STELLINGEN behorende bij het proefschrift van Erik Gommeren

1. Het ontwerp en de optimalisatie van een industrieel maalproces berust nog grotendeels op ervaringsregels. Dit zal zo blijven zolang de beschikbare procesmodellen geen beschrijving geven van de fenomenen op microschaal.

2. De parametrisatie van de semi-empirische relaties voor het jetmill-proces wordt bemoeilijkt door het niet-lineaire karakter van de fysische verschijnselen. Hierbij speelt de massa en de deeltjesgrootteverdeling van het produkt aanwezig in de molenkamer een belangrijke rol.

3. In een stationaire bedrijfstoestand is het jet mill proces zelfstabiliserend als gevolg van de fysische terugkoppeling van de moleninhoud op het breukproces en de interne classificatie. Deze terugkoppeling geeft echter geen garantie voor de produktkwaliteit.

4. Evenals bij andere industriële deeltjesprocessen, zoals kristallisatie en granulatie, speelt bij jetmilling het stochastische karakter van het transport en de interactie, alsook van de onregelmatigheden in de structuur van deeltjes, een overheersende rol in de werking van het apparaat.

5. Kleinere deeltjes zijn gemakkelijk te versnellen, maar moeilijk te raken.

6. Jetmilling, malen met een luchtje.

7. De ontwikkelingen in de informatie technologie zullen niet zozeer tot uiting komen in nieuwe electronica, maar vooral in de manier waarop individuen met informatie omgaan. De belangrijkste vooruitgang ligt dus niet in de hardware, maar in de hoofden van de mensen.

8. Naast de technische en economische levensduur van een artikel, bestaat er ook zoiets als een marketinglevensduur. Na het verstrijken hiervan zijn er geen toeters en bellen meer aan het produkt te hangen om de consument met reklame te verleiden tot aanschaf.

9. Het is niet terecht dat rokers een hogere ziektekostenpremie zouden moeten betalen. Als ze na hun produktieve periode eerdeer overlijden levert dit zelfs een besparing op.

10. De plotselinge ophef die stofzuigerfabrikanten maken over de toepassing van het aloude cycloonprincipe voor het ontstoffen van een luchtstroom door een nieuwe concurrent, doet vermoeden dat ze bij hun produktontwikkeling al die jaren andere dan technologische motieven zwaarder hebben laten wegen.

11. Een goede systeembeheerder heb je niet nodig.

12. Het feit dat, ondanks de moderne communicatiemiddelen, volkeren een gebrekkige kennis van elkaars culturele achtergronden hebben ligt niet aan de techniek, maar is vooral het gevolg van gebrek aan interesse.

13. 'Vooruitgang': Het gebruik van mobiele systemen in auto's die aangeven waar files staan en vervolgens alternatieve routes aangeven, zal mogelijk de gemiddelde lengte van de files doen dalen. Het aantal en de totaal lengte van de files echter zullen er waarschijnlijk door toenemen.

Study of a closed circuit jet mill plant using on-line particle size measurements

Study of a closed circuit jet mill plant using on-line particle size measurements

PROEFSCHRIFT

ter verkrijging van de graad van doctor
aan de Technische Universiteit Delft,
op gezag van de Rector Magnificus Prof. dr. ir. J. Blaauwendraad,
in het openbaar te verdedigen ten overstaan van een commissie,
door het College van Dekanen aangewezen,
op maandag 17 november 1997 te 16.00 uur
door

Henricus Jacobus Cornelis GOMMEREN

werktuigbouwkundig ingenieur

geboren te Bergen op Zoom

Dit proefschrift is goedgekeurd door de promotoren:
Prof. B. Scarlett M.Sc.
Prof. ir. O.H. Bosgra

Toegevoegd promotor:
Dr. ir. H.J.M. Kramer

Samenstelling van de promotiecommissie:

Rector Magnificus, voorzitter
Prof. B. Scarlett, M.Sc. Technische Universiteit Delft
Prof. dr. ir. O.K. Bosgra, Technische Universiteit Delft
Dr. ir. H.J.M. Kramer, Technische Universiteit Delft
Prof. K. Heiskanen, Technical University of Helsinki, Finland
Prof. J.A. Dodds M.Sc., Ecole des Mines D'Albi, Frankrijk
Prof. Dr.-Ing. K. Schönert, Technische Universität Clausthal, Duitsland
Dr. ir. W. de Bruyn, Ico Europe, Rotterdam

Cover: Fabrique Delft 1997

Table of Contents

Voorwoord

Allereerst wil ik mijn promotors Brian Scarlett en Okko Bosgra bedanken voor hun inspiratie, ondersteuning en de vrijheid die ze me hebben gegeven tijdens het werken aan dit onderzoek. Daarnaast wil ik Sjoerd Dijkstra en Herman Kramer, tevens co-promotor, bedanken voor hun begeleiding.

Verder hebben een groot aantal studenten een belangrijke bijgedrage geleverd. Dit waren René van Eerten, Ed Hanenberg, Marc Ramondt, Albert van de Bos, Maarten Volker, Hans Moolenaar, Tys van Elk, Danny Post, Jan van Rhee en Michael Phillipse. En Joke Talman, die onderzoekster in Japan is geweest. Bedankt voor de motiverende samenwerking en inzet. Succes met jullie carrières en ik hoop jullie met enige regelmaat terug te zien.

Op deze plek wil ik tevens Camiel Heffels en Daniel Heitzmann bedanken voor hun inhoudelijke bijdragen aan het project. Maar belangrijker vind ik natuurlijk de vriendschap die we hebben opgebouwd. Ook wil ik Arief Dahoe bedanken voor zijn hulp.

Daarnaast wil ik mijn waardering uitspreken over de ondersteuning door de werkplaats en het secretariaat van het lab API, alsook over de samenwerking met de firma Barth, JMS, Novem en Wedco. Iedereen bedankt voor het meedenken aan de bouw van de proefopstelling, de nuttige reacties op het onderzoek en de plezierige omgang.

En natuurlijk zal ik mijn collega-AIOs op API en Deeltjes niet vergeten. Bedankt voor de gezelligheid zoals tijdens het koffiedrinken en de sportieve uitjes.

Tot slot gaat mijn dank uit naar mijn familie, vrienden en vriendin Aster. Dat spreekt voor zich.

Rotterdam, 1997
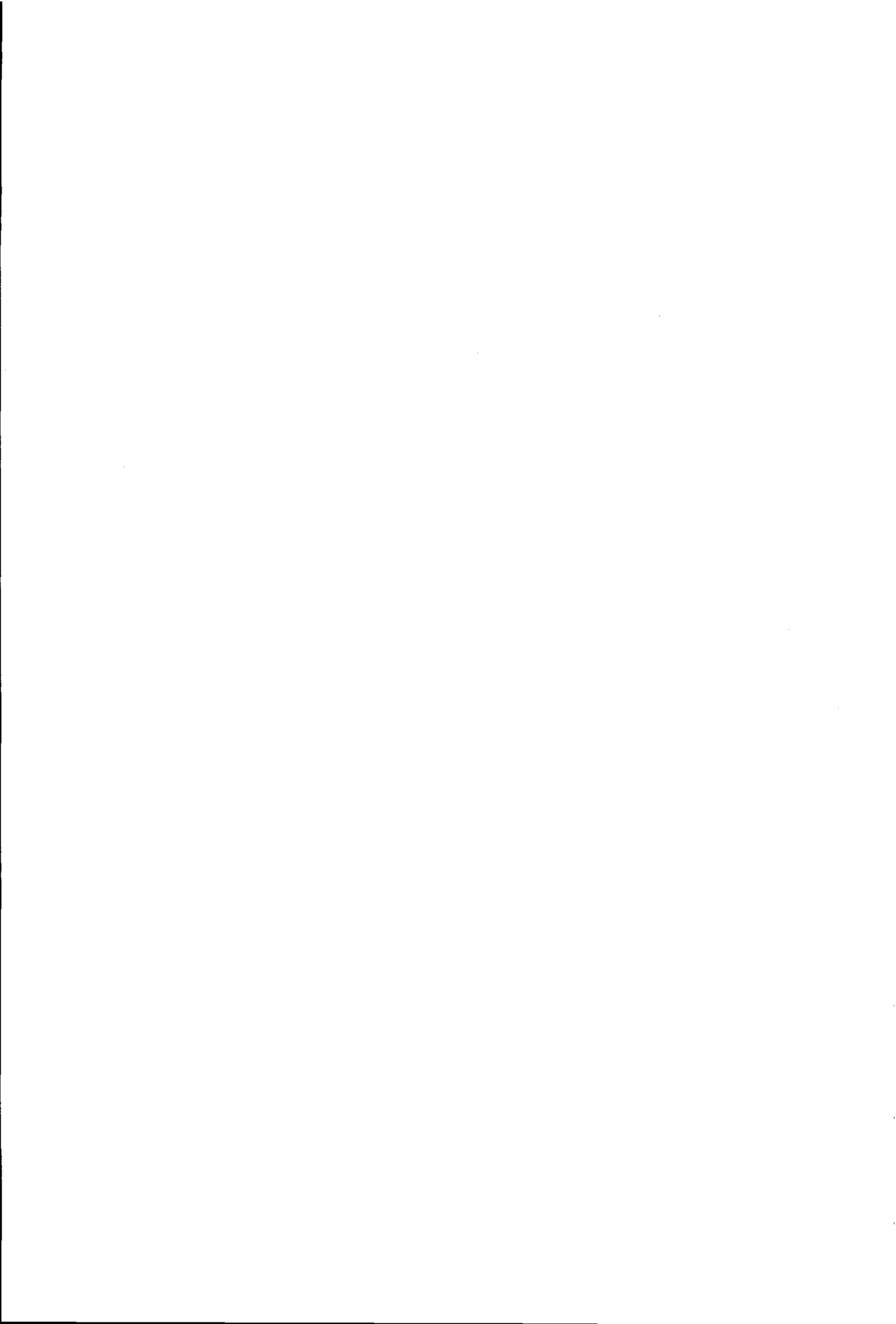
Summary

Study of a closed circuit jet mill plant
using on-line particle size measurements

Jetmilling is a grinding technique which is typically used to produce a fine powder with a narrow particle size distribution (PSD) from a brittle feed material. The PSD determines greatly the behaviour of the material in succeeding unit operations such as chemical reactions, combustion, printing or coating.

Advantages of jetmilling, besides the well defined PSD, are the avoidance of excessive heat and contamination during processing. This makes jetmilling very suitable for the processing of plastics, pharmaceuticals and food additives. The major disadvantage of the process is the very poor energy efficiency.

In jet mills, which are also called fluid energy mills, expanding air jets entrain and accelerate the particles which are dispersed into the mill chamber. Turbulence is the main mechanism for the mutual collisions that create the mechanical loading required for particle breakage.

In this project two types of jet mills were investigated, namely the spiral jet mill and the opposed jet mill. In spiral jet mills, both the size reduction and the separation of particles depend on the two phase flow inside the mill chamber. The optimal hold-up required for each of these sub-processes conflicts and makes a simultaneous optimisation impossible. For this reason the jet mill plant was extended with an external classifier and operated in a closed circuit mode.

As a comparison, an opposed jet mill was tested. In this mill the jets are directed at a focal point. The fines are discharged by an integrated classifier rotor. Set points of the solid feed, air supply and rotorspeed were systematically studied and an optimisation procedure was suggested.

Disturbances on the air supply and variations in the composition of the feed cause the product quality to fluctuate. Therefore, in industrial practice jet mills have to be operated below their maximum capacity in order to avoid the production of off-specification material. Start-up and shut-down of the grinding plant is a matter of trial and error, which is laborious and makes the product quality vulnerable to operator errors.

This underlines the importance of an automated grinding plant equipped with a real-time PSD instrument for quality control. A special in-line sampling cell on the mill outlet was designed and built for use with laser diffraction (LD) instruments. As a more robust and cheaper alternative to LD a prototype of an incoherent scatter device was investigated.

For control purposes an absolute accuracy of the produced PSD is not required. With principle component analysis (PCA) the raw scatter signals of the LD instruments was studied. This data reduction technique allowed a faster and simpler processing of the measured data into a control signal compared to the usual deconvolution techniques.

The real-time size information of the mill product was measured and stored together with the operating variables. The collected process knowledge was used to validate and optimise a population balance model of the closed circuit jet mill plant. Separate impact tests and compression tests were carried out to characterise the breakage behaviour of the test materials.

The plant automation improved the reproducibility of grinding batches as a result of the exclusion of operator errors. The real-time particle size monitoring of the jetmilling process reduced the production of off-specification material. A simple feedback control based on the on-line PSD measurements allowed an operation of the mill that was closer to the specification limit, thus avoiding a considerable amount of overgrinding.

The last part of the research project focused on a more detailed study of the flow patterns in the jet mill. Computational fluid dynamic (CFD) simulations were made of the rotating flow in the mill chamber. The Phase Doppler technique was used to study the entrainment of particles by the expanding air jet.

Chapter 1

General introduction

1.1 Motivation and background

1.1.1 Powders in chemical process industry

In the chemical process industry the majority of products is treated in some particulate form during its life cycle. Unit operations like granulation, grinding, crystallisation and classification modify the properties of particle collections without a chemical reaction. The aim of these so-called particulate processes is to obtain a desired behaviour of the powder in a following process step or final application.

A large variety of products ranging from high value fine chemicals to bulk materials consists of powders and granules. Examples are fillers for paint, toners, ink, food additives, coatings and powders for rotational moulding. The material can be a catalyst or a carrier constituent that is mixed with liquids and other compounds. The scales of operation vary from several litres to cubic meters, operated batch wise or in continuous way.

The desired properties of a powder depend on the application [CARR]. For instance, the reactivity or solubility of the product is usually related to the maximum surface area, which, depends on the relative amount of fines present in the powder. Complete conversion in combustion, chemical reaction and solution processes are determined by the largest particles. Other characteristics affected by particle size are the flowability and bulk density. For a smooth coated surface the top size of paint/coating particles is critical. Furthermore the brightness and colour of pigments are related to the whole particle size distribution as a result of light diffraction [BRAMEKAMP]. Other examples are the strength of cement and the taste of chocolate. Finally dust problems and explosion risk during handling can be controlled by a proper particle size.

The above examples illustrated how the product specification is often related to the size distribution of the particles. As a result of new applications and products such as

energy mills. Mutual collisions cause particle breakage. Figure 1-4 (right) shows that the energy efficiency drops sharply in the fine particle range [HUKKI].

Relevant process characteristics: A combination of criteria determines whether a particulate process can be applied. First of all, the required product quality has to be attained. Secondly, an economic basis must exist, which is a function of investment cost, operational cost and added value of the end product. In most cases the energy supplied to the mill is not effectively used for size reduction. Only a fraction is used for breakage of particles, as most of the energy is simply dissipated or lost by heat development.

Process integration: As an enormous dissipation of energy is inherent to size reduction, especially in the fine particle range, it is useful to first consider alternative processes before choosing for grinding. Processes like crystallisation, precipitation or spraying are far less energy intensive. Also the study of unit operations previous to or following the grinding step should get attention. Slight modifications in these processes might benefit the overall energy efficiency of the production. KLIMPEL [1994] gave a number of examples how to modify grinding environments in order to improve downstream product performance. HULS [1990] discusses the effect of grinding on flotation. Furthermore it should be realised that in some cases grinding processes can simultaneously be used for de-agglomeration, coating [TAKEBAYASHI] and mixing of particles.

1.2 Fluid energy grinding

1.2.1 General operating principle

Jetmilling, also called fluid energy grinding, is an increasingly used process in chemical industry for processing brittle, heat sensitive materials into very fine powders with a narrow size distribution. More than 90 years jet mills are being built and applied successfully on a semi large scale in the chemical industry. A number of famous design are extensively described in a number of patents and publications [AKUNOV, ALBUS, ALBANAO, KARVINEN, RUMPF, NIED].

Most of such mills are variations on one of the fundamental configurations that are depicted in Figure 1-5. The designs differ from each other by the arrangement of the nozzles and the classification section. In the following paragraphs the jet mill types will be briefly discussed.
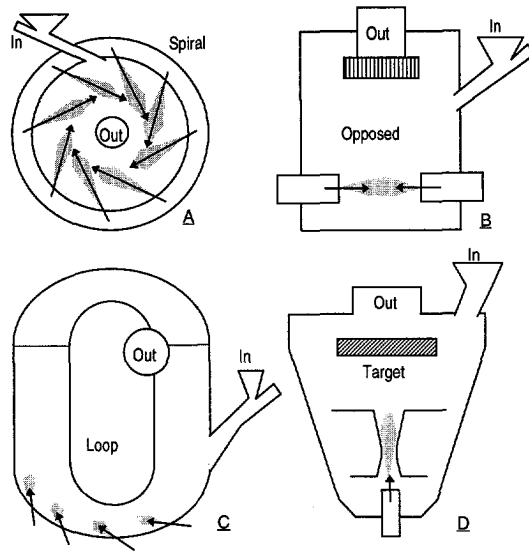
Figure 1-5 Schematic representation of basic jet mill designs. A: Spiral, B: Opposed, C: Loop, D: Target.

The key feature of jet mills is the conversion of high pressure into kinetic energy. The operating fluid enters the grinding chamber through nozzles placed in the wall. The feed particles brought into the mill through a separate inlet, are entrained by expanding jets and accelerated to velocities as high as the velocity of sound. In fact three collision geometries can be distinguished:

1. Inter particle collisions due to turbulence in a free jet.

2. Collisions between particles accelerated by opposed jets.

3. Impact of particles on a target.

The turbulent nature of the jets causes particles to have differences in velocities and directions. Particle breakage in jet mills is mainly a result of inter-particle collisions: wall collisions are generally thought to be of minor importance only, except mill type D (Figure 1-5). Fluid energy driven mills are a class of impact mills with a considerable degree of attrition due to eccentric and gliding inter-particle impacts. The grinding mechanism through mutual collisions means that jet mills operate with virtually no product contact. In other words, the contamination grade is low.

The classification of product leaving the mill depends on a balance between centrifugal forces and drag forces in the flow field around the mill outlet. Mill types A and C create a free vortex at the outlet, while jet mill D makes use of gravity. Type B has an

integrated rotor. The final product quality is largely determined by the success of classification.

1.2.2 Spiral jet mill

The original design of the spiral jet mill is shown in Figure 1-5, and was first described by ANDREWS in 1936 and patented under the name Micronizer. It has a cylindrical chamber of which the height is considerably smaller than the diameter. Other names are: Micron Master, Orba-Jet, or pancake mill. A number of nozzles is placed in the outer wall of the mill through which the grinding medium, a gas or steam, enters the mill. Initially it was equipped with a double row of nozzles, but the first production mill has a single row.

A spiral jet mill combines both grinding and classification by the same jets. The vortex causes coarse particles of the mills contents to be transferred to the outer zone, as fines can leave through the central outlet. The solid feed is brought into the mill by an air pusher. The outlet is placed in the centre of the mill chamber. The working principle of this mill was extensively investigated by RUMPF.

Spiral jet mills are notable for their robust design and compactness. Their direct air operation avoids the need for separate drive units. Another significant argument for the use of jet mills is the lower risk for dust explosions. The spiral jet mills used for experiments in this research project were built by Wedco.

1.2.3 Opposed jet mill

Opposed jet mills are fluid energy driven mills that contain two or more jets aligned towards each other (see Figure 1-5, B). Different versions are on the market, based on a design patented by WILLOUGHBY [1917]. In this type of jet mill opposed gas streams entrain the mill hold-up. At the intersection of the jets the coarse particles hit eachother. The grinding air carries the particles upwards in a kind of fluidised bed to the classification zone.

Adjustment of the rotor speed allows a direct control of the particle size of the end product. The feed is entered by a rotary valve. Drawbacks are the higher cost of investment and maintenance. These types of mills are described by VOGEL and NIED.

1.2.4 Other jet mill designs

Figure 1-5 D shows one of the earliest jet mill designs (around 1880), but still in use today. In this mill a jet loaded with particles is impacting on an anvil. Consequently the impact efficiency is high for relatively large particles. Very fine grinding becomes

difficult as small particles are decelerated in the stagnant zone in front of the target. Fines are dragged out in an air stream by a fan, as coarse material is recirculated to the jet entry. Points of improvement have been a better classification and abrasive resistant target material. This device is suitable to incorporate as a pre-grinder.

The loop mill (Figure 1-5, C), also called Torus mill, was designed by KIDWELL AND STEPHANOFF [1940]. Today this mill type is being built by Aljet Equipment Company, under the name 'Reductionizer'. The grinding fluid is brought into the grinding section. The fines leave the mill through the classification section.

1.3 Modelling of grinding processes

RUMPF [1960] showed that many variables affect the size reduction process. The question with respect to plant optimisation is: How can the desired product quality be achieved at minimum energy use and a reasonable throughput. In order to improve the grinding systems knowledge must be collected at different aggregation levels and during process steps. Figure 1-6 shows the aspects to be concerned with the investigation of comminution processes.
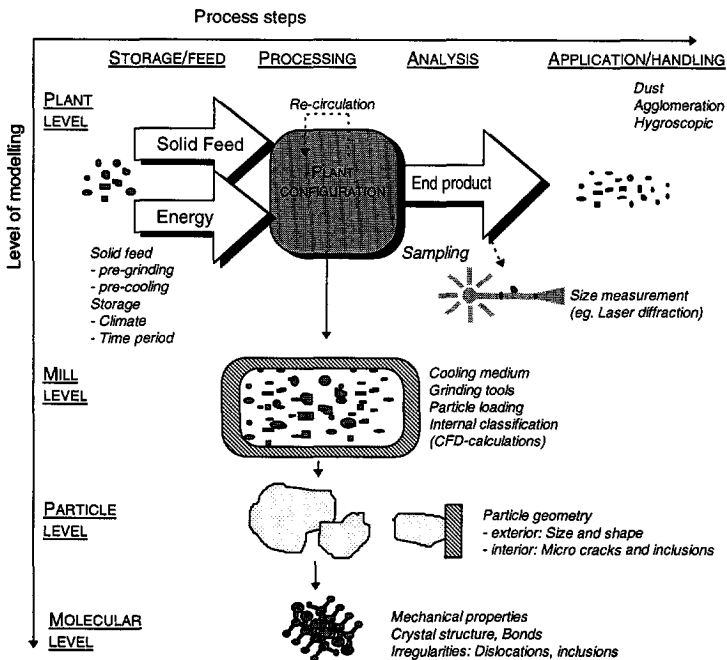
Figure 1-6 Ways of looking at comminution dividing it in process steps (horizontal) and levels of modelling (vertical)

Process steps: The key issue is whether the desired product quality can be obtained by applying a certain grinding technique. Therefore the process steps will be discussed in the reverse order.

Handling and application: The desired behaviour during application is the determining factor. It dictates which aspects of the particle size distributions are relevant and how the product specifications have to be defined.

Analysis: Particles that are within specification need to be discharged from the grinding plant while keeping the mill in optimal working conditions. In order to control and optimise the process a monitoring system is required. Particles are analysed to check whether they meet the product specification, several methods can be used. Sampling techniques and analysing methods determine the reliability of the particle size measurement. The frequency of sampling as well as the location of sampling play a role.

Processing: Disturbances like changing ambient conditions and machine wear influence the grinding process. It is important to know the dynamic behaviour of the plant and its ability to suppress fluctuations. Which actuators variables are available and most suitable for set point tracking. In case the product specification can not be effectively achieved in one stage, re-circulation or serial processing might bring a solution. Accurate determination of mill type and operating conditions will have to be determined by pilot plant tests.

Storage and feed: The grinding process starts with the input of energy in some form and the supply of solid feed. It is important to know the history of the material such as pre-treatment and previous unit operations. Also the storage conditions (summer/winter) have an influence as the material might have been submitted to heat or moisture. Finally, when the feed material is of natural origin or supplied by different producers it is important to check if it is of constant quality.

Levels of modelling: Levels at which size reduction process can be described are presented along the vertical line in Figure 1-6.

*Plant level*ː The highest level describes the behaviour performance of the grinding plant for different combinations of set points. The product is characterised by bulk properties such as bulk density, PSD, flowability or moisture content.

A black box model can be determined by recording the transients in plant performance due to appropriate test signals. According to EEK [1995] a relatively simple

mechanistic model is suitable for control purposes. This semi-empirical model can be based on pilot plant experiments.

A model that can serve as tool for plant design or scale-up needs to be obtained by physically based modelling. Such a model should be able to predict how the separate units of the plant interact dynamically. The accurate formulation of events such as particle breakage and transfer is crucial in this approach. Insight in mechanisms at the lower model levels contributes to better understanding of the mill performance at plant level.

Mill level: This is the second level on which milling process can be investigated. Due to the improvement of computational fluid dynamics software packages and increasing computer power simulations can be useful tools that provide information about loading conditions and movement of the particles inside the mill. TALMAN [1995] set up a rigorous model including a discrete simulation of particle movements in a turbulent vortex flow. Much progress is expected in this field.

Particle level: On the level of the particle itself modelling work was done by CAMPBELL ET ALL [1993]. Grid cells are attached to another by a 'virtual' glue. This glue incorporates the mechanical properties of the material. Realistic simulation results were produced, but there is a lack of physical basis. In the ideal case size reduction is governed by crystal structure and bonding energy. Irregularities, in practice, overshadow the idealised structure concepts.

Grindability is related to the molecular structure (amorphous, poly-crystalline) and the forces between the molecules. One step down is the modelling of mechanical behaviour of solids by molecular modelling software.

First grinding models appeared at the beginning of this century in the mineral industry. AUSTIN gave an overview of the models describing breakage process in mechanistic manner using the concept of population balances. Power laws and statistical expressions express the breakage behaviour of materials in specific mills. These models could be used for process tuning and control, but have limited applicability to different mill designs.

Many literature contributions exist on the performance of various types of mills since the fifties. RUMPF who studied the working principle of jet mills. Rigorous modelling based on the processes of particle breakage and two phase flow patterns in the mill can provide transferable insight in the dominant physical mechanisms principles of grinding and classification. This should allow a more rationally based design and scale

up of grinding plants. In fact output of the lower levels of modelling in Figure 1-6 can provide inputs for the higher levels, together with experimental modelling.

An other purpose of a mill model can be control. A mechanistic model has to be built that is able to predict relevant conditions inside the mill and changes in product quality for different operating conditions. On-line process data can be used for verification and optimisation of the model parameters. Based on this information setpoints of the grinding plant can be adjusted such that the desired product quality is obtained at minimum energy consumption.

Remark on the use of literature: Comparison of data from different sources should be done with care, as different sampling and measurement techniques might have been used. Furthermore differences in grindability provide large spread in results. Therefore actual performance should be measured at a pilot plant scale.

1.4 Scope of the problem

Economic importance and scale of operation: On a world basis one can speak about an economic revival leading to an increased demand for intermediates. Competition on a global market requires guaranteed product quality produced in an efficient way. On top of all the model levels discussed in the previous section, a model determining whether the process has an economic basis (see Figure 1-7).
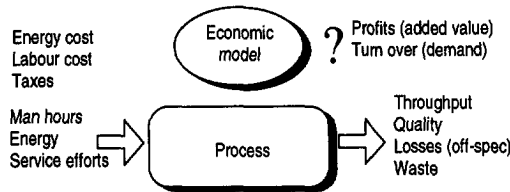
Figure 1-7 The economic model on top of process model

Of all grinding processes, jet milling is the most energy inefficient as virtually all energy supplied to a jet mill is being dissipated in the turbulent flows. On the other hand turbulence creates differences in velocities and directions of particles (motion) that leads to collisions needed for particle breakage. The product quality depends on the internal classification of the mill which is negatively affected by turbulence. Optimisation for grinding and classification performance can not be achieved simultaneously, because this jet mill is normally operated in such a way that the number of particles larger than the desired product size is minimised. This leads to a highly inefficient grinding process in terms of energy consumption.

RUMPF [1966] estimated that 5% of the world energy is used for grinding. Jet mills use between 800 and 4500 kWh per ton ground product, so energy cost are a significant part of the total production cost. To put this figure in context, the estimated total energy use for jet milling in Europe is about 600 million kWh and in the United States, 1000 million kWh on annual base.

1.5 Objective and approach

The work which forms the basis of this thesis originated from a research program sponsored by the Dutch Association for Environment and Energy (Novem) and the company Wedco Holland. The project aimed at a 50% energy reduction of the jetmilling process by developing a control system and improved design of the grinding plant. For this purpose a jet mill plant was built at TU Delft. The approach was two fold:

1. Plant and mill re-design: As it appeared that grinding and classification could not be optimised simultaneously, the pilot plant has been extended with an air classifier. A part of the mill product flow was removed and re-circulated. The next step was to get the most out of the existing jet mill plant. During the last stage of the project the mill design was studied.

2. Process monitoring and control: An important feature of this new grinding system will be an operation control system based on in-line size measurement of the ground product. This offered the opportunity to study dynamic performance, rapid exploration of operating conditions of the plant.

This included the implementation of a distributed control system and better control arrangements to capitalise on variations in product quality and off spec batches.

1.6 Organisation of this thesis

After an introductory period the pilot plant was designed and prepared for the mechanical and electrical workshops. **Chapter 2** deals with the lay out of the grinding plants that were investigated in this research project. The major parts of equipment and the control system of the grinding plant are described. Two most commonly used types of jet mills, namely the spiral and opposed types, were subject of study.

Chapter 3 is concerned with the set up of a real-time size measurement system based on the principle of light scattering. An on-line sampling cell was designed and tested on the pilot plant. Experiments were carried out to access effects on the measured PSD due to sample errors, concentration fluctuations. The raw detector data was

studied to serve as a control signal. As an alternative to laser diffraction an instrument based on the scattering of incoherent light was tested.

Chapter 4 provides a theoretical background for size reduction of plastics. Single particle impact tests and compression tests were performed to determine the grindability of the test materials used for the jet mill experiments.

Chapter 5: The application of classifiers in grinding plants are important with regard to the obtained product quality as well as for the optimisation of the grinding plant. The basic principles of air classification and their implementation in grinding plants are described. Finally methods are presented to characterise the performance of classifiers.

Chapter 6 presents the experimental data of the grinding plant. Real-time particle size measurements played an important role in the study of dynamic mill performance. The operating ranges were explored. Finally open and closed loop test runs were compared with respect to specific energy use and product quality.

Chapter 7 presents a mechanistic model based on population balances to describe the dynamic behaviour of the closed circuit jet mill plant. The jet mill is divided into several zones exchanging particles. The stochastic behaviour of the particles is not described by the classical residence time distribution, but directly by the probability of the particles to move from one zone to another. For the breakage and selection function in the model, traditional equations were used that were extended with terms for process conditions.

Chapter 8: Flow simulations and Phase Doppler measurements were carried out in to investigate the flow patterns in the expanding jets and the vortex in the mill chamber.

In **Chapter 9** the general conclusions and perspectives are given.

Literature

Akunov, W.J., Strahlmühlen. Translation into German of a Russian text issued by the State, *Scientific-Technical Publishers,* 1952

Albus, F.E., The modern fluid energy mill, *Chem.Eng.Proc. CEP,* vol. 60/6, 102-106, 1964

Albus, F.E., Fluid Energy Grinding or Jet Milling, *12th annual Powder and Bulk Solids Conference,* , 437-447, 1987

Albus, F.E., Fluid energy grinding-versatile process tool, *Chem.Eng.Prog.,* 57, 90, 1961

Alfano, G., Saba, P., Surracco, M., Development of a new jet mill for very fine mineral grinding, *Int. J. Miner. Process.,* vol.44-45, 327-336, 1996

Alfano, G., Saba, P.; Surracco, M., Fine particle technology - development of a new jet mill, *Recents Prog. Genie Procedes 96, 10(45, Procedes de Broyage)* 143-148, 1996

Austin, L.G., Rogers, R.S.C.,, Powder technology in industrial size reduction, *Powder Technology,* 1985

Austin L.G., Klimpel R.R, Luckie P.T., Process engineering of size reduction: Ball Milling, *Trans SME/AIME,* 1984

Barnard, B.; Laverick, W.T., Metal phosphate-coated titanium dioxide pigments, *Ger. Offen.,* 17 pp., Pat.

Barsukov, E.Y., Soskind, D.M., Jet pulverization of solid particles in fluidized bed apparatus, *int.chem.eng.,* 13/1, 84-86, 1973

Bignell, J.D., Newton, S., Recent progress in solids processing: comminution- a review, *Chem. Eng. res. des.,* 64, March, 91-93, 1986

Bokii, Y.F., Purification of Metal Powders from Oxide Films in a Jet Mill, *Sov Powder Metall Met Ceram,* 21/2, 81-84, 1982

Bouchillon, C.W., Steele, W.G., Burnett, J.D., Ultra-fine grinding of low rank coals in a fluid energy mill, *Particulate science and technology,* 7 (3), 4-5, 1989

Boyd, H., Fine Grinding-high speed mechanical mills, *Short course on size reduction and classification, A'dam (Hand out),* 1-10, 1990

Campbell, C.S., Potapov, A.V, Computer simulation of particle fracture, *int. fine. part. research. institute (IFPRI), report ifpri.5,* arr-18-5

Chan, R.C.; Chung, D. D. L., Superconducting pastes and paints, *Supercond. Its Appl., Proc. Annu. Conf. Supercond. Appl., 2nd,* 2nd, 208-13, 1988

Chang, Y.-H.; Jernigan, J.C.; Treece, L.C., Powder coating compositions prepared by jet milling to give fine particles, *PCT Int. Appl., 37 pp.,* Pat.1995

Cheng, Y.S, Marshall, T.C., Henderson, R.F., Newton, G.J., Use of a jet mill for dispersing dry powder for inhalation studies, *am.ind.hyg.assoc.J.*, 46(8), 449-454, 1985

Dunn, R.M., An innovation for the efficient production of superfine materials, *12th annual powder and bulk solids conf. 1987*, ,427, 1987

Dobson, B., Rothwell, E., Particle size reduction in a fluid energy mill, *Powder technology*, 3, 213-219, 1969

Forssberg, E.; Zhai, H., Liberation modeling of base metal ores in autogenous grinding, *Scand. J. Metall.*, 14(1), 9-17, 1985

Garbagnati, G., Turbine micronization of powders, *ICP*, 12(2), 68-72, 1984

Goodspeed, N.C.; May, R. R., Jr.; Ross, J., Two-stage fluid-energy milling of titanium dioxide pigments, *Brit. Amended, 8 pp.* Pat.

Heiskanen, K., Soo, S.L., Scarlett, B., Kievit, O., Powder processing, *Diktaat Deeltjestechnologie II*, ST68, 1993

Hohensee, M.; Mertins, E., Reduction of specific energy consumption in liberation grinding of iron ores through improvement of autogenous and subsequent fine grinding, *Aufbereitungs-Technik*, 31(3), 138-46, 1990

Hommel, H., Preparation of ultrafine ammonium perchlorate in an air jet mill, *Int. Jahrestag. - Inst. Chem. Treib- Explosivst. , (Mod. Technol. Treib- Explosivst.)*, 161-97, 1978

Hukki, R.T., Reddy, I.G., The relationship between net energy input and finess in comminution, *Dechema, Symp. Zerkleinerung, 1966/67*, teil I, 313-320, 1966

Huls, B.J.p.m., Interaction between grinding and flotation, specifically column flotation and column scale-up,, *Ph.D Thesis, TU Delft, The Netherlands*, 1990

Huwald, E., Clements, M., Mahlung und verschleiss in einer Gegenstrahlmühle, *Chem.Ing.Techn.*, 47nr 299, 216/75, 1975

Ionchev, V. D., Jet mills and their use in the production of daylight fluorescent inks, *Khim. Ind. (Sofia)*, 44(10), 463-4, 1972

Jimbo, G., New pulverization technology for preparation of ultrafine particles, *Kagaku Gijutsushi MOL*, 21(1), 40-5, 1983

Kaiser, R., Fluisized bed jet milling. Key to purify Si, Si3N4 powders, *Metal Powder report*, 42, 851-853, 1987

Kaiser, R., Fluid bed jet mill makes fine pure powder, *ceramic industry*, 30-43, 1988

Karvinen, R., Kauramaki, T., Nieminen, P., Grinding Principle and Experiences with a new type of opposed jet mill, *Grinding Principle and Experiences with a new type of opposed jet mill,* 3-2, 123-128, 1991

Kingston, H.E., The fluid energy mill for grinding solids to sub sieve ranges, *Brit. Chem. Eng. Mag.,* 30-38, 1956

Klimpel, R.R., Some industrial experiences in modifying fine grinding environments for improved downstream product performance, *8th European Symposium on Comminution, Stockholm,* I, 141-151, 1994

Mohanty, B., Narasimhan, K.S., Fluid energy grinding, *Powder Technology,* 33, 135-141, 1982

Nakagami, H.; Nada, M., The use of micronized cellulose disintegrants as insoluble swellable matrixes for sustained-release tablets, *Drug Des. Delivery (1991), 7(4),,* 7(4), 321-32, 1991

Nakayama, N., Pulverizing of various Materials by Super-Sonic Jet Mill, *Bulk Solids Handling,* 6-1, 157-160, 1986

Nakayama, N., Development of toner production process with super sonic jet mill and dispertion separator, *Kagaku Kogaku,* 55(6), 441-4, 1991

Nied, R., Fluidized bed counter- jet mill - recent findings and new applications, *Aufbereitungs-Technik,* 23(5), 236-242, 1982

Nied, R., CFS - HD: A new classifier for fine classification with high efficiency, *8th European Symposium on Comminution, Stockholm,* II, 35-69, 789-801, 1994

Nishibori, S., Pulverization of gelatins, their resin films and coatings, *Jpn. Kokai Tokkyo Koho,* , 11 pp., Pat.

Orlov, V. M.; Sannikov, A. K.; Toldina, L. A., Modification of red iron oxide pigment during jet grinding, *Novoe v Tekhnol. Polucheniya Dvuokisi Titana.,* 175-80, 1976

Pacek, A.W.; Nienow, A.W., An Application of Jet Grinding to Fluidised Bed Granulation, *Powder Technology,* 65/1-3, 305-310, 1991

Rumpf, H., Uber grundlegende physikalische Probleme bei Zerkleinerung, *Symposium Zerkleinern, Frankfurt,* , 1-31, 1962

Schönert, K., On the limitation of energy saving in milling, *1st world congress Part.techn,* 2, 1986

Shiau, S. Y.; Yang, S. P., Effect of micronizing temperature on the nutritive value of sorghum, *J. Food Sci.,* 47(3), 965-968, 1982

Takebayashi, H., Coating technology of ultrafine particles, *Kagaku Sochi,* 29(5), 67-71, 1987

Temperly, H.N.V, Blythe, G.E.K., Mills which grind to micron size without moving parts, *Nature,* 219, 1218-1220, 1968

Tkacova, K., Stevulova, N., Lipka, J., Sepelak, V., Contamination of quartz by iron in energy-intensive grinding in air and liquids of various polarity, *Powder Technology,* 83, Issue 2, May 1995, 163-171, 1995

Vil'shanskii, A. I.; Kuz'min, V. G.; Sitnikov, I. S.; Stepanova, V. V.; Khodakov, G. S., Production of fillers for plastics in counter current jet mills, *Stroit. Mater.,* 2, 10-11, 1972

Vogel, A., The Alpine fluidized bed opposed jet mill with examples for special fields of application, *TIZ International Powder Magazine,* 114-10, 1990

Wicke, R.; Pahl, M. H., Disaggregation of compacted bulk materials using a jet mill, *Aufbereitungs-Technik,* 32(1), 1-9, 1991

Willoughby, A., Andrews, N. Opposed jet mill, *Am. pat,* 1917

Wolfram, H.G., An interesting new grinding process, *Bull American Ceramic Soc.,* 18 (10), 374-375, 1939

Chapter 2

Jet mill plants

This chapter describes the jet mill plants that were investigated in this research program. Section 2.2 deals with the pilot plant at TU Delft comprising a spiral jet mill connected to an external air classifier. Section 2.3 describes the central monitoring and control system. Information about the auxiliaries can be found in section 2.4. Finally section 2.5 gives a brief description of the industrial scale opposed jet mill plant.

2.1 Introduction

Experimental work had to be done in order to investigate the jetmilling process. Therefore a pilot plant was designed and built at TU Delft comprising a spiral jet mill and an external classifier. The performance of the plant was characterised by means of a real-time particle size measurement system. In this chapter the lay-out of the pilot plant will be described.

In addition, experiments were performed with an opposed jet mill in a similar experimental set-up at the location of Wedco Holland. A brief description is given in the last section of this chapter.

For a general description about grinding plants one is referred to DARLING [1949] and WAYNE [1990].

2.2 Pilot plant at TU-Delft

The lay out of the pilot plant is schematically shown in Figure 2-1. A screw feeder drops the feed material, normally granules or flakes with a size of several millimetres, into the solids inlet of the mill.
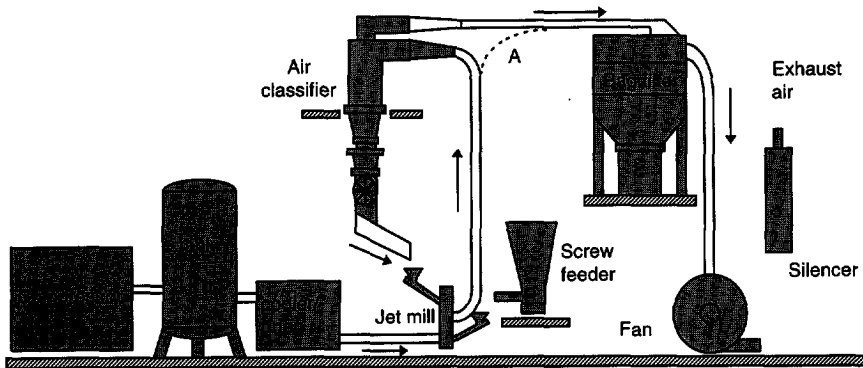
Figure 2-1 Lay-out of the closed circuit jet mill pilot plant.

Two configurations of this plant were tested. In the open circuit mode the exhausted grinding air conveyed the ground material directly to the bag filter where it was collected as end product. The external classifier was by-passed (path A).

In the second mode, closed circuit grinding, an external classifier was incorporated in the grinding plant which recirculated the coarse fraction of the ground product to the jet mill. The fines outlet of the classifier was connected to the product collection.

Generally, the feed enters at the centre of the mill chamber where it is submitted to grinding. As an alternative the feed can be added to the classifier inlet. This may be advantageous when pre-ground feed is used, that already contains a significant percentage of fine particles. In this way the grinding of feed particles which are already undersize can be avoided. The coarse rejected from the product flow is added to the fresh feed (mock-up) for re-grinding.

2.2.1 Spiral jet mill

The design of the the spiral jet mill, or Micronizer, is described in a number of publications [ALBUS]. For this research project a 10-inch spiral jet mill was fabricated out of stainless steel by Wedco. The cylindrical mill chamber with a inside diameter of 254 millimetre housed a number of replaceable nozzles that were tangentially directed. Figure 2-2 shows the geometry of the pilot plant jet mill.
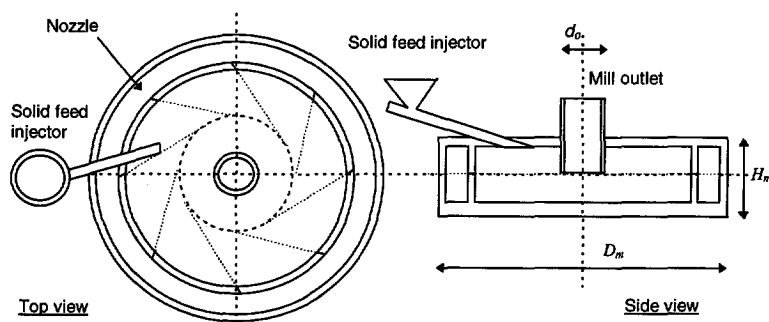
Figure 2-2 Top view and side view of spiral jet mill.

A characteristic feature of a spiral jet mill is the absence of moving parts, which results in lower wear than in mechanical mills. Furthermore the construction could be compact and cheap. The dimensions of spiral jet mills typically used for grinding plastics range from 15 to 100 centimetres. The operating pressure of the carrier gas, in this case air, varied from 3 to 7 bar. The material present in the mill accelerate to high velocities due to the mutual exchange of momentum between the gas and the particles. Photo 2-1 shows the jet mill with the top plate removed.
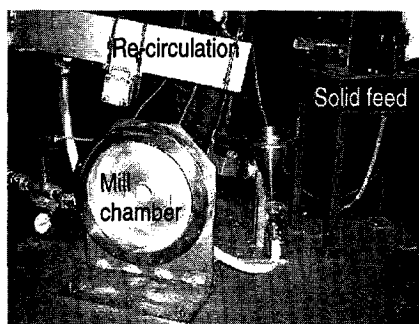
Photo 2-1: 10-inch spiral jet mill used in pilot plant at TU Delft.

Mill chamber: In the centre of the spiral jet mill classification takes place where centrifugal and drag forces are acting on the particles. Smaller particles are relatively more sensitive to the drag forces and are dragged to the central mill outlet. A cylinder in the outlet can be positioned to adjust the outlet height. Larger particles, being relatively heavier, are sent back to the outer zone of the chamber for further grinding.

Table 2-1 Specifications of the 10" and 6" jet mill. Measures in mm.

Model	D_m	H_m	d_i	r_i	d_o	h_0	# [-]	d_n	δ_n
6"	101.6	15	1.5	...	37.0	6	6		70°
10"	254.0	25.0	3.0	102.0	60.3	14.0	4; 8	2.0; 2.5	71°, 80°
24"	609.4	3.0; 5.0	?		150.0	25.0	12	5.55	

Nozzles: Different nozzles configurations used during pilot plant experiments, of which the specifications are listed in Table 2-2. These nozzles sets, placed equidistantly in the periphery of the mill chamber, could vary in number, diameter and injection angle.
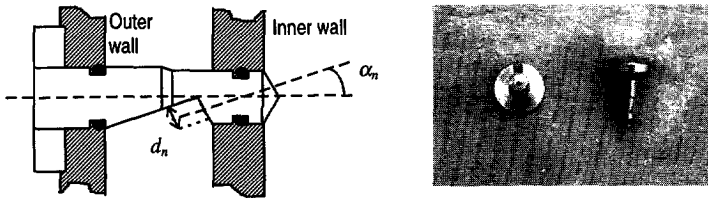
Figure 2-3 Geometry of a nozzle as used in 10-inch spiral jet mill.

The nozzles used during experiments were of the abrupt type, as shown in Figure 2-3. An alternative could have been the use of Laval shaped nozzles, which in principle allowed super sonic velocities in the expansion zone. However, with the large particle concentration present in the vicinity of the nozzle outlet the jets never achieve their full velocity. Furthermore, depending on the operating pressure a specific nozzle shape is required. Benefits are relatively low, production cost are high and flexibility is low. For Laval nozzle design rules one is referred to work of VISWANATHAN and RUMPF.

MUSCHELKNAUTZ reported that the optimal angle was around 30 degrees. For plastics it appeared to be the same [Smi86]. For combination with the external classifier nozzle sets with smaller angle have been used.

Table 2-2: Nozzle sets for 10" Wedco mill

Set no.	d_{nozzle}	a_{nozzle}	N_{nozzle}
1	2.0	20.0	8
2	2.0	20.0	4
3	2.5	20.0	8
4	2.5	20.0	4
5	2.5	10.0	8
6	2.5	10.0	4

Action in a solid feed injector: An solid injector, shown in Figure 2-4, was mounted on the top plate of the mill chamber. The feed solids were dropped in the injector cone and pushed into the mill chamber by high pressure air supplied to the injector nozzle.

The size of the feed particles can be up to 10 millimetres. Pilot plant experiments were generally done with granulate or flakes with an average size of 3 to 5 millimetres.
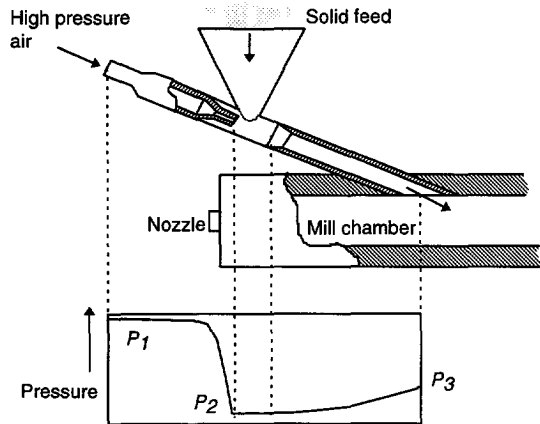
Figure 2-4 Principle of the solid feed injector mounted on a spiral jet mill.

In case that the injector pressure was too low the mill contents was blown back. Especially when grinding very fine feed material this occurred easily. A high injector pressure could overcome this problem. However, more injector air caused a stronger disturbance of the vortex flow which had a negative effect on the internal classification of the mill. Therefore it is preferable to restrict the ejector pressure and tune it to the minimum level. Literature reported that the amount of false air is about 20 to 30 percent of the injector air, depending on the material and scale of the mill [CHELLAPAN, MUSCHELKNAUTZ]. In smaller scale jet mills relatively more false air was taken in. In the test plant the amount of pushing air brought in by the solids feed injector was approximately 30 normal cubic meters per hour.

2.2.2 Free vortex classifier

In a closed circuit configuration of the spiral jet mill plant the recirculation of product was performed by a free vortex air classifier mounted on the mill outlet (see Figure 2-5). The exhausted grinding air conveying the dispersed mill product entered the cylindrical section tangentially, generating a free vortex. Coarse particles deposited on the walls of the body and moved downwards to the under outlet. Fines were dragged to the fines outlet. At several points in the classifier body extra air flows were added to adjust the performance of the classifier.
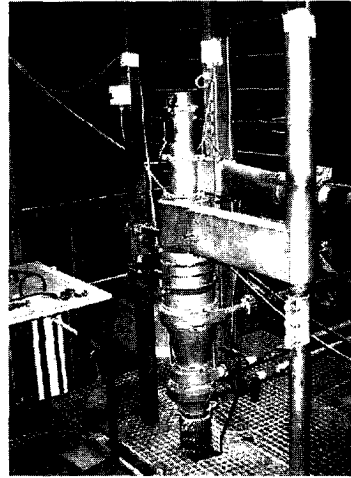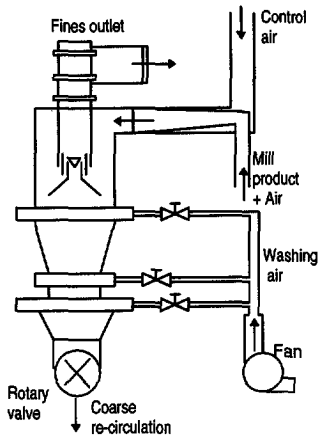
Figure 2-5: The LaCAD Oy free vortex air classifier.

The control air enters the classifier parallel with the dispersed product stream. Depending on the level of negative pressure, created by the fan, an extra air flow was taken in, enforcing the vortex flow. In the lower section washing air is blown in by a separate blower. This air is used for redispersion and entrainment of fine particles back to the fines stream in the upper section.

The particles that are carried downwards, are re-dispersed by three flows of washing air. By adjusting the amount of washing air the cut point and the sharpness of separation can be adjusted. The position of the cone and a cylinder could be adjusted so that a desired flow between the two sections of the classifier was achieved. The cone separated the upper and lower section of the classifier. In the lowest position of the cylinder the upper part of the vortex finder is totally closed.

A rotary valve is used on the coarse side of the classifier to maintain a negative pressure in the system after the mill when operating with the closed loop configuration.

Remark: Though the free vortex classifier will not give a precise size control as a forced vortex classifier, the absence of moving parts, combined well with the concept of spiral jet mills.

2.3 Distributed control system

2.3.1 Functional lay out

This section describes the control system as it was installed on the jet mill pilot plant. The process computer was connected by RS485 digital lines to controllers, actuators and sensors in the plant. The functional lay out of the control system is shown in Figure 2-6.
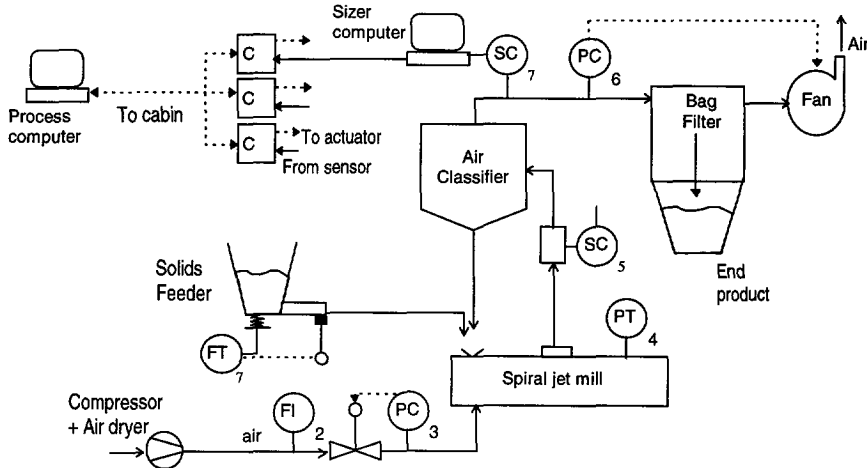
Figure 2-6 Functional lay out of distributed control system.

The control and acquisition package ETP was installed on the process computer for the downloading and setting of the parameters of the local controllers as well as the logging of the sensors in the pilot plant. Software routines were implemented for the automatic start-up/shut-down and the data handling of the system.

The grinding plant could be remotely operated from a separate cabin, which was convenient as jet mills produce much noise and the danger of dust explosions exists. The automated mill plant also improved the reproducibility of the test runs.

Control loop PC$_3$ kept the pressure on the nozzles at the desired setpoint by adjusting a valve. The feed hopper was placed on a load sensitive resistance to monitor the feedrate. Control loop FC$_7$ adjusted the screw speed of the solid feed unit. The pressure sensor in the inlet of the bag filter was connected to UC$_6$ which kept the pressure level constant by adjusting the fan speed. PT$_4$ measured the pressure level in the mill chamber.

The real-time particle size instrument was connected to the sizer computer which continuously stored the size data. This computer also transmitted a signal through an

analogue PC output card to the controller SC_5. This signal was related to a specific aspect of the particle size distribution, which could be selected in the software.

2.3.2 Sensors and actuators

<u>Pressure transmitter</u>: In the grinding plant a number of pressure transmitters is installed. On places where the product flow is in contact with the sensor a flat membrane process connection is used. A pressure transmitter (1-10 bar, E&H) was mounted on the top plate of the mill to measure the static pressure level in the chamber. In order to avoid abrasion a ceramic process connection was used (see Photo 2-2).

Photo 2-2: Pressure sensor with flat process connection

<u>Vortex flow meter</u>: A vortex flow transmitter (FT_2) was used to monitor the amount of air supplied to the nozzles. The measuring principle of this sensor (E&H Swingwirl II, DN25) is based on vortex shedding which occurs when a fluid flows around a delta shaped obstruction. Figure 2-7 shows the Von Karman vortices after the cone inside the probe.
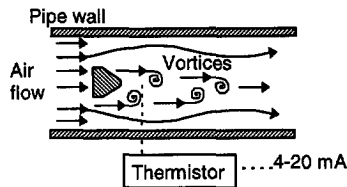
Figure 2-7 Principle of vortex flow-meter

The pressure pulses from the vortices were causing a small sensor deflection in the flow meter's body. This shedding is sensed by thermistors. The frequency (f_k) was determined by

$$f_k = \frac{K \cdot \Phi_l}{3.6} \hspace{4cm} (2.1)$$

where K is the calibration factor. The measured frequency was transformed to a current output signal that is linear to the actual air volume flow (Φ_l) under local

pressure conditions. For a conversion to normal cubic meters this flow had to be multiplied by the local pressure, assuming ideal gas behaviour. The calibration was verified with the formulas for isentropic air flow through the nozzle [RUMPF].

$$\Phi_{air} = 143 \cdot d_n^2 \cdot N_n \cdot P_n \tag{2.2}$$

Particle sizing sensor: An on-line particle size measurement system was used on the grinding plant and connected to the DCS. This instrument based on laser diffraction will be described in Chapter 3 'On-line particle size measurements'.

2.3.3 Actuators

Valve for grinding air: The air supply to the mill was adjusted by an air-to-open type of control valve in control loop PC_3.

$$\Phi_{air,N} = 514 \cdot K_v \cdot f \sqrt{\frac{\Delta p \cdot p_2}{\rho_N \cdot T_1}} \tag{2.3}$$

The valve characteristic is given by equation 2.3 in which f is the relative valve stroke, a value between 0 (closed) and 1 (opened).

Speed controllers: An invertor was used to adjust the speed of the fan to keep the grinding plant at a negative pressure. A lower pressure caused more washing air to be taken in by an extra air classifier inlet. In this way the operation the classifier could be manipulated. A second speed controller was used to adjust the solid feedrate.

2.4 Auxiliaries

In a jet mill plant the air flow is both the transport medium as the energy carrier. Figure 2-8 depicts the air supply system to which the fluid energy mill was connected.
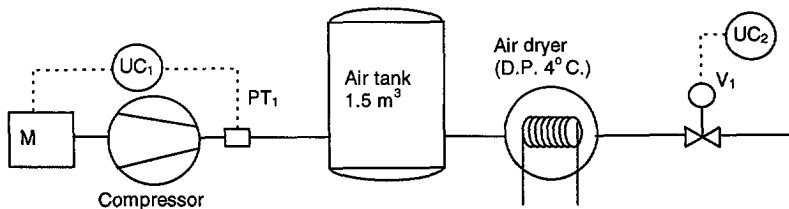
Figure 2-8 High pressure air supply.

2.4.1 Compressor

The high pressure air was generated by a 30 kilowatt screw compressor, Atlas Copco GA30 pack, with a maximum capacity of 300 normal cubic meters per hour at a pressure of 7.5 bar. The compressor operates at a constant speed. The on/off controller, UC_1 ,caused the air pressure to fluctuate between an upper and a lower limit. A 1000 litre air tank was installed in order to minimise these pressure fluctuations. In this way the air flow was generally constant through each stage of the system.

2.4.2 Air dryer

The compressed air was dried to assure air supply of constant quality. This was desirable for further processes/storage (agglomeration, moisture) and for reproducibility of the experiments. The air dryer used in the plant was an Atlas Copco FD100 operated at a dew point of 4°C. At this temperature water was removed from the airflow. Before leaving the dryer the grinding air was reheated to 20°C.

2.4.3 Solid feed unit

Fluctuations of the solid feedrate affect the mill performance and therefore during the experiments the particle flow had to be hold as smooth as possible. It was desirable to select a feeder which could deliver a constant solid feed. The pilot plant was equipped with a screw feeder with three sets of screws for the different operating ranges. The solid feed was stored in a hopper. The feed unit is shown on Photo 2-3.

screw set	Range of flowrate
type 1	0.4-16 [kg/hr]
type 2	1.0 - 45 [kg/hr]
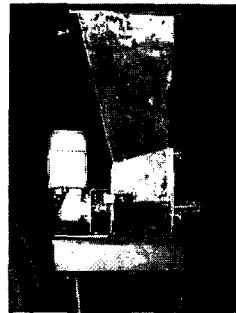
Photo 2-3: Screw feeder and hopper (Gericke GLD175)

Two types of feed control systems can be distinguished, namely volumetric feeding and gravimetric feeding. In a gravimetric feed system, also called loss-in-weight, the feedrate is based on the massflow of the feed leaving the hopper. Though this method is more flexible, the response time of this feed control is longer due to the required integration time [ALLENBERG].

For the jet mill experiments volumetric control was used. In this case a direct relation between the mass flow and the screw speed had to be determined by calibration for each new test material. Over each time span the derivative of the hopper mass was calculated to obtain the calibration curve.

2.4.4 End product collection
The end product is collected by a bag house, DCE 104, 10 bags with a total surface area of 10 m², as shown in Figure 2-9. The bags were cleaned by pneumatic pulses. The bag house was kept at a negative pressure by the fan. In the course of an experiment the filter blocked causing a pressure drop. The pressure at the filter inlet was maintained at a desired level by the controller UC_3 to exclude effects on the rest of the system.
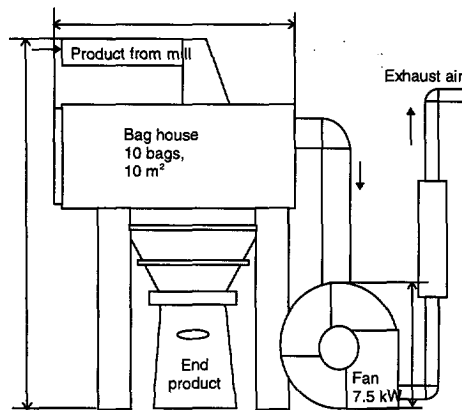
Figure 2-9 Bag filter with constant inlet pressure.

Normally the air entering the injector generates a significant level of noise. To counteract this, the mill has been designed with effective silencer. The bag house has an explosion relief plate installed to vent to the outside.

2.5 The opposed jet mill plant

Part of the experimental program was performed at an opposed jet mill which was part of an industrial plant. The general lay-out of this plant was similar to the one described earlier in this chapter.

The opposed jet mill is depicted in Figure 2-10. The mill body is constructed as a cylinder. The lower section contains three opposed nozzles. Particles in the vicinity of the jets are entrained and accelerated towards the intersection point of the jet streams. In this section most of the grinding takes place. The expanded air fluidizes the product to the top section where a forced vortex classifier rotor is mounted.
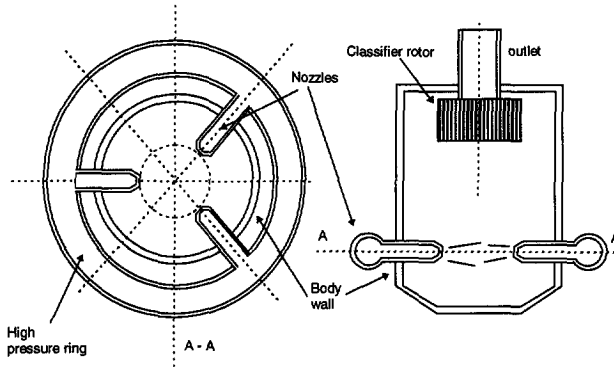
Figure 2-10 Dimensions of the opposed jet mill.

In the top section of opposed jet mill a classifier wheel is placed. All air entering the house, mill chamber will leave the AFG mill through the rotor blades. The upward gas flow conveys the ground particles into the classifier section. The classification of the particles occurs in a centrifugal field produced by the upper rotor. By changing the rotor speed the product top size can be varied. The air flow carries particles that are fine enough to pass the centrifugal field through the rotor. The coarse rejects are returned to the grinding chamber. A forced vortex classifier is integrated in the upper section and forms the classification section. The particle mixture enters the forced vortex force field generated by the rotating vanes of the classifier. The forced vortex force field will impede the larger fraction of the mill product to exit the mill. Coarse particles that do not pass the classifier are rejected to the grinding zone. Where they are accelerated by the opposed jet. Thus creating a fluidised bed that influences the amount of particle entrained into the gas jet. For a more complete description of the AFG mill one is referred to the work of VOGEL [1991].

The coarser particles can not enter the blades of the classifier and are rejected to the grinding zone where they undergo further size reduction.

Solids are brought into the mill chamber by a screw feeder. A rotary valve serves as a pressure lock. The end product is collected in a bag filter.

Table 2: *Tested jet mills*

Model AFG	200	400	630
d_n (mm)	2x4+1x5	3x8	4x11
D_r (mm)	100	200	315

List of symbols

d	diameter	[mm]
D	diameter	[mm]
f	frequency	[1/s]
K	constant	[-]
N	number	[#]
p	pressure	[bar]
r	radius	[mm]
T	temperature	[°C]

Greek

α	nozzle angle	[°]
δ	complement of α	[°]
Φ	flowrate	[m³/s]
η	viscosity	[Pa.s]
ρ	density	[kg/m³]

Indices

n	nozzle
N	normal conditions
v	valve
r	rotor

Abbreviations

C	controller
F	flow
I	indicator
P	pressure
X	general name instrument
T	transmitter

Literature

Allenberg, B., Requirements on a Continuous Weigher in a Quality Assurance System, *Bulk Solids Handling,* 13,2, 314-318, 1987

Bates, L., Feeding of particulate solids, *RELPOWFLO II,* 587-614, 1993

Butler M.E., How to facilitate start up, *Chemical Engineering,* June, 82-92, 1993

Chellapan, S., Ramaigan, G., Gas solid injector, Experimental Study of design parameters of a gas-solid injector feeder, *Powder Technology,* 48, 141-144, 1986

Darling, C.S., Industrial grinding and reduction plant, *Mechanical world monographs 53,* 1949

E+H, Granuflow gmr130 microwave flow indicator, *brochure im 008g/01e/09.94,* 1994

Eckhoff, R.K., Prevention and Mitigation of Dust Explosions in the Process Industry State of the Art, *REPOWFLO II, Oslo 1993,* 801, 1993

Fahlenbock, T., The principles of dynamic weighing applied to chemical feeding equipment of the loss-in-weight type, *12th annual Powder and Bulk Solids Conference 1987,* 147-158, 1987

Gühne, H.P., Prinzip und betriebsergebnisse einer gegenstromprallmuhle, *verfahrenstechnik,* 14 no. 5, 326-329, 1980

Moersky, P., Klemetti, M., Knuutinen, T., Kalapudas, R., Koivistoinen, P., The development of laboratory testing for autogenous grinding, *Int. J. Miner. Process.,* 44-45, 261-271, 1996

Mular, A. L.; Jull, Norman A., The selection of cyclone classifiers, pumps and pump boxes for grinding circuits, *Miner. Process. Plant Des., [Symp.],* 376-403, 1978

Nayar, M.P., Wheeler, M.E., Butler, M.E., How to facilitate start-up, *chem.eng,* 82, 1993

Nimmo I., Start up plants safely, *Chemical Engineering Progress,* December, 66-69, 1993

Ridder-Van den Berg S., Gevaar voor Stofexplosies Voortdurend Onderschat, *Poly Technisch tijdschrift,* 4, 32-34, 1993

Vogel, A., The Alpine fluidized bed opposed jet mill a case history, *Powder handling and processing,* 3, no.2, 129-132, 1991

Wayne, E., Frey, A., The Complete (Grinding) System, *Short course on size reduction and classification, A'dam (Hand out),* 1990

Viswanathan, K., Jet-mill design-a complete method, *Bulk Solids Handling,* 7-4, 585-593, 1987

Chapter 3

Real-time particle size measurements

Paragraph 3.1 discusses particle size analysis methods currently used in process industry and the need for real-time measurements. Furthermore, definitions of particle size and shape, as well as the statistical basis for particle size distributions are given. Paragraph 3.2 describes the working principles of two optical particle sensors used in this project, one based on laser light and the other based on incoherent light. Paragraph 3.4 deals with the sampling of powder flows and the design of an in-line sampling cell for the jet mill. Paragraph 3.5 discusses the numerical treatment of scatter signals. The chapter concludes with a performance test of the light scattering instruments used in this project.

3.1 Introduction

3.1.1 The motivation for real-time size measurements

Improvements in process measuring and control are commonly driven by traditional goals of safety, cost control and last but not least the product quality. Enhancement of process efficiency and control of product specification created a demand for real-time particle size measurements at the production site. The advantages of real-time measurements over off-line analysis carried out in a quality assurance laboratory are several:

1. Direct correlation between grinding conditions, powder properties and product quality. No time delay between sampling and analysis. Process conditions stored in a database can serve as a tool for system analysis. Traceability of disturbances can lead to process improvements and better customer support.

2. Real-time measurements can be used as a feedback signal to a central control system that automatically adjusts the operating set-points when necessary [CRAIG].

3. Better statistical basis for quality analysis as a result of the larger number of measurements that are continuously taken from a moving product flow. Further advantages are the exclusion of operator effects and segregation problems on sampling [HEIDENREICH].

Despite these advantages on-line particle size measurements are not widely applied in the process industries, unlike pressure, pH or flow measurements. Probably this is partly due to the lack of expertise to install and maintain the sizing instruments on the plant. Above that most of these devices were originally developed for laboratory application with user friendly software and sophisticated features. All this made them too expensive and complicated to implement in an industrial environment. HEISKANEN [1995] discussed the difficulties of implementing size analysis sensors in particulate processes.

3.1.2 Requirements to the sizing sensor in a jet mill plant

HEYWOOD [1947] stated that particle size analysis is not an objective in itself, but a means to correlate powder properties with some process of manufacture, usage or preparation. The requirement for on-line instruments is how to organise the transmission of the measured signals to the process control computer without requiring the interference of an operator for continuous cleaning and calibration. Further requirements for installation in a grinding plant are:

1. Robust and compact housing that is explosion proof (10 bar) and can withstand operating temperatures up to 50 degrees Celsius and is not sensitive to vibrations.

2. Real-time data acquisition, numerical processing and transmission of the measured signal to the digital control system of the grinding plant.

3. Ability to detect process changes that are related to the aspects of the PSD that are to be controlled. Or providing additional/complementary information in combination with another sensor. Absolute accuracy of the signal is not essential.

4. Proper sampling conditions: Fine particles, in the range from 1 to 100 microns, dispersed in a high velocity air flow (>25 m/s) pass through the cell. The solid concentration lies around 0.1 - 1 volume percent. The outlet diameter of a jet mill can vary from 30 for a pilot plant model to 250 millimetre for industrial scale mills.

5. Instrumentation cost that are lower than 20% of total installed equipment cost.

3.1.3 Particle size distribution

In the chemical industry powders with all kinds of properties are processed. The final application or the next process step demand a specific behaviour of the powder [RALPH]. For example, the diameter based on equivalent area can be a relevant variable in defining the quality of paints or pigments. Reaction rates change with the specific surface of the powder, while the suspension of particles in water is dependent on the Stokes diameter.

Graphical representation: A powder consists of a collection of particles with different sizes and shapes. The particle size distribution (abbr. PSD) describes the spectrum of sizes in a powder sample. Two commonly used ways to represent the PSD are the density distribution and cumulative undersize distribution. Figure 3-1 shows a typical size distribution of an industrial powder, which is usually considered to be a continuous curve.
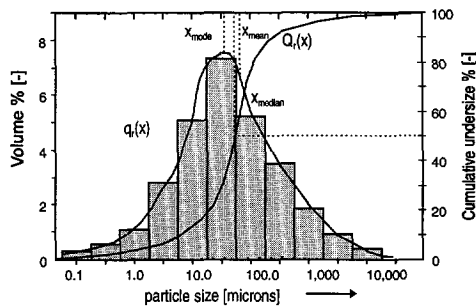
Figure 3-1 Particle size density q(x) on the left-hand axis and cumulative under-size Q(x) on the right-hand axis expressing the PSD of a powder.

Density distribution: The particle size density distribution $q(x)$ of a powder expresses the amount of material present in each size class related to the amount of total sample.

Cumulative distribution: The cumulative undersize distribution $Q(x)$ describes the volume percentage of the powder that is finer than a specified size. This is the intergral of $q(x)$ and is represented by the S-shaped curve in Figure 3-1 which corresponds with the right-hand axis. The use of these curves is common in industrial practice as product specifications can easily and fast be compared.

Discrete size vector: In practice it is convenient to depict PSD curves as a histogram. Traditionally used sieves produced discretised results as do many of the modern devices, such as electrical resistance, light scattering or ultrasound instruments, due to numerical processing. Finally, for modelling purposes it is often convenient to work

with particle size distributions that are represented by discrete vectors of restricted length.

Basis of the distribution: A physical property has to be chosen to characterise the size of particles. In Figure 3-2 particle size distributions $q_n(x)$ as fractions of the total sample are presented on different bases in terms of equivalent spheres. The PSD is called to be volume based ($n=3$) when it is expressed as the volume of particles present in each size class. When the surface area is of interest the PSD can be based on surface area per size class ($n=2$). The number of particles per size class is given by the number density ($n=0$).

In the case of attrition the number of fines produced is very large, whilst the volume of these fractions will be low. With respect to thermodynamics it is interesting to look at the newly created surface area. Since in the population balance model the mass balances during the grinding process are to be solved for each size class (Chapter 7 "Modelling") the volume diameter is most appropriate. So depending on the application a specific basis has to be chosen.
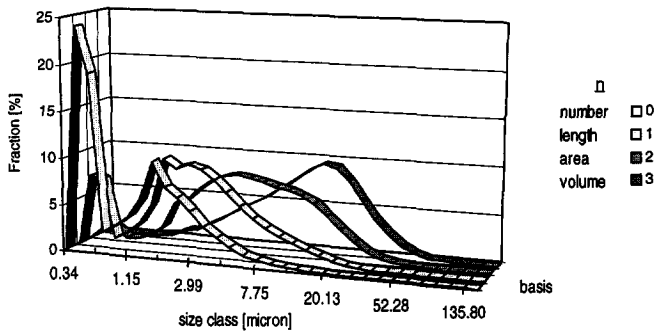
Figure 3-2 Representation of a particle size distribution $q_n(x)$ the PSD on different bases: volume $q_3(x)$, area $q_2(x)$, length $q_1(x)$, number $q_0(x)$.

Moments: The moments are in fact the average values of these distributions. The general expression for the kth moment m with basis n is

$$m_{k,n} = \int_{x_{min}}^{x_{max}} x^k \cdot q_n(x)dx \qquad (3.1)$$

The modal size, x_{modal}, is the particle size at which the $q_n(x)$ shows a maximum as can be seen in Figure 3-1.

The median size, x_{50}, is the 50%-value, while the mean size, x_{mean} is defined as

$$x_{mean} = \frac{m_{1,n}}{m_{0,n}} \tag{3.2}$$

Effect of milling method on PSD: Figure 3-3 shows the comparison of a sample of conductive carbon which was ground in a ball mill and in a jet mill. In both cases the end product had the same median size of 7.4 microns. If the fines are the desired product, as for light scattering by pigments, the jet mill product is superior. For particle packing as with ceramics, a maximum density is required. This can best be achieved with the ball milled product.
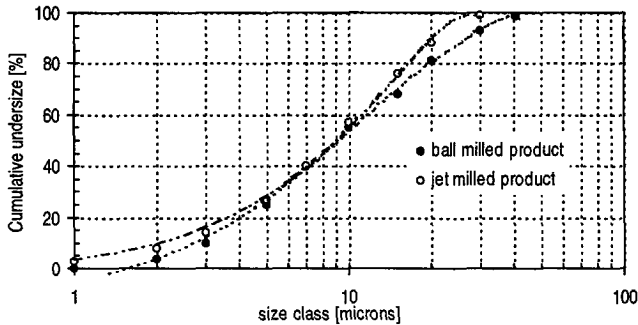
Figure 3-3 Cumulative undersize distributions of ground conductive carbon ground on two different mills. Measured with laser diffraction.

The use of different instruments: As mentioned earlier, powders are produced for a variety of applications. For each aspect related to particle size the choice of a certain particle size representation and a proper measurement technique depends on the process variable of interest. An alternative is the use of calibration factors to interpret results obtained with different sizing instruments.

3.1.4 Particle shape

Grinding machine induced shape bias: Up till this section the criterion for particle characterisation has just been size, assuming that all particles are equivalent spheres. During a grinding process not only is the particle size reduced, but often the shape of the particles also changes. Photo 3-1 (A) shows pre-treated test material CW ground on a coffee mill. The end product is much finer with a narrow distribution. Also the particles are more spherical due to attrition.

A   B
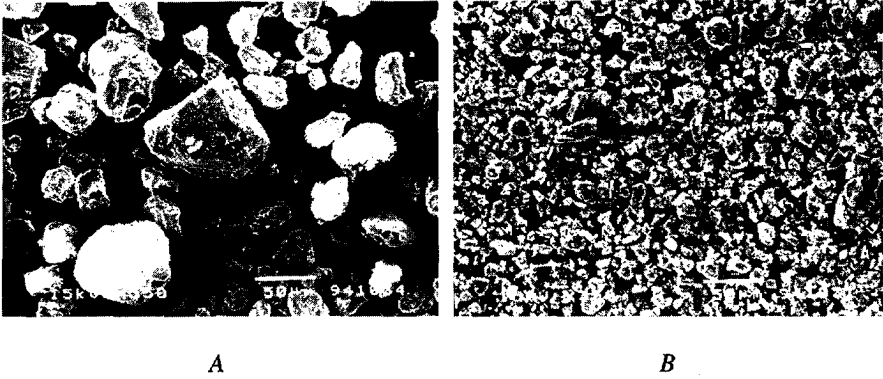
Photo 3-1: Test material CW ground on a coffee mill (A) and on a jet mill (B).

Instrument effects on PSD curve: Practically all size instruments show a difference while measuring the PSD of irregular shaped particles as they are based on different physical concepts that are described in Paragraph 3.1.5. The PSD-curves, commonly represented as a two-dimensional plot have a shortcoming. For a conversion between particle size distributions measured with different instruments, additional information is required about the shape of the particles over the size range and what the shape biases are of each specific instrument. This is illustrated in Figure 3-4.
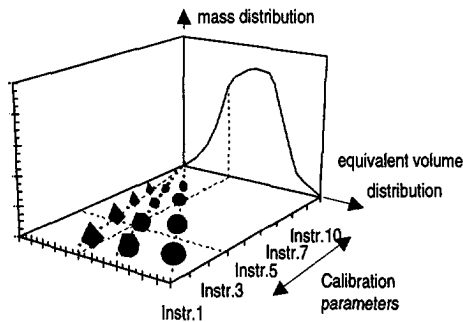
Figure 3-4 Conversion of size distributions measured on different instruments.

Shape factors: A particle can only be completely described by a single geometric variable, which contains full information about the surface and the volume, if it is a sphere or a regular polyhedron. However, in the case of irregular shaped particles, it is not possible to the identify the complete geometry by a single parameter. In this case the description of a particle shape requires a geometric recording of the surface as a function of two variables. This is not practical in industrial practice and therefore a number of single variable shape factors are commonly used as a simplified alternative [HOUNSLOW].

Aspect ratio is the largest linear dimension of the particle divided by the smallest linear dimension. In formula: $AR = l_{max}/l_{min}$. The *sphericity* (Ψ) is defined by WADELL as the surface area of volume-equivalent sphere (A_{sphere}) divided by the surface area of the particle (A_*). Or $\Psi = A_{sphere}/A_*$. HEYWOOD proposed a *volumetric shape factor*, which is the ratio between volume of that particle V and the surface equivalent diameter x_a to the power three. $k = V_*/x_a^3$.

Many attempts have been made do find general descriptions of particle geometries. KAYE and MELOT used fractals and other mathematical techniques for this purpose. HEFFELS derived some sort of optical shape factor by interpreting non-concentric diffraction patterns.

3.1.5 Particle size instruments

<u>Working principles</u>: A wide variety of particle sizing devices, ranging from sieves to particle imaging with CCD cameras, are available on the market for the measurement of the PSD for both suspended and dispersed particles. ALLEN gave an overview of different sizing methods. Figure 3-5 lists the different particle size instruments together with the related quantities which are determined with a specific measuring techniques. Basically four groups exist as indicated in the scheme. There is a tendency from the measurement of geometrical properties (group 1) towards physical quantities that are indirectly related to the particle size (group 2, 3 and 4). Models and numerical processing to calculate a PSD out of measured signals are becoming more complex which makes the role of the software equally important as the hardware.

GROUP	RELATED QUANTITY	SENSOR MODEL	PARTICLE GEOMETRY	BASIS OF PSD
1. Sieve / Hegmann wedge	grid width / Wedge depth			Mass / Number
2. Andreasen's pipet / Aerosizer / Centrifuge / Electrical zone	Settling time / Time of flight / Trajectory / Resistance	Direct Model	St-diameter / St-diameter / St-diameter / volume	Cum.Mass / Number / Mass / Number
3. Light scattering / Acoustic device	Scatter pattern / Extintion	Model & Inversion	Projected area / idem	Volume/Area / Volume
4. CCD camera	2D image	Imaging	Shape/size	Flexible

Figure 3-5 Size measurement techniques and their signal processing.

The first group contains instruments that are traditionally used in the mineral and paint industries such as sieves and Hegmann wedges. Normal sieves measure down to about 70 microns, while air swept screens are able to sieve till about 40 microns. The procedures are well documented in DIN, ISO and ASTM standards. The analysis is laborious and difficult to automate. The small amount of product sampling and the delay time before analysis make the result less useful. An advantage is the direct and absolute determination of some geometrical properties of the particles as the particle size is directly related to the measured quantity.

The second group is characterised by a direct relationship between the measured signal and the particle size distribution that is reconstructed by a one-to-one model. The determination of the settling time (Andreasen's Pipette), the time of flight (Aerosizer) and the electrical resistance (Coulter Counter) of each individual particle can be used to characterise the PSD of a powder. Though the related quantities (measuring signals) do not have a geometric basis, there exists a direct and unique relationship between the equivalent behavioural sphere and the signal.

The third group of instruments is characterised by an optimisation or deconvolution problem. Examples are the acoustic instruments for suspended solids and the light scattering instruments for both wet and dry media. The algorithms implemented in sophisticated instrument software convert the measured signals, light intensities under scatter angles or sound extinction, into a corresponding size distribution by means of deconvolution methods. The back-calculation is not unique and a-priori knowledge has to be added to stabilise and converge to a realistic solution. Analysis of the individual instruments shows good reproducibility, but the results on different instruments shows deviations, especially in the extremes of the PSD. Furthermore these methods require calibration. As a result of the numerical processing of data these methods are easier to automate and to be used on-line in a distributed control system.

Technical developments have made CCD camera's more compact and cheaper, with higher resolution. Faster computers allow on-line image processing which gives both size and shape information about individual particles in the product flow [BEYERS]. An in-line imaging probe is manufactured by Lasentec [BECKER] which can be used as a monitoring system for the particle geometry or contamination level in industrial processes.

Compatibility of size measurements: Though the software interfaces might suggest conversion between particle sizes determined with different methods to be possible, the reliability is poor. Each method has its own specific resolution, statistical errors,

sampling errors and model imperfections. Reliable information can be obtained by combining a process model with the measurement techniques.

3.2 Optical particle sizing

3.2.1 Working principle

Of the sizing instruments discussed in the previous section the optical devices were found to be the most suitable for on-line measurements in the jet mill plant. The product stream that leaves the mill is well dispersed and is optically accessible. In this project three different instruments based on light scattering were used for on-line measurements in the grinding plant. The Malvern MSX and the Insitec EPCS have a laser beam inside, while the Jena PSI contains a halogen lamp.

These instruments make use of visible light, which is in fact electromagnetic radiation with a wavelength λ lying between about 400 (violet) and 700 (red) nanometers. Figure 3-6 schematically shows the four major phenomena which occur when light is incident on a particle. A fraction of the light is diffracted around the edges of the particle in the near-forward direction. Part of the light is reflected from the particle surface. Finally, some of the light is refracted into the particle and partially absorbed and transformed into other forms of energy. The remainder leaves the particle as emergent rays.
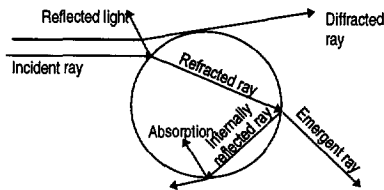
Figure 3-6 Beam of light hitting a particle. After HULST.

3.2.2 Laser diffraction instruments used in the project

<u>Malvern MSX</u>: The MasterSizer, MSX, shown in Figure 3-7 was used for the real-time measurements, though it is actually an instrument intended for laboratory use. An in-line sampling cell that could be mounted directly on the jet mill outlet was designed and built for use with this instrument. The MSX was interfaced with the monitoring and the control system of the grinding plant by protocols that were written in SizerBasic, a programming language delivered with the instrument. This software allowed a flexible handling and processing of the measured data which was found convenient for research purposes.
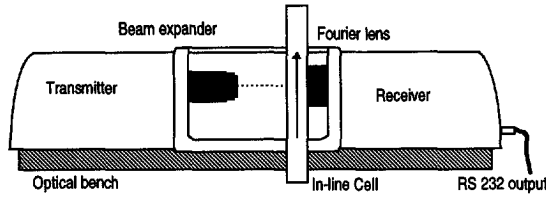
Figure 3-7 Laser diffraction instrument Malvern MSX.

Insitec EPCS: The optical components and electronics of the EPCS, Ensemble Particle Concentration Size, are built into a robust probe that was especially designed for use in an industrial environment. Figure 3-8 shows the on-line version which was used on the industrial plant as the large pipe diameter did not allow in-line sampling. In this case a part of the product stream was withdrawn from the main flow and lead through the probe.
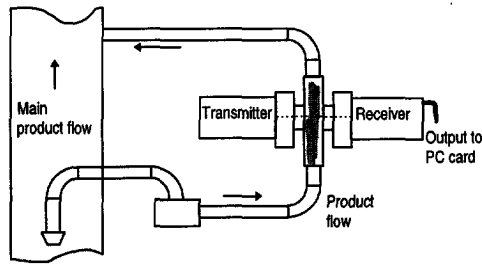
Figure 3-8 Installation of Insitec probe on mill outlet.

The Malvern MSX and the Insitec are both laser diffraction instruments which have a similar optical configuration as shown in Figure 3-9.
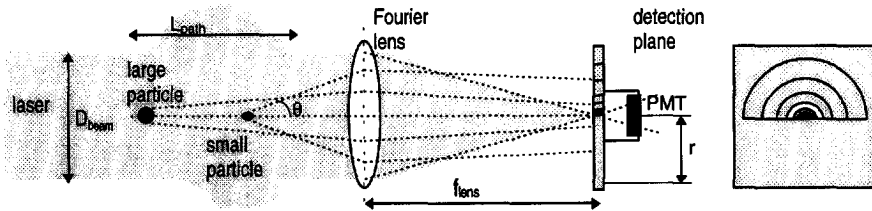
Figure 3-9 Optical lay-out of laser diffraction instruments.

A low power Helium-Neon laser (λ=632.8nm) forms a collimated and monochromatic beam. A collective of particles is introduced into the laser beam in the sampling volume. A Fourier lens projects the far field diffraction pattern of the scattered light at the focal plane. This optical configuration has the characteristic that a moving particle at any position in the laser beam always causes a stationary light intensity pattern that

is centred on the optical axis. The diffraction pattern is collected by a multi-element detector along the radial direction, r, of the focal plane. By means of a scatter model, discussed in paragraph 3.3, and a numerical optimisation technique, see paragraph 3.5, the particle size distribution can be back calculated.

The unscattered light passes through a pinhole in the detection plane and is measured by a photo multiplier, PMT. This signal is monitored to determine the sample volume concentration by applying BEER-LAMBERT'S law, dealt with in paragraph 3.3.2.

3.2.3 Incoherent light scatter instrument

Jena PSI: As a robust and low cost alternative to the laser diffraction instruments discussed in the previous section, the principle of diffraction by incoherent light was tested. The PSI, Particle Size Inspection, uses a halogen lamp as a light source that illuminates the mask. The optical configuration, shown in Figure 3-10, projects the mask onto a plane. A single photo multiplier collects the light that passed the pinhole in the centre of the plane. The multi-channel programmable LCD mask determins the integration zone in the diffraction pattern based on incoherent space-frequency analysis [THORWIRTH].
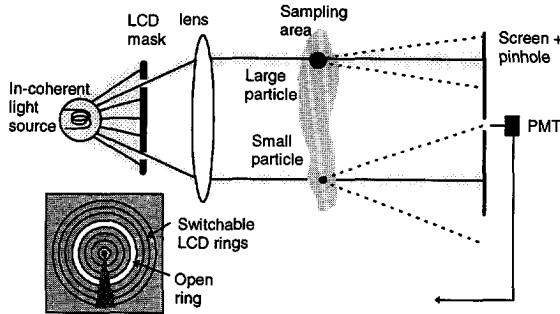
Figure 3-10 Set-up of light scattering device using an incoherent light source

The light incident on a particle present in the sampling zone is scattered and projected on the image plane creating an AIRY pattern centred around the pinholes. The numerous incoherent point sources in the mask- plane cause a superimposed intensity pattern. During a measurement sweep the light sensitive detector behind the pinhole records the sum of the intensities in the diffraction pattern as if all Airy patterns are centred around the optical axis [HEFFELS]. Figure 3-10 shows the LCD mask that consisted of 31 switchable rings. By sequentially making a specific ring in the mask plane transparent, the signals of a ring shaped multi-element detector in a coherent set-up, as described in the previous section.

The combination of a single detector with a halogen light source makes this instrument attractive. Since the development cost of a liquid crystal based programmable mask is relatively low compared to a photo detector array, it is possible to design a dedicated robust instrument for the size classes required in the specific industrial application. Disadvantages of this method are the facts that the sequential signal acquisition makes the instrument slower and the instant correlation of raw detector data (see paragraph 3.6.5) is not possible.

3.3 Scatter models

3.3.1 Calculation of particle size distribution

<u>Definition of parameters</u>: A scattering function defines how the incident light intensity with wavelength λ is distributed as a function of the scattering angle θ for each particle size x. The angle θ is measured from the direction of the incident beam to the scattered beam. In the ideal case of one single particle with a known geometry and optical properties, the scatter pattern can be predicted from theory. The main parameters in the model are:

1. Dimensionless size parameter $\alpha = \frac{\pi x}{\lambda}$. This is the ratio of the particle size (x) to the wavelength of the incident light.

2. The wave number, k, which is the reciprocal of the wavelength. $k = 2\pi / \lambda$.

3. The optical behaviour of both the particle and its surrounding medium are expressed by the relative refractive index $m = n_{real} - in_{imaginary}$.

<u>Scatter theories</u>: The general theory of light scattering by transparent particles was originally developed by MIE. The FRAUNHOFER approximation assumes that scattering is independent of the relative refractive index, which means that measurements do not require knowledge of the material or medium optical properties. The scattering is mainly caused by the diffraction of light around the particle. This makes the Fraunhofer theory only valid for a limited range of the scattering angle θ, the relative refractive index m and the size parameter α. For the calculation of the PSD the following assumptions were made:

1. Light does not pass through the particle itself. Light that falls onto the particle is absorbed and can be ignored.

2. Particles are assumed to be spherical.

These assumptions imply that the application of the Fraunhofer theory is restricted to sufficiently large particles with diameter d compared to the wavelength λ of the laser. According to VAN DE HULST the size of the particle and its refractive index must be such as $2\alpha(m-1) >> 30$. For powders measured in air this means that below 3 microns errors in the calculated PSD with the Fraunhofer theory can be significant. In this project the Fraunhofer approximation was used to describe the scatter properties of the mill product.

The Fraunhofer model: The diffraction pattern resulting from a uniformly illuminated spherical particle consists of a central bright region, known as the Airy Disc, surrounded by a number of fainter rings as was illustrated in Figure 3-11. Each ring is separated by a circle of zero intensity.
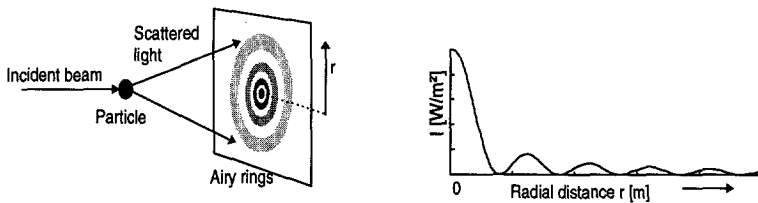
Figure 3-11 Projection of an Airy pattern on the measuring plan (left). Shape of a BESSEL function (right).

The irradiance intensity distribution of this pattern $I(\theta,\alpha)$ at angle θ and given α is represented by:

$$I_{individual}(\theta,\alpha) = \frac{I_0}{k_{wave} \cdot l_{dist}^2} \cdot \alpha^4 \left[\frac{J_1(\alpha \sin\theta)}{\alpha \sin\theta} \right]^2 (\frac{1+\cos^2\theta}{2}) \qquad (3.3)$$

where l_{dist} is the distance between the plane of observation and the particle. J_1 is a first-order Bessel function) and I_0 is the intensity of the incident beam. This equation learns that the measured light intensity on the detector rings of a LD-instrument is proportional with the square of the particle size.

A diffraction through a mono-disperse powder will create the same co-axial Airy rings. However, smaller particles diffract light over a wider angle than larger particles. Thus, in case of poly-dispersity of size a monotonic distribution will be found which is the superposition of numerous BESSEL functions. In practice many particles are present simultaneously in the laser beam which causes the diffraction pattern to be the sum of all individual patterns overlaid on the central axis. In order to evaluate the scattering properties of an ensemble of particles, it is enough to know the scattering functions for the individual particles. A composite scattering pattern is:

$$I_{sum}(\theta) = \int_0^\infty I_{individual}(\theta, \alpha) \cdot f(\alpha) d\alpha \qquad\qquad (3.4)$$

Here $f(\alpha)$ is the distribution function, which represents the fraction of the total number of scattering particles in any size range.

3.3.2 Calculation of particle concentration

The use of the in-line sampling cell, through which the main product flow passed, offered the possibility of using the blockage of laser light to determine the volume concentration of the powder flow leaving the mill. The total extinction of a cloud of particles, measured in the forward direction is defined as:

$$Obs = 1 - \frac{I}{I_0} \qquad\qquad (3.5)$$

where I and I_0 are the light intensities into and out of the sample respectively.

BROWN AND FELTON suggested that the particle concentration of the dispersed powder can be obtained from the extinction signal using the BEER-LAMBERT relationship. For this purpose the optical path length and the PSD must be substituted. In formula

$$C_s = \frac{V_s}{V_{sample}} = \frac{ln\left(\frac{I}{I_0}\right)}{-3\sum\left(\frac{q_i}{x_i}\right) \cdot l_{beam}} \qquad\qquad (3.6)$$

As the air flow through the mill $\Phi_{V,air}$ was measured the flowrate of solids leaving the mill $\Phi_{M,s}$ could determined:

$$\Phi_{M,s} = \rho_s C_s \Phi_{V,air} \qquad\qquad (3.7)$$

3.4 Sampling of dry powders flows

3.4.1 Off-line particle size measurements

Photo 3-2 shows the dry powder cell mounted in the Malvern MSX for the off-line size analysis. During the pilot plant experiments the ground product was collected in the bag filter. Samples of 200 grams were taken from the bag filter after the test run and analysed with the Malvern Mastersizer. The sample was re-dispersed with the ejector nozzle that was operated at a low pressure of 2.0 bar in order to avoid particle breakage. After passing the sampling cell, the powder was collected in an industrial vacuum cleaner.
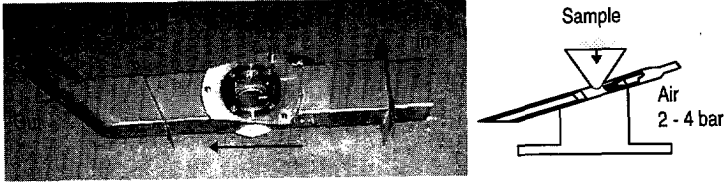
Photo 3-2 The Malvern dry powder cell (model MS24) for off-line measurements.

3.4.2 In-line sampling

The pilot plant was equipped with a tailor-made sampling cell on the product outlet. The criteria for the proper design and operation of this in-line sampling cell were as follows:

1. The obscuration of the light during operation of the grinding plant had to be within upper and lower limits in order to avoid multiple scattering effects. The solid concentration in the jet mill outlet varied from 100 grams to 400 grams per cubic meter air.

2. The path length of the laser light through the powder was limited to 3 centimetres to avoid vignetting of the scattered light by the second cell window and the collector lens.

3. Segregation of the particles on their way through the sampling zone had to be minimised by reducing gradients in velocity and direction of the flow.

4. Operating time had to be sufficiently long. For industrial applications maintenance frequencies should be reduced to once every week.
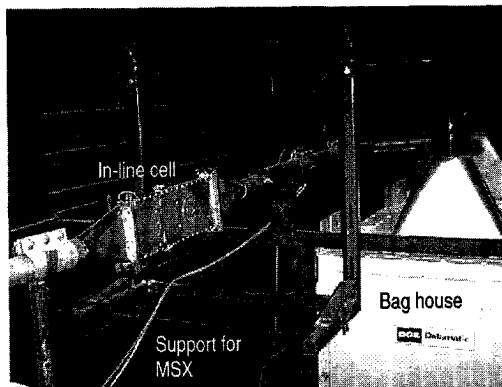
Photo 3-3 Installation of the in-line sampling cell in the jet mill plant.

Photo 3-3 shows the in-line cell mounted before the bag house. The Malvern MSX was placed in the supports.

Actual design: The dimensions of the in-line cell are depicted in Figure 3-12.

The cross sectional area was maintained constant to avoid acceleration of particles in the probe as this would lead to segregation.

Washing air to avoid window contamination was entrained and created a stream of clean air parallel with the product flow. This washing stream had to reduce the deposition of particles on measurement windows, but at the same time not disturb the flow pattern in the sampling volume.
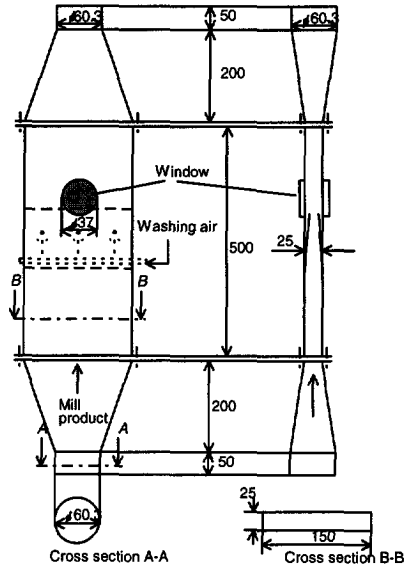
Figure 3-12 Dimensions of the in-line sampling cell mounted on the mill outlet.

Typical operating times were 2 to 3 hours for the first model pilot plant cell. Then the plant was shut down and the windows had to be removed from the cell and cleaned with alcohol. Based on trials with the first cell and flow simulations modifications were made on the design.

3.4.3 On-line sampling probe

The scale up of in-line probes to larger diameters is restricted due to the maximum optical path length of the light beam through the sample. Up to diameters of 10 centimetres the cross section can be flattened.

For the larger diameters this becomes impractical and on-line sampling (by-passing) has to be employed instead. From an operational point of view on-line sampling has an advantage over in-line measurements since the plant does not need to be shut down for maintenance or installation.

In the case of on-line sampling a pass-by of the product flow is used. Figure 3-13 shows how the sample nozzle attached inside a tube takes in a part of the product flow. The effects of inlets, outlets and constrictions were minimised by mounting the sampler fifteen pipe diameters downstream from the classifier outlet and five diameters upstream from the bag house. A homogeniser distributed the particles uniformly across the cross-section of the product pipe. After analysis the product is returned to the main product flow.
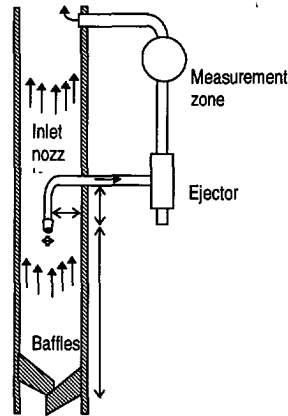
Figure 3-13 On-line sampling probe

<u>Tuning the on-line sampling probe</u>: A sample taken from the main product flow will only be representative when the velocity of aspiration into the nozzle to the measuring device is equal to the gas velocity in the tube at that point. Under these so-called iso-kinetic conditions there is no disturbance of the gas streamlines and all the particles approaching the nozzle will enter it. Work about the sampling of dispersed powders was published by AGUILLON, ALLEN, BURKHOLZ, STENHOUSE and GY.

A jet mill operated at a constant operating pressure has approximately a constant air throughput. For each pressure the on-line sampling was compared with in-line measurements. In this way the required air flow through the sampler was determined. The effect of under- and over-iso kinetic sampling was tested in the pilot plant. The measurements for both lower and higher sampling inlet velocities were compared with off-line measurements. The results are presented in Figure 3-14.
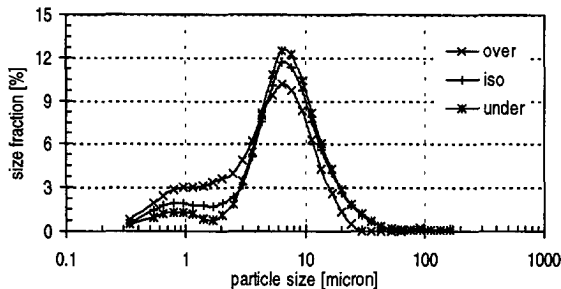
Figure 3-14 The effects of under- and over iso-kinetic sampling.

At low nozzle inlet velocities relatively more coarse particles were measured. When the inlet velocity was much higher than the iso-kinetic velocity fines were preferentially sucked into the nozzle. The PSD-curve shifted to the fine particle range.

The inlet diameter of the sampler should be larger than the scale of the turbulence in the region of the inlet. This depends on the flow regime and the particle size range. The flow pattern in the jet mill outlet is highly turbulent. The eddies were considered small compared to the sampling inlet nozzle.

In order to achieve iso-kinetic sampling conditions several approaches are described in the literature. Sampling units with integrated velocity measurement devices can be used. Recently more elegant approaches are discussed based on the information of the PSD shift by varying the inlet velocity. This information can be used to tune the sampler to iso-kinetic conditions.

3.5 Numerical treatment of scatter data

3.5.1 The deconvolution problem

The measured light intensity signal $I(\theta)$ is a linear combination of the single particle signatures. Scatter models written in a matrix form A are used for the calculation of the contribution by particles in a given size class $q(i)$ on each detector ring $r(j)$. The original particle size distribution has to be back-calculated from the measured scatter signal. Numerical quadrature methods are commonly used for the optimisation of the q-vector in such a way that the error function $e=[I-Aq]$ is minimised. The main complication is that the particle size distribution that might have caused the scatter pattern is not unique.
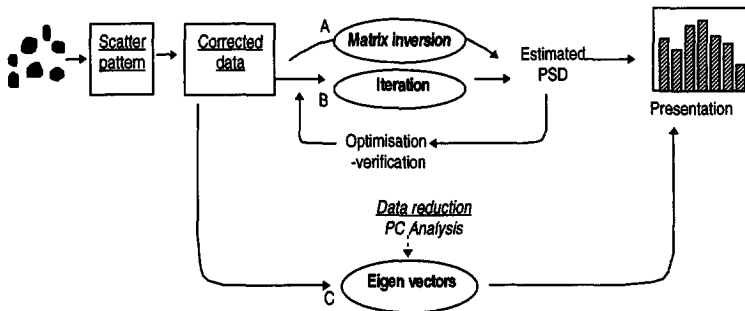
Figure 3-15 Three different routes A,B and C for the back-calculation of the particle size distribution that might have caused the measured scatter pattern.

The scheme in Figure 3-15 shows different methods that can be used to solve the deconvolution problem. Matrix inversion, iteration and principal component analysis will be discussed in respectively paragraph 3.5.2, 3.5.3 and 3.5.4.

Before the numerical processing starts, the scatter signal normally undergoes pre-treatment. First of all the signal will be discretised as a result of the multi-elements on the detector. The second step is averaging of the signal over a number of measurement sweeps. Finally a background signal, that was determined for an empty measuring cell, is subtracted.

As a result of the instabilities of the solution all the methods add a-priori knowledge during the deconvolution to stabilise the solution. These can be weighing factors, smoothing parameters or fit parameters based on process data.

3.5.2 Matrix inversion

The data acquisition of laser diffraction instruments is milliseconds. The matrix inversion is a direct method for the back calculation of the PSD that caused the scatter signal. The problem is the ill-conditioned matrix. PHILLIPS-TWOMEY regulation is mostly used by laser diffraction instruments that consists in conditioning the set of linear equations by introducing smoothness constraints on the solution. This normally takes a few seconds.

In Figure 3-16 the points I-I and $i+1$ are linearly connected. The deviation a_i between this line and point i is minimised together with the error e_i. The function to minimise becomes $e^2 + \gamma a^2$ instead of e^2. The scalar γ determines the extent of smoothing in the final solution

$$q = \left(A^T A + \gamma H^T H \right)^{-1} A^T L \tag{3.8}$$

$$a_i = \tfrac{1}{2}(q_{i-1} - q_{i+1}) - q_i$$
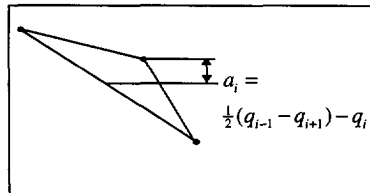
Figure 3-16 Definition of the optimisation criterion a_i

The matrix H determines how points on the curve are to be connected. The asked connection is linear when a smoothing matrix of the second order is chosen. Then the matrix has the following form.

$$
H = \begin{bmatrix}
0 & 0 & 0 & 0 & \dots & 0 \\
-1 & 2 & -1 & 0 & \dots & 0 \\
0 & -1 & 2 & -1 & \dots & 0 \\
\dots & \dots & \dots & \dots & \dots & \dots \\
0 & 0 & \dots & \dots & \dots & -1 \\
0 & 0 & 0 & 0 & 0 & 0
\end{bmatrix}
$$

The major difficulty is the conditioning of the inversion problem. The choice of γ must be determined by trial-and-error. A value too low will not eliminate oscillations, while a high value adds too many constraints, moving the solution away from the true one. BOXMAN introduced a weighting matrix to stabilise the inversion derived from the variances of the detector signals. Large fluctuations resulted in under-relaxation of these signals during deconvolution. $W_{ii}=cov^{-1}(L)$ were the elements on the diagonal matrix W. The solution, which was in fact a weighted least square method, became

$$
q = \left(A^T WA \right)^{-1} A^T WL \tag{3.9}
$$

A non-negativity constraint was added to avoid non-physical solutions.

3.5.3 Iteration

HEFFELS studied the iterative approach of CHAHINE for obtaining a particle size distribution. In this procedure the solution vector q was approximated by iterative correction of a start value.

$$
q_m^{i+1} = C_m^i C_m^{i-1} \dots C_m^0 q_m^0 \tag{3.10}
$$

In which:

$$
C_m^i = \sum_{j=1}^n a_{jm} r_j \bigg/ \sum_{j=1}^n a_{jm} \; ; \; r_{m'} = \frac{L_{m'}}{\tilde{L}_{m'}^i} \; ; \; \tilde{L}_{m'}^i = \sum a_{m'j} q_j^i \; ; \; m = 1, M \text{ and } m' = 1, n
$$

The number of detectors is denoted by n and the number of size classes by M. The advantage of this method over the inversion method is the absence of negative values in the solution vector. Drawbacks are the low speed and oscillations in the curves leading to non-converging solutions.

3.5.4 Principle Components Analysis

Jet mill product is typically characterised by a mono-modal particle size distribution. AZZAM used Principle Components Analysis, PCA, as a data reduction technique to describe the size of the product. PCA can also be used as an alternative way to process

the raw scatter data of LD instruments. This method was applied by EEK on real-time data obtained from a pilot plant crystalliser. PCA can be used to describe a set of data in terms of a reduced set of principle components which contain most of the variations present in the original set of data. This implies the reduction of the dimension of the data set consisting of many interrelated variables, while retaining as much as possible of the relevance in the original set. This is achieved by transforming to a new set of variables, the Principal Components, PCs, which are not correlated.

In this project PCA was applied to find the principle components in the Malvern data obtained from the jet mill plant. The principal component vector z that contains the principal components, z_k, $k=1,...,p$ of the correlated elements of the original vector L, is obtained from a linear transformation:

$$z = M^T L \qquad (3.11)$$

Here M is an orthogonal matrix whose k^{th} column, denoted as a_k is equal to the kth eigenvector of the covariance matrix Σ of L

$$\Sigma = E\{(L - \overline{L})(L - \overline{L})^T\} \qquad (3.12)$$

Furthermore

$$\Sigma M = M\Gamma \qquad (3.13)$$

where Γ is the diagonal matrix whose k^{th} diagonal element is λ_k, which is the kth eigenvalue of Σ. The eigenvalues directly represent the variance of the principal components:

$$\lambda_k = \text{var}(a_k^T I) = \text{var}(z_k) \qquad (3.14)$$

If the eigenvalues and eigenvectors are ranked in decreasing order, the best linear combinations of elements in x, representing the largest signal variance (energy), is represented by the eigenvector a_1 and the corresponding eigenvalue λ_1 then represents the signal energy in this specific signal direction. A reduced representation of the original representation of the original vector I is obtained by omitting the least significant signal directions, which mainly represent a noise contribution to the signal.

<u>Required number of elements</u>: In order to determine the number of components, as many eigenvectors are selected that reproduce a sufficiently large part of the signal energy. This can be done on the basis of a direct plot of the eigenvalues. The location in the plot where large eigenvalues cease and small eigenvalues begin is taken as an indicator [EEK].

Relationship between PCs and PSD: How the principal components relate to the PSD
is shown with

$$z = M^T L = M^T A q \qquad (3.15)$$

Here A is the scatter matrix (depending on the particle size instrument, i.e. the
geometry of the detector, the focal distance), q is the particle size distribution. It is to
be expected that there is a relationship between the median particle size, x_{50}, and
principal components z. When more of the PCs are used, the median will be
reconstructed more precisely. Assuming only a regression between z_1 and x_{50} the
equation will be:

$$x_{50} = c_1 + c_2 z_1 \qquad (3.16)$$

In which c_1 is a scalar and c_2 is a vector.

3.6 Testing the particle sizers

3.6.1 Sources of error

SCARLETT stated that the equivalent light scatter diameter depends on the scattering
parameters and thus the wavelength of the incident light and the refractive index of the
surrounding medium. Any equivalent diameter relates exactly only to the precise
circumstances in which it is determined and the translation of it to different
circumstances requires some assumptions to be made.

The consequence is that commercially available laser diffraction instruments often
give different results, even though they are based on the same principle. The origin of
the errors can be categorised as follows in:

1. Theoretical errors such as incorrect light scattering models or different
   deconvolution procedures.

2. Differences in the nature of the product such as non-homogeneity of particles or
   shape effects.

3. Experimental errors such as a concentration of particles too high, non-
   representative sampling or the presence of particles outside the measuring range of
   the optics.

4. The lay-out of the instrument such as the lenses and the detector geometry might
   cause a bias in the final measurement results.

All of these factors make the prescription of a standard procedure for measurements very difficult, if not impossible. In the next sections some of the important points enumerated above will be discussed with respect to the performance of the Malvern MSX for the measurement of the product of the jet mill. The Jena PSI instrument will also be considered.

3.6.2 Conditioning of raw detector signals

Before deconvolution the raw signals measured by the multi-detector undergoes pre-treatment. As a result of process instabilities or disturbances the conditions in the sampling volume can fluctuate.

Figure 3-17 shows how gradients and peaks (not related to the PSD of the product) in the signal of the 15th ring are reduced by normalisation of the signal with the obscuration.
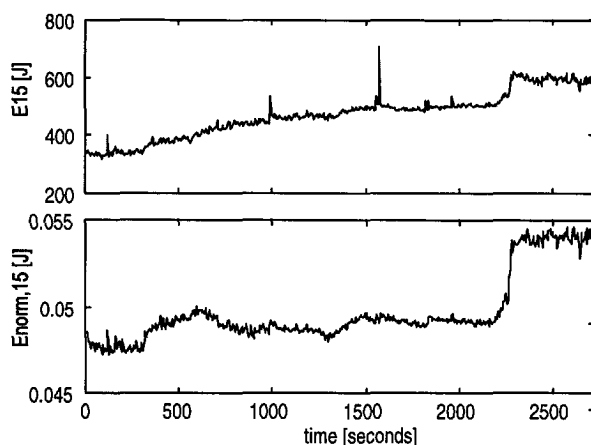
Figure 3-17 Light energy on the 15th ring before (upper curve) and after normalisation (lower curve). At t = 2250 seconds a step change on the feed is done.

Figure 3-18 shows how the median particle size, x_{50}, of the jet mill product is correlated in time with the normalised detector signals. These plots indicate that the jet milling process can be monitored with a simplified detector which has a smaller amount of detectors.
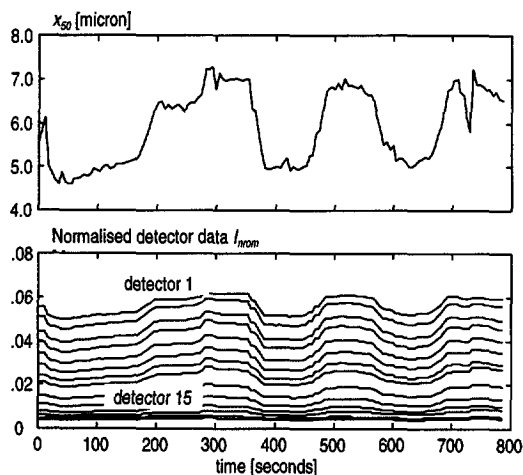
Figure 3-18 Median particle size (upper) and first fifteen normalised Malvern detector data (lower) for run 249.

3.6.3 Numerical deconvolution method

Figure 3-19 gives the particle size distributions obtained based on the same set of raw data measured with the MSX Malvern, but by applying two numerical methods, namely Chahine iteration and Phillips-Twomey (see paragraph 3.5.2 and 3.5.3).
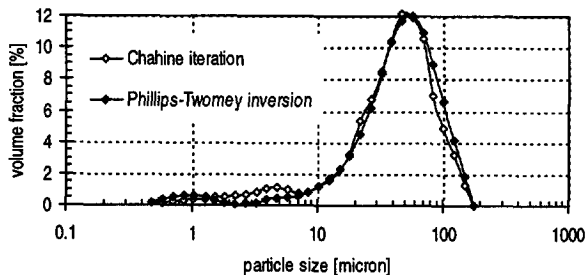
Figure 3-19 Differences in calculated PSD using the iteration and inversion method.

The curve obtained with the Phillips Twomey method, which is used in the standard Malvern software, is smoother and wider than the curve calculated by the Chahine iteration method. Irregular particles scatter more light on the outer rings than the Fraunhofer theory predicts. Inversion of the measured light signals using the Fraunhofer theory thus interprets this light to becaused by fines. The differences of the Chahine results and the Phillips-Twomey results were assumed to be due to a modification of the Fraunhofer model below the 10 micron range in the Malvern software.

3.6.4 Number of measurement sweeps

A sweep is the instantaneous scan of values on the detector rings by the instrument. Statistical errors which occur can be reduced by averaging the light signals over a number of sweeps. The total light intensity on detector i used for the deconvolution is calculated by

$$L_i = \frac{\sum_{k=1}^{N_s} L_{i,k}}{N_s} \qquad (3.17)$$

In which $L_{i,k}$ = Signal on detector i of an individual sweep k

A sample of glass particles with sizes ranging from 40 to 100 micron was suspended in water to investigate the influence of the number of sweeps on the particle size distribution. This sample was analysed with the off-line wet cell in the Malvern Mastersizer using different numbers of sweeps.
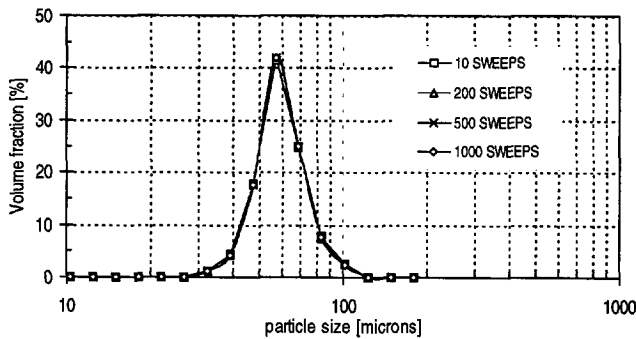
Figure 3-20 Influence of number of sweeps on measurement results with Malvern MSX. Obscuration: 20%. Glass: ref.ind. 1.52 and density 2.46 g/cm^3, Medium: water

From Figure 3-20 it is clear that reliable results are already obtained with a low number of sweeps. Poisson statistics predict the low variance in number when the sampling volume contains many fines, which on its turn produced a constant scatter signal.

In case of fine particles and sufficient obscuration levels the deconvolution of single sweep data already gave reliable results. This was also found during the real-time measurements on the outlet of the mill. Only a low number of sweeps was needed to measure reproducible particle size distributions, which was explained by the fact that the product of the jet mill consisted of very fine particles.

3.6.5 Detection of coarse particles

Sometimes the problem arises that a small number of larger particles were found in the end product of the milling process. These are not easily detectable with Laser Diffraction instruments. In the extremes of the PSD the accuracy of most laser diffraction instruments is reduced.

Experiments were done with the MSX in order to investigate the detection of a relatively number of large particles. The large test particles had sizes ranging from 250 to 425 micron. The small tests particles varied from 40 to 70 micron. Aliquots of large particles were added successively to a sample of smaller particles. The results are presented in Figure 3-21. Two percent by weight of the large particles was still detectable within a sample of fine particles.
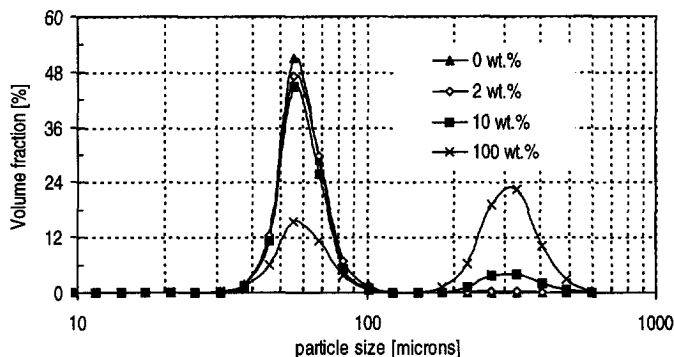
Figure 3-21 Influence of large particles (250 - 425 µm) in weight percentage of the small particles (40 - 100 µm) on the PSD. Media: glass in water.

Detection of a single large particle: The experiments described above indicated that below two percent by weight coarse particles were not easily detected. In this section the particle statistics in the sampling zone of the laser diffraction instrument will be discussed.
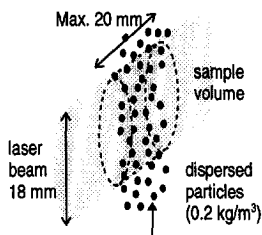
Figure 3-22 Sampling volume of laser diffraction instrument.

Figure 3-22 illustrates the situation in the sampling cell. The path length of the laser beam through the powder flow had to be restricted to 25 millimetre, thus creating a sample volume of approximately 3 cubic centimetres. The airflow leaving the jet mill contained about 0.2 kilograms per cubic meter of air, so the amount of product in the sampling volume was 1.0 milligrams. Two virtual samples of particles were compared with nearly identical size distributions. Sample A had a smooth PSD, as shown in Figure 3-23. Sample B, however, contained 1.5 grams of coarse particles with a size of 334 micron in 100 grams of sample.
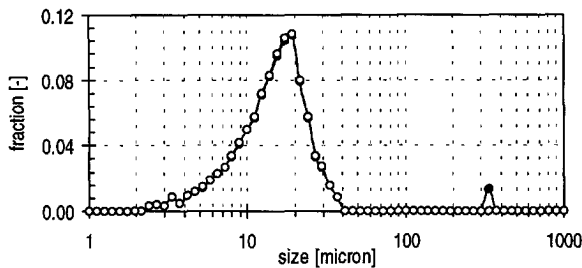
Figure 3-23 PSD curves of sample A, all fines, and B almost equal, but with 1.5 volume percent of 334 micron particles.

The scattered light on the detector rings is fluctuating instantaneously as it is caused by new particle collectives during each measurement sweep. Figure 3-24 shows the calculated light intensities on the detector caused by a collective without any coarse particles and by a collective containing 5 coarse particles.
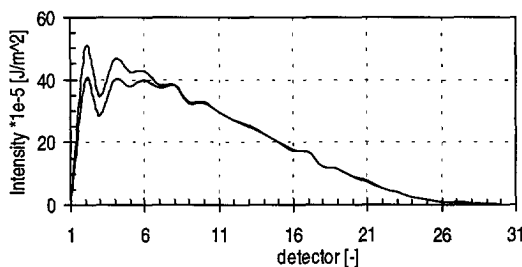
Figure 3-24 Calculated intensity pattern for a single sweep measurement for the PSD of sample A (lower) and sample B.

Normally the light intensities are time averaged over a large number of sweeps to obtain a reproducible value. After deconvolution of the averaged scatter data the original peak in the PSD at the 334 micron of sample B had disappeared, which indicated that the coarse particles would not have been detected with the current sizer software.

As mentioned, many LD instruments use time averaging of the intensity fluctuations or underrelaxation during the deconvolution by a weighing factor. However, the fluctuating single sweep detector data contains useful information about the presence of coarse particles. Correlation of the fluctuations on the inner detector rings for individual measurement sweeps can be useful for the detection or actual counting of small amounts of large particles in a fine powder.

The information can be completed with Poisson statistics. The weight of one coarse particle m_{334} is 0.2 milligrams. The average number of coarse particles, N_{334}, present in the sampling volume can be calculated by

$$N_{334} = \frac{m_{sample}}{m_{334}}$$
(3.18)

Here m_{sample} is the total mass of product present in the sampling volume. A volume percentage of 1.5 coarse particle corresponded with an average of 5 particles per measurement sweep. Figure 3-25 shows the probability of the number of particles present in the sampling volume.
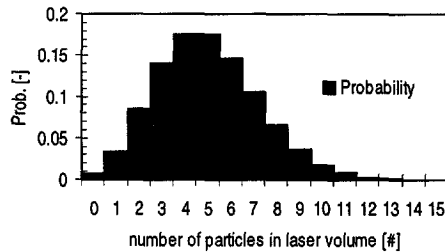
Figure 3-25 Probability of the number of particles in the sampling volume.

3.6.6 Measurement of irregularly shaped particles

Grinding processes always produced irregularly shaped particles. The feed material for these jet mill experiments were mostly flakes, while the end product was more rounded as a result of the attrition mechanisms in jet mills.

The detectors of most laser diffraction instruments as well as the software are not programmed to handle scatter signals caused by non-spherical particles. The bias that particle shape causes to the final measurement results was tested by using a transparent film with a distribution of particle outlines of different shape arrayed in random positions and orientations. The particle images were characterised by their equivalent projected area. Figure 3-26 contains the measured results.
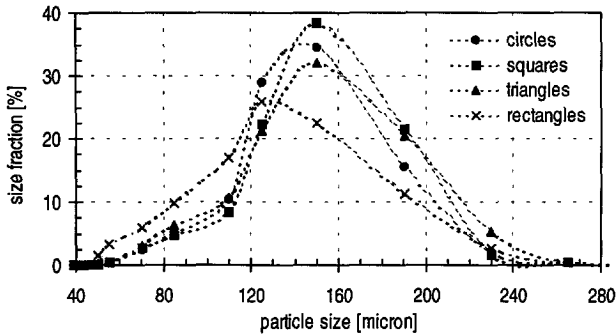
Figure 3-26 Reticules with differently shaped but equivalent projected areas measured by laser diffraction. MSX.

Figure 3-26 indicates that the shape must substantially differ from spherical in order to get a large difference in the modal size. The instrument undersizes particles which are platelets. For circles, squares and triangles the same modal size was found. The largest deviations were found for rectangles with an aspect ratio of 5. In jet milling practice the end product mostly consists of rounded particles with an aspect ratio of 1.4 or lower.

3.6.7 Upper and low limits of particle concentration

Minimum concentration: The sensitivity of the laser diffraction instrument to concentration fluctuations was tested by measuring a suspension of particles (glass beads, 40-70 micron) in water with the MSX. After each measurement the solid concentration was increased leading to higher obscuration levels. The results are shown in Figure 3-27.
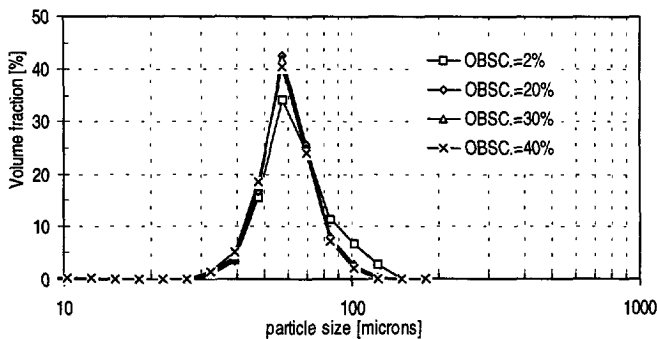
Figure 3-27 Influence of obscuration. Glass beads suspended in water. MSX.

Reproducible measurements were obtained at relatively low obscuration levels, but deviations were found for obscuration levels below 2 percent. This corresponded to

0.005 volume percent of particles in the suspension. The experiments were extended until an obscuration level of 40% and no deviations were found. During the in-line measurements on the jet mill outlet the product concentration varied from 0.01 up to 0.04 volume percent. The obscuration level was typically 30%. Therefore. no side effects due to too low or too high particle concentration were assumed.

Multiple scattering: At higher particle concentrations the light may be scattered more than once before reaching the detector. The application range of models that are based on single scattering are normally restricted to obscuration levels until 50 percent. This can be a problem for in-line measurements in product flows with a high particle concentration. Especially for finer particles, as they cause higher obscuration values with the same volume concentration.

Software solutions were implemented in the Insitec instrument for treatment of multiple scattering. Reliable measurements were reported in obscuration levels up to 90 volume percent [HIRLEMANN, HOLVE].

3.6.8 Comparison of laser and incoherent light scattering

The objective was to compare the performance the Malvern MSX and Jena PSI, based respectively on the scattering of laser light and incoherent halogen light. Two samples of mill product, a fine and a coarse fraction, were dispersed in air by an ejector and analysed in a flow-through cell. An equal number of 500 measurement sweeps was taken by both instruments. In order to compare the results the raw data of both the MSX and PSI were processed with the Chahine iteration method. The results are presented in Figure 3-27.
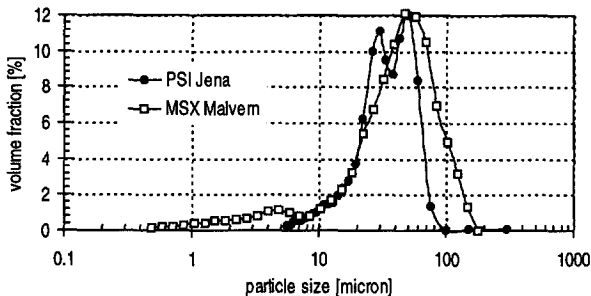
Figure 3-28 Alumina powder ground on a jet mill measured with Malvern MSX and Jena PSI sizing instruments. Chahine iteration.

In both cases the same numerical method was used. The Chahine iteration scheme gives physically more realistic results since the distribution is less effected by noise

[HEFFELS]. Though the shape of the curves differ considerably, the mean size has about the same value.

3.6.9 Processing scatter data with principle component analysis

When a jet mill is operated under normal conditions the PSD of the mill product is usually characterised by a mono-modal curve. Due to interference of the light also particles scatter light on several neighbouring rings. This means that the signals on the detectors will be correlated which on its turn reduces the number of intensity distributions that can be expected on the detector rings of the LD instrument. The correlation will be strongest on those rings recording the maximum intensity of the most prominent size classes.

PCA was applied to six data sets of historical process data that were measured under different operating conditions of the grinding plant. Figure 3-18 shows the strong correlation between the detector signals in the raw data measured during a test run. In Figure 3-29 the first four eigenvectors *a1, a2, a3* and *a4* corresponding to the first four eigenvalues of each set are presented. Figure 3-30 plots the eigenvalues of the covariance matrix for several test runs.
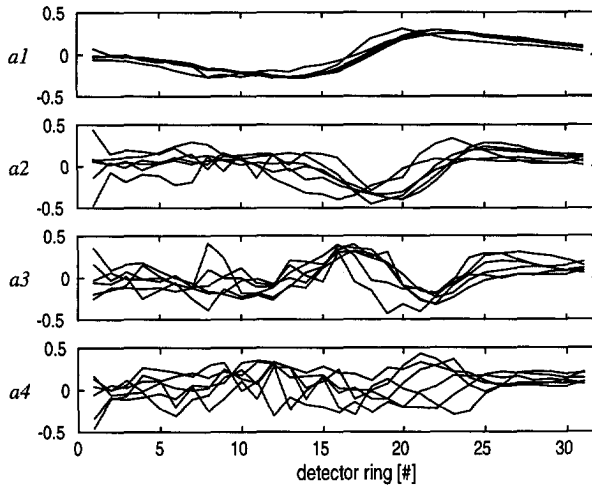
Figure 3-29 First four principal eigenvectors of the covariance matrix for the jet mill runs 243, 247, 248, 249, 254 and 276

By means of PCA an empirical scatter model is derived for the specific mill configuration and test material within the range of tested operating conditions. For these circumstances the PSD could be retrieved by use of a reduced set of parameters.
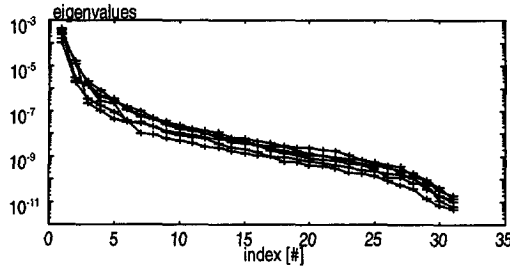
Figure 3-30 Eigenvalue plot of eigenvalues corresponding to all 31 principal components (test runs 243, 247, 248, 249, 254 and 276).

These experiments indicated that all the data sets contained the same principle signal directions. The directions were most reproducible for the first eigenvector; at higher order the coherence between the eigenvectors disappeared rapidly.

It appeared that more than 95% of the PSD information was covered by three principle components for a large number of different operating conditions. In other words, the PSD of the jet mill product could be accurately represented by a linear combination of three intensity vectors.

As an example the evolution of the PSD over run 249 was evaluated. During this run the process inputs were strongly excited which resulted in a fluctuating PSD in time. Figure 3-31 indicates a sharp transition in the trend of the eigenvalues. This implied a change in the ratio of the desired signal variance and noise variance.
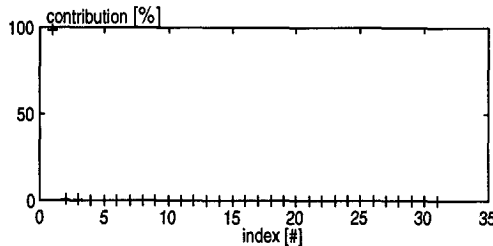
Figure 3-31 Contribution of the eigenvalues corresponding to all 31 principal components for run 249.

This plot shows that the variance of the first principle component of run 249 described more than 99 percent of the variance of the original data.

Figure 3-32 presents the first four principle components that were derived from run 249. The variance of the first PC is the largest and strongly correlated with the fluctuations of the PSD. The variance of the remaining PCs decreased rapidly down the sequence.
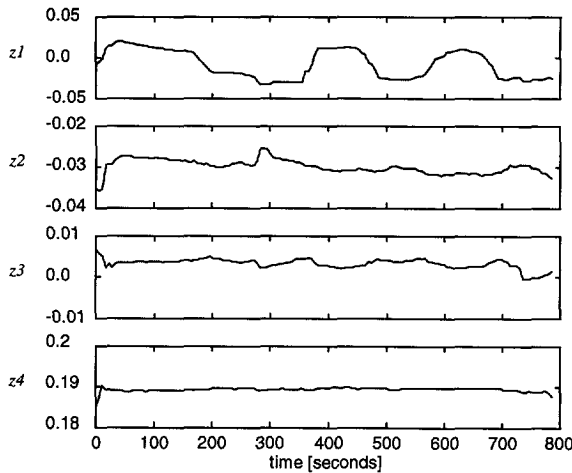
Figure 3-32 Principal components z1, z2, z3 and z4 for jet mill run 249.

Figure 3-33 shows that the first principle component correlated mainly with particles in the size range between 5 and 100 micron. The sensitivity to variations became smaller above this range.
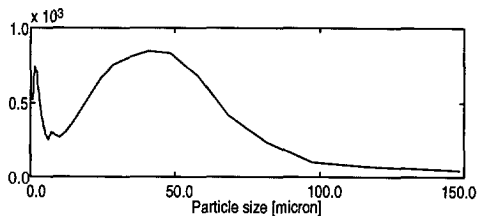
Figure 3-33 Major direction of the particle size domain related to the first principal component z_1 (run 249)

During run 249 the operating conditions were varied, resulting in a fluctuating median size of the end product. In Figure 3-34 the value of the median size x_{50} (dashed line) is reconstructed with the first principle component. For a control of the x_{50} the first PC is most suitable as it is sufficiently sensitive to the process variations.
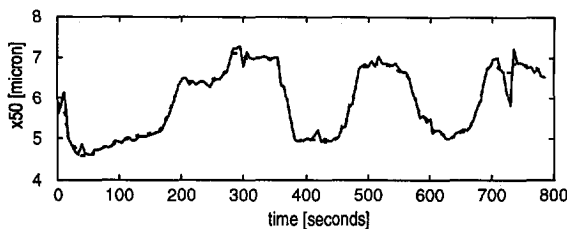
Figure 3-34 Reconstruction of the median size x_{50} with the first PC for run 249.

This plot shows that an estimation of the median particle size of the product of the jet mill could be given by assuming a linear relation between the first principle component and the median size.

3.7 Conclusions

From all particle size measurement techniques that were reviewed the optical techniques were found most suitable for on-line particle size measurements on air driven mills and classifiers. The main advantages are the data acquisition speed, the digital output signal that can easily be transmitted to the central control system and the ability to measure in a high velocity dispersed air flow. Two diffraction instruments were tested, one using laser light and the other using incoherent light. Both instruments were able to measure transients in the PSD of the product of the jet mill. However, the final measurement results of the sizing instruments depended on device lay-out (optical configuration), scatter model and sampling conditions. This made the comparison of measurement results with the different instruments difficult and a mutual calibration is essential.

Most diffraction instruments which are commercially available were not designed for use in an industrial environment, where they are exposed to dust, heat and vibrations. Furthermore the investment costs are high and the installation needs quite some preparation.

For the control of an existing grinding plant a simplified and robust sizing probe is required that provides one or more output signals (e.g. currents) that can be used as feedback signals for the aspects of the PSD to be controlled. Absolute accuracy is not a necessity, only the ability to monitor relevant process changes. Last but not least, the maintenance and calibration of sizer instruments and sampling units on an industrial grinding plant demand expertise.

Continuous measurements on the jet mill outlet are statistically better than off-line size analyses of samples taken from the bag filter. In the case of on-line measurements the total amount of material analysed is larger. Furthermore the risk for segregation or agglomeration during transport and handling of the material is avoided since the product remains well dispersed in the main flow. Another benefit of on-line measurements is the strongly reduced time delay, which allows a better correlation between changes in the product quality and the process conditions.

On smaller jet mills an in-line sampling cell can be mounted on the product outlet, which allows, besides the PSD, the mass flow to be continuously monitored. Larger

pipe diameters require the by-passing of a part of the main product flow through an on-line sampling probe. In this case attention should be paid to the (iso-kinetic) conditions of sampling.

From the performance tests of the light scattering instruments it appeared that these instruments were capable to measure the median size of powders with great reproducibility. The absolute accuracy at the extremes of the PSD was poor. In the fine particle range, <1 micron, the optical model based on the Fraunhofer theory caused deviations. Mixtures of fine and coarse powders were measured with LD-instruments. Below a volume percentage of 2 percent the coarse particles were difficult to detect. It is suggested to use the correlation between detector rings for fluctuating single sweeps in order to enhance the measurement of small number of coarse particles in fine powder.

Jet mill product is usually characterised by a smooth mono-modal size distribution. The data reduction technique PCA is an alternative way to monitor the grinding process. The median size of the product can be described with one component. Information about the PCs and process inputs can be stored in a data base and used for mill tuning and control. The PCs derived from the jet mill data were mainly sensitive to PSD changes within the 5 to 100 micron range. PCs are less sensitive to obscuration changes and fouling of the cell windows. For PCA it is necessary to observe the system for a period of time. Deconvolution applied for the estimation of the PSD will be necessary for process monitoring and presentation of understandable physical quantities. PCA offers a means to avoid deconvolution which can be useful for faster data processing or the interpretation of measured data from a simplified sizing sensor.

List of symbols

A	scatter matrix	
A	surface area	[m^2]
C_s	solids concentration	[-]
Dbeam	diameter laser beam	[mm]
f	focal distance	[mm]
H	smoothing matrix	
I	light intensity	[J/m^2]
k	wave number	[nm^{-1}]
k_v	volumetric shape factor	[-]
l	length	[m]
L	vector with light signals	
m	relative refraction index	[-]
n	refraction index	[-]
Obs	Obscuration	[%]
q	particle size density	[-]
Q	cumulative undersize distribution	[-]
x	particle size	[m]

Greek

r	radial position on detector plane	[mm]
α	dimensionless size parameter	[-]
Φ	flow rate	[kg/hr]
λ	wavelength	[m]
λ_i	i^{th} eigenvalue	
ρ	density	[kg/m^3]
θ	scatter angle	[°]
Ψ	sphericity	[-]

Literature

Aguillon, J., Shakourzadeh, K. and Guigon, P., Comparative study of non-isokinetic sampling probes for solids flux measurement in circulating fluidized beds, *Powder Technology*, Vol. 83, 79-84, 1995

Allen, T.A., Particle size measurement, *Powder Technology Series*, 3rd ed. 1986

Azzam, M. I. S.; Jutan, Arthur; Rodriguez, E., II, Particle size characterization of a jet mill product via principal component analysis, *Part. Sci. Technol.*, 6(1), 95-104, 1988

Azzopardi, B.J., Instrumentation for particle size analysis by far field diffraction: accuracy, limitations and future, *Proceedings of the 25th anniversary conference Particle size analysis, 17-19 Sept. 1991, Loughborough*, 1-12, 1991

Becker, R., lasentec, *manual,* 1995

Boxman, A., Particle size measurement for the control of industrial crystallizers, *Ph.D thesis TU Delft*, 1992

Boxman, A.,Merkus, H.G., Verheijen, P.J.T., Scarlett, B., Deconvolution of light scattering patterns by observing intensity fluctuations, *Appl.Opt.,* 30, 4818-4823, 1991

Brown, D.J., Felton, P.G., Direct measurement of concentration and size for particles of different shapes using laser light diffraction, *Inst. of chemical engineers chem eng res des,* 63, 1985

Burkholz, A., Sampling Probes as Precollectors for Cascade impactor measurements of Aerosols in Gas Flows, *Partec 86,* , 537 -540, 1986

Byers, R.L., Davis, J.W., Matson, W.L., McKinstry, H.A., Particle size and shape characterization by scanning electron microscope, *Recent Advances in air Pollution Control,* vol.170, 389, 1974

Chahine, M.T., Inverse problems in radiative transfer, *J.Atmos.Sci.,* 27, 960-967, 1970

Cooper, D.J., Clough, D.E., Optical real-time monitoring of particle size distribution in a fluidized bed, *AIChE Journal,* 32, no.3, 389-395, 1986

Craig, K., Hulbert D.G., Metzner, G., Moult, S.P., Extended particle size control of an industrial run-of-mine milling circuit, *Powder Technology,* 73, 203-210, 1992

Gy, P.M., Sampling of particulate materials, theory and practice, 1979

Harvill, T.L., Hoog, J.H., Holve, D.J., In-process particle size distribution measurements and control, *Part.part syst.charact. 12,* 309-313, 1995

Heffels, C.M.G., On-line particle size and shape characterisation by narrow angle light scattering, *Ph.D.-thesis TU Deft*, 1995

Heidenreich, E., Stintz, M., Evaluation of particle size analysis data regarding reproducibility and accuracy, *Proceedings of the 25th anniversary conference Particle size analysis, 17-19 Sept. 1991, LOUGHBOROUGH,* 436-445, 1991

Heiskanen, K., On the difficulties of implementing particle size control in particulate processes., *Powder Technology,* 82, 13-19, 1995

Heitzmann, D., Optical measurement of particles and particle flows, *Paon course Delft*, 25-27 mei, 1994

Heuer, M., Schwechten D., In-line particle size analysis in the fines outlet of an air classifier, *Partec 95,,* 301-310, 1995

Heywood, H., Symposium in particle size analysis, Inst.Chem.Eng.Suppl., 25, 14, 1947

Hirleman, E.D., Optimal scaling of the inverse fraunhofer diffraction particle sizing problem: the linear system produced by quadrature, *part.charact.*, 4, 128-133, 1987

Hirleman, E.D., Response characteristics of laser diffraction particle size analyzers: optical sample volume extent and lens effects, *optical engineering*, 23(5), 610-619, 1984

Holve, D.J., Using ensemble diffraction to measure particle size distribution, *powder & bulk Engineering,*, 1991

Holve, D.J., Harvill, T.L., In-process particle size distribution measurements and control, *Partec 95*, 291-300, 1995

Hong, J. and Tomita, Y., Measurement of distribution of solids concentration on high density gas-solids flow using an optical-fiber probe system, *Powder Technology*, 83, Issue 1, April 1995, 85-91, 1995

Hosokawa, In-line particle size analysis, *brochure Hosokawa Alpine*, 1995

Hughes G.N., Andres R.F., Neutral time of flight mass spectroscopy a technique for analysis of aerosols, *Recent Advances in air Pollution Control*, 70, 317-321, 1974

Hulst, van de, H.C., Light scattering by small particles, Wiley, New York, 1981

Kaye B. , Trottier R., The many measures of fine particles, *Chemical engineering*, April, 78-86, 1995

Löffler, W., Bartz, P., On-line Partikelgrössenmessung mit inkoheren-optischen Methoden, *Pulver & Schüttgut Verfahrenstechnik*, 1.2, 1-7, 1995

Logan, T.J., Felder, R.M., Ferrell, J.K., Experimental investigation of isokinetic and an-isokinetic sampling of particulates in stack gases, *r.adv. in air poll. control*, v.170, 389, 1974

Plessis, P., Kaye, B.H., Investigation of some factors affecting optical reflectivity from powders, *Powder and Bulk Solids, Proceedings*, 1992

Rolland, T.; Pons, M. N.; Vivier, H.; Dodds, J. A.; Thomas, A., Quantitative analysis of particle shape during grinding: case of hydrargillite, *Recents Prog. Genie Procedes 96, 10(45, Procedes de Broyage)*,, 10(45), 111-116, 1996

Santschi, M., Bock, A.H., Continuous particulate monitoring, *Powder & Bulk Solids Conf. proceed. 1992, Illnois*, 1992

Scarlett, B., 25 years of particle size conferences, *Proc. of the 25th anniversary conference Particle size analysis, 17-19 Sept. 1991, Loughborough*, 1-12, 1991

Scarlett, B., Monitoring of Particulate Processes, *REPOWFLO II, Oslo 1993*, , 829, 1993

Schwechten,D., In-line Partikelgroessenanalyse fuer Mahlsichtanlagen, *CAV*, 74-78, 1993

Snow, R.H., Allen, T., Effectively measure particle-size-classifier performance, *Chem. Eng. Progress*, may, 29-35, 1992

Stanley-Wood, N., Llewellyn, G., Lim, T.H., In stream particle size characterisation by a micro computer based data analyser, *Particle Size Analysis*, 329-335, 1981

Stenhouse, J.I.T., Lloyd, P.J., Sampling errors due to inertial classification, *Recent Advances in air Pollution Control, AIChE series, no. 137*, 70, 307-310, 1974

Svarovsky, L., Svarovsky, J., A new method and apparatus for monitoring of particle size distributions in industrial processes, *Proc. of the 25th anniversary conference Particle size analysis, 17-19 Sept. 1991, Loughborough*, 436-445, 1991

Thomas, A., Pons, M.N., Rolland, T., Vivier, H., Dodds, J.A., Perrin, H., Thomas, D, Particle morphological analysis in high velocity air jet mills, *IFPRI annual meeting, June* 1995

Thorwirth, Optical spatial frequency analysis principle and results, *Jena review*, 2, 95-97, 1990

Twomey, S., Introduction to the mathematics of inversion in remote sensing and indirect measurments, *Elseviers Scientific Publishing Compant*, Amsterdam, 1977

Wadel, H., Sphericity, *Physics*, 5, 163, 1938

Whiteman, M., Ridgway, K., The application of principal components analysis to particle shape description, *Proc. of the 25th anniversary conference Particle size analysis, 17-19 Sept. 1991, Loughborough*, , 340-349, 1991

Witt, W., Rothele, S., Laser diffraction - unlimited?, Sympatec, *Partec,*1995

Wolowec, V., Selection of a reliable On-line and In-line Monitoring System for Solids, *REPOWFLO II, Oslo 1993*, 853, 1993

Wright, H., Ramkrishna, D., Solutions of inverse problems in population balances, I aggregation kinetics, *Comp.chem.eng.*, 16-12, 1019-1038, 1992

Chapter 4

Fine grinding of heat sensitive materials

In this chapter the size reduction of heat sensitive materials is discussed. Paragraph 4.2 deals with the effects of size, shape and mechanical properties of the solids on breakage. Paragraph 4.3 discusses the loading conditions that the particles experience inside the mill. The next paragraphs deal with the state of stress and the propagation of cracks. Paragraph 4.5 presents the results of impact and compression tests that were carried out to assess the grindability of the materials used during the jet mill experiments.

4.1 Introduction

During grinding the size distribution of a particle collective, which can be a powder or granulate, shifts to smaller sizes. Consequently, the specific surface area, *SSA*, will increase. Figure 4-1 illustrates what occurs during the breakage of a single particle.
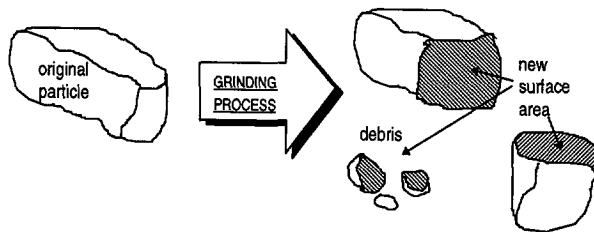
Figure 4-1 Effects of particle breakage: The reduced particle size and the increase of total surface area.

Due to the lack of insight into the physical mechanisms of the size reduction the design and operation of grinding plants is largely based on trial-and-error. This chapter deals with the many parameters that control and affect the size reduction process.

A review on crushing and grinding is given by LOWRISON. RUSSEL discussed a number of techniques for fine grinding. HIXON handled the selection of grinding equipment, while PEBWORTH dealt with grinding of heat sensitive materials.

Little corresponding literature exists with regard to the grinding of polymers. In the last sections of this chapter the assessment of breakage parameters of the test material will be described. These parameters will be used for the dynamic model described in Chapter 7.

4.2 Theory of particle breakage

4.2.1 Mechanisms of breakage
The key issue in all grinding processes is the creation of a stress field inside the particle that is intense enough to cause breakage. The state of stress and the breakage reaction are affected by many parameters that can be grouped into particle properties and loading conditions as is shown in Figure 4-2. Publications on the fundamentals of grinding were written by RUMPF, SCHÖNERT and AUSTIN.
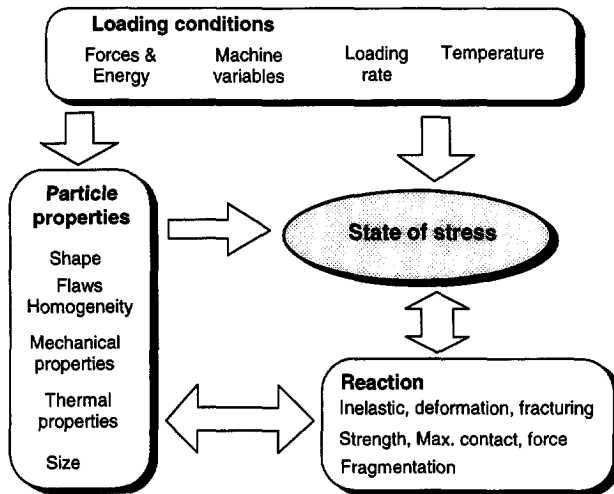
Figure 4-2 Factors affecting the breakage of a particle. After HEISKANEN [1995].

The reaction of a particle to the state of stress is influenced by the material properties, the state of stress itself and by the presence of micro cracks and flaws. Size reduction will start and continue as long as energy is available for the creation of new surface. The stresses provide the required energy and forces necessary for the crack growth inside and on the surface of the particle. However, a considerable part of the energy supplied during grinding will be wasted by processes other than particle breakage such as the production of sound and heat as well as plastic deformation.

4.2.2 State of stress

During a grinding process particles are loaded by external forces that create a three-dimensional state of stress inside those particles. The state of stress were geometrically represented by the Mohr-circle as forces exerted on the unit cube. This is illustrated in Figure 4-3.
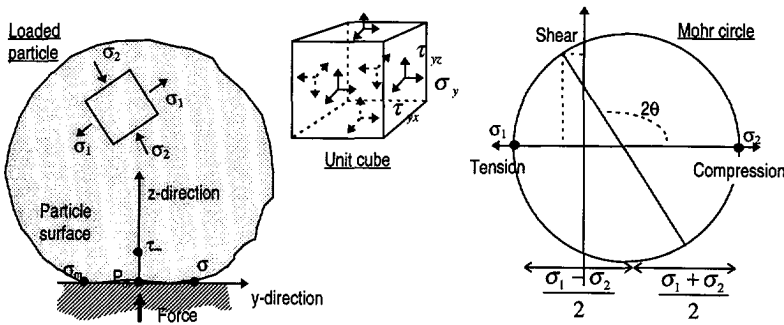
Figure 4-3 External force acting on a spherical particle (left). Stresses acting on a unity cube (middle). Construction of the Mohr-circle (right).

The compressive and tensile stresses are expressed respectively as positive and negative values on the horizontal axis. The shear stresses are represented as values on the vertical axis. There exist no shear stresses in the directions of the principle axes. The shear stress τ_θ at an angle θ to the principle axes can be calculated by

$$\tau_\theta = \frac{(\sigma_1 - \sigma_2)}{2}\sin 2\theta \qquad (4.1)$$

The normal stress σ_θ is

$$\sigma_\theta = \frac{(\sigma_1 + \sigma_2)}{2} + \frac{(\sigma_1 - \sigma_2)}{2}\cos 2\theta \qquad (4.2)$$

<u>Contraction</u>: Besides a compressive stress in the direction of the maximum principle stress, contraction of the material also causes tensile stresses in the direction of the

other principle stresses. The relationship between longitudinal strain and the concomitant lateral strain is given by the Poisson's ratio, v. A stress σ_l causes extra shear forces in a plane at an angle θ perpendicular to the direction of the stress. The Poisson's ratio may be as high as 0.55 for materials such as rubber. A typical value for v is 0.33.

On the basis of Figure 4-3 the maximum value of the shear stresses is found when the angle θ is 45 degrees. The value of the compressive or tensile stresses is highest for θ = 0. If a body breaks through tension, it will break along a surface perpendicular to the stress represented by the largest co-ordinates on the x-axis, i.e. the break will be flat across the section of a rectangular piece. If the body breaks in shear, it will be at an angle of about 45 degrees to the minimum cross section of a rectangular piece.

Internal friction: In practice however a lot of materials appear to break in shear at larger angles. In order to explain this phenomenon Coulomb introduced the concept of internal friction expressed by the parameter ζ. The equation for the shear stress caused by the principle stresses extends to

$$\frac{(\sigma_1 - \sigma_2)}{2} sin 2\theta - \zeta \left[\frac{(\sigma_1 + \sigma_2)}{2} + \frac{(\sigma_1 - \sigma_2)}{2} cos 2\theta \right] \qquad (4.3)$$

Assuming that a particle breaks in shear, this will occur in a plane where the shear stress is highest. The angle of this plane to the principle axes can be found by differentiation of equation 4.5 to the angle θ and equate the result to zero. Thus the material will fail at the angle

$$\theta = tan^{-1}(\zeta \pm \sqrt{\zeta^2 + 1}) \qquad (4.4)$$

The values for ζ, are approximately 1 and therefore the angle θ will always be larger than 45° [LOWRISON].

Stress distribution in a particle: As an illustration the pressure distribution in two colliding linearly elastic spheres will be discussed. HERTZ found that for contacting surfaces the stress system satisfying the compatibility of displacement for mutually contacting points enclosed within the contact region and the condition of surface stresses in the absence of friction. For the geometry depicted in Figure 4-4 TIMOSHENKO gave the following solution

$$\sigma = \sigma_{max} \sqrt{1 - \frac{r^2}{a^2}} \qquad (4.5)$$
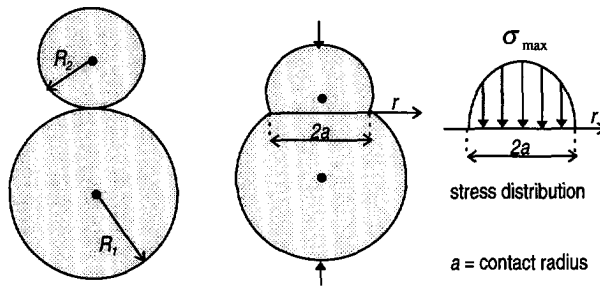
Figure 4-4 Contact of two spherical particles. Deformation and stress distribution.

The maximum compressive stress, σ_{max}, at the centre of impact of an elastic collision can be calculated by [MORI]

$$\frac{\sigma_{max}}{E} = 0.52 \cdot E \cdot \left(u \middle/ \sqrt{E/\rho} \right)^{2/5} \qquad (4.6)$$

A size effect is not included in the equation, which would mean that the key problem would be sufficient acceleration of the particles. Often the critical stress is not reached resulting in rebouncing, especially for smaller particles. This can be explained by the differences in deformation of differently sized particles at the same impact velocity. Furthermore, the impact deformation varies with size due to a change in yield stress with strain rate.

Stress concentration: Most industrial solids contain irregularities like microscopic cracks and weaknesses caused by dislocations, non-stochiometric composition, solid solutions, gas and liquid filled voids or grain boundaries. INGLIS showed that these irregularities play a predominant role in particle breakage as the local stresses, σ_i, generated at the tips of the crack, as shown in Figure 4-5, were much higher than the gross applied stress σ_N.
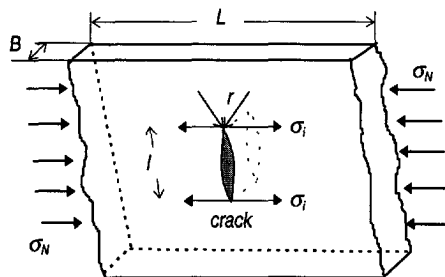
Figure 4-5 A micro-crack in an infinitely large plate.

The effect of a crack can be expressed by stress concentration factor k

$$k = \frac{\sigma_i}{\sigma_N} = \frac{l}{r} \qquad\qquad (4.7)$$

which is a function of the crack length, l, and the tip radius, r.

GRIFFITH found that tensile stresses always occur in the vicinity of crack tips, even when the applied gross stresses are compressive. It also appeared that the largest tensile stresses are produced at cracks having a 30 degree angle to the compressive stress. Thus cracks play a key role in propagation and their effects greatly overshadow the theoretically calculated values for particle breakage.

4.2.3 The breakage reaction

Fracturing criteria: If the absorbed energy exceeds a certain value it will be used to break the particle, to deform the particle and to supply the broken particles with an amount of kinetic energy. If the absorbed amount of energy is less than the critical amount, the energy will be divided between energy for plastic deformation and kinetic energy of the rebounding particle. For crack propagation it is necessary to satisfy two conditions, namely

1. The *force condition* states that the bond forces between ions, atoms and molecules, respectively, are overcome by the local stress.

2. The *energy condition* demands that the energy from the stress field, the external forces, the internal thermal energy or energy from chemical reactions have to exceed the energy necessary for crack extension. The material in the neighbourhood of the crack tip is always deformed irreversibly, even with the so-called brittle materials such as glass.

Force conditions: In paragraph 4.2.2 it is was shown that a compressive stress can cause shear stresses. The body will break in shear at locations where the shear stress occurring, τ, is higher than the ultimate shear strength, τ_u. Differentiating equation 4.5 with respect to the angle θ and putting the resulting equation gives the angle along which *breakage by shear* will occur [LOWRISON].

$$\theta = \tfrac{1}{2}\cot^{-1}\mu \qquad\qquad (4.8)$$

Substitution leads to the following condition for breakage by shear

$$\left[(1+\upsilon)\sqrt{(1+\mu^2)} - (1-\upsilon)\mu\right]\sigma_{r,u} > 2\tau_u \qquad\qquad (4.9)$$

If typical values of $\mu = 1.0$ and $\nu = 0.25$ are used the ratio between the ultimate tensile stress and ultimate shear stress under a compression will be $\tau_u < \frac{1}{2}\sigma_{c,u}$.

The condition for a solid subjected to a compressive force to *break by tensile stresses* is

$$\nu\sigma_{c,u} > \tau_u \qquad\qquad (4.10)$$

Most solids processed in the chemical industry are inhomogeneous. During compression of the particle certain parts will deform more than the rest. This results in shear forces and explains why in many grinding processes particles breaks in shear. For these materials the ultimate shear stress, τ_u, should be used in calculations of mechanical strength [JOISEL].

Energy condition: During crack propagation energy is absorbed for new surface formation, plastic deformation close to the crack, as well as heat and electronic processes. For a static crack in a particle the *energy balance* is given by

$$U = (-U_p + U_\varepsilon) + 2U_s = U_m + 2U_s \qquad\qquad (4.11)$$

where U_s is the free surface energy, U_m is the total mechanical energy of the system consisting of the energy of the applied load, $-U_p$, and the elastic strain energy, U_ε.

If there is no propagation of the crack, an equilibrium exists between the terms with respect to any incremental change in crack surface area.

$$\frac{dU}{dA} = \frac{dU_m}{dA} + \frac{dU_s}{dA} = -G + R = 0 \qquad\qquad (4.12)$$

The crack propagation is determined by the balance of two energies. Elastic energy, described by the *energy release rate G*, is supplied to the crack tip and absorbed for the generation of new surfaces.

The *crack resistance, R,* is the result of the local cohesive forces of the material surrounding the crack. This energy is required to create new surface area.

$$R = dU_{s,req}/dA \qquad\qquad (4.13)$$

The energy release rate G is

$$G = \frac{-dU_m}{dA} \qquad\qquad (4.14)$$

The change in mechanical energy after crack growth can be expressed as

$$dU_m = \frac{\sigma^2}{2E} \cdot 2\pi a \cdot dA \qquad\qquad (4.15)$$

In which $\sigma^2/2E$ is the elastic energy per unit of volume.

For breakage the energy release rate has to be larger than the crack resistance. Parameter G can be calculated from the measured values of σ and a and the heat can be measured. This gives limiting values for crack resistance. Typical values for plastics are 10 to 1,000 J/m^2. Compared to the specific surface energy these values are 2 to 5 decades higher. Thus the major amount of energy is consumed by the inelastic deformation and the heat generation at the advancing tip [SCHÖNERT].

Critical crack length: At maximum crack propagation velocity this is a material constant. During crack propagation both energies are balanced. Due to the interaction of the field of stress and the advancing micro-crack the situation is unstable depending on the second derivative of the energy d^2U/d^2A. The energy for cracks to propagate can only come from the stress field. The critical crack length a_c for a stress σ is given by

$$2a_c = \frac{ER}{\pi\sigma^2} \qquad\qquad (4.16)$$

Propagation of a crack continues provided there is enough strain energy stored in the particle. As long as this criterion is met or until they are stopped by the boundary of the particle or irregularities the crack will propagate. Work on the breakage of crystalline materials was published by CLARKE.

Other phenomena: The speed of crack propagation approaches the velocity of sound in the material and can be more than 1000 meters per seconds. Furthermore the local temperatures at the cracks can rise up to thousands of degrees. The breakage of single particles was analysed with numerical tools by KIENZLER.

4.3 Particle properties

In literature different formulae are used to define the energy required to break the material. The problem with these mostly empirical relationships is how to differentiate between the energy dissipated by the mill and the energy absorbed by particles during the comminution. Furthermore, many phenomena interact during the process of breakage. This makes data in literature difficult to compare and therefore this discussion will only be qualitatively. In the following sub-paragraphs the effects of

respectively size, shape and mechanical properties on breakage behaviour will be discussed.

4.3.1 Effect of particle size

Grinding limit: The strength of a particle becomes larger as its size decreases and therefore the critical energy for breakage has to be higher. This is explained by the fact that smaller particles can contain consequently smaller irregularities. KENDALL stated that a lower limit exists to the size of particles produced by grinding. The minimum particle size which can break using elastic energy stored in the particle during deformation can be calculated with equation 4.17. The elastic energy stored temporarily during impact can be calculated by equation 4.7. This equation does not contain the particle size.

Substitution of typical values for plastics shows that a minimum particle size produced by single step breakage lies around several microns. Therefore comminution of particles finer than the limit need either external energy to be imported or repeated loading. This value coincides with the experimentally found limit of brittle materials starting to show plastic behaviour. Work of HESS dealt with the brittle-plastic transition in small particles.

Energy requirements: The energy use for breakage in relation to particle size is often described by three empirical relationships that are each applicable for a specific size range. Figure 4-6 shows the composite plot of these 'laws' over the whole size range introduced by HUKKI. For each material a similar plot can be determined.
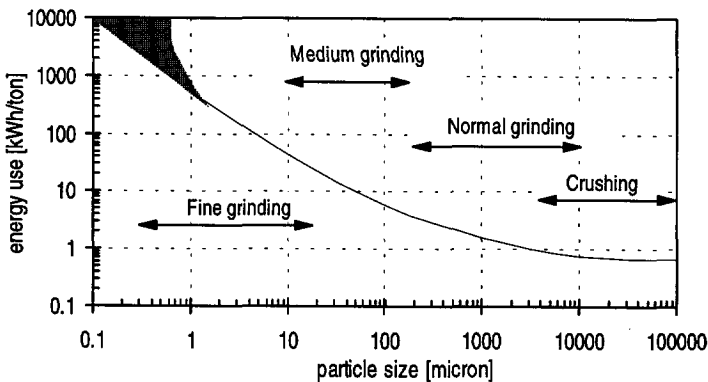
Figure 4-6 Required energy as function of produced particle size. After HUKKI.

RITTINGER [1867] stated that the energy consumed is proportional to the new surface produced. This law can be written as

$$E = C\left(\frac{1}{x_2} - \frac{1}{x_1}\right) \qquad (4.17)$$

Figure 4-6 indicates that Rittinger's law is applicable to particles in the size range from 0.1 to 1000 microns.

KICK [1885] postulated that the energy requirement is related to the volume/weight of the particles. In other words: The work required for crushing a given quantity of material is constant for a given reduction ratio, irrespective of the original particle size. In formula

$$E = C\ln\left(\frac{x_1}{x_2}\right) \qquad (4.18)$$

BOND [1952] found that the energy content of a material is based upon the reciprocal of the square root of the screen size through which 80% passes. This empirical equation is applied for the transition region. In formula

$$E = 2 \cdot C \cdot \left(\frac{1}{\sqrt{x_2}} - \frac{1}{\sqrt{x_1}}\right) \qquad (4.19)$$

The proportionality constant C is called the work-index. This parameter is a function of particle size range and breakage mode.

The above mentioned curves usually are some power law fit of the average size reduction ratio of the particles, such as by WALKER.

$$\frac{dW''}{dx} = -Cx^{-n} \Rightarrow W'' = \frac{C}{n-1}\left(\frac{1}{x_P^{n-1}} - \frac{1}{x_F^{n-1}}\right) \qquad (4.20)$$

where $n=2.0$ for Rittinger, $n=1.0$ for Kick and $n=1.5$ for Bond's law. KAPUR wrote a review on size reduction laws. Other work concerning grindability and energy consumption was done by FUERSTENAU.

Theoretical description: WEICHERT stated that the theoretical dependence of the mass specific energy W_m is a function of the particle properties, material properties and the loading condition. This theoretical equation, which was derived by WEIBULL statistics and HERTZ theory, is given by

$$W_m = \left(cx^2 k^{(1-z)}\right)^{-\frac{1}{z}} \cdot \Gamma\left(\frac{1}{z} + 1\right) \qquad (4.21)$$

The k-value accounts for the loading condition, and equals 1 for impact tests and 2 for compression tests. The theoretical dependence of the required mass specific energy W_m on the particle size is given by:

$$W_m \propto (x)^{-2/z} \qquad (4.22)$$

This means that the mass specific energy is proportional to the particle diameter to a power which depends on the material. The applicability of the theory to fragmentation of particles was tested on data from single particle experiments (paragraph 4.5.2) and compression tests (paragraph 4.5.3) carried out with our test materials.

4.3.2 Particle shape and texture

Differently shaped particle, though having the same volumetric diameter, have different breakage behaviour. Based on the thermodynamic principle of free surface energy a spherical particle is most stable, as its surface energy is lowest per unit of volume.

Non-spherical particles subjected to external forces lead to stress distributions that differ sharply from the spheres. Therefore the breakage behaviour of such particles is different from what can be expected based on the HERTZ theory due to in-homogeneity and uneven surfaces of the particle. For example; elongated particles tend to break more easily due to the fact that they are more vulnerable to bending forces which are more effective than compressive forces.

The particles fed to a mill often have irregular shapes. They can be granules produced by extrusion, flakes or crystals. During a grinding process the particle shape often changes. The individual particles in the end product after jetmilling will normally be more spherical as a result of attrition. The irregular and angular particles become rounder and smaller during grinding as their corners are knocked off during collisions. Spherical particles are least sensitive to attrition and when broken the fragments have more or less equal sizes, but a more angular shape. HONMA investigated the effects of particle shape of feed particles on jetmilling.

According to SCHÖNERT the energy required for crack propagation through a particle is proportional to its cross-sectioned area. Figure 4-7 illustrates how the grindability can be related to the particle shape. Elongated particles are experience more bending forces that are more effective for breakage than compression. In industrial practice most particles have an aspect ratio around 1.4.
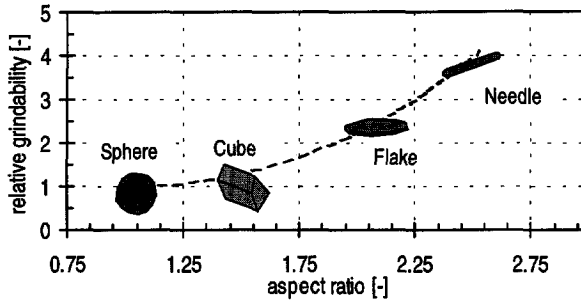
Figure 4-7 The relationship between grindability and particle shape.

Texture or irregularities in the material as a result of previous unit operations, such as crystallisation, can greatly affect the size reduction process. An important factor is the natural grain size of the material. Grain boundaries or heterogeneities obstruct crack extension and make the material more difficult to grind. Amorphous and poly-crystalline materials resist the propagation of cracks more than purely crystalline materials. This can explain why amorphous materials usually tend to break locally at the edges in an attrition mode. Crystals are more likely to break in parts of equal sizes as the stress is more evenly distributed over the whole particle [LOWRISON].
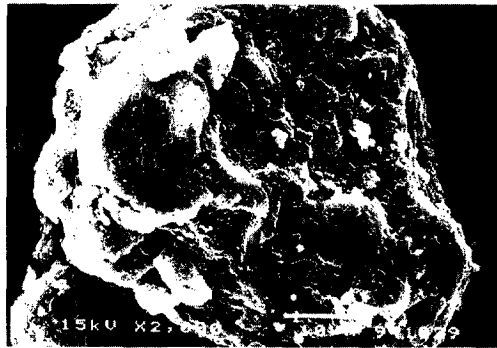
Photo 4-1 Texture of the model material CW. SEM photo (1500x).

Photo 4-1 shows a CW particle that is built up of layers. Grinding tests showed that breakage occurred along these layers, and new fragments appeared as flakes. Finally, when the particle size was reduced to a size in the order of the layer thickness the particles became more spherical. Then the particle was less vulnerable to attrition and further size reduction on a jet mill was difficult.

The other way around, a grinding process can affect the structure of the processed materials. LEITEL reported about changes of the porosity of several metal oxides after jetmilling.

4.3.3 Mechanical properties

The mechanical properties of the material affect the built-up of a stress field in a particle during loading. They also determine the ultimate stress levels a material can sustain. Polymeric materials like PE, ABS, PVC, POM, PC and PC are increasingly used and represent eighty percent of the world production [YOUNG]. The mechanical properties of these polymers are plotted in Figure 4-8. The fracture mechanics of polymers were described by HULL.
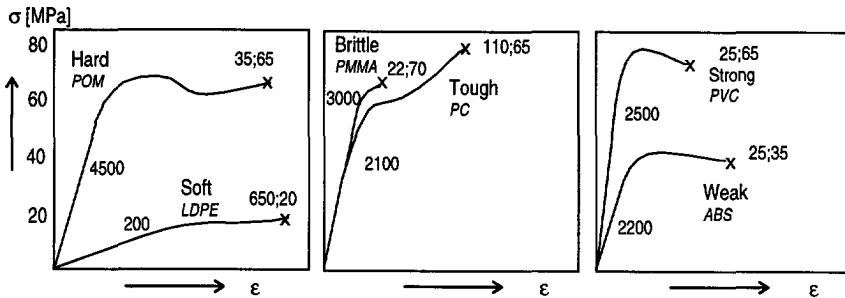
Figure 4-8 Features of stress-strain curves for polymers. The marker X represents the ultimate tensile stress at which breakage occurs.

Inter-molecular forces: The ultimate comminution process is the reduction of solids into single molecules, which would be theoretically mean evaporation. However, in this case one cannot speak about a particulate process anymore. The smallest assembly of molecules that still behaves in the manner associated with solids consists of 10^3-10^4 molecules, which corresponds to a size of 2 to 5 nanometer. Below this size range particles grow to larger entities [HOUNSLOW].

Van der Waals forces between particles act over a longer range than those between molecules. For two spherical particles of diameter x the attractive potential, Φ_A in Joule, is given by

$$\Phi_A = -\frac{A \cdot x}{24s} \tag{4.23}$$

Repulsive forces acting on particles are of electrostatic nature

$$\Phi_R = \frac{32\pi dc_\infty RT\zeta_0^2}{\kappa^2}\exp(-\kappa s) \tag{4.24}$$

Combination of these effects shows that below one micron range particles become quite sensitive to these forces. Grinding below this size will become more difficult.

Molecular modelling software, as used in crystallisation research, allows the calculation of attachment energies between crystal planes as well as mechanical properties of the ideal pure substance. Simulation results might be useful for the study of the effects of chemical impurities on size reduction.

MENYHART studied the structural changes of materials after processing on a jet mill. LEITEL reported about a different porosity of metal oxides using jet mills and ball mills.

Bending strength: The effect of bending strength on the grindability on jet mills was investigated by SMIT [1980] on specimens of the three waxes. The correlation between bending strength and obtained feedrates with comparable x_{99} is shown in Figure 4-9.
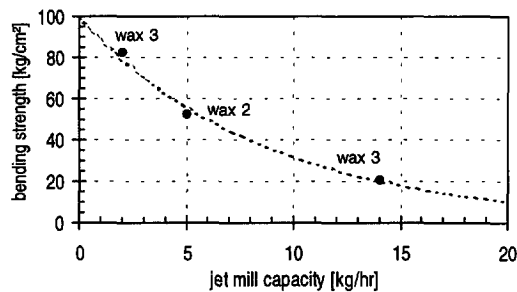
Figure 4-9 Bending strength versus mill capacity. After SMIT.

Lower bending strength leads in case of waxes ground at room temperature to higher mill capacities. Tests were done at elevated temperatures, but no improved grindability was found. In fact the same polymer can sometimes be made either brittle or ductile by changing the operating temperature or the rate of loading.

4.4 Loading conditions

4.4.1 Forces on the particles

Loading of solids: In order to break a solid it is necessary to satisfy the force and energy conditions, as discussed in paragraph 4.2.3, in order to create a state of stress beyond certain limits. This is generally done by applying a mechanical load to the particle that introduces three dimensional stresses inside the particle. Alternative ways of particle loading are the use of ultrasound or electrical principles [HALBEDEL,

KUSTERS]. Figure 4-10 illustrates basic methods of particle loading as they occur in most grinding equipment.

| Compression | Tension | Shear | Bending | Torsion |
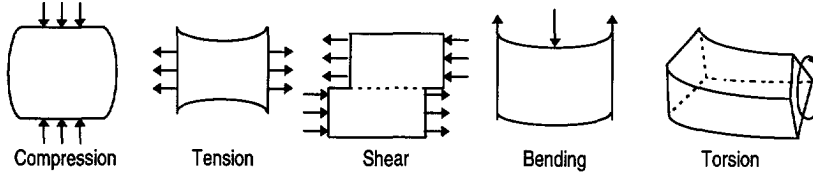
Figure 4-10 Ways of applying a mechanical load to a solid.

Machine variables: The type of tool that is used to apply the loading on a particle plays an important role. Different modes of comminution are distinguished according to the direction and magnitude of the forces applied. Figure 4-11 lists the modes of particle loading as they occur in industrial mills. This loading can take place either by slow compression between two planes or by impact against a target. In these cases the force is normal to the plane. An alternative way of particle loading is by applying a shear force by moving the loading planes horizontally. The table lists commonly used comminution equipment indicates that compression and impact are more used for coarse grinding, while attrition and abrasion are usually applied in the fine and super fine comminution.

	COMPRESSION	IMPACT	ATTRITION	ABRASION
COARSE				
crushers	XX			
hammer crusher		XX		
MEDIUM				
roller mills	XX			X
high pressure	XX			X
rolls	XX	XX	XX	X
tumbling mills				
FINE				
vibrating mills	X	XX	XX	
planetary mills	X	XX	X	
hammer mills		XX		
cutter mills		XX	X	
SUPER FINE				
pin mills		XX	XX	
micro impact mills		XX	XX	X
opposed jet mills		XX	XX	X
spiral jet mills		X	XX	X
stirred ball mills			XX	XX

Figure 4-11 Breakage modes in industrial mills [HEISKANEN, 1995]

Compression and impact: For the breakage mode the force is normal to the particle surface and affects the whole particle. The resulting breakage is producing fragments that are substantially smaller than the original particle.

Attrition: If the applied normal forces are too weak to affect the whole of the particle and are restricted to a partial volume at the surface of the particle, the comminution mode is attrition. The result is that the original particle remains large and rounded. In addition much finer particles are produced. Normally this mode results in a very narrow PSD as the relatively coarse particles can be separated by classification from the fines. The end product is characterised by a narrow PSD. Attrition has been extensively studied as an undesired effect in fluidised beds [RAY, KONO].

Abrasion: In this breakage mode the major force is tangential. The result is usually similar to attrition, but the fine particles are even finer, the original particle is smoother but little changed in size and shape. SUH described abrasion in terms of a de-lamination theory, based on the behaviour of dislocations at the surface of the particle, sub-surface crack and void formation, with subsequent joining of cracks by shear deformation of the surface. Wear of particles will be in the form of thin plate-like sheets and surface layers undergo large plastic deformation.

Autogenous grinding: In autogenous mills the product serves as the grinding medium (see Figure 4-12). This means less intensive contact between the product and the machine parts. Autogenous mills are therefore suitable for the grinding of abrasive materials such as minerals. AUSTIN investigated the autogenous grinding in tumbling mills. In autogenous jet mills the highly turbulent flow field makes particles collide against each other. OKUDA compared the grinding mechanism in a fluid energy mill with secondary nucleation in crystallisers.
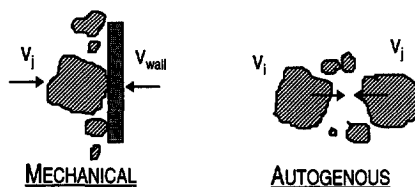
Figure 4-12 Grinding media used for particle loading.

In the chemical industry a wide variety of mills are used. The forces acting on a particle in these mills grinding are complex and usually employ a combination of the loading modes described in this section. However, in each type of mill one mode will normally be predominant and typically affect the properties of the ground material.

4.4.2 Grinding temperature

In grinding processes much of the supplied energy appears as heat in the broken particles. Operating temperatures of mill can easily rise up to hundreds of degrees in mechanical mills. This causes undesired effects like agglomeration, adhesion on the equipment walls and degeneration of the product.

Cooling media: Plate mills, pin mills and ball mills are air swept for conveying and cooling purposes. In fluid energy mills the product present in the grinding chamber is coincidentally cooled by the expanding air jets. Solid carbon dioxide or liquid nitrogen can be added as cooling media to reduce temperatures [VOLKER, KLUMPAR]. Alternatively, a part of the mill is cooled by water. In jet mills the fluid flow, which is the energy carrier, provides at the same time excellent cooling of the product. Practically the temperature rise of the flow leaving the mill can be neglected as the heat development by breakage and friction is compensated by the temperature drop caused by adiabatic expansion. For this reason jet mill are suitable for the treatment of heat sensitive materials, like plastics.

Plastics: When a polymeric material is subjected to tensile or shear stress of sufficiently high magnitude it will rupture. Crystalline polymers are often brittle below the glass temperature, Tg. Amorphous polymers also have a transition region, below Tg, in which the impact strength decreases. Therefore plastics can often be characterised by some sort of brittleness temperature [BROEK].
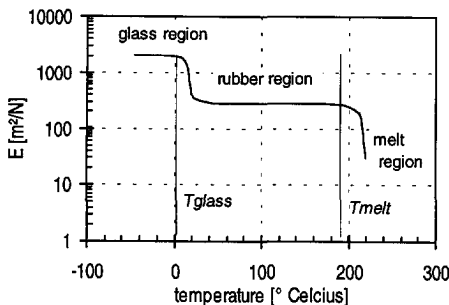
	T_g	T_m
CW	-	50
POM	-50	110
LDPE	-120	-
PMMA	110	-
PC	150	-
PVC	87	-
ABS	105	-

Figure 4-13 Elasticity modulus for a semi-crystalline plastic as function of temperature (left). Table with glass and melt temperatures of polymers (right).

In the case of rupture above the glass transition temperature where the polymer chain backbones are able to change their configurations before the sample breaks. The crack propagation which ends in rupture can be strongly affected by the relief of stress through visco-elastic relaxation or by crystallisation at large extensions. Also the presence of filler particles and the mechanical history in periodic stressing can play a

role. Experiments showed that the dependence of ultimate properties on temperature and rate of deformation is closely related to that of visco-elastic properties and therefore reflected the rates of molecular rearrangements.

Below the glass transition temperature the molecular configurations are immobilised. In general for polymers below T_g rupture is usually associated with the breaking of the primary chemical bonds. Here the chain backbone configurations are immobilised during the time of the breakage avoiding long-range rearrangements. Nevertheless, dissipation of energy by local relaxation processes appears to be important in determining the degree of stress concentration at the tip of a crack, and the breaking strength under impact.

The material used in this project is ground with high pressure air at a temperature of 20 degrees Celsius. For certain materials it may be advantageous to use cryogenic grinding. Cooling increases brittleness and hardness. The comminution mode changes from attrition to breakage, leading to a wider PSD. In accordance with thermodynamics, a higher grinding temperature should help comminution. At elevated temperatures the breaking force decreases while the wax becomes more difficult to grind. This can only be explained by a considerable increase in plasticity of the wax at higher temperatures at higher temperatures. These effects were reported by SMIT.

4.4.3 Rate of loading

Despite the complicated nature of polymers, various experiments showed the correlation of mechanical properties at different temperatures and different rates of deformation [NADAI]. This general equivalence between time and temperature, illustrated in Figure 4-14.
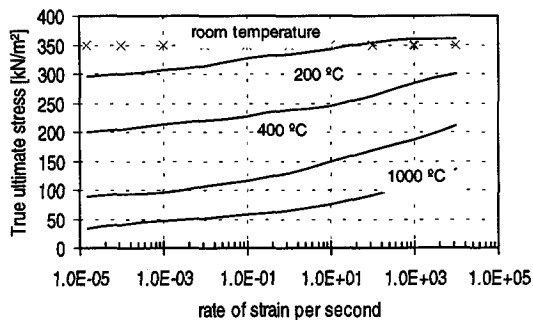
Figure 4-14 Effect of the rate of deformation and the processing temperature on mechanical strength. After NADAI. Copper.

The ultimate stress seemed to be stronger if the loading is faster. It is also thought that there exists an equivalence with regard to the visco-elastic behaviour and the temperature. A polymer that shows a rubbery behaviour at a given test condition can be induced to show glassy behaviour by either reducing the temperature or increasing the rate of loading. It may be possible to interrelate the time and temperature dependence of the visco-elastic properties of polymers. For instance, a polymer which displays rubbery characteristics under a given test condition can be induced to show glassy behaviour by either reducing the temperature or increasing the testing rate or frequency [FERRY].

Repetitive loading: Many materials suffer failure under cyclic loading at stresses well below which they can sustain during static loading. This phenomenon is known as fatigue. Closely related to this is multiple collision breakage, which means that the energy may be supplied in small portions. The total energy required for a desired degree of fragmentation can be substantially reduced as by the repetitive process the kinetic energy is better utilised. This phenomenon was described by RUPPEL AND BRAUER.

4.5 Breakage tests

Model describing grinding processes typically contain an energy balance, and mass balances over the mill that describe the evolution of the PSD in time. The model is completed by the kinetic expressions which relate the population events such as attrition and breakage to the process conditions. SANKARA gave an overview of principles and applications of particle breakage tests to comminution. SHIPWAY investigated the fracture of brittle materials under compression and impact loading. Investigation of particle breakage at the micro-scale level were described by MIDDLEMISS.

A more detailed understanding of the size reduction process of our test material was done by impact experiments presented in paragraph 4.5.2 and compression experiments presented in paragraph 4.5.3. In these tests the velocity, respectively force and energy input into the particles could be measured in addition to the resulting fragment size distributions. The information was used to estimate the parameters for the statistical description of the breakage process in Chapter 7 Modelling.

4.5.1 Measures for size reduction

However, the interpretation of the results can be difficult, especially when the shapes of the PSD curves for various materials differ widely. In the study of fragmentation, it

is necessary to define a parameter to quantify the modification of structure of the particle.

Reduction Ratio, *RR*: The measurement of the PSD before and after comminution can be used as a guide to the extent of size reduction. This method is commonly used in grinding practice and was originally based on sieve sizes. It is defined as the ratio of the size of the feed particles divided by the size of the broken particles. In this project the median diameter of the feed particles $x_{50,F}$ and the product collected after breakage $x_{50,p}$ were used

$$RR = \frac{x_{50,F}}{x_{50,p}}$$ (4.25)

Changes in the extremes of the size distribution related to the grinding action are not taken into account. Therefore the reduction ratio is a simple way to judge the breakage performance as it says little about the breakage modes in the fragmentation process.

For some applications it is more useful to express the degree of size reduction as the increase of the specific surface area of the powder. The relationship between the PSD and the specific surface area was described by KIHLSTEDT.

Increase in specific surface, *ISS*: The specific surface of a powder is defined as the surface of all particles divided by their collective mass. The increase of specific surface is defined as the ratio between the difference in specific surface area (abbr. *SSA*) of product and feed, divided by the specific surface area of the feed:

$$ISS = \frac{\left(SAA_P - SAA_F\right)}{SAA_F}$$ (4.26)

Changes in specific surface between feed and product are widely used as a measure of size reduction. The advantage of this parameter is that the ISS takes into account the whole range of the particle size distribution. Problems are that one specific surface value can be obtained from a variety of particle size distributions and that the finer particles contribute largely to the surface and the coarser particles contribute largely to the mass of the product.

Comment: Only when the relevant shape information of particles in different size classes is available, the increase in specific surface area can theoretically be derived from the particle size distribution. However, in most size analyses it is assumed that the shape does not change over the size range. Furthermore, each sizer instrument produces a specific bias/error caused by shape effects.

4.5.2 Particle impact experiments

Impact tests were carried out by a number of researchers such as OKUDA, YUREGIR, KIENZLER, LESCHONSKI, DAN, CLEAVER and LeCOQ, either to investigate the target wear or to study fragmentation of the impacting granules. A jet impingement tester developed by MEBTOUL was used in this research project to assess the grindability of a set of materials ground on the jet mill plant.

Test equipment: The lay-out of the test rig is shown in Figure 4-15. The vibratory feeder brought the sample, a specific sieve fraction of test material, into the ejector nozzle. The particles were accelerated in the converging/diverging tube up to 300 hundred meters per second by an expanding air flow. The concentration of particles was kept low, assuming that inter-particle collisions were of minor importance.
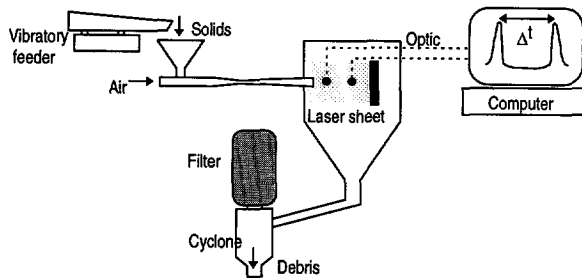
Figure 4-15 Test rig for single particle impact.

The impact velocities on the target were determined by measuring the light reflectance by particles travelling in a laser sheet parallel with the particle loaden air jet. The signals of the optic fibres were cross-correlated by

$$\phi_c(t) = (1/T)\int f_1(t) * f_2(t + \Delta t)dt \qquad (4.27)$$

The velocity is the distance between the optical fibres divided by the time delay. The debris after impact was collected by a cyclone and analysed with a particle sizer.

Experimental program: Particle breakage of the test materials was investigated by impacting sieve fractions on a target at different velocities. The tested samples are listed in Table 4-1 and Table 4-2 together with the impact velocities.

Table 4-1 Test material: CW

Size [micron]	Impact velocity [m/s]					
500 - 600	60.6	112.1	149.6	187.6	231.7	260.5
420 - 500	97.5	132.6	158.7	197.9	236.2	---
250 - 420	120.7	166.4	178.8	223.4	240.3	---
150 - 250	133.5	189.1	206.5	247.3	286.9	---

Table 4-2 Test material: PE

Size [micron]	Impact velocity [m/s]					
500 - 600	140.2	146.5	177.5	221.3	252.0	260.2
420 - 500	100.0	155.1	173.6	225.9	264.6	---
250 - 420	123.2	168.8	178.9	232.5	262.5	---
150 - 250	144.5	185.1	206.3	240.0	274.6	---
90 - 150	158.4	202.4	229.5	277.2	316.6	---

<u>Impact test results</u>: The Figure 4-16 presents the results of the impact tests carried out with different sieve fraction of material CW.
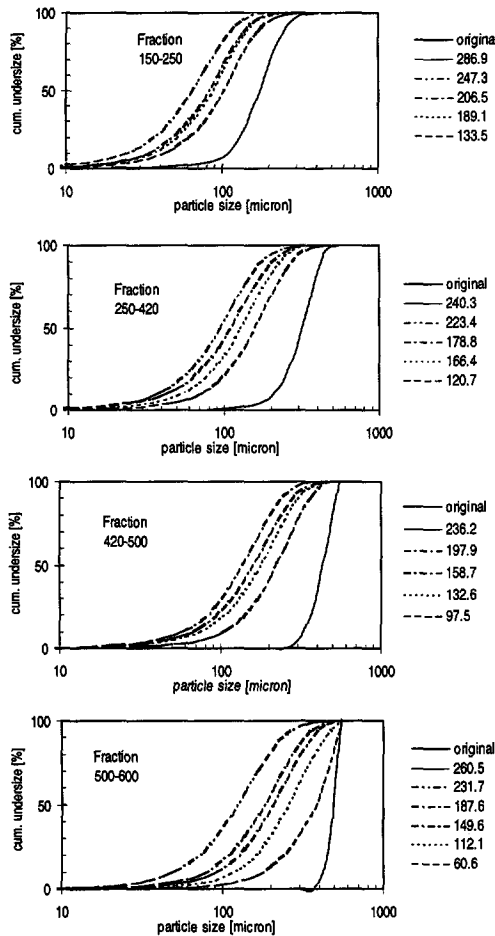
Figure 4-16 Different sieve fractions of model material CW impacted on a fixed SiC target. Impact angle 90°.

The solid lines at the right represent the particle size distribution of the feed sample. The dashed lines are the PSDs of the debris after impact at different velocities. The PSD of the debris shifted to the finer side for higher impact velocities.

Assessment of breakage parameters: The impact experiments with CW and PE were used to determine the grindability related to particle size and impact energy. Figure 4-17 shows that the data points of the reduction ratio, RR, and the increase of the specific surface area, ISS. It appeared that the RR for the materials CW and PE could be fitted well with a linear function of the velocity.
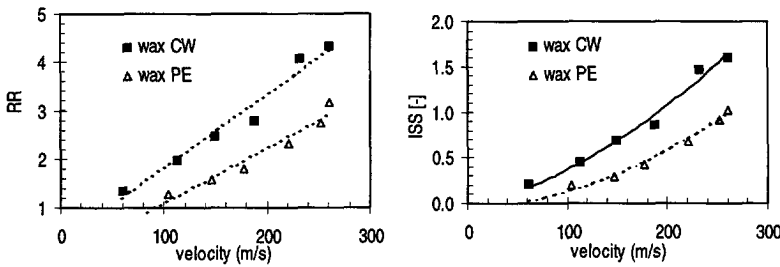
Figure 4-17 RR (left) and ISS (right) for the model materials CW and PE for sieve fractions of 500-600 microns impacted on SiC target.

The increase of specific surface area, ISS, was proportional to the square root of the velocity, which implied that it was proportional to the kinetic energy of the particle.

The results show that the required impact velocity to achieve an equal degree of fragmentation for a 500-600 micron sieve fraction was significantly lower for CW compared to PE. For a RR-value of 3.0 the impact velocity of PE particles had to be 260 meter per second, while for a CW particle 180 meter per second was sufficient. In this case the mass specific energy of CW was 48 percent of the value for PE.
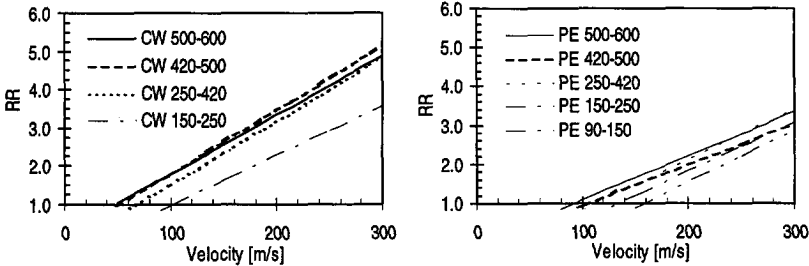
Figure 4-18 Reduction ratio, RR, versus impact velocity for different size fractions. Material CW (left), Material PE (right).

Figure 4-18 contains the linear fits of the *RR* data for the different sieve fractions and impact velocities for CW and PE. The intersection with the velocity axis gave the velocity where the reduction ratio *RR* was unity. Physically this meant that under these impact velocities no particle breakage occurred.

During the event of impact the kinetic energy of the particles was temporarily used for loading of the particles. The impact energy is calculated with

$$E_{impact} = \frac{1}{2}mv_p^2 \qquad\qquad\qquad (4.28)$$

The mass specific energy required for breakage was described by WEICHERT. The points of intersection of *RR*-curves with the velocity axis for CW were fitted with a power law derived from his equation

$$v_{p,crit} \propto (x_p)^{\left(-\frac{1}{z}\right)} \qquad\qquad\qquad (4.29)$$

For material CW the Weibull coefficient was 0.70. For material PE a *z*-value of 1.7 was found.

Effect of the impact angle: Impact tests with CW particles (250-420 microns) showed that at equal impact velocity, a 70 degrees angle lead to finer debris than the default 90 degrees angle. Experiments at 45 and 60 degrees showed no effect.
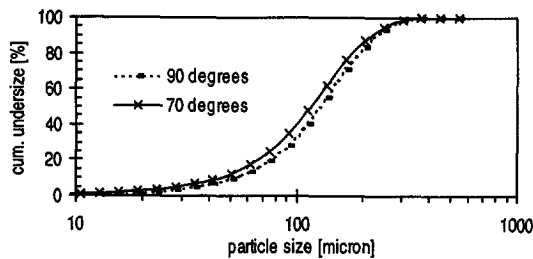
Figure 4-19 Effect of impact angle. Material CW. Sieve fraction: 250 - 420 microns.

BRAUER reported about an optimal impact angle of 45 degrees for rock, which he explained by the importance of shear stresses for particle breakage. MEBTOUL found that only the normal component of the impact velocity contributes to size reduction. Following the discussion about breakage criteria in paragraph 4.2.3, both findings can be true, depending on the fact whether the shear or tensile stresses are critical.

Literature review: RINKS compared opposed jet comminution and target comminution. Glass spheres were impacted on a target and brought into opposed jets at different combinations of velocities and loading factors. Results were obtained for two particle

sizes: 45 micron and 100 micron. At equal jet velocities of 235 meter per second, the target impact tests attained finer debris. A sample of 45 micron particles diminished to 24 micron by target impact and to 34 micron in an opposed jet. The size of 100 micron particles was reduced to respectively 40 micron and 90 micron. This effect was explained by the higher collision probability for target impact, which was 100 percent. The mutual collisions in opposed jets depended on the loading factor and particle velocities. Most of the energy is not effectively used and dissipated. Therefore target impact grinding should be preferred. However, size reduction by moving or static targets, such as in mechanical mills is limited to relatively coarse particle sizes. Below a size of about 20 micron particles will be decelerated and even dragged away by the streamlines around the target object.

4.5.3 Compression tests

Compression tests can be used to characterise grindability. SHIPWAY compared the results obtained from compression and impact tests. The compression tests described in this section were performed with the materials listed in Table 4-3.

Table 4-3 Sieve fractions of materials prepared for compression tests.

fraction	PS	PW	PC	NL	SL	CW	PE
0.50-0.60	x	x	x	x	x	x	x
0.60-1.00	x	x	x	x	x	x	x
1.00-1.18	x	x	x	x	x	x	x
1.18-1.70		x	x			x	x
1.70-2.00					x	x	
2.00-2.36	x				x		
3.35-4.00		x		x			

The device for the compression tests is schematically drawn in Figure 4-20.
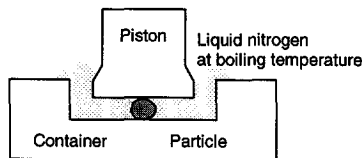
Figure 4-20 Test rig for compression experiments.

The experiments were carried out in liquid nitrogen at a temperature of minus 195.8 degrees Celsius. The mass specific breakage energy was calculated by integrating the resulting compression curves and dividing the energy by the average mass of the particles in the tested sieve fraction. The compression energy required for breakage was compared with the data determined by the impact tests. The assumptions for the interpretation of the data were

1. The tested particles were spherical

2. The particles in compression and impact tests broke into the same fractions

3. The virtual brittleness for impact (velocity effect) and compression (cooling effect) were the same

4. The impact effect in compression could be ignored, since the tests were done at low rates

Figure 4-21 presents the measured compression energies for the test materials.
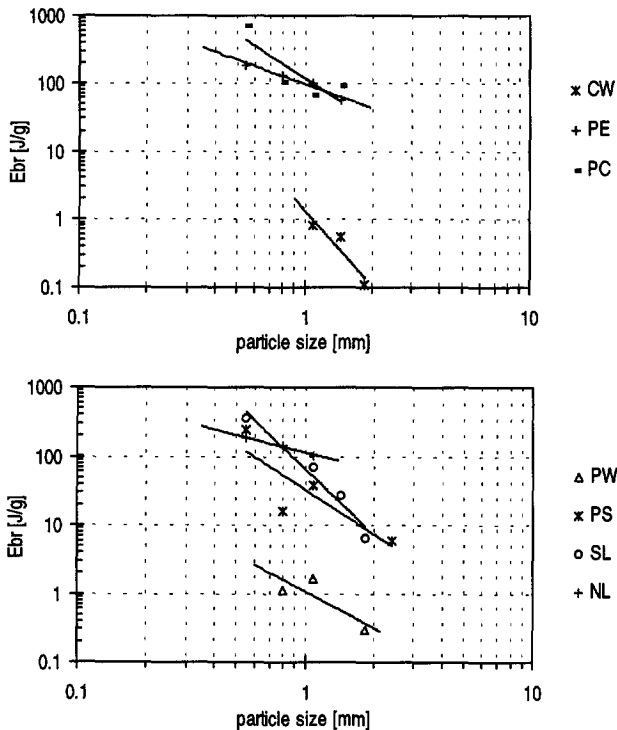
Figure 4-21 Compression tests of polymeric materials CW, PC and PE (upper plot), materials PW, PS, SL and NL (lower plot).

These plots indicated that CW and PW, commonly ground on jet mills, required relatively low energy for breakage. The other materials PC, PE, SL, PS and NL are tougher and are normally ground on mechanical mills such as rotating disc mills.

The experimental values, represented by the markers, were fitted with a power relation and the Weibull coefficient as described in paragraph 4.3.1. These lines had different

angles indicating that for larger feed sizes PW required more compression energy, while at smaller feed sizes CW started to require more energy. Nevertheless CW is far more better ground on jet mills than PW. This was assumed to be due to the high brittleness of CW compared to PW which is beneficial for the attrition process in jet mills. The parameters are listed in Table 4-4.

Table 4-4 Weibull coefficients determined by impact and compression tests.

	CW	PW	PS	PC	PE	SL	NL
impact	0.70	1.71	-	-	-	-	-
compression	0.54	1.13	0.936	0.93	1.68	0.63	2.43

A larger z-value indicates that a material is more homogeneous. A smaller variation in crack lengths will result in a narrower particle size distribution of the debris. PE and NL had the most uniform texture, while CW and SL showed a wider spread.

Description of the breakage process at the machine level adopts a statistical approach due to the complex interaction of particle properties and loading conditions. For this non-microscopic approach the behaviour of a large number of particles is described by parameterized breakage functions in population balance models. This will be the subject of Chapter 7 'Modelling'.

4.5.4 Attrition tests

Attrition is a predominant breakage mode in jet mills. Figure 4-22 shows how a cubic particle changes to a spherical particle due to attrition and looses 52 percent of its original mass.
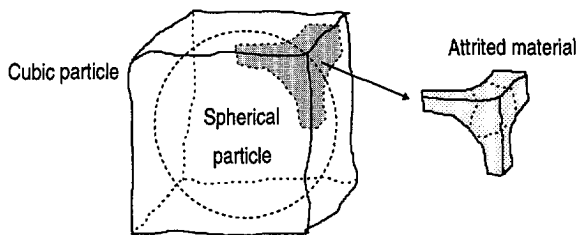
Figure 4-22 Change of particle shape from cubic to spherical as result of attrition.

The picture also illustrates how the broken edges of the particle themselves are more vulnerable to attrition due to the sharp edges.

Attrition experiments were carried out on an AFG100 opposed jet mill operated at a very low pressure of 2.0 bar. Under these conditions particle collisions were weak enough to avoid normal breakage, so they could only cause attrition. For the batch run

100 grams of polymer particles with a median size of 8 micron was placed in the mill chamber. The classifier rotor was operated at a high speed to keep the original (unbroken) particles inside the mill chamber. The fines caused by attrition could leave the mill through the rotor and were collected by a cyclone. After about 30 minutes no mass was leaving the mill, indicating that the attrition had stopped. It appeared that the median size of particles in the mill chamber had reduced to 6.5 micron. The remaining mass inside the mill was 45 grams. The collected fines had a median size of 1.2 micron. This corresponded with a reduction ratio of 6.7 for this attrition process. The results obtained with this experiments agreed with the concept based on the change of shape of particles during attrition depicted in Figure 4-22.

Remark: Attrition is a typical surface effect and extensively studied in fluidised beds by researchers such as RAY, ZENZ, BLICHINEV and YUREGIR. A stochastic analysis of attrition is given by DUGGIRALA.

4.6 Conclusions

The final performance of a mill grinding a material depends on a combination of machine, material and operation depending factors. Lab scale tests will be necessary that apply similar loading conditions to the industrial scale mills in order to characterise grindability.

The traditional empirical breakage laws do not provide practical information for the choice and the operation of mills in order to grind a specific chemical into a desired size distribution.

It is extremely difficult to characterise the grindability accurately and uniquely. Effects of cracks and other irregularities and the stochastic nature of the loading conditions particles in real mills makes an theoretical description of the breakage process not possible. Therefore the characterisation of the grinding process is based on semi-empirical and statistical equations.

The results of the off-line single particle tests gave an indication of the grindability of the test materials. The impact tests were assumed to be more reliable as the mechanisms are closer to the jetmilling process.

The impact tests are useful to characterise the breakage behaviour of relatively coarse particles. At higher impact velocities the PSD shifted to smaller sizes, while the curves showed similar shapes. In case of CW an impact angle of 70 degrees gave a finer product. The PSD of the breakage product of the impact tests showed a self-

similarity. For a impact velocity of 200 meter per second the average reduction ratio was 2.5.

Breakage parameters derived for the materials by impact and compression tests showed agreement. The Weibull coefficients for material CW and PE derived by impact were about 25 percent higher than the compression values.

For the production of very fine particles attrition tests attrition is a a pre-dominant breakage mode and is important for the description of jetmilling processes. Attrition could not be measured by the single particle breakage tests. Therefore an attrition test was set up with a small laboratory opposed jet mill operated at a very low nozzle pressure and high rotor speed. The reduction ratio for attrition was 6.7 and the attrited mass was 45 percent. These measurements corresponded with the theoretical values. However, it was not possible to quantify the attrition rate.

List of symbols

P_{max}	max. compressive stress	[N/m^2]
u	velocity	[m/s]
E	Young's modulus	[1/MPa]
k	loading parameter (1=impact, 2=compression)	[-]
x	particle diameter	[micron]
T	temperature	[° Celsius]
R	Crack resistance	[]
x	particle size	[micron]
z	material constants	[-]

Greek

α	nozzle angle	[°]
ρ	density	[kg/m^3]
γ	Poisson ratio	[//]
v	contraction	[-]
Φ	flow	[kg/s], [m^3/s]
τ	shear stress	[N/m^2]
η	viscosity	[Pa s]
σ	stress, tension	[N/m^2]
Γ	gamma function	

Indices

e	end product
a	area based
m	mass based
v	volume based
C	coarse re-circulation
i	size class

Abbreviations

RR	reduction ratio
SSA	specific surface area
ISSA	increase of specific surface area
PSD	particle size distribution

Literature

Andrews, E.H., Developments in polymer fracture-1, *Applied Sc.Publishers Ltd*, 1979

Austin, L. G., Barahona, C. A., Menacho, J. M., Investigations of autogenous and semi-autogenous grinding in tumbling mills, *Powder Technology*, vol.51(3), 283-94, 1987

Austin, L. G.; Barahona, C. A.; Menacho, J. M., Fast and slow chipping fracture and abrasion in autogenous grinding, *Powder Technol.*, vol.46(1), 81-7, 1986

Austin, L.G., Luckie, P.T., Methods for determination of breakage distribution parameters, *Powder Technology*, 5, 215-22, 1971 - 72

Barsukov, E.Y., Soskind, D.M., Jet pulverization of solid particles in fluidized bed apparatus, *int.chem.eng.*, 13/1, 84-86, 1973

Blinichev V.N., Strel'tsov V.V. , Lebedeva E.S., An investigation of the size reduction of granular materials during their processing in fluidized beds, *International chemical engineering*, 8 no 4, 615-618, 1968

Bond, F.C., Crushing and grinding calculations parts I and II, *British Chemical Engineers*, 6, 378-385; 543-548, 1961

Bouchillon, C.W., Steele, W.G., Burnett, J.D., Ultra-fine grinding of low rank coals in a fluid energy mill, *Particulate science and technology*, 7 (3), 4-5, 1989

Broek, D., Materiaalkunde 1, *college diktaat Mt1*, TU Delft, 1978

Cheng, Z., Redner, S., Scaling theory of fragmantation, *Center for polymer studies and department of physics-Boston*, 1987

Cleaver, J.A.S., Ghadiri, M., Rolfe, N., Impact testing of sodium carbonate monohydrate crystals, *Powder technology*, 76, 15-22, 1993

Dahlstrom, D.A. and Kam, W.P., Potential Energy Savings in Comminution by Two Stage Classification, *Int J Miner Process*, 22/1-4, 239-250, 1988

Dan, C.C.,Schubert, H., Breakage probability, progeny size distribution and energy utilization of comminution by impact, *7th European Symposium on Comminution, Ljubljana*, 169-178, 1990

De Silva, S.R., Gühne, H.P., Probleme der Feinmahlung von Hartmineralien und ihre Lösung, *Aufbereitungs-Technik*, 19 (1978) 10, 472-480, 1978

De Silva, S.R., Tech, B., Gühne, H.P., Fine Milling By the impact of opposed material streams the Majac Air Impact Mill, *Donaldson Europe N.V.*,

Dogan, Z. M., Autogenous grinding practice in Turkey, *DECHEMA-Monogr.*, 79(1549-1575), 297-305, 1976

Duggirala, S.K., Fan, L.T., Stochastic analysis of attrition- A general cell model, *Powder technology*, 1989

Egorov, V. P.; Blinichev, V. N.; Strel'tsov, V. V.; Guyumdzhyan, P. P., Impact grinding of single spheroidal particles of brittle materials, *Izbr. Dokl. Nauch.-Tekh. Konf. Ivanov. Khim.-Tekhnol. Inst. Meeting 1972*, 55-60, 1973

Ferry, J.D., Visocelastic properties of polymers, 3rd ed., *John Wiley & Sons Inc.*, 1980

Fuerstenau, D. W.; Kapur, P. C., A new approach to assessing the grindability of solids and the energy efficiency of grinding mills, *Miner. Metall. Process.*, 11(4), 210-216, 1994

Fuerstenau, D.W. and Kapur, P.C., Newer energy-efficient approach to particle production by comminution, *Powder Technology*, 82, Issue 1, 51-57, 1995

Gardner, R.P., Austin, L.G., A radio-active tracer technique for the determination of breakage functions, *Symposium Zerkleinern Fragmentation size reduction, Frankfurt*, , 217-231, 1962

Ghadiri, M., Arteaga, P., Cheung, W., Impact attrition of particulate solids, *Proceedings of the second congress of particle technology, Sept. 19-22 Kyoto, Japan*, 1990

Ghadiri, M., Zhang, Z., Impact attrition of semi-brittle particulate solids, *Proceedings of the fine particle society*, 8, 87-88, 1990

Griffith, A. A., The theory of rupture, *Proc. 1st Inter. Congr. Appl. Mech. Delft*, , 55-60., 1924

Häse, U., Production of finest grains by opposed jet milling, *Verfahrenstechnik (Mainz)*, 10(6), 369-378, 1976

Halbedel, B., Killat, U.K., Electro-mechanical autogenous grinding of ferrites, *Aufb.Technik.*, 34(10), 512-520, 1993

Hertz, H., Über die beruhrung fester elastischer korper, *Jl. fuer Mathematik von Crelle*, 92, 156-171, 1882

Hess, W., Schönert K., Brittle-plastic transition in small particles, *The Institution of Chemical Engineers Symposium No. 63 march 10-13*, 63, 1981

Hixon, L., Pryor, M., Prem, H., Van Cleef, J., Sizing materials by crushing and grinding, *Chemical Engineering*, , 94-104, 1990

Honma, T., Grinding probability in jet milling. Possibilities of preferential selective pulverization accompanied by autogenous grinding, *Yamagata Daigaku Kiyo, Kogaku*, 22(1), 1-9, 1992

Honma, T.; Hasegawa, M.; Kanda, Y., Jet pulverization using grinding medium, *J. Chem. Eng. Jpn.*, 15(3), 240-242, 1982

Honma, T.; Hasegawa, M.; Kanda, Y., Effects of feed particle shapes on jet pulverization, *J. Chem. Eng. Jpn.,* 17(2), 221-3, 1984

Hull, D., Nucleation and Propagation processes in Fracture, Ch.9, Polymeric Materials, Relationships between Structure and mechanical Properties, *book,* 1973

Huwald, E., Clements, M., Mahlung und verschleiss in einer Gegenstrahlmühle, *Chem.Ing.Techn.,* 47nr 299, 216/75, 1975

Jimbo, G., New pulverization technology for preparation of ultrafine particles, *Kagaku Gijutsushi MOL,* 21(1), 40-5, 1983

Joisel, A., Dechema, Zerkleinern Symposium, 49, 1962

Kapur, P.C., Self-preserving Size Spectra of Comminuted Particles, *Chemical Engineering,* 27, 425-431, 1972

Karna, A., Studies of pressurized grinding, *Dissertation,* 1984

Karvinen, R., Kauramaki, T., Nieminen, P., Grinding Principle and Experiences with a new type of opposed jet mill, 3-2, 123-128, 1991

Kendall, K., The impossibility of comminuting small particles by compression, *Nature, 20 April,* 272, 710-711, 1990

Kendall, K., McAlford, N., Birchall, J.D., Elasticity of Particle Assemblies as a measure of the Surface Energy of Solids, *Proc.R.Soc.Lond. A,* 412, 269-283, 1987

Kienzler, R., Schmitt, W., On Single particle comminution: Numerical analysis of compressed spheres, *7th European Symposium on Comminution, Ljubljana,* 149-158, 1990

Kihlstedt, P.G., The relationship between particle size distribution and specific surface in comminution, *Symposium Zerkleinern, Frankfurt,* 205-216, 1962

King, R.P., Bourgeois, F., Measurements of fracture energy during single particle fracture, *Minerals engineering,* 6-4, 353-367, 1993

Kono, H., Attrition rates of relatively coarse solid particles in various types of fluidized beds, *AIChE Symp.series,* 77 (1981), 205, 96-106, 1981

Kusters, K.A., Pratsinis, S.E., Ultrasonic fragmentation of agglomerate powders, *Chem.eng.sc.,* Nov. 1992

Lecoq O.; Mebtoul, M.; Chouteau, N.; Guigon, P., Characterization test of grindability of different granular materials, *Recents Prog. Genie Procedes, Procedes de Broyage,* 10(45), 31-36, 1996

Leitel, E.; Heinicke, G.; Paudert, R., Changes in the porosity of some metal oxides after jet and vibratory ball milling, *Z. Chem.,* 10(4), 157-158, 1970

Leschonski, K., Matsumara, S., A single impact against a solid wall as a basis for impact grinding, *7th European Symposium on Comminution, Ljubljana,* , 211-223, 1990

Leschonski, K., Menzel, U., Experimental investigations on single plate fluid energy milling, *preprints 1st world congress particle technology, Nurnberg,* part 2, 297-323, 1986

Leschonski, K.; Menzel, U., Possibilities and limits of impact-plate jet milling, *Freiberg. Forschungsh. A,* 778, 53-75, 1988

Lewandowski, M., Milling in air-pressure centrifugal mills, *Inz. Apar. Chem.,* 14(1), 24-7, 1975

Liu, J., Schönert, K., Modelling of interparticle breakage, *8th European Symposium on Comminution, Stockholm,* , 102-115, 1994

Lowrison, G.C., Crushing and grinding; The size reduction of solid materials, *Chemical engineering series,* 1974

Manne, F.; Benhassaine, A., Micronic grinding with air jet as engineering unit process, *Recents Prog. Genie Procedes, Genie de l'Elaboration des Materiaux,* 7(28), 163-8, 1993

Mebtoul, M., Etude du broyage fin au moyen d'un test d'impact a garnde vitesse. Aplication aux broyeurs a jets d'air, *PhD-thesis,* 1995

Mebtoul, M.; Large, J. F.; Guigon, P., High velocity impact of particles on a target - an experimental study, *Int. J. Miner. Process.,* 44-45, 77-91, 1996

Mebtoul, M.; Large, J. F.; Guigon, P., Very high-velocity impact of alumina particles on a target. Modeling of a   jet mill, *Recents Prog. Genie Procedes , Etudes et Conception d'Equipements,* 7(30), 207-12, 1993

Menyhart, M., Miskiewicz, L., Comminution and structural changes in a jet mill, *Powder Technology,* 261-266, 1976

Menyhart-Kocsis, M.; Miskiewicz, L., Changes in structure of materials after grinding in jet mill, *Int. Congr. Chem. Eng., Chem. Equip. Des. Autom., [Proc.], 5th Congr. CHISA, Prague, Czech.,* C, 12 pp., 1975

Middlemiss, S., King, R.P., Microscale fracture measurements with application to comminution, *8th European Symposium on Comminution, Stockholm,* 57-69, 1994

Mohanty, B., Narasimhan, K.S., Fluid energy grinding, *Powder Technology,* 33, 135-141, 1982

Müller, H., Weichert, R., Probability of breakage of particles in compression tests under single particle and packed bed conditions, *7th European Symposium on Comminution, Ljubljana,* 159-167, 1990

Nakashige, Akira; Kamino, Yoshitaka; Sodeyama, Kenichi; Tabata, Ichiro, Fine pulverization of Shirasu, *Kenkyu Hokoku - Kagoshima-ken Kogyo Gijutsu Senta,* 6, 21-4, 1992

Nakayama, N., Pulverizing of various Materials by Super-Sonic Jet Mill, *Bulk Solids Handling,* 6-1, 157-160, 1986

Occella, E., Effect of the nature of the rock on the grinding particle-size distribution products, *DECHEMA-Monogr.,* 57(993-1026), 847-66, 1966

Ocepek, D., Problems in colloidal grinding of nonmetallic materials, *Rud.-Metal. Zb.,* 3, 281-5, 1966

Okuda, S., The grinding mechanism in a fluid energy mill and its similarity to secondary nucleation, *Ind. Cryst., [Proc. Symp. 1975],,* 6th, 67-76, 1976

Okuda, S., Choi, W.S., Grinding characteristics of polymeric materials by target type fluid energy mill, *5th European Symposium on Comminution,* , 171-183, 1980

Okuda, S., Choi, W.S., Fracture characteristics of single particle of polymeric materials under impact loading, *Journal of chemical engineering of japan,* 12-5, 383-388, 1979

Okuda,S., Choi, W.S., Grinding characteristics of target type fluid energy mill, *J.Chem.Eng.Japan,* 13-3, 219-225, 1980

Owe Berg, T.G., Avis, L.E., Exploratory experiments on kinetics of comminution, *Powder Technology,* 1970 -71

Pebworth, J.T., Selecting mills for heat-sensitive materials, *Solids handling magazine, section III processing,* August, 193-200, 1972

Pitchumani, B., Ramanujam, M., Venkateswarlu, D., Fluid energy mill: Statistical analysis of performance, *Particle Technol.,* 1971

Prasher, C.L., Crushing and grinding, process handbook, 1987

Rajendran Nair, P.B., Ramanujan, M., Circular fluid mill, *TIZ International Powder Magazine,* 114-10, 1990

Ramanujam, N., Venkateswarlu, D., Studies in fluid energy grinding, *Powder Technology,* 3, 92-101, 1969 -70

Ranguis, I.; Pineau, J. L.; Blazy, P., Grindability of gibbsite during grinding in a mill with opposed air jets, *Mines Carrieres: Tech.,* 4-5, 147-58, 1993

Ratcliffe, A., Crushing and Grinding, *Solids Handling, section III processing,* 1972

Ray, Y.C., Jiang, T.S.,Wen, C.Y., Particle attrition phenomena in a fluidized bed, *Powder Technology,* 49, 193-206, 1987

Rumpf, H., Beanspruchgungstheorie der Prallzerkleinerung, *Chem.Ing.Techn.,* 31-5, 323-337, 1959

Rumpf, H., Versuche zur Bestimmung der Teilchenbewegung in Gasstrahlen und des Beanspruchungsmechanismus in Strahlmühlen., *Chem.Ing.Techn.,* 38-5, 335-342, 1960

Rumpf, H., Prinzipien der Prallzerverkleinering und ihre Anwendung bei der Strahlmahlung, *Chem.Ing.Tech. (api bieb),* 32-3, 129-135, 1960

Ruppel, P. , Brauer, H., Comminution of single particles by repetitive impingement on solid surfaces, *1st world congress Particle Techn. comminution,* 2, 1986

Sankara Narayanan S., Single particle breakage tests: a review of principles and applications to comminution modelling, *Bull. Proc. Australas. Ins. Min. Metall.,* 291 no. 4, 49-58, 1986

Schönert, K., Physical and technical aspects of very and micro fine grinding, *2nd world congress particle techn., Kyoto, Japan,* 257-271,

Schönert, K., Advances in communition fundamentals and impacts on Technology, *Aufbereitungs-Technik,* 32-9, 487-494, 1991

Schönert, K., Weichert, R., On the temperature rise at the tip of a fast running crack, *Journ.Mech.Phys.Solids,* vol.22, 127-133, 1971

Shipway, P.H., Hutchings, I.M., Attrition of brittle spheres by fracture under compression and impact loading, *Powder Technology,* 76, 23-30, 1993

Skelton, R., Kayyat, A.N., Temple, R.G., An investigation of micronizer performance, design and operational parameters, *Eur. Symp. Particle Technology,* 1980

Smit, W.A.J., Air milling of heat sensitive materials, *first world congress particle technology, Nuerenberg,* , 1986

Steiner, H.J., The significance of the Rittinger-equation in present-day comminution technology, *xvii intern. mineral processing congress, dresden,* 1, 177-188, 1991

Stiess, M., Schönert, K., Dehnungen und spannungen in der oberflache gedruckter PMMA Kugeln, *Coloid & polymer Sci.,* 252, 743-748, 1974

Timoshenko, S., Goodier, J.N., Theory of Elasticity, 3rd ed., 1969

Tornery, M., Verney, S., Le broyeur a jets alternes a lit fluidise, *L'industrie ceramique,* 855, 830-833, 1990

Vanangamudi, M.; Ramanujam, M., Fluid energy milling, *Chem. Eng. World,* 13(6), 41-50, 1978

Veldkamp, J. D. B., A description of jetmilling in terms of plastic deformation and fracture, *EFCE Publ. Ser., 5th European Symposium Particle Technology. A'dam,* 7(PT A), 399-409, 1980

Vervoorn, P.M.M., Austin, L.G., The analysis of repeated breakage events as an equivalent rate process, *Powder Technology,* 63, 141-147, 1990

Vervoorn, P.M.M., Hoekstra, J.K., Scarlett, B., Particle impact testing, *7th European Symposium on Comminution, Ljubljana,* 195-209, 1990

Volker, W., Fine grinding of hard-to-grind products, *DKV-Tagungsber.,* 15(1), 41-59, 1988

Volker, W., Horschkes, S., CMS-Technik ermoglicht Cryogen Feinstmahlen, *Gas Aktuell,* 40

Weichert, R., Theoretical prediction of energy consumption and particle size distribution in grinding and drilling of brittle materials, *part.part.syst.charact,* 8, 55-62, 1991

Yashima S., Kanda Y., Sano S., Relationships between particle size and fracture energy or impact velocity required to fracture energy or impact velocity required to fracture as estimated from single particle crushing, *Powder Technology,* 51, 277-282, 1987

Young, R.J., Lovell, P.A., Introduction to Polymers, 1991

Yuregir, K.R., Ghadiri, M., Clift, R., Impact attrition of sodium chloride crystals, *Chemical engineering science,* 42-4, 843-853, 1987

Yuregir, K.R., Ghadiri, M., Clift, R., Observation of impact attrition of granular solids, *Powder Technology,* 49, 53-60, 1986

Zenz, F.A., and Kelleher, E.G., Studies of attrition rates in fluid-particle systems via free fall, grid jets and cyclone impact, *Journal of powder and bulk solids technology,* 4 (2/3), 13-20, 1980

Chapter 5

Air classification

In paragraph 5.1 the motivation is given for the use of classifiers in grinding plants. Paragraph 5.2 describes the various operating principles of air classifiers. Paragraph 5.3 deals with the classifiers used in this project. In paragraph 5.4 two methods are discussed to express the classifier performance, while paragraph 5.5 handles the processing of experimental classifier data. Paragraph 5.6 presents the test results. Finally conclusions are given.

5.1 Introduction

5.1.1 Definition of classification

Classification is a process unit operation that divides particles into discrete fractions on the basis of a shared property. In industrial classifiers this property is mostly size, but it can also be another characteristic of the particle such as shape or density. The feed is normally separated into two flows, called the coarse flow and fines flow. Some types of classifiers, as will be shown later, are able to produce multiple fractions.

5.1.2 Purpose of classifiers in grinding plants

Air classifiers are used in grinding plants for the following reasons:

1. *More accurate control of the particle size distribution* of the grinding product as the internal classification of the mill is often not sufficient. Mostly a specific aspect of the PSD is to be controlled, such as the top size or the specific surface area. New applications, such as toner materials, printing inks and pigments, ask

better defined and more specific distributions which can not be achieved with mills directly, or can be very costly and inefficient.

2. *Optimisation of grinding plants.* Each mill posses its own internal classification keeping a selected part (merely coarse particles) of the hold-up, whilst discharging the fines. However, the optimal conditions inside the mill for comminution and classification often do not coincide. Thus tuning the optimal grinding performance can be a dilemma. In such circumstances an external classifier is useful, because the comminution process can be optimised for size reduction without producing off-spec material [DAHLSTROM, USUI].

5.1.3 Classification of dry powders

In the classification of dry powders two techniques are used. The first group, sieves are commonly used, but they have the following limitations:

1. Very large quantities cannot be handled (up to several tonnes per hour).

2. Below 100 microns the separation becomes unacceptably poor.

3. Irregularly shaped particles cause problems.

4. Sensitivity to moisture.

Figure 5-1 shows the typical ranges of application as presented by SENDEN. Separation trials were made with particles down to one micron by SUGANUMA and ZHANG.
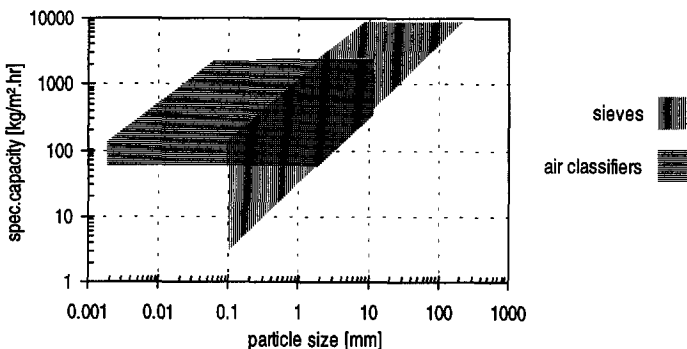

Figure 5-1 Application ranges of sieves and air classifiers. After Senden.

Air classifiers are preferred for the situations where the performance of sieves becomes poor. Furthermore it is advantageous to use air classifiers in combination with air swept mills as an air flow is already available and the product remains well dispersed, thus avoiding agglomeration problems.

5.2 Theory

5.2.1 Forces acting on particles

The working principle of the air classifiers is based upon the different trajectories of the particles moving through the classifier caused by the forces that the particles experience in the flow field inside the classifier. These forces can be due to the interaction of the particle with the fluid such as drag or dynamic buoyancy, and are roughly proportional with the square of the particle diameter. Another category are the field forces like gravity and inertia. The latter are typically proportional to the volume of the particle. DE SILVA [1981] listed the forces that can act on particles in a fluid flow.

Other forces that can occur in classifiers are caused by particle-particle interaction, wall collisions and electric or magnetic charging [ANDRES]. Generally these forces have a negative effect on the classifier performance, but they can also serve as a driving force for separation.

5.2.2 Types of air classifiers

The driving force for separation in most air classifiers is created by a sudden change of the direction of an air flow containing the particles. Differently sized particles tend to follow a trajectory different from the air flow due to inertial or centrifugal forces. LESCHONSKI categorised air classifiers in two groups with regard to the flow field.

1. Cross flow classifiers

2. Centrifugal classifiers

Cross flow air classifiers: In this type of classifier the particles move perpendicular to the direction of the main air flow. Typical examples are the GONELL [1928] classifier and the Zig-zag classifier investigated by SENDEN [1979]. The application range of these systems typically lies above 100 microns.

Another example, actually a semi-cross flow type, is the Coanda classifier originally developed by RUMPF and LESCHONSKI [1967]. This classifier, also called Elbow Jet air classifier is shown in Figure 5-2. The working principle is based on the Coanda effect which describes how a freely flowing jet-stream in the vicinity of a curved surface tends to flow along that surface.
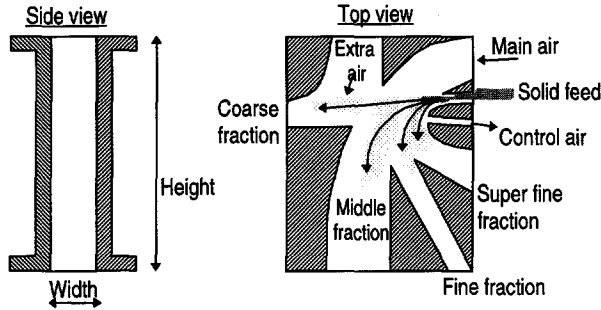
Figure 5-2 Schematic representation of the Elbow jet air classifier. The Coanda principle.

Small particles will be able to follow the curved flow whilst larger particles will be less affected by the Coanda effect and follow straighter trajectories due to their inertia. Tuning of the air flows and repositioning of the internal blocks of the classifier gives another classification performance.

The smallest unit, with a capacity of 50 kilograms per hour requires an airflow of 420 normal cubic meters per hour. A jet mill with a comparable capacity uses approximately 300 normal cubic meters per hour. The large air flows of these classifiers makes them attractive for use in combination with air swept mills. Throughputs up to 2000 kilograms per hour can be achieved with the largest models with an air consumption of 6000 normal cubic meters per hour and with a corresponding power consumption of 120 kilowatt.

Besides the fact that this classifier does not contain moving parts, it has the advantage of producing more than two fractions in one unit operating step. The finest fraction has a narrow particle size distribution with a median size below 5 microns.

Centrifugal air classifiers: The second group of classifiers make use of a rotational flow field or vortex. Small particles will find an equilibrium at small radii where the flow is moving into the overflow. Coarse particles will stay on large radii, in the downward flow, and finish in the under-flow. The radial velocity of a vortex stream depends on the air flow to the central outlet.

For a cylinder classifier section with height h the radial velocity, v_r, at a distance r from the central outlet is given by

$$v_r = \frac{\Phi_{air}}{2\pi hr} \qquad\qquad (5.1)$$

The tangential velocity, v_t, varies over the radius according to

$$v_t = \frac{const}{r^n}$$ *(5.2)*

Figure 5-3 shows the working principles of rotational classifiers.
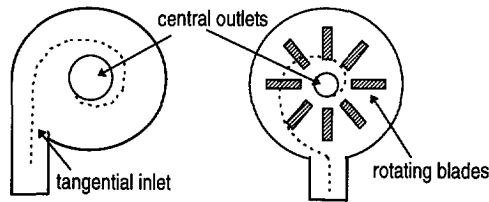
Figure 5-3 Schematic representation of a free vortex and forced vortex classifier.

Based on the nature of the rotating flow design air classifiers are categorised into

1. *Free vortex classifiers (n=+1)*: The rotation is created by the tangential direction of the air inlet or in some models by static vanes. The force of the vortex is determined by the airflow. Towards the central outlet the tangential velocity drops gradually described by equation 5.2 for *n~1*. The hold-up of mass in the classifier slows down the vortex and leads to an increased cut-size. The LaCad-Oy classifier used in this project is based on this principle.

2. *Forced vortex classifiers (n=-1)*: The tangential velocity is determined by the angle velocity of the rotating blades and remains constant in a radial direction. Forced vortex classifiers are less sensitive to loading until a transition point were the dense particle bed is squeezed through the vanes. Then the cut size drops sharply.

Comment 1: In a free vortex classifier particles can form stabilised trajectories in certain zones depending on their size, which leads to unstable vortices. Particles in a forced vortex either leave the central outlet or are transferred to the outer wall of classifier.

Comment 2: True forced vortex classifiers do not exist as the forced vortex only continues between the vanes. Outside the rotating vanes the flow changes into a so-called mixed vortex flow (*n=0.5*).

Flow patterns in air classifiers: Design of classifiers requires a detailed knowledge of the velocity profiles in the classifier body. The scale-up of cross flow classifiers is relatively simple as the flow field is two-dimensional. For example in the case of the Coanda classifier, this is a matter of changing the width of the unit (see Figure 5-2).

The scale-up of centrifugal classifiers is generally more complicated. The capacity of the classifier is related to the dimensions of the inlet and outlet cross sections, while the separation performance depends on the diameter of the rotor or classifier body. Larger classifiers have more difficulty with the separation of fines.

The equilibrium orbit theory, which was originally proposed by DRIESSEN AND CRINER, stated that there exist particles on which the centrifugal and drag forces are in balance. A number of analytical classifier models were developed and described in the literature by MOTHES, LÖFFLER, DIETZ, LEITH AND LICHT. In reality the particle demonstrates a random movement, due to turbulence and particle interactions. Models have been proposed to include this stochastic behaviour [MOLERUS].

Numerical simulations of the flow pattern and particle trajectories in air classifiers were carried out by JOHANSEN. Initially simplified descriptions of flow fields and the calculation of particle trajectories were used, assuming no turbulence, particle-particle or particle wall interaction. With increasing computer power and improving computational fluid dynamics software these phenomena can be included in the simulations.

5.2.3 Installation in grinding plant

Classifiers can be implemented in a grinding plant in alternative ways. Examples of typical flow-sheets are presented in Figure 5-4.
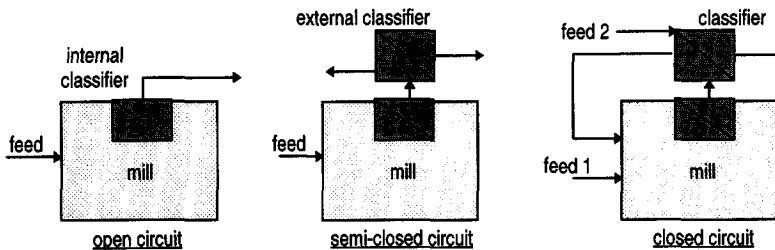
Figure 5-4 Schematic representation of grinding circuits.

Open circuit operation: A stand-alone mill, without an external classifier is said to be operating in a open circuit configuration. The internal classification of the mill itself determines directly the particle size distribution of the mill product. The tuning for optimal classification performance often does not coincide with the tuning for most efficient grinding.

Semi-closed circuit operation: In this plant configuration an external classifier is connected to the mill outlet. This mode is particularly interesting when more grades

are desired. The fines are collected as an end product, grade A. Grade B is collected at the coarse outlet.

Closed circuit operation: Two configurations are commonly used in industry [DE SILVA]:

1. In the *forward mode* the solid feed is brought into the mill at point 1 (see Figure 5-4). This mode is most useful if the top size control in the product is an important criterion. The product quality is independently controlled by the external classifier. A disadvantage is the passage of fine through the mill causing unnecessary loading. The coarse fraction from the classifier is recirculated to the mill.

2. The *reverse mode* is chosen when the fresh feed already contains a considerable amount of in-spec particles (feed 2, Figure 5-4). The fines are removed from the fresh feed to the mill, allowing a more efficient grinding operation. The PSD of the end product is narrower due to better internal classification. Pregrinding may be an option to increase the fines content of the raw feed.

An option to improve the product specification is the use of a multistage mill-classifier plant, similar to the concept of distillation columns. Different grades can be produced in a continuous process.

5.3 Characterisation of classifier performance

In the literature many universal models have been described to predict classifier performance in practice. They are based on the description of size dependent particle trajectories in the internal flow field of the classifier. Due to complex flow patterns in real classifiers, the influence of irregularities in particle properties and measurement errors such general models are not able to give a reliable output, although they give insight into the working and provide rough scale up rules.

In order to obtain more realistic predictions, test classifications would give more useful information, made under a known set of operating conditions [FEGAN]. In this case, the classifier performance was described by semi-empirical equations. This experimental grade efficiency curve is one way of evaluating classifier performance. However, it should be used with caution, especially when comparing different materials and using different measurement techniques.

5.3.1 Expressions for classifier efficiency

Air classification is a unit operation in which the feed particles, Φ_F, dispersed in air are selectively divided over a coarse flow, Φ_C, and a fines flow, Φ_f.
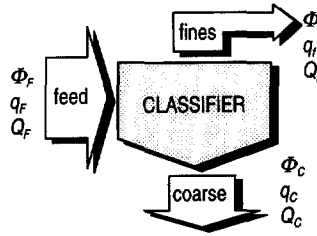
Figure 5-5 Mass flows and particle size distributions of the solids entering and leaving the classifier.

The mass balance for each particle size x can be written as

$$\Phi_f \cdot q_f(x) + \Phi_c \cdot q_c(x) = \Phi_F \cdot q_F(x) \qquad (5.3)$$

where $q(x)$ and $Q(x)$ represent the density and cumulative weight distributions of the flows respectively, whilst Φ is the flowrate in kilograms per hour.

The overall *mass efficiency*, η_o, gives the ratio between the coarse and the feed flow.

$$\eta_o = \frac{\Phi_c}{\Phi_F} \qquad (5.4)$$

The classifier efficiency per size class is traditionally expressed by the *Tromp-curve*, which is defined as the recovery of particles in the coarse flow.

$$T(x) = \eta_o \frac{q_c(x)}{q_F(x)} \qquad (5.5)$$

The grade efficiency defined in this way describes how efficiently a given particle size is recovered from the feed flow and taken up by the coarse flow. Therefore the Tromp curve is important for analysing the operation of closed circuit grinding plants.

As the Tromp curve depends upon the mass flows and the particle size distributions of both the feed and the product, this function does not express the improvement of the product quality compared to the feed quality. For this purpose the *Treasure-curve* is more useful as it plots the PSD of the feed flow, Q_F, against the PSD of the coarse flow, Q_c, and the fines flow, Q_f.

Both types of efficiency curves and their construction from experimental data are illustrated in Figure 5-6.
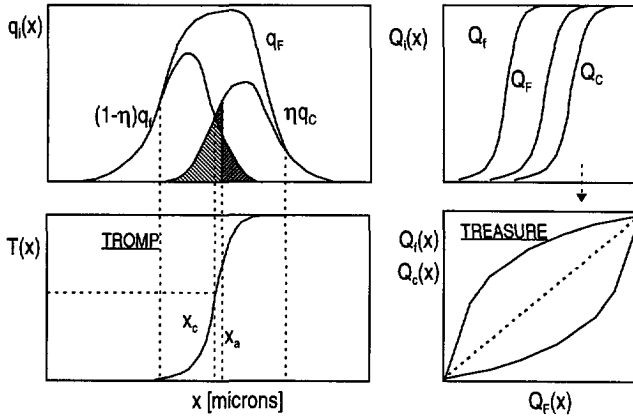
Figure 5-6 Construction of classifier curves. Tromp (left) and Treasure (right).

The use of the Treasure curve is discussed in more detail in Paragraph 5.5.5.

5.3.2 Classification parameters

The *cutsize*, x_c, of a classifier is the operating condition at which a particle with this size has a fifty percent probability to leave through either the coarse or the fines outlet. Mathematically the cut-size is defined as the median value of the Tromp curve.

$$\frac{q_F(x_{cut})}{2} = \eta \cdot q_c(x_{cut}) = (1-\eta) \cdot q_f(x_{cut}) \qquad (5.6)$$

Inside the classification zone the separation conditions vary for the individual particles due to stochastic disturbances. This implies that the effective value of the separation cut point varies too. RUMPF [1972] pointed out that $T(x)$ can be interpreted as being the cumulative distribution function of separation cut points.

Imperfection (I): In the case of ideal classification the Tromp curve would be a straight vertical line through the x_c value on the horizontal axis. In practice classifier performance mostly shows a spread around the cut point which gives the Tromp curve its characteristic S-shape. A commonly used parameter to express the sharpness of classification is the imperfection I, which is defined as

$$I = \frac{x_{T75} - x_{T25}}{2 \cdot x_{cut}} \qquad (5.7)$$

where x_{T75} is the particle size that has 75 percent chance of reporting to the coarse outlet.

The *top-size*, x_t, defined as the largest particle size present in the fines flow, is an important quality parameter for industry when the fines flow is the end product. Pilot plant experiments showed that the classifier throughput decreased sharply with slight decreases of the top-size. A $Q(15)=100\%$ corresponded with a capacity of 6.8 kilograms per hour, whilst a $Q(20)=100\%$ allowed a classifier feed of 15.3 kilograms per hour. This sensitivity was due to the asymptotic curvature of the grade efficiency at the coarse end of the particle size range.

Finally it should be realised that the accurate determination of the Q=100% value is very difficult. Laser diffraction particle sizers are not capable of detecting small amounts of coarse particles present in a powder sample with the standard software as was illustrated in Chapter 3. Modifications of the instrument software by correlating the fluctuations on sensor rings can be used to count the coarse particles present in the product flow. Nowadays in industry sieves (e.g. air swept sieves) are often used to determine the topsize of a product. Sieve analyses must be interpreted with care because of shape effects.

5.3.3 Dead flux

The separation efficiency defined in the previous paragraph assumes no short-circuiting in the classifier. In practice a part of the product flow is sometimes not affected by classification leaving directly through the coarse or fine outlet. This effect is known as dead flux, R_d.

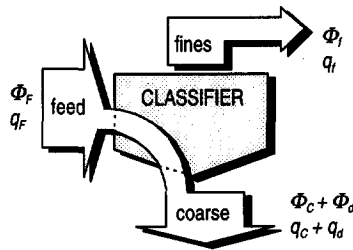*Figure 5-7 Dead flux: Part of the feed flow is not affected by the classifier action and directly passed to the coarse outlet.*

In this case the mass balance for each size class has to be extended to

$$\Phi_f \cdot q_f(x) + \Phi_c \cdot q_c(x) + \Phi_d \cdot q_d(x) = \Phi_F \cdot q_F(x) \qquad (5.8)$$

MAYER proposed to correct the Tromp-curve as follows.

$$T^*(x) = \frac{(T(x) - R_d)}{(1 - R_d)} \qquad (5.9)$$

A corrected grade efficiency curve lies between from 0.0 and 1.0. Normalised by the corrected cut-size this Tromp curve is assumed to be scale and device independent.

In the case of total by-pass the corrected separation efficiency will be zero. For a complete separation the value will be unity. A description about the performance of classifiers is given by HEISKANEN.

5.3.4 Statistical model

PLITT used the following equation to fit experimental classifier data.

$$T(x) = 1 - \exp\left(-0.693\left(\frac{x}{x_{cut}}\right)^m\right) \qquad (5.10)$$

The Plitt function was used to describe the operation of the free vortex classifier in the dynamic model of the closed loop grinding plant in Chapter 7. The parameters were determined from the experimental data of the LCC20 classifier in the pilot plant.

5.4 Classifiers used in this project

5.4.1 LCC20 free vortex air classifier

In Figure 5-8 the implementation of the LCC20 classifier in the grinding plant is illustrated. The product leaving the 10-inch spiral jet mill in the pilot plant contained fine particles dispersed in air. In the closed circuit plant configuration the powder flow entered the LCC20 air classifier.

This free vortex classifier built by LaCad Oy is in principle a high efficiency cyclone, with several extra features. The first one is the addition of control air to the main product inlet. The second extra feature is the supply of washing in the lower section of the classifier for the recovery of fines from the re-circulating flow. Finally two adjustable internals, the cone and the cylinder, direct the flow patterns inside the classifier body.

Small particles in the mill product are separated in a vortex flow field and dragged to the classifier outlet. These fines are collected in the bag filter as the end product. The coarse particles settle on the classifier wall and move downwards. A rotary valve brings the underflow back to the jet mill for regrinding.
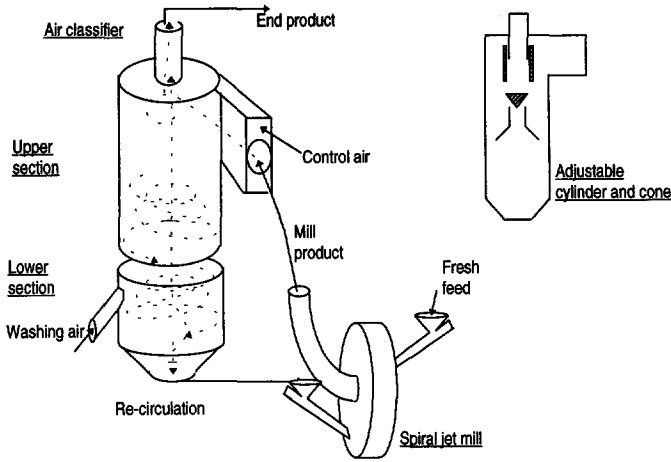
Figure 5-8 Two stage free vortex classifier. Model LCC20.

The lower section of the classifier works as a fines recovery step by adjusting a washing air flow that re-disperses the particles. The fines are carried upwards in a fluidised bed to the upper section by a chute and added to the upper section for re-classification [OVASKAINEN].

5.4.2 ATP classifier unit incorporated in AFG mill

The AFG opposed jet mill that was used for tests contains a classifier rotor with a diameter of 315 millimetre and the height of 187 mm. The number of vanes is 60. The lay-out is presented in Figure 5-9.
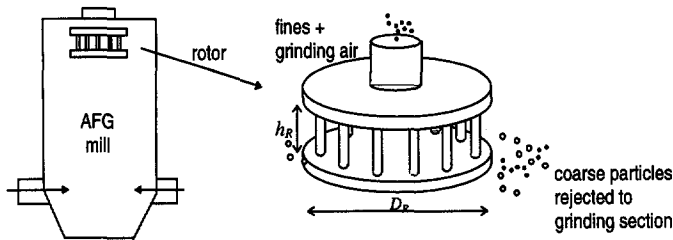
Figure 5-9 Classifier rotor in top section of opposed jet mill.

The particle bed in the bottom section of the AFG630 opposed jet mill is continuously hits by the jets. The expanded grinding air carriers the particles to the top section where fines are dragged by the air through the rotor vanes. Coarse particles are rejected by the centrifugal forces and taken downwards by a circulation flow in the mill chamber. A more detailed description about this classifier can be found i

The cut-size, which is related to the rotor speed and the amount of grinding air, can be calculated using the equations for the drag and centrifugal forces on a particle. The air flow is a function of the nozzle pressure and the nozzle diameter.

When the centrifugal forces are in equilibrium with the drag forces a particle has an equal chance of leaving through the outlet classifier, or of being rejected into the fluidized bed. In formula:

$$\frac{1}{2} C_D \rho_f v_r^2 \frac{\pi}{4} x^2 = \frac{\pi}{6} x^3 \rho_s a_c \qquad (5.11)$$

Substitution of the Reynolds number for the transition range gives

$$a_c = \left(2\pi N_R\right)^2 \tfrac{1}{2} D_R , \; v_r = \frac{143 \cdot n_n \cdot d_n^2 \cdot P_n}{\left(\pi D_R\right) h_R} \quad \text{and} \quad C_D = 18.6 \cdot \left(\frac{\rho_f v_r x}{\eta_f}\right)^{-0.6}$$

Based on this concept the cut-size of the classifier rotor can be estimated from the operating set-points and the classifier geometry by

$$x_{cut} \propto \left(\frac{\eta_f^{0.375} \rho_f^{0.25}}{\rho_s^{0.625}}\right)\left(\frac{P_n^{0.875}}{N_R^{1.25}}\right)\left(\frac{d_n^{1.75} n_n^{0.875}}{D_R^{1.5} h_R^{0.875}}\right) \qquad (5.12)$$

The first term contains the material properties, the term in the middle represents the operating variables and the third term contains the design parameters of the opposed mill.

5.4.3 Acucut forced vortex classifier

Experimental set-up: The Acucut A12 is a forced vortex classifier built by Mikropul. The flat cylindrical body contains a rotor with a diameter of 300 millimetres and a height of approximately 25 millimetres. Experiments were carried out with this classifier as a stand-alone unit, as well as in combination with a 6-inch spiral jet mill. The latter configuration is shown in Figure 5-10.
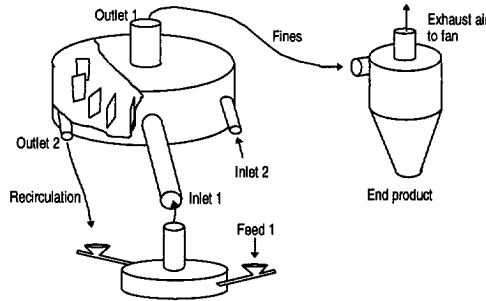
Figure 5-10 Acucut A12 used in combination with 6-inch spiral jet mill

During normal use of the Acucut, without the jet mill connected, the feed enters the classifier at the periphery through inlet 1 which is in the radial direction. Rotating vanes mounted between two discs create a forced vortex flow field. The space between the outer edge of the wall and the periphery of the rotor forms the classification zone. The fines leave through the central outlet, while coarse particles exit through outlet 2. Inlet 2 is normally used for the recirculation of product. This type of classifier was extensively investigated by DE SILVA.

5.5 Processing of classifier data

5.5.1 Choice of the sampling points

The separation curves described in the previous sections can be determined in different ways by relating the mass-flows and the particle size distributions of the feed, the over and under flows. Figure 5-11 contains typical experimental data from the LCC20 free vortex classifier.
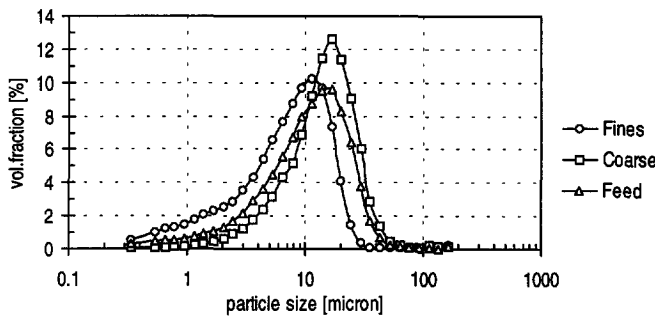
Figure 5-11 Volume fractions of the feed, coarse and fines flows. LCC20 air classifier. Mass flows: $\Phi_F = 19.0$ kg/hr; $\Phi_C = 12.02$ kg/hr; $\Phi_f = 6.98$ kg/h.

5.5.2 Calculation of Tromp curve

In this section three methods will be investigated to determine the Tromp-curves.

Method 1: Sampling of coarse flow and feed flow

$$T_1(x) = \eta_M \cdot \frac{q_c(x)}{q_F(x)} \qquad\qquad (5.13)$$

Method 2: Sampling of feed and fines flow

$$T_2(x) = 1 - (1 - \eta_M) \cdot \frac{q_f(x)}{q_F(x)} \qquad\qquad (5.14)$$

Methods 3: Sampling of fines and coarse flow

$$T_3(x) = \left[1 + \left(\frac{1}{\eta_M} - 1\right)\frac{q_f(x)}{q_c(x)}\right]^{-1} \qquad (5.15)$$

The Tromp-curves determined with these methods are shown in Figure 5-12 based on data of Figure 5-11. A significant off-set with the horizontal axis was found, which indicated a dead flux.
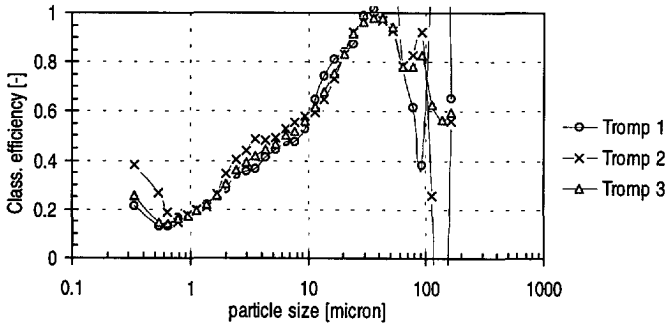
Figure 5-12 Tromp curves calculated with the methods 1,2 and 3.

Furthermore the separation curves show large fluctuations at the coarse end of the operating range that are a result of measurement and sampling errors. The different calculation methods amplify these errors in a specific way as will be discussed in the next section.

The Tromp curve is a good way of characterising classifier recovery, but it does not give any information about the quality and quantity of feed and product streams.

5.5.3 Error estimation of Tromp curve

At the coarse end of Tromp-curves large fluctuations are often found, which are a result of stochastic errors in the PSD and mass flow measurements. The sensitivity of the error in the T-curve (reliability) for inaccuracies of the absolute mass fractions can be calculated by taking the first derivative of the T-function.

$$\Delta T_1(x) = \frac{q_c(x)}{q_F(x)}\Delta\eta_M + \frac{\eta_M}{q_F(x)}\Delta q_c(x) + \frac{\eta_M \cdot q_c(x)}{q_F^2(x)}\Delta q_F(x) \qquad (5.16)$$

$$\Delta T_2(x) = \frac{q_c(x)}{q_F(x)}\Delta\eta_M + \frac{1-\eta_M}{q_F(x)}\Delta q_f(x) + \frac{(1-\eta_M)\cdot q_f(x)}{q_F^2}\Delta q_F(x) \qquad (5.17)$$

$$\Delta T_3(x) = \left[1 + \left(\frac{1}{\eta_M} - 1\right)\frac{q_f(x)}{q_c(x)}\right]^{-2} \cdot$$

$$\left\{\frac{1}{\eta_M^2}\frac{q_f(x)}{q_c(x)}\Delta\eta_M + \frac{\left(\dfrac{1}{\eta_M} - 1\right)}{q_c(x)}\Delta q_f(x) + \frac{\left(\dfrac{1}{\eta_M} - 1\right)\cdot q_f(x)}{q_c^2(x)}\Delta q_c(x)\right\} \qquad (5.18)$$

These equations express the sensitivity of the Tromp curve for errors in the mass efficiencies and PSDs of the fines, coarse or feed.

The error plots for the different methods are presented in Figure 5-13. These plots are based on equal measurement accuracies for feed, coarse and fines flow.
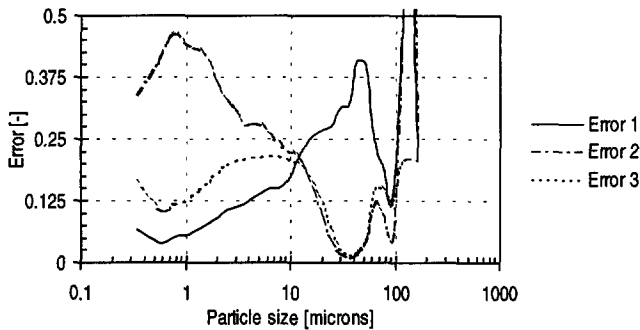
Figure 5-13 Error plots of Tromp curves determined with methods 1, 2 and 3.

Depending on the size range of interest, one of the methods should be chosen. If the interest is in the coarse recovery, one should use method 3. Method 1 is more accurate for the finer sizes, but inaccurate in the coarse particle range. And method 2 is the best option for the middle range. Of course also practical consideration will determine the location of sampling points.

5.5.4 Verification of classifier data

In this section the original data on which the classifier curves were based will be verified. Figure 5-5 showed the measured particle size distributions and mass flows over the classifier. The measured overall mass efficiency can be calculated with

$$\eta_O = \frac{\Phi_C}{\Phi_F} = \frac{12.0}{19.0} = 0.63 \qquad (5.19)$$

In theory it should be possible to determine the overall mass efficiency of the classifier out of the masses balances of each individual size class.

$$\eta_0 = \frac{\left(Q_F - Q_f\right)}{\left(Q_C - Q_f\right)} \qquad\qquad (5.20)$$

The original data set was substituted in equation 5.20. Figure 5-14 shows the deviations of the mass efficiencies over the whole size range.
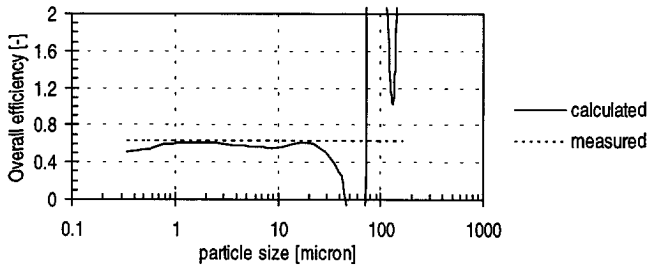
Figure 5-14 Mass efficiencies based on equation 5.16 and measured (dashed line).

These differences can be due to errors in the determination of the mass flows as well as errors in the PSD measurements. Though laser diffraction instruments are quite able to determine a median particle size, their accuracy at both the fines and the coarse ends of a particle size distribution drops rapidly.

These errors cannot be eliminated by statistical treatment and are considered to be an artefact of the measurement method. Also particle breakage can occur and give deviations from the expected overall mass curve. Higher values will be found in the small particle range. Each of the method, described in paragraph 5.5.3 used to calculate the Tromp curve will deal with these errors in a different way. Depending on the range of interest one of the methods is preferred.

ZISSELMANN [1985] wrote about the mathematics for the assessment of comminution and classification processes.

5.5.5 Construction of Treasure curve

An alternative way of presenting classifier data is the Treasure curve. A plot based on the same data as the Tromp curve discussed earlier, is shown in Figure 5-15.
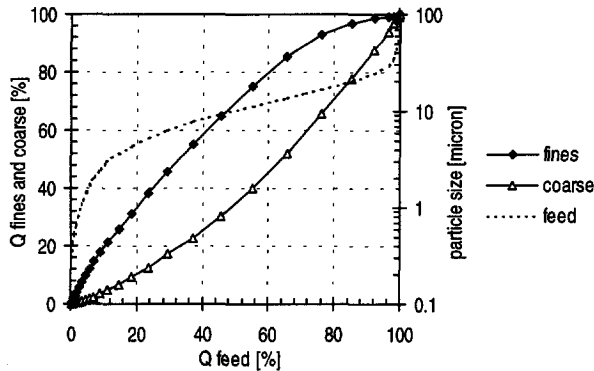
Figure 5-15 Treasure-curve expressing classifier performance.

The Treasure curve presents the classifier data as the cumulative undersize distributions of the coarse flow and fines flow plotted against the cumulative undersize of the feed flow. It provides the full information about the quality improvement of the product stream.

The dashed line represents the particle size distribution of the feed read from the horizontal axis corresponding with the sizes on the right-hand axis. The upper curve expresses the quality improvement of the fines flow, while the lower curve shows the coarse flow.

Particles with a size of 5 micron will be taken to illustrate the use of this graph. First the size is located on the right-hand axis of Figure 5-15. From the dashed line the cumulative undersize of the feed can be read on the horizontal axis. In this case $Q_F(5)$ = 28 percent. The corresponding distribution of the fines and coarse flows are found at the cross points of an imaginary vertical line from the x-axis, whilst reading the left-hand axis. This shows that the mass of particles smaller than 5 micron $Q_f(5)$ increased to 42 percent. In a similar way it was found that the amount of fines smaller than 5 micron in the coarse flow $Q_c(5)$ decreased to 19 percent.

The mass efficiency can be calculated by substitution of the cumulative undersize distributions of the feed, fines and coarse flow in equation 5.19.

5.6 Testing of air classifiers

5.6.1 Free vortex classifier connected to spiral jet mill

The performance of the LCC20 free vortex classifier shown in Figure 5-8 was investigated. During the closed circuit grinding experiments the 10-inch spiral jet mill was operated at a constant nozzle pressure and feed rate.

The mill product dispersed in air entered the classifier body through the tangential inlet. The particle size distribution of the fines flow was measured in-line before it was collected as end product in the bag filter. Samples of the coarse recycle were collected and analysed off-line at a later stage with laser diffraction instrument.

The major control variable of the classifier was the primary control air. This air flow, which was added to the mill air, could be adjusted by changing the negative pressure level at the classifier outlet. The effect of the air flow is shown in Figure 5-16.
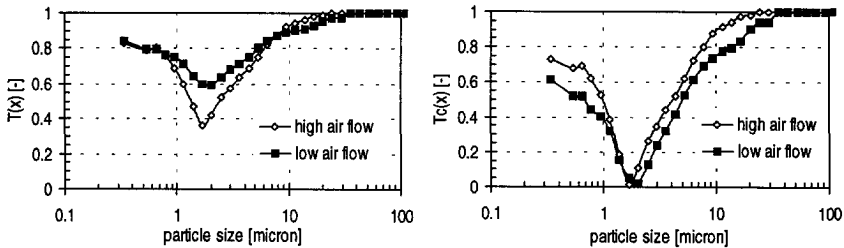
Figure 5-16 The Tromp curve and corrected Tromp curve for a high and a low primary air flow

The high air flow corresponded with a negative pressure of 40 mbar, while the low air flow was obtained at a negative pressure of 30 mbar. A control loop consisting of a pressure transmitter and a speed controller on the fan maintained the desired pressure level under different operating conditions of the closed circuit jet mill plant.

The same classifier data is plotted as a Treasure curve in Figure 5-17.
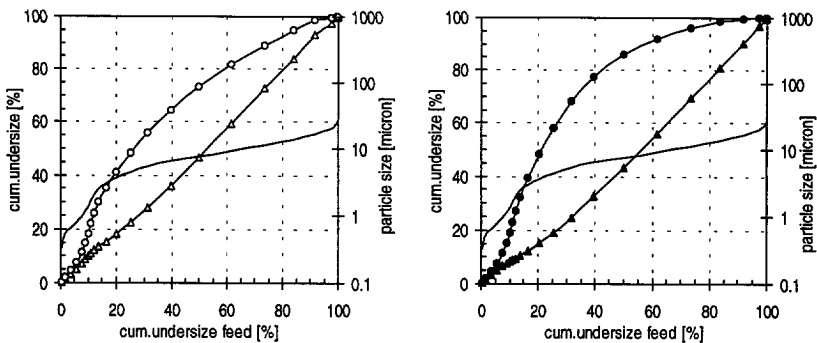
Figure 5-17 Treasure curves for a low (left) and high (right) control air flow.

The curves representing the size distribution of the coarse flow lays close to the 45 degrees line, indicating that the composition of this flow did not differ much from the feed flow. In fact, much of the feed was not affected by the classification process and

is passed through to the re-circulation as dead flux. At a higher air flow the coarse recycle did not change much. More important was that the quality of the fines flow improved significantly.

The qualitative effects of the air flow on the air classifier performance can be summarised as follows. An increase usually gave

1. Finer cutsize

2. Decrease of the dead flux

3. Slightly more concentrated underflow

4. Narrower PSD of the overflow

An increase of the solid feedrate at constant airflow caused the opposite effects. In the case of very high inlet flows, for example at high recirculating flows, the local maximum concentration was exceeded leading to blockage of the vortex and a disrupt in the discharge of a portion of the classifier contents. A similar phenomenon was also observed through a window in the base of the spiral jet mill. Turbulent bursting phenomenon re-entrain some of the particles in the main flow. The boundary layer becomes overloaded with particles. The vortex collapsed and the mill contents was re-mixed and left through the central outlet.

LCC56: After pilot plant experiments the dimensions of a larger LCC model were determined. A number of design studies can be found in the literature that relate body diameter, inlet geometry, vortex finder and other design features to classifier performance [COKER, DIETZ, LICHT].

From industrial runs with a LCC56 classifier in combination with a 24-inch spiral jet mill it appeared that the throughput could be increased while avoiding coarse particles to be present in the end product [VALIZE]. However, this larger classifier had a larger cut-size and a larger deadflux compared with the smaller pilot plant model at equal cut-sizes.

Remark: Long operating times require a drain of the recirculation flow as this flow is likely to accumulate inert particles which cannot be broken by the jet mill. Finally this accumulation might lead to coarse particles in the product flow. Scaling inside the classifier body and outlet pipe can cause similar problems.

5.6.2 Forced vortex classifier in opposed jet mill

The AFG opposed jet mill tested in this project had an integrated ATP-classifier rotor in the top section (see Figure 5-9). The operation point of this classifier was a function of the air flow supplied through nozzles in grinding zone and the rotor speed.

Effect of rotor speed: Figure 5-18 shows how the median size of the mill product depended on the rotor speed for three AFG models, the AFG200, AFG400 and AFG630.
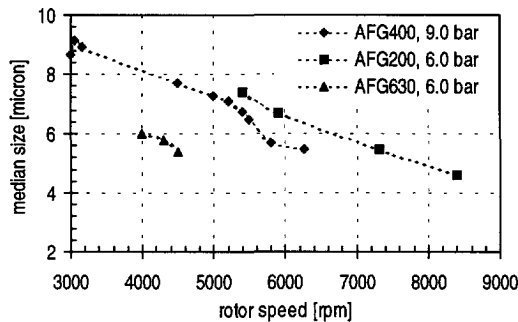
Figure 5-18 Product fineness as function of rotor speed at constant hold-up level for different opposed jet mills.

For these mills the median size varied almost linearly with the rotor speed.

$$x_{50} \propto \frac{1}{N_R^{1.03}} \qquad\qquad (5.21)$$

The vertical position of these linear curves were related to the dimensions of the classifier rotor, the diameters and number of nozzles and the operating pressure of the opposed jet mill.

In order to produce a certain topsize x_{90} the setpoints of the classifier and the feedrate can be found by following the lines. According to equation 5.3 an exponent of 1.25 was expected for the rotor speed N_R. The effect of an higher air flow due to higher grinding pressure is twofold. Besides the an increased grinding rate, also the internal classification of the rotor changed. As a result the composition of the mill contents changed. The fineness of the mill product is determined by the classification action of the rotor as well as the particle bed in the vicinity of the rotor. The classifier rotor was preferably operated at the highest rotor speed in order to use the highest air flow, which meant the highest throughput of the mill for the smallest unit.

When the grinding rate was not able to keep up with the internal classifier discharge an accumulation of particles occurred in the mill chamber. The particle concentration in the vicinity of the rotor rose and the friction between rotor and particles increased. This effect could be measured by a larger power consumption of the classifier rotor. The classification sharpness dropped due to mis-classification and bouncing of the particles. Higher particle concentration hitting the fast rotating blades also caused heat development and lead to streamers and the deposition of material near to the mill outlet.

As discussed earlier, the performance of the classifier unit is mainly determined by the dimensions of the rotor and the rotational speed. For scale up to higher capacities from the cut-size, sharpness, feedrate and product fineness from a test unit, the same loading (ratio of air to solids) will be used. To maintain the same cut-size, the balance between the centrifugal and drag forces must be the same. Due to strength limitations, the larger rotor is limited to lower speed. For scale-up, that means to handle more air flow under equal classification conditions the option for more rotors is often preferred.

At higher loading the rotor developed a significant amount of heat that caused operation problems like the formation of streamers and deposition of melted material in product pipes.

5.6.3 Tests with Acucut A12 forced vortex classifier

The Acucut A12 built by Mikropul was first tested as a stand-alone unit. During these tests with the Acucut A12 inlet 1 (see Figure 5-10) was used for the classifier feed, while a cyclone and ejector were connected to outlet 2 for the recovery of the coarse particles. Fines present in the coarse fraction were redispersed and brought back into the classifier through inlet 2.

Tests with CW were carried out at lower rotor speeds, up to 5000 rpm. Above this limit heat development caused operational problems, especially at higher loading. The relatively small volume of the classifier body combined with high rotor speeds caused problems with the heat development. Initial tests with material CW caused fouling in the classifier body and in the outlet tube. Experiments at higher rotor speeds were performed with Alumina powder with particle with a broad particle size distribution ranging from 1 to 40 micron. The classifier feedrate was 5.1 kilogram per hour. The overall mass efficiency was 0.24 and the imperfection, I, was 0.31. Results are presented in Figure 5-19.
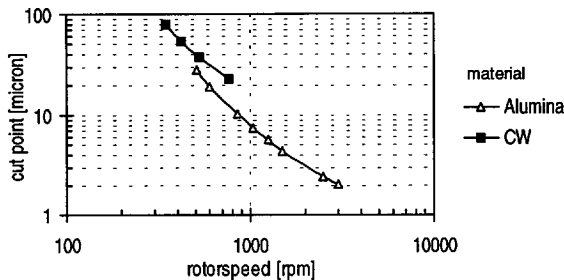
Figure 5-19 Effect of rotorspeed Acucut A12. Test materials Alumina powder (1-40 micron) and CW (1-60 micron). Airflow ~ 110 m³/hr. Feedrate ~ 5 kg/hr.

Trial runs were done with the Acucut connected to the 6-inch spiral jet mil. The inlets were not capable of handling the air flow leaving the mill. The mill was operated at lower pressure levels to reduce the air flow. However, at these pressures the grinding capacity of the mill was insufficient, which resulted in an overloading of the recirculating loop. The placement of a row of tangentially directed nozzles in the cylindrical wall of the Acucut was proposed by De Silva, thus creating a hybrid classifier/mill.

5.7 Conclusions

Air classifiers are very suitable for combined use with air swept mill, such as jet mills. Benefits are that the air can be effectively used to create a flow field in which particles are separated. The product flow remains dispersed thus avoiding agglomeration and segregation.

The Tromp curve expresses the performance of a classifier. This is useful for investigating the closed loop jet mill plant as it gives an indication what the composition and massflow of a recirculation flow will be. Due to measurement inaccuracies the absolute accuracy of the separation curves is low. How these errors appear in the final separation function depends on the sample locations and the calculation methods.

For the evaluation of quality improvement of powders the Treasure curve gives better information. All particle size data, both of the feed, coarse and fines flow is contained in the curve. The shape of the Treasure curve indicates how much the feed and product flow differ.

The free vortex classifier LaCad Oy LCC combined well with the principle of jet milling. Simple construction and low installation cost are advantages. Also the product was more gently treated than in forced vortex classifiers. Application of this

free vortex classifiers is limited to cutsizes above 5-10 microns. Below this range the dead flux increased dramatically and the classifier operated as a splitter. The current deadflux at higher re-circulating flow is in the order of 30 to 40%. The use of the washing air required a careful tuning. Coarse particles were easily re-entrained in fines flow.

The testing of a free vortex classifier with an industrial jet mill plant showed that coarse particles in the mill product could be collected. Creation of a large recirculating load for plant optimisation was not possible as the cut size of the units is higher due to the larger dimensions.

The median size of the product ground on the AFG mill could be well predicted. Use of the forced vortex classifier allows a more direct control of the topsize. The response of the system was faster, due to shorter residence time in the classification section. At higher loading the rotor developed a significant amount of heat that caused operation problems like the formation of streamers and deposition of melted material in product pipes.

The Acucut classifier produced a very narrow size distribution, but was not able to handle large air flows. At higher solid loading heat development became a problem for the processing of plastics. This was caused by the classifier rotor that introduced a considerable amount of mechanical energy in the small classifier body.

The Coanda type of classifiers offers opportunities to achieve lower cutsizes in closed circuit plants than the free vortex classifier. Especially a combination with jet mills is attractive.

List of symbols

d_n	nozzle diameter	[mm]
D_r	diameter of rotor	[mm]
L_r	height of rotor	[mm]
n_n	number of nozzles	[#]
N_R	rotorspeed	[rps]
p	pressure	[bar]
R_d	dead flux	[-]
q	particle size density distribution	[-]
Q	cumulative undersize distribution	[-]
v	velocity	[m/s]
x	particle size	[micron]

Greek

Φ	massflow	[kg/hr]
η	efficiency	[-]
η	viscosity	[Pa s]
ρ	density	[kg/m^3]
τ	delay time	[s]

Indices

c	cut-size
C	coarse fraction
d	dead
f	fines
F	feed
M	mass
n	nozzle
o	overall
R	rotor

Literature

Andres, U.; Sivashinsky, G., Separation of Minerals in Electric Field by Ponderomotive Forces (Classification in High Voltage Vertical Capacitor), *Powder Technology*, 12, 7-10, 1975

Austin, L.G., Klimpel, R.R., An improved method for analysing classifier data, *Powder Technology*, 29, 277-281, 1981

Bernard, J.G., Andries, J., Scarlett, B., Statistical analysis of cyclone grade efficiency measurements, *Proc. of the 25th anniversary conference Particle size analysis, 17-19 Sept. 1991, Loughborough*, p.426-435, 1991

Biddulph, Mixing effects in a simple air classifier, *AIChE Journal*, 32, no2, 317, 1986

Clift, R., Ghadiri, M., Hoffman, A.C., A critique of two models for cyclone performance, *AIChE Journal,* 37 no.2, 285-290, 1991

Coker, A.K., Understand cyclone design, *Chemical Engineering Progress,* 51-60, 1993

Dahlstrom, D.A. and Kam, W.-P., Comminution Energy Reduction by Two Stage Classification, *Proceed Intl Symp Adv Fine Part Pro,* 3-17, 1990

Dahlstrom, D.A. and Kam, W.-P., Classification for Energy's Sake, *Comminution-Theory & Pract SME Symp,* Ch.18, 249-260, 1992

De Silva, S.R., Air classifiers: principles, evaluation, performance, *Powder & bulk solids conf/exh. ring band,* 1981

De Silva, S.R., Neuer windsichter zur herstellung superfeiner fullstoffe, *chem.technik,* 8 no5, 219-225, 1979

De Silva, S.R., Walsh, D.C., Johansen, S.T., Bergstrøm, T.Bernotat, S., Simulations versus experiment in an Acucut air classifier, *Powder and bulk solids conference,* Chicago, 1991

Dietz, P.W., Collection effciency of cyclone separators, *AIChE Journal,* 27, no 6, 888-895, 1981

Fegan, S.D., Hasbrouck, J.F. ,Snow, R.H., Luckie,P.T., Allen, T., Blackwood,T., Klumpar, I., Scarlett, B., Karuhn, R., Leschonski, K., Summers, J.S., Wood, B., Particle size classifiers: testing procedures, *AIChE Journal* 64, 1993

Frey, R.E., Principles and Application of Air Classification, *SME/AIME,* no.85-93, 1-4, 1985

Gibson, K.R., Particle classification efficiency calculations by geometry, *Powder Technology,* 18165-170, 1977

Gonell, H.W., Cross flow classifier, *Z. VDI 72,* 27, 945-950, 1928

Hanly, J., Petchonka. J.J., Equipment selection for solid gas separation, *chem.eng,* july, 83-90, 1993

Heiskanen, K., Classification handbook, *Larox Oy,* 1987

Heiskanen, K., Particle Classification, Chapmann & Hall, London, 1993

Hukki, R.T., About the ways and means to improve the performance of closed grinding circuit, *4th Europ.Symp.Comminution,* p.319-330, 1975

Ishito, Carl K., Air Classification Technologies Update, Powder & Bulk Solids, *Conf/Exhib 1992, Illinois,* 1992

Johansen, S.T., Anderson, N.M., De Silva, S.R., A two phase model for particle local equilibrium applied to air classification of powders, *Powder Technology,* 63, 121-132, 1990

Kalen. B., Zenz, F.A., Theoretical-empirical approach to saltation velocity in cyclone design, *Recent Advances in air Pollution Control,* vol.170, 389, 1974

Klumpar I.V., Measuring and optimizing air classifier performance, *Sep.Techn.,* 2, 124-130, 1992

Koch, P.; Bohlmann, S., Modelling by Classification in Concentrator Process Control, *Aufbereitungs-Technik,* 31/1, 1-6, 1990

Leith, D., Licht, W., The collection efficiency of cyclone type particle collectors - a new theoretical approach, *Aiche symposium series,* 68, no126, 196-200, 1972

Leschonski, K, Die Bedeutung des Dispergierens und Dosierens bei Fienstrennung in Windsichtern, *Particle Technology,* Amsterdam, 1980

Luckie, P.T., Particle size classifiers, *Short course on size reduction and classification, A'dam (Hand out),* 1990

Maunz, M., Buettner, H., Ebert, F., Particle collection in cyclones, *Proceedings Partec '95,* 1995

Mayer, F.W., Berechnung des neues Trennscharfe, Kennwertes aus den Teilungszahlen., *Aufbereitungs-Technik,* vol.2, 82-90, 1971

Molerus, O., Stochastisches Modell der Gleichgewichtssichtung, *Chem.Ing.Techn.,* 39, 792-796, 1967

Molerus, O., Hoffman, H., Darstellung von Windsichtertrennkurven durch ein stochastisches Modell, *Chem.Ing.Techn.,* 5+6, 340-344, 1969

Mothes, H., Löffler, F., Prediction of particle removal in cyclone separators, *International Chemical Engineering,* 28, 231-240, 1988

Nied, R., Sickel, H., Modern Air Classifiers, *Powder Handling & Processing,* 4-2, 203-205, 1992

Onuma, E., An analysis of closed circuit grinding system with an imperfect classifier, *J. Chem. Eng. Jpn.,* 9(6), 481-484, 1976

Ovaskainen, P., LaCad Oy LCC20 air classifier, *operating manual,* 1993

Pervis, A.B. (Jr), Goree, E.G. and Simmons, G.A., Pneumatic Classification of Ultrafine Powders, *Proc Symp Ultrafine Grind Sep Ind,* , 98-104, 1983

Plitt, L.R., Finch, J.A., Flintoff, B.C., Modelling the hydrocyclone classifiers, *Proc.Eur.Symp. Part.Technolgy,* Amsterdam, 790-804, 1980

Rajendran Nair, P.B., Ramanujan, M., Classification function in fluid energy grinding, *Powder Technology,* 68, 79-84, 1991

Rosenbrand, G.G.,Senden, M.M.G., Tels, M., Modelling of zigzag air classifiers at high feed rates, *Partec 86*, 469-483, 1986

Rumpf, H., Leschonski, K., Principles and recent methods of air classification, *Selected translated papers,* vol.1., 1972

Rumpf, H., Borho, K.,Reichert, H., Optimale dimensionierung von Zyklonen mit Hilfe vereinfachender Modellrechnungen, *Chem.Ing.Techn.*, 21/22, 1072-1082, 1968

Rumpf, H.,Leschonski, K., Prinzipien und neuere Verfahren der Windsichtung, 1967

Schlepp, D.D. and Turner, P.A, Influence of Circulating Load and Classification Efficiency on Mill Throughput, *SME/AIME 119th Annual Meeting, UT,* no.90-94, 1-9, 1990

Schmidt, P., Cyclone separator with a diffusor slot in a long outlet tube, *Partec 86,* 1986

Senden, M.M.G., Stochastic models for individual particle behaviour in straight and Zig-Zag air classifiers., *Dr.Ing Thesis, TU Eindhoven,* 1979

Senden, M.M.G., Vortsman, M.A.G., Tels, M., Schmidt, P., Air classification and sieving, *Particle Technology Workshop,* 1981

Suganuma, A., Yamamoto, H., Yoshie, K., Machida, M., Trials of Pneumatic Classification in the neighbourhood of 1 micron, 443-455, 1986

Svarovsky, L., Hydrocyclones, Technomic, 1984

Svrcek, W.Y., Design two-phase separators within the right limits, *Chemical Engineering Progress,* October, 53-60, 1993

Tromp, K.F., Neue Wege für die Beurteilung der Aufbereitung von Steinkohlen, *Glueckauf 73,* 6, 125-131, 151-156, 1937

Usui, K., Influence of classification characteristics on the capacity in closed-circuit system, *Kagaku Kogaku (7),* 31(3), 295-6, 1967

Valize,Th., Report: LaCad Oy classifier, *Internal report,* 1994

Yamada, Y., Yasuguchi, M., Iinoya, K., Development of an Air Classifier for Fine Particle Use, *Partec 86,* 1986

Yoshida, H., Saeki, T., Hashimoto, K. and Fujioka, T., Size Classification of Submicron Powder by Air Cyclone and Three Dimensional Analysis, *J Chem Eng Jpn,* 24/5, 640-647, 1991

Zisselmar, R. and Kellerwessel, H., Approximate Mathematical Description of Particle Size Distributions Possibilities and Limitations as to the Assessment of Comminution and Classification Processes, *Part Charact,* 2/2, 49-55, 1985

Chapter 6

Pilot plant experiments

This chapter presents the grinding experiments conducted on two types of jet mills. Paragraph 6.1 gives information about the grinding plants, default operating conditions and test materials. Paragraph 6.2 describes the experiments with the spiral jet mill, while paragraph 6.3 deals with the opposed jet mill tests. This chapter ends with conclusions.

6.1 Introduction

6.1.1 Grinding plants

Most of the jet mill experiments described in this chapter were conducted on the pilot plant at TU-Delft, which was operated in an open circuit or closed circuit configuration. This plant comprised a 10-inch spiral jet mill and a LCC20 free vortex classifier. The mill was equipped with replaceable nozzles. The sets of nozzles are listed in Table 2-2.

Part of the experimental program was carried out on an AFG opposed jet mill at the location of Wedco Holland. Both plants were equipped with on-line particle size instruments that were used for system analysis. More detailed information about these jet mill plants is given in Chapter 2.

6.1.2 Default operating conditions

Jet mills can be operated with different fluid such as steam, helium, nitrogen or air. In this project the energy required for grinding was supplied by expanding air jets through nozzles that were mounted in the cylindrical wall. Before the high pressure air entered the mill it was dewatered at a dew point of 4 degrees Celsius and reheated to a constant temperature of 20 degrees Celsius. All the experiments were carried out with nozzle pressures that were higher than the critical pressure for mass limiting flow. For the calculation of the energy use one is referred to Appendix A, Nozzle flow.

The organic test materials were stored in a hopper and dosed by a screw feeder. A useful parameter to compare the grinding performance of a jet mill is the loading factor, which is defined as the mass ratio of the feed and the air flow [RUMPF]. In formula:

$$\mu = \frac{\Phi_F}{\Phi_{Air}} \qquad\qquad (6.1)$$

6.1.3 Test material

Jet mills are used for the grinding of numerous materials [KÖHLER, YOON].The model test material used for the experiments with the spiral jet mill was a natural wax, referred to as CW. The feed particles were flakes with an average thickness of 0.8 millimetres and length of 3 millimetres.

A number of experiments were done with a different wax referred to as PW. This material was primarily ground on the opposed jet mill. The feed particles were pastilles with a diameter of approximately 4 millimetres.

Table 6-1 summarises the results of trial runs conducted on a 6-inch spiral jet mill with different test materials to asses the grindability.

Table 6-1 Results trial runs with different materials on 6-inch spiral jet mill.

Material	Φ_F	P_n	Φ_A	x_{ini}	x_{after}	RR	run time
	[kg/hr]	[bar]	[Nm³/hr]	[micron]	[micron]	x_{ini}/x_{after}	[s]
CW	12.1	6.3	14.7	165	5	33.0	600
PW	12.3	6.2	14.5	220	31	7.1	550
SL	10.7	6.1	14.3	376	320	1.1	750
PE	8.9	6.1	14.3	415	330	1.3	750
PS	10.1	6.2	14.4	460	385	1.2	750
PC	6.6	6.2	14.4	575	563	1.1	750

Material CW, which is very brittle, was found very suitable for grinding on a spiral jet mill as it had a reduction ratio of 33.

The PW feed had a reduction ratio of 7.1 indicating that this material is more difficult to be ground on a jet mill. This was explained by the fact that the loading of the large PW pastilles was insufficient in the free jets, where sliding contacts more prevalent. In opposed jets the grindability of PW pastilles improved as a result of the frontal collisions during which more kinetic energy was available for particle loading. The other materials SL, PE, PS and PC showed very low degrees of size reduction and were considered not to be grindable on jet mills with air at ambient temperature.

6.2 Tests with the spiral jet mill in pilot plant

This paragraph presents a systematic analysis of the performance of the 10-inch spiral jet mill. This information can be used for plant tuning [BAZIN] and for the verification of the model described in Chapter 7. First a global description of the product quality of the mill as a function of the process conditions is given in paragraph 6.2.1. Then a deeper analysis is described of the operational and design aspects of the air supply in paragraph 6.2.2, and of the rate and composition of the feed in paragraph 6.2.3. Finally the effects of a stabilising controller and the closed loop configuration are discussed.

6.2.1 Exploration of operating range of 10-inch spiral jet mill

The first experiments were aimed at the exploring of the working range of the open circuit jet mill plant with the use of the on-line size measurements. After start-up the pilot plant was brought to a series of steady states by the central control system. The particle size of the end product was continuously stored in a database together with other process data. Figure 6-1 shows the median size of the mill product for combinations of the solid feedrate and the nozzle pressure.
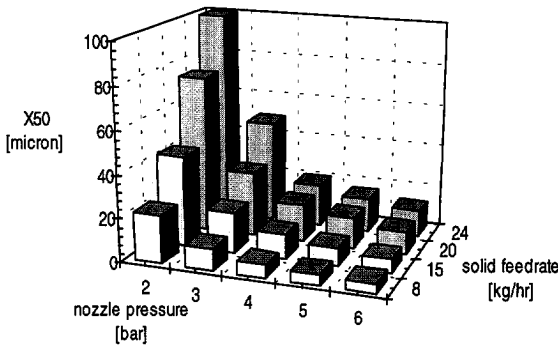

*Figure 6-1 Median size of mill product versus the nozzle pressure and solid feedrate.
Material CW. 10-inch spiral jet mill. On-line MSX.*

The reproducibility of the measurements was high, as there was no operator interference during sampling and the mill was brought automatically to the desired operating condition.

The median size of the mill product as a function of the two process input variables was described by the following equation for the material CW ground on the 10-inch spiral jet mill.

$$x_{50} = \frac{1180}{(P_n + 2.1)^{2.2} + (24.1 - \Phi_{M,F})^{1.8}}$$ (6.2)

Equation 6.1 is in fact a black box model of the jet mill for this specific test material and mill configuration, which predicts the median size of the mill product as function of the process inputs. It appeared that the same median size was obtained by various combinations of pressure and feedrate. All these points lay on a curved line formed by the crossing of the plane with a horizontal plane at the value of the x_{50}.

Figure 6-1 shows that for lower solid feedrates and higher nozzle pressures the x_{50} of the mill product gradually decreased to a minimum value of approximately 4.0 micron. A finer product could not be obtained with this mill. Either the mill design has to be modified or a different fluid has to be used if a finer product is required. An alternative can be the operation of the mill in closed circuit with an external classifier that has a low enough cutsize.

For certain applications the increase of specific surface area, SSA, as defined in Chapter 4, is a good basis for the comparison of grinding performance. Figure 6-2 shows that the highest increase of the SSA was obtained for combinations of low feedrates and high nozzle pressures.
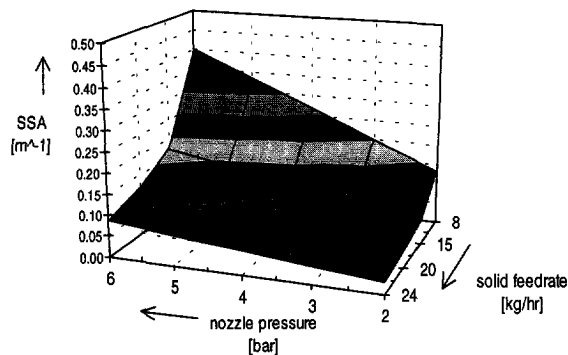

Figure 6-2 Increase of SSA for combinations of pressure and solid feed. Material CW. 10-inch spiral jet mill. On-line MSX.

The SSA increased linearly with the nozzle pressure, which indicated that the energy input (see Appendix A) was proportional to the newly created surface. This implies that the jet mill was operating in the region where Rittinger's empirical breakage law ,equation 4.17, is valid.

A more specific measure of the mill performance is obtained when the increase of the SSA is divided by the energy supplied. The specific grinding energy, *SGE*, in the case of jet mill is the pneumatic energy supplied through the nozzles divided by the solid throughput.
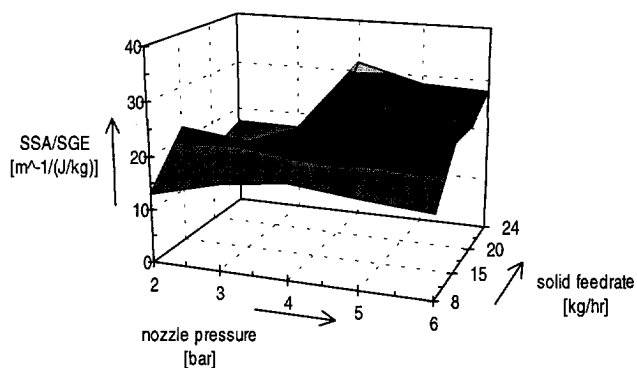
Figure 6-3 Increase of SSA divided by the SGE for combinations of nozzle pressure and solid feed. 10-inch spiral jet mil. Material CW. On-line MSX.

Figure 6-3 shows that the profile of the SSA/SGE-curve is rather flat. The degree of size reduction varied relatively little for the combinations of solid feedrate and nozzle pressure tested for this mill configuration.

6.2.2 Effect of air supply on jet mill performance

In jet mills the air serves both the energy carrier for grinding as well as the transport medium of the solids. Therefore the air flow has a direct effect on the comminution and the internal classification in the mill. This section presents the effects of the operating pressure and the diameter, angle and number of the nozzles.

Nozzle pressure: A higher operating pressure results in a higher energy input to the mill. Figure 6-4 shows the PSD of the mill product. The solid feed was kept at a constant level of 22 kilograms per hour during these experiments. The cumulative undersize curves, with a typical S-shape, shifted to the fine particle range for higher nozzle pressures.

Figure 6-4 Effect of the nozzle pressure on the PSD of the jet mill product. Constant feed rate 22 kg/hr. Nozzles 8x2.0mm. Material CW. MSX 100mm lens.
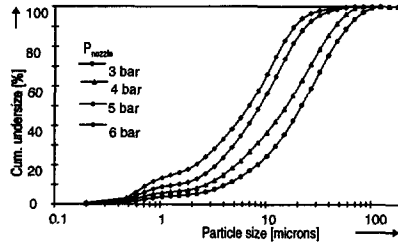
Number of nozzles: The spiral jet mill was equipped with a replaceable set of nozzles mounted in the cylindrical wall. Figure 6-5 shows the effect of the number of nozzles in the spiral jet mill. The total cross section of the nozzles was kept at a similar magnitude by using 4 nozzles with a diameter of 2.5 millimetre and 8 nozzles with a diameter of 2.0 millimetre. The loading factor for both of these experiments was 0.20.
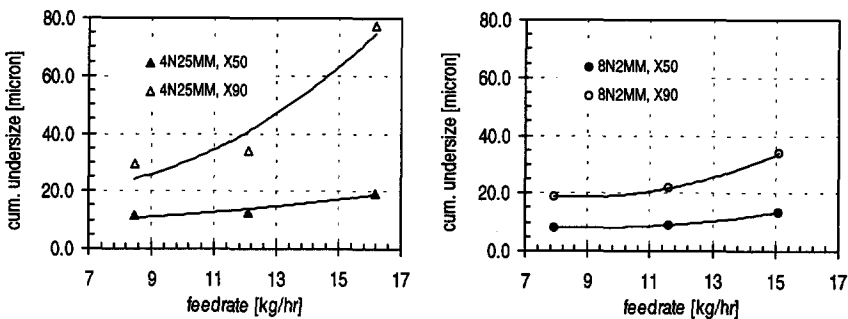
Figure 6-5 Cumulative undersizes (x_{50}; x_{90}) of the mill product versus the solid feedrate for 8x2.0mm (right) and 4x2.5mm (left) nozzles. μ= 0.20

The median size produced by the 8x2.0mm nozzles was slightly smaller, at these feedrates, than the median size for the 4x2.5mm set. More significant were the differences in the topsizes. The internal classification of the spiral jet mill became bad for the 4 nozzle configuration which caused coarse particles to escape through the mill outlet. The 8 nozzles created a more axi-symmetrical vortex and thus better classification.

Nozzle angle: The nozzle angle is defined as the angle of its indentation to the radius of the mill chamber, as is shown in Figure 2-2. The nozzle angle has an effect on the internal classification of the spiral jet mill. Figure 6-6 shows the results of experiments with the 10-inch spiral jet mill. Two nozzle angles were tested. The default angle was 19 degrees.
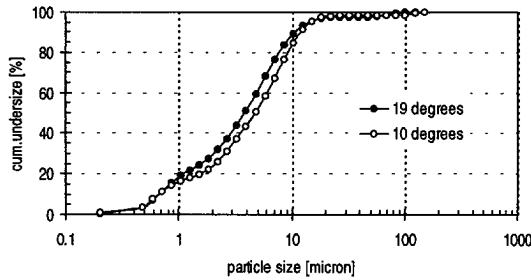
Figure 6-6 Effect of nozzle angle. 10-inch jet mill. Nozzles 8x2.5mm.

When a narrow PSD was desired the spiral jet mill had to be operated at a low feedrate with the larger nozzle angle of 19°. In situations were larger throughputs were required, such as in closed circuit grinding, a smaller nozzle angle gave better results. At higher mill loading the 10 degrees configuration was able to maintain a stronger vortex at the outlet.

Generally a larger nozzle angle (with the radius) gives a better internal classification as it creates a larger circle where the jets formed a stable vortex. This makes the risk of misplaced coarse particles in the product flow smaller. When the angle is too large and the number of nozzles, the jets hit the outer wall causing machine wear. The optimal angle depends on the desired product quality, mill loading and the scale of the jet mill. However, no general rules exist.

KURTEN, RUMPF AND MUSCHELKNAUTZ studied the flow patterns in spiral jet mills related to the nozzle configuration.

Air pressure on solids injector: The feed particles were brought into the mill chamber by a solids injector which was mounted on the top plate of the spiral jet mill. Figure 6-7 shows the PSD of end product at different injector pressures.

Figure 6-7 Effect of the injector pressure on the PSD of the mill product. Spiral jet mill. 8x2.5mm nozzles. Nozzle pressure: 6.0 bar

Figure 6-7 shows the two effects of the ejector pressure. First, the mill product ground at a high injector pressure was f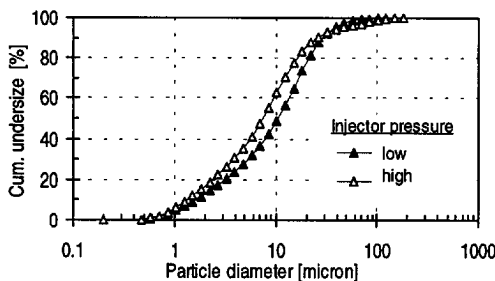iner. A higher ejector pressure resulted in a higher energy input and caused an extra grinding action. The large feed particles were sucked into the ejector tube and rubbed against the wall and against other particles in a highly turbulent flow. Secondly, at approximately 20 microns the cumulative undersize curves crossed, which means that the mill product contained relatively more coarse particles at the enhanced ejector pressure. This had a negative effect on the product quality, which is often defined by the top size.

Remark 1: During start-up of the spiral jet mill a high injector pressure was required to overcome the pressure level in the chamber. After sufficient material had built up the pressure level in the mill chamber dropped and the ejector pressure could be reduced to minimise the disturbance of the vortex flow.

Remark 2: In Chapter 8 the design of a solid injector with an enhanced pregrinding action is described. This device comprises an ejector and a fixed target and can be used for the grinding of non-abrasive materials, such as polymers or organic waxes. This pregrinding injector is particularly useful for grinding tougher pastilles down to particles that are sufficiently small for entrainment and breakage by the free jets.

Remark 3: When extra injection air is required, such as for the regrinding of very fine material or in a closed circuit jet mill plant, the injector inlets should be tangentially mounted in the outer cylindrical wall. In this way the extra ejector air will not disturb the vortex.

6.2.3 Effect of throughput on performance of spiral jet mill

The on-line size measurements based on laser diffraction allowed a dynamic study of the mill performance. Figure 6-8 shows how the solid feed and the output flow of the spiral jet mill were changing in time over the course of a test run. During the run the operating pressure was kept at a constant level of 6.0 bar.

During the start-up stage the solid feed was brought to a level of 20 kilograms per hour by the control system. The mass flow of the product leaving the mill, determined from the obscuration signal as discussed in Chapter 3, stabilised at the level of the feed rate with a delay of approximately 60 seconds. Then the grinding rate was apparently in equilibrium with the discharge rate at the central mill outlet and no extra hold-up was being accumulated. The product flow was smooth and the mill was operating under steady state conditions.
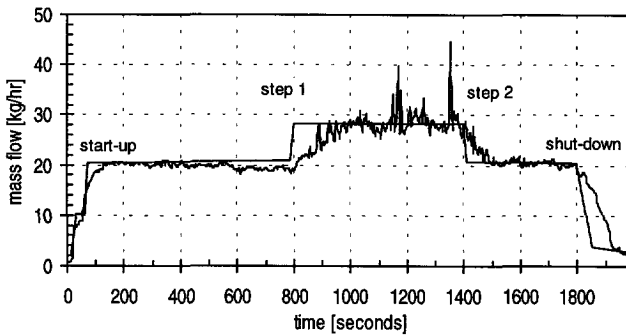
Figure 6-8 Evolution of feed flow and product flow during a test run. On-line MSX.
Nozzles 8x2.5mm, Operating pressure 6.0 bar, Material CW.

At t = 800 seconds the solid feed rate was increased from 20 to 28 kilograms per hour. The average product flow stabilised at the level of the solid feed after a time delay of 200 seconds. During this period extra hold-up was accumulated. Figure 6-8 shows that the output flow was fluctuating strongly due to unstable performance of the mill. This transition was explained by the fact that the grinding rate of the mill was not able to keep up with the discharge rate which caused the hold-up to increase and finally reached the physical limit of the amount of material that fitted in the mill chamber. The vortex collapsed resulting in an instant discharge of a large part of the mill contents. For several seconds the mill operated stably until the physical limitation was reached again. Experiments showed that the frequency of the instabilities increased with higher feedrates from 3 up to 20 seconds. This periodic collapsing of the vortex was also observed during experiments made with the transparent mill base plate described in Chapter 8.

At t = 1400 seconds the feed rate was brought back to 20 kilograms per hour and the product flow stabilised at the original level. Finally the jet mill plant was shut down. The product flow continued until the mill chamber was empty.

Effect of solid feedrate on product fineness: During the same test run the particle size distribution was measured continuously. The results are shown in Figure 6-9. The cumulative undersize distribution of the mill product is plotted on the left-hand axis, while the solid feed is plotted on the right-hand.

The start-up of a spiral jet mill is a critical phase during which coarse product is easily produced. In the first 60 seconds peaks in the particle size were detected that were caused by choosing wrong combinations of feedrate and nozzle pressure.
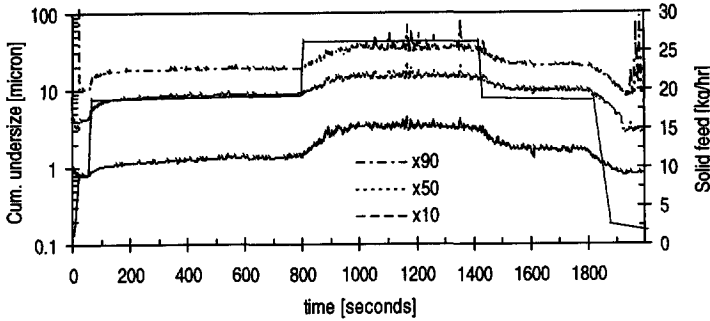
Figure 6-9 Evolution of x_{10}, x_{50} and x_{90} of mill product in time. 10-inch spiral jet mill, nozzles 8x2.5mm, pressure 6.0 bar, material CW.

At t = 150 seconds the product fineness reached a constant value. After the step on the solid feedrate from 20 to 28 kilograms per hour, the PSD of the mill product changed. The median size increased from 7.5 to 14 microns and the top size changed from 18 to 35 micron. Peaks in the topsize of the mill product, x_{90}, were found up to 100 microns. Particles with diameters larger than 150 micron were found in the end product by sieve analysis. The latter were not detected with laser diffraction as their concentration was too low.

Figure 6-10 shows how the topsize of the mill product was related to different feedrates. For the lower feedrates the top size was constant. At increased feedrates a transition to unstable mill performance was found. This transition occurred rapidly at 20 kilograms per hour the profile of the topsize was still smooth, whilst at 24 kilograms per hour large peaks appeared which were caused primarily by material in the coarse size classes that escaped to the central outlet due to vortex instabilities.
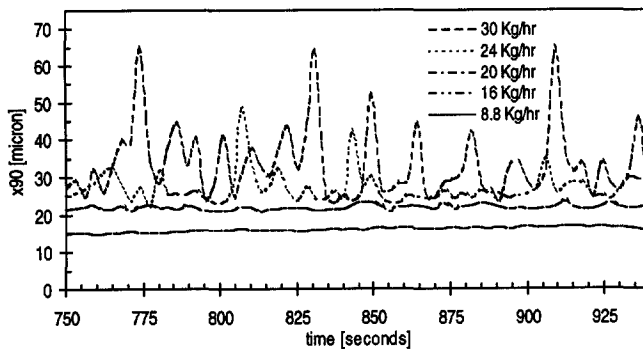
Figure 6-10 Fluctuations of the cumulative undersize of mill product (x_{90}) during runs with different levels of solid feed rates. 10-inch spiral jet mill. P_n = 6.0 bar

Figure 6-11 presents the variance of the fluctuations of the topsize during the course of the test run. The plot shows that the variance remained below 1.0 for feedrates up to 20 kilograms per hour. At higher feedrates the fluctuations increased rapidly due to unstable mill performance.
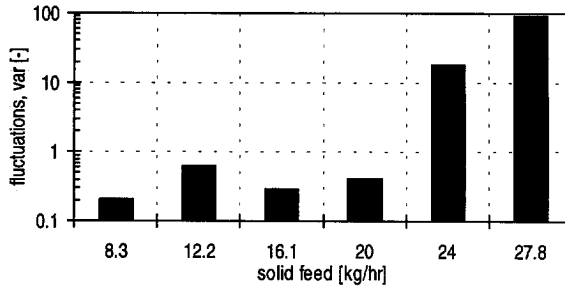
Figure 6-11 Fluctuations of the x_{90} expressed as the variance versus the solid feedrate.

Effect of pregrinding: The particle size of the feed can affect the grinding performance [HÄSE]. Pilot plant experiments were conducted with feed materials having different initial particle size distributions. The standard CW feed particles, as it was supplied, were flakes with a thickness of 0.8mm and of length 3mm. Pre-ground CW material was produced on a mechanical mill. These particles were more cubic with a median size of 0.6 millimetre. Approximately 20 percent by weight were attrited fines.

The results of jet mill experiments with the original and preground feed are presented in Figure 6-12. At a low throughput pregrinding did not significantly affect the mill performance, as can be seen in the left hand graph. During experiments with high throughputs the feedsize had a significant effect, as the right hand plot shows.
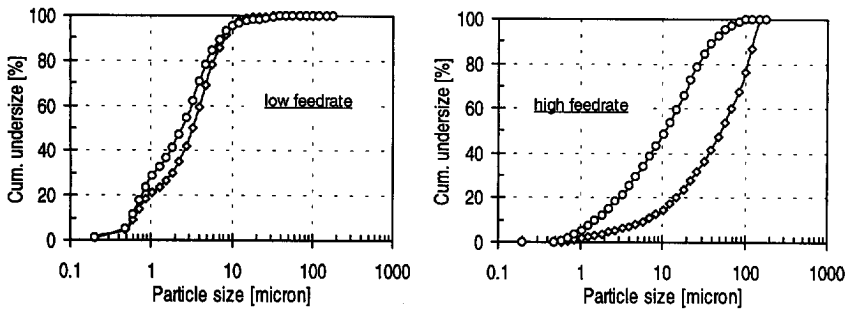
Figure 6-12 Pregrinding the solid feed. Effect at lower feedrates (left). Effect at higher feedrates (right . Operating pressures: 4.5 bar; 10-inch spiral jet mill; 8x2.0mm.

The difference can be explained by the fact that in the case of high throughputs the grinding rate of the mill became insufficient in comparison to the internal classification. In the case of low capacities the classification function determined the PSD.

Remark: HOMMA investigated particle size and shape effects on jet mill performance. Besides particle size, also the shape of the feed particles plays an important role on the grinding performance of a jet mill. During pure attrition the edges of the particles are broken off and the particles become more spherical. During this process the attrition rate drops gradually until all particles are turned into spheres. Normal breakage creates sharper particles that are more vulnerable to attrition.

6.2.4 Conditions inside the mill chamber

In this section the conditions in the mill chamber are discussed. The amount of material present in the mill has a strong influence on the processes.

Hold-up: A manifold on the mill outlet was used to achieve an instantaneous closure of the mill. Simultaneously the solid feed and the air flow to the nozzles were stopped. After the plant was shut down, the mill contents was removed and weighed. The results of a series of hold-up measurements are plotted in Figure 6-13. The lowest feedrate tested was 6.5 kilograms per hour, whilst the highest was 17.8 kilograms. A polynomial function was fitted through the data points for experiments with a constant nozzle pressure.
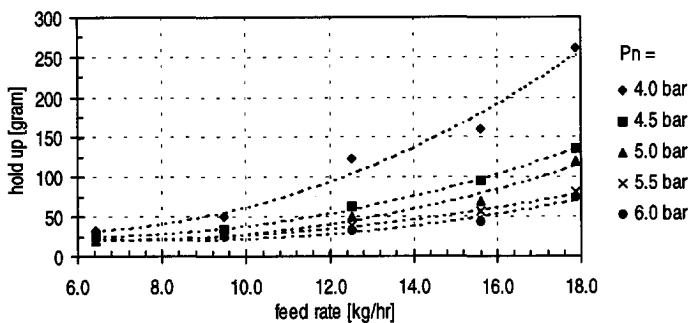
Figure 6-13 Effect of feed rate and nozzle pressure on hold-up in mill chamber. 10-inch spiral jet mill. nozzles 8x2.5mm. Product CW.

For an operating pressure of 6.0 bar the hold-up increased from 26 to 75 grams. All the experiments were carried out in duplicate. The hold-up measurements at a low mill loading were well reproducible. For lower nozzles pressures higher hold-ups were found. As the mill loading increased the reproducibility of the hold-up measurements

decreased. This was probably due to the sudden discharge during unstable operating conditions of the mill.

Pressure level in mill chamber: In the literature it is reported that the pressure drop over the mill chamber was correlated with the hold-up [RUMPF, MUSSCHELKNAUTZ]. In order to investigate this effect a pressure sensor was mounted on the top plate of the 10-inch spiral jet mill at a radial distance of 7 centimetres from the centre. In Figure 6-14 the pressure level in the mill chamber is plotted against the solid feedrate as in the previous section.
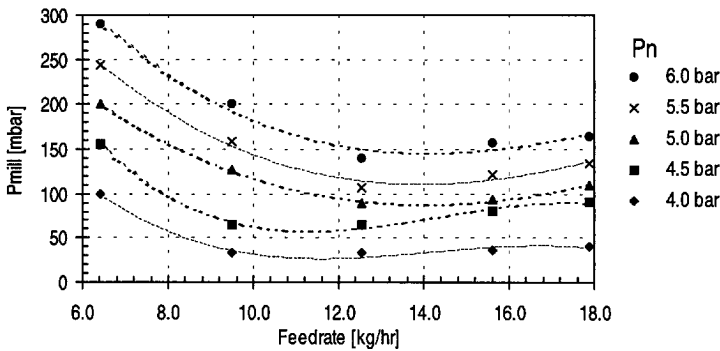
Figure 6-14 Effect of feed rate and nozzle pressure on pressure levels in mill chamber (P_{mill}). Test material CW. Nozzles 8x2.5mm.

At relatively low feedrates the pressure level in de mill decreased with increasing feedrates. For feedrates higher than 12 kilograms per hour the mill pressure started to increase again. The minimum pressure level shifted to higher feedrates for test runs conducted with higher nozzles pressures.
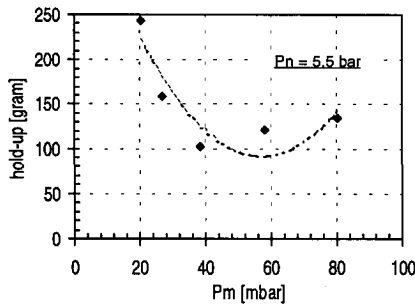
Figure 6-15 Hold-up versus pressure level in jet mill chamber, Pm, for constant nozzle pressure Pn of 5.5 bar.

In Figure 6-15 the hold-up is plotted against the mill pressure for a series of testruns with a nozzle pressure of 5.5 bar. This curve shows that the mill pressure is not uniquely related to a hold-up, it does vary.

6.2.5 Control experiments

Step responses: Figure 6-16 shows the evolution of the solid feed, the pressure level in the mill chamber and the median size of the product. During the start-up a peak in the mill pressure was measured that corresponded with a coarse mill product.
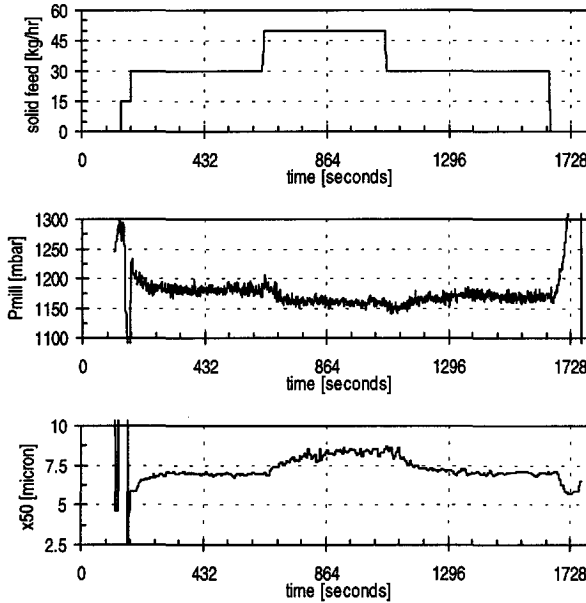
Figure 6-16 Solid feedrate, pressure level in mill chamber and the median size of the ground product evolving over a test run. Step upwards and downwards. $P_n = 5.5$ bar.

After approximately 100 seconds the mill pressure stabilised at a value of 1175 mbar. The median size reached a stationary value of 7.0 micron at the same time. At t = 420 seconds a step change to the feedrate was made. This resulted in a lower pressure level in the mill chamber and a larger median size of the product of 8.4 microns.

During the following test run the feedrate was kept constant at a level of 15 kilograms per hour. The effect of a step change on the nozzle pressure is shown in Figure 6-17.
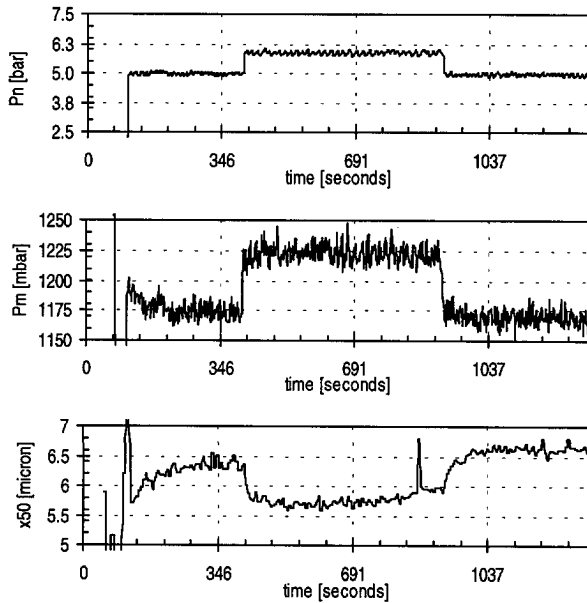
Figure 6-17 Nozzle pressure (Pn), pressure in mill (Pm) and median size (x50).
Feedrate 15 kg/hr.

After start-up the mill was operated with a nozzle pressure of 5.0 bar. The mill product had a median size of 6.4 micron. At t = 420 seconds the nozzle pressure was increased stepwise to 6.0 bar. The median size of the mill product decreased and stabilised at 5.75 micron after 15 seconds. Compared to a step change on the feedrate the mill pressure reacted faster to a step change of the nozzle pressure.

These pilot plant experiments implied that simple proportional feedback controllers, which manipulate the feedrate and high pressure air supply, can be used to control the PSD.

In an industrial environment fluctuations in the air supply easily occur due to the start-up and shut down of jet mill plants that are connected to a central high pressure air supply unit. In the following sections the ability of the feedback controller to compensate for the pressure disturbances is presented.

<u>Feedback control based on the pressure level in the mill chamber</u>: The hold-up is an important variable for the performance of the mill and the pressure level in the mill appeared to be related to it. This section deals with control experiments during which the mill pressure, *Pm*, was used as a feedback signal with the objective of stabilising the median size. Figure 6-18 shows the evolution of the pressure level in the mill and the median size.
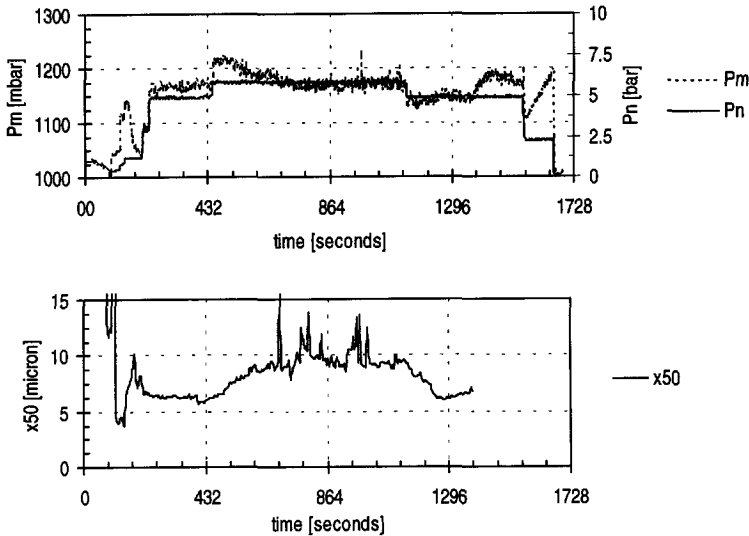
Figure 6-18 Excitation of the P_n and stabilisation of the mill pressure by feedback on the solid feedrate (upper plot). Effect of control using the P_m-signal (lower plot).

Stabilisation of the pressure level in the mill chamber (P_m) resulted a constant x_{50} as long as the pressure on the nozzles was constant. A disturbance on the nozzle pressure at t = 435 led to an increase of the median size even though the pressure level in the mill chamber was kept constant. This control loop, based on the pressure level in the mill, was not able to keep the median size accurately at the desired value of 6 micron. This can be understood since different combinations of nozzle pressure and feedrate can lead to the same P_m.

Feedback control loop based on real-time particle size measurements: The on-line laser diffraction instrument mounted on the mill outlet measured continuously the PSD of the product leaving the mill. Two control loops were tested. The first one adjusted the solid feed and the second one adjusted the nozzle pressure. As a control signal the median size of the particle size distribution was chosen. In principle other aspects of the PSD such as specific surface area or topsize can also be selected as a manipulated variable as well.

Adjustment of solid feedrate: Figure 6-19 shows how the median size of the product was brought to the new setpoint. The controller was able to keep the actual value within 0.5 micron accuracy at the desired setpoint.
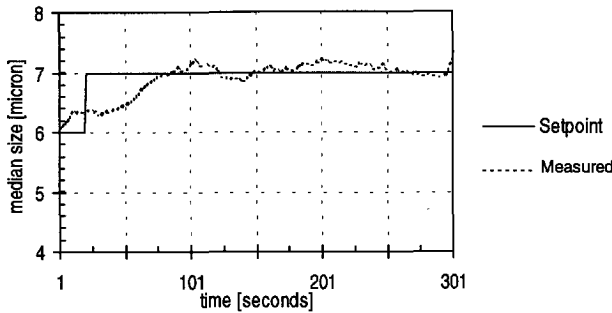
Figure 6-19 Set point change from 6.0 to 7.0 micron (median size). Feedback control on solid feedrate.

Adjustment of air supply: In this experiment the valve on the air inlet to the nozzles was used as an actuator. The median size of the mill product reacted quickly and stabilised at 7.0 microns. The product quality was controlled with an accuracy of 0.4 microns. The high pressure supply had a two-fold effect on the performance of the mill. The energy available for grinding dropped as did the internal classification.
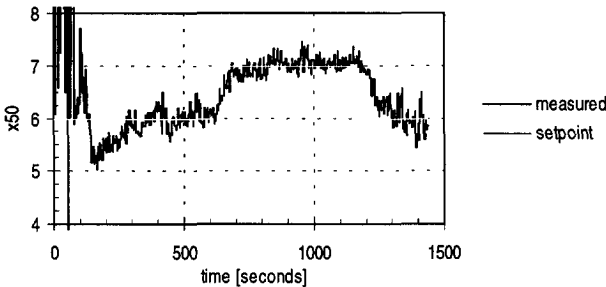
Figure 6-20 Change of set point by adjustment of the nozzle pressure. Feedback control on nozzle pressure

Remark: The feedback on the air supply worked well, but is not preferred in industrial practice since the pressure drop due to friction over the control valve causes considerable energy losses.

Remark: In Chapter 3 the use of PCA was described to reduce the light scatter data measured with laser diffraction instruments in a jet mill plant. Control experiments indicated that PCA is effective for set point tracking. However, for unstable mill performance at higher feedrates and low nozzle pressures the accuracy dropped. The advice is to use PCA in combination with a sensor that can indicate process fluctuations.

6.2.6 Scale-up effects of spiral jet mills

Experimental data from the pilot plant was compared with data from other jet mills. Table 6-2 contains scale-up data for material CW. This data indicated that generally larger mills operate in a more energy efficient way.

Table 6-2 Scale-up effect of spiral jet mills. Test material CW. $P_n = 6.0$ bar

	Φ_s [kg/hr]	Φ_a [Nm³/hr]	Spec. Energy
6-inch	3	40	13.3
10-inch	15	175	11.7
24-inch	220	1800	8.2

* Part of the data is obtained from industrial mills by SMIT

A number of publications about the scale-up of spiral jet mill exist, such as by KANO and MORI. The latter proposed the correlation

$$\Phi_s = K \cdot W^a \qquad\qquad (6.3)$$

The power a varied from 2.0 to 2.5. It should be realised that this equation varies for different test materials and mill configurations. The improved energy efficiency can be explained by the fact that in larger mills the number of nozzles increases. This results in a larger contact area between circulating particle bed and the entraining jets.

MÜLLER derived dimensionless numbers for scale-up based on mill dimensions, throughput and energy input.

6.2.7 Performance of the closed circuit jet mill plant

HERBST, HUKKI AND ZIMMELS described the application of external classifiers for the optimisation of grinding plants. During the closed circuit grinding experiments carried out in this project the coarse flow of the external classifier LLC20 was recirculated to the 10-inch spiral jet mill. Figure 2-1 shows the lay-out of the closed circuit plant.

Accumulation of hold-up: Figure 6-21 presents a series of hold-up measurements made on the 10-inch spiral jet mill.

At a recirculation rate of 7.5 kilograms per hour the hold-up increased linearly with the solid feed. When operating with a 15 kilograms per hour recirculation the hold-up rose sharply, but did not exceed a value of 220 grams.
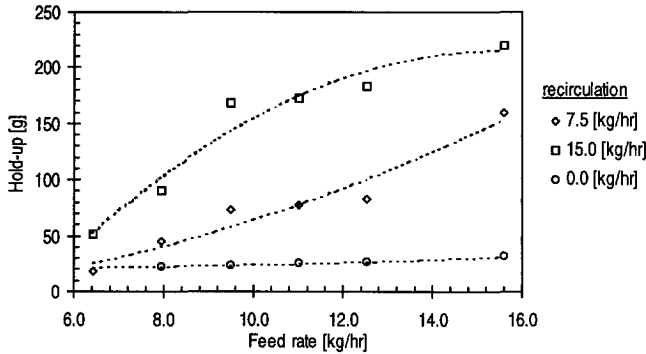
Figure 6-21 Hold-up of the 10-inch spiral jet mill for open and closed circuit grinding for different feed rates. Nozzles 8x 2.5 mm; Test material CW.

Dynamics of closed circuit jet mill plant: Figure 6-22 shows the development of the mass flow in time after a step change on the solid feed to the mill.
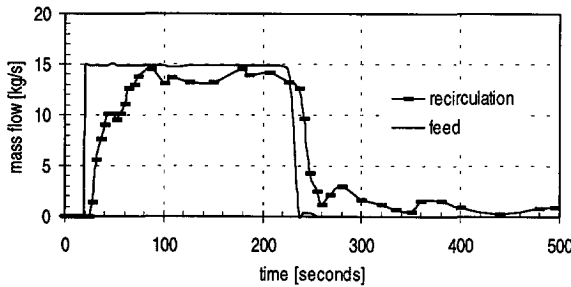
Figure 6-22 Evolution of feedrate and recirculatiion rate in time.

At t = 20 seconds the solid feed to the mill was brought to 15 kilograms per hour. Shortly after the start-up no recirculation was detected due to the residence time of the coarse flow in the classifier body and the rotary valve. Gradually the recirculation rate increased and stabilised at approximately 13 kilograms per hour after 80 seconds. Oscillations in the recirculation flow occurred with a frequency of 90 seconds. The time span between two oscillations was of the order of the total residence time of the mill and external classifier. At t = 220 seconds the feed to the mill was stopped. The oscillating recirculation continued until the closed circuit was empty.

Energy use of jet mill per kilogram ground product: Energy consumption is responsible for a major part of the cost of most grinding processes [AKUNOV]. In this section the energy consumption of the open and closed circuits will be investigated. The results will be compared on the basis of the energy consumption per kilogram

throughput. Two different product qualities, defined by the median size of the mill product were investigated.

Figure 6-23 shows curves of the specific energy, *SE*, required for the grinding of a product to a median size of 7.0 microns. The upper curve represents the SE-values for the open circuit jet mill plant that varied from 0.75 to 1.05 MJ per kilogram. The reduction of specific energy used for closed circuit grinding in comparison to open loop was a factor of three. For nozzle pressures higher than 5.0 bar the SE-curve was horizontal, indicating that the optimal operating pressure was reached.
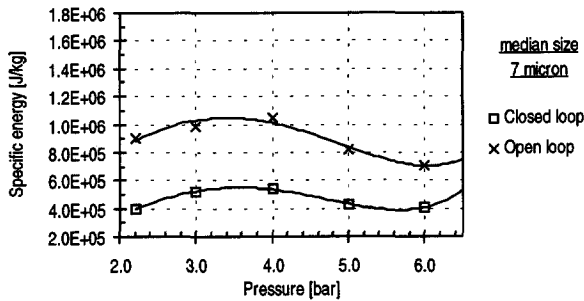
Figure 6-23 Curves of equal median size x$_{50}$ for open and closed circuit grinding. 10-inch jet mill and LCC20 air classifier. Material CW.

Figure 6-24 shows the SE consumption in the case of a product with a median size of 5.0 microns. The average SE for the open circuit plant changed from 1.0 to 1.6 MJ per kilogram. The increase for the closed circuit plant was 0.4 to 0.6 MJ per kilogram.
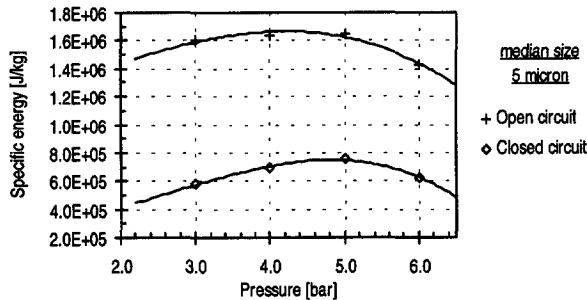
Figure 6-24 Curves of equal median size x$_{50}$ for open circuit and closed circuit grinding. 10-inch jet mill and LCC20 air classifier; Material wax CW.

The closed circuit grinding experiments showed that significant energy savings were obtained. For finer products these savings were larger.

6.3 Experiments with opposed jet mill plant

The previous sections described experiments carried out in the spiral jet mill plant. This section deals with experiments conducted with the opposed jet mill. The materials used here were PW pastilles. More experimental work on this type of jet mill is reported by RINK.

6.3.1 Effect of hold-up in the mill chamber

As in any autogenous mill the hold-up of material plays an important role in the grinding performance of opposed jet mills. There are different ways to measure the hold-up. The first one was an instant closure of the mill chamber. This was quite laborious as the plant had to be shut down, emptied and the mill contents weighed.

An alternative was the use of a weight cell placed under the opposed jet mill. Unfortunately this was practically not possible as the whole unit had to be mechanically uncoupled from the environment by flexible inlets and outlets. Though weight cells would have been the most accurate solution, a more practical way of measuring the hold-up was chosen. The power consumption of the rotor was taken to be a measure for the mill hold-up. A number of manual hold-up measurements were carried out to determine the calibration curve in Figure 6-25.
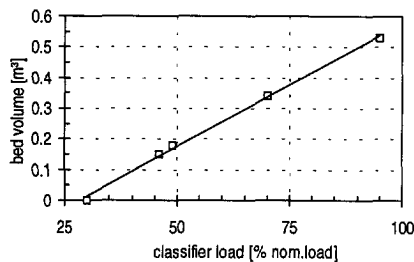
Figure 6-25 Bed volume as a function of the power consumption of the rotor.

A rotor turning in an empty mill used of 30 percent of the nominal power of the engine. Calibration experiments were carried out. The bed volume, measured by opening the mill after a sudden shut down appeared to rise linearly with the power consumption. This relationship was used for real-time hold-up measurements.

6.3.2 Effect of rotor speed

In Chapter 5 the correlation between the median size and the rotor speed of the opposed jet mill is discussed. KHAN derived a similar correlation for the opposed jet mill.

The particle size distribution of a product ground on an opposed jet mill depends on the nozzle pressure and the rotor speed for a given mill configuration. Figure 6-28 shows the PSDs of the mill product for different rotor speeds.
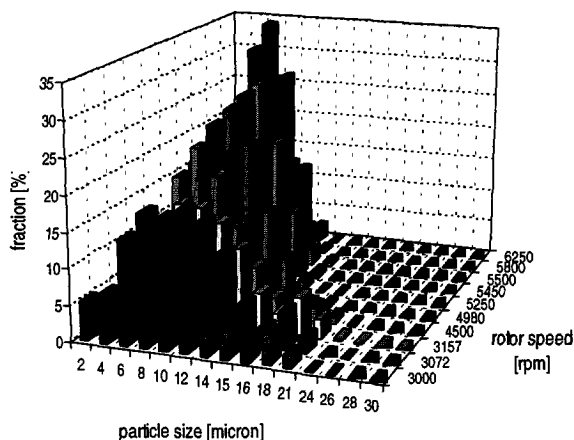
Figure 6-26 Shift of the PSD of mill product on a AFG400 opposed jet mill with changing rotor speed. Feedrate 22 kg/hr. Pn = 8.0 bar.

The feedrate was relatively low and the grinding rate was sufficient to maintain a constant discharge rate. Under these conditions the classification by the rotor was the determining factor. As the rotor speed increased the PSD shifted to the finer particle size and the range decreased. These effects are shown in Figure 6-26.

6.3.3 Control experiments with the opposed jet mill

Figure 6-27 shows the control scheme of the tested opposed jet mill. Control loop 1 measured the particle size distribution of the ground product with a realtime LD-instrument. The measured topsize of the end product, x_{90}, was chosen as a feedback signal. This primary loop directly determined the product quality by manipulation of the rotor speed. This loop was used to compensate for disturbances on the pressure supply or changes in feed material.

Conrol loop 2 measured the hold-up by the power consumption of the rotor using the calibration curve of Figure 6-25.
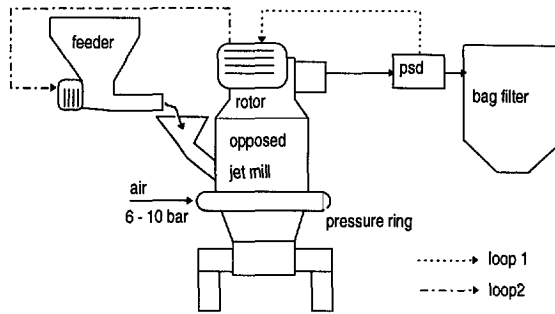
Figure 6-27 Set-up for control experiments with opposed jet mill.

For each experiment with the opposed jet mill the hold-up was maintained at a constant level whilst the PSD was continuously measured.

In Figure 6-28 the mill throughput and the x_{90} of the end product are plotted against the corresponding mill hold-up. The experiments were performed at a constant rotorspeed of 4120 rpm. The throughput, plotted on the right hand axis, was varied from 75 to 130 kilograms per hour.
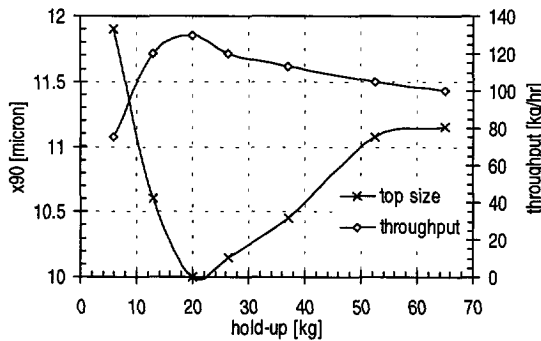
Figure 6-28 Product fineness and throughput as function of the hold-up. AFG630 opposed jet mill. Product PW. Rotorspeed 4120 rpm.

These curves indicate the existence of a value of the hold-up were the throughput was highest and the product was finest. In this situation the mill was grinding most efficiently. This phenomenon was also reported by ØZMERIH for grinding minerals.

6.4 Conclusions

A systematic analysis has been made of the performance of the spiral jet mill plant with respect to process conditions and plant configuration. The results of the open circuit and closed circuit grinding research demonstrated the following:

1. A spiral jet mill has a tendency to show unstable classification behaviour at higher solids loading, the transition being rapid. This fact urges the user to operate the mill at a safe distance from the maximum allowable throughput in order to avoid the risk of product that is out of specification.

2. The use of an external classifier that recirculated the coarse fraction to the jet mill allowed an increase of the throughput of 25 to 50%, whilst maintaining the energy input at the same level. This means a considerable decrease of the specific energy used, as well as reduced operator costs.

Current on-line particle size instruments can provide a signal for stabilising feedback control. The use of a stabilising controller makes it possible to operate the mill closer to the specification limit. The risk of producing material out of specification is greatly reduced.

Stabilising control based on the mill pressure failed due to the non-uniqueness of the relationship between the pressure in the mill and the hold-up.

The use of the external free vortex classifier in combination with the spiral jet mill allowed a considerable reduction of the specific grinding energy. Gains on the basis of equal median size were largest for the finest mill product (5 microns). The location of the minimum specific energy shifted to higher pressures for finer products.

The PSDs of jet mill product showed self similarity as long as the mill performance was stable. Thus the results for different median sizes could be compared with equal x_{90}. In case of large instabilities due to overloading multi-modal PSD were found.

The free vortex classifier was operating at the limit of its size range. Large dead fluxes caused unnecessary loading of the mill. The large volume of the classifier body served as a buffer for unstable product flows leaving the mill.

The use of a second ejector positioned on the opposite site of the mill chamber of a spiral jet mill gave an improved internal classification.

Both the classifier rotor in the opposed jet mill and the free vortex classifier are sensitive to pressure fluctuations on the nozzles. Spiral jet mills are more sensitive to hold-up variations than opposed jet mills.

List of symbols

d_n	nozzle diameter	[mm]
K	constant	[-]
m	mass	[kg]
N_r	rotor speed	[rpm]
P	pressure	[bar]
RR	reduction ratio	[-]
SSA	specific surface area	[1/m]
W	power draw	[W]
x	particle size	[micron]

Sub- and superscripts

a	area based
s	solid
rec	re-circulation
v	volume based
i	size class
f	feed
m	mill
cl	classifier
p	product

Literature

Akunov, V.I., Calculation of unit energy expenditure and communition costs for countercurrent jet mills, *Soviet Mining science*, vol. 22 (2), 122-127, 1986

Austin, L.G., Bhatia, V.K., Experimental methods for grinding studies in laboratory mills, *Powder Technology*, 5, 261-266, 1971 - 72

Bazin, C., Girard, B., Hodouin, D., Time series analasis: a tool for operators training? application to the direct reduction of ilmenite concentrate, *Control of particulate processes, Kananaskis, Canada*, 1995

Benz, M.; Herold, H.; Ulfik, B., Performance of a fluidized bed jet mill as a function of operating parameters, *Int. J. Miner. Process.*, 44-45, 507-519, 1996

Callow, M. I., Start-up autogenous grinding circuits successfully, *Chem. Eng. Prog.*, 87(5), 45-50, 1991

Dotson, J.M., Extending the range of jet mills, *Ind. Eng.chem.*, 54 (1962) 62, 62-65, 1962

Ghadiri, M.,Yuregir, K.R. et al, Influence of processing conditions on attrition of NaCl crystals, *Powder Technology*, 65, 311-320, 1991

Gommeren, H.J.C., Progress reports no 1-8, Jet Mill Project, *Internal reports*, 1992-96

Häse, U., Influence of feed particle size and a nozzle shape in the opposed jet grinding of lime-stone, *Zement-Kalk-Gips,* 12, 1985

Herbst, J.A., Lo, y.c., Optimization of grinding circuits, *xvii intern. mineral processing congress,* 1, 259-265, 1991

Honma, T., Hasegawa, M. and Kanda, Y., Effects of Feed Particle Shapes on Jet Pulverization, *J Chem Eng Japan,* 17/2, 221-223, 1984

Hukki, R.T., Allenius, H., A quantitative investigation of the closed grinding circuit, *Trans.Soc. Min. Eng. AIME,* 241, 482-487, 1968

Huwald, E,; Clement, M,, Investigations on grinding in an opposed jet mill, *Erzmetall,* 29(11), 503-8, 1976

Jacobs, W., Mertins, E., Energy efficiency in autogeneous grinding, *Partec 86,* , 249-255, 1986

Kano, O., Yamada, Y., A new scale-up method of jet pulverizers, *Powder and bulk solids conference/exhibition,* 306-311, 1989

Khan, A., Ramanujam, M., Improved correlation for superfine grinding in a condux air jet mill, *Indian Chem. Eng.,* 20(4), 49-51, 1978

Kneile, R., Wring more information out of plant data, *chem.eng.,* march, 1995

Köhler, R., Grinding of waxes by air jet mills and the application of micronized waxes in paintings, *Fette, Seifen, Anstrichm.,* 87(5), 214-216, 1985

Mani, B.P., Venkateswarlu, D., Untersuchung uber die Zerkleinerung in Strahlmühlen, *Aufbereitungs-Technik,* 1.20, 238, 1980/81

Mori, Y., Studies on jet pulverizing, *Symposium Zerkleinern, Frankfurt,* 515-530, 1962

Müller, F.; Polke, R.; Schädel, G., Spiral jet mills: hold up and scale up, *Int. J. Miner. Process.,* 44-45, 315-326, 1996

Ocepek, D., Salatic, D., Grujic, M., Energy saving in the comminuton processes, *ljubljana, partec 86,* 1986

Onuma, E.; Asai, N.; Jimbo, G., Estimation of steady-state characteristics of closed circuit grinding system from locked-cycle test data, *J. Chem. Eng. Jpn.,* 9(6), 485-488, 1976

Pauw, O.G., The minimization of overbreakage during repetitive impact breakage of single ore particles, *Powder Technology,* 56, 251-257, 1988

Pauw, O.G., Mare, M.S., The determination of optimum impact breakage routes for an ore, *Powder Technology,* 54, 3-5, 1988

Rao, T. C., Improvement of plant performance: A few Indian case studies, *Miner. Process.: Recent Adv. Future Trends, Proc. Conf.,* 299-310, 1995

Rink, N., Ciersiepen, C., Vergleichende Untersuchungen an Strahlmühlen, *4th European Symposium on Comminution,* 387-402., 1975

Rowe, R.M. and Baltich, L.K., Energy Efficiency of Comminution Processes Crushing, Grinding, and Classification Program, *AMAX Res Dev Inc,* 1984

Schädel, G., Wellmann, J.P., Eine Moglichkeit fur die Mass-stabsvergrosserung von Spiralstrahlmuhlen, *BASF AG, Ludwigshafen,* 1990

Schäfer, W., Sommer, K., Influences of Dispersion and Convection during grinding on the solid distribution in a spiral-type Jet Mill, *1st World Congress Part.Techn. Comminution,* 2, 325-343, 1986

Schäfer, W., Sommer, K., Particle size distribution of hold-up and product in a jet mill, *TIZ International Powder Magazine,* vol. 114-10, 1990

Viswanathan, K., Mani, B.P., Analysis of a closed grinding circuit, *Journal of powder and bulk solids,* 8-2, 25-28, 1984

Weyher, L.H.E., Richards, R.G. and Trawinski, H.F., Innovative Grinding Circuits through Staged Classification and Concentration, *SME/AIME,* no.85-120, 1-40, 1985

Yamada, Y., Kano, O., Yabuta, K., Coupling system of air jet pulverizer and air classifier, *Powder and Bulk Solids,* 1992

Yoon, S. H.; Kim, S. Do; Kang, Y.; Cho, S. H.; Kim, Y. J., Pressure fluctuation in a fluidized-bed jet mill, *Nonmunjip - Ch'ungnam Taehakkyo Sanop Kisul Yon'guso,* 9(1), 175-184, 1994

Yoon, Suck Ho; Kim, Sang Do; Kang, Yong; Kim, Young Joo; Cho, Seung Ho, Effective comminution of diatomaceous earth in a vertical type jet mill, *Korean J. Chem. Eng.,* 12(4), 436-441, 1995

Zimmels, Y.; Feldman, C., Economic modeling and optimization of closed - circuit grinding processes, *Trans. Soc. Min., Metall., Explor.,* 292, 1805-13, 1993

Øzmerih, L., Optimization of a fluid bed opposed jet mill, *Ph.D. thesis Norwegian Inst. of Technology,* 1989

Chapter 7

Dynamic modelling of a closed circuit jet mill plant

This chapter considers the dynamic modelling of the jet milling process combined with an external classifier. Paragraph 7.2. discusses the mathematics of grinding models based on population balances. Paragraph 7.3 describes the system boundaries and process variables of the grinding plant. Functional forms of the breakage and selection for breakage are examined as well as terms for particle transfer between the subsystems in paragraph 7.4. Simulation experiments initialised with process data of the open and closed circuit jet mill plant are presented in paragraph 7.5. This chapter ends with conclusions.

7.1 Introduction

7.1.1 Objective

The increasing power of computers allows a more quantitative approach to problems in the operation of grinding processes that require the solution of complex systems of mathematical equations. This approach offers a wider scope in investigating alternative configuration and more efficient operation of the jet mill plant. In addition, the numerical analytical approach provides a deeper understanding of the internal mechanisms of the processes studied. The interaction of the spiral jet mill and the air classifier was investigated by dynamic experiments presented in Chapter 6 and model simulations presented in this chapter. This knowledge can be used for the following purposes.

Stabilising control: In the black box model the product quality and throughput were related to the process inputs with a simple power law expression. Such a model can be used as a basis for control and the implemented in a control strategy. The disadvantage of these models is their limited predictive capabilities as for each new test material or plant geometry new tests have to be carried out to update and adapt the model. In case of stabilising control some model errors will not pose major difficulties, especially in the lower frequencies [EEK]. Work on the use of grinding models for control purposes was published by BASCUR.

Process optimisation: An important state variable is the hold-up which is to be predicted by the model on the basis of the same process inputs as the real mill plant. This state estimation can be an alternative to direct measurements of the hold-up, which require expensive sensors and plant modifications. The articles by FRÜHWEIN and HARTLEY deal with the use of models used for the optimisation of grinding plants.

Remark: Re-design and scale-up of grinding plants requires a fairly accurate description of the physical processes at the machine level, as illustrated in Figure 1-6, Chapter 1. Computational fluid dynamic simulations are discussed in the Chapter 8.

This chapter deals with mechanistic input-output models at the process level.

7.1.2 System description

The system boundary is defined as the interface between the parts of grinding plants that are of interest with respect to the model purpose and the rest of the system and its environment. Only the behaviour of the interior of the system boundary is modelled, as is shown in Figure 7-1.
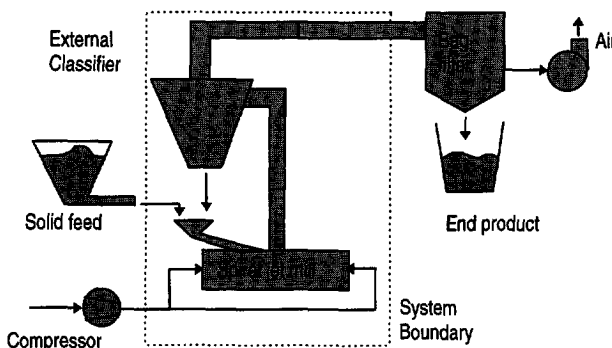

Figure 7-1 Lay-out of closed circuit jet mill plant comprising a spiral jet mill and an external free vortex classifier.

The jet mill and the external classifier are assumed to be inside the system boundary. Auxiliaries such as the solid feed unit, high pressure air supply and the bag filter are considered to be a part of the surrounding system.

For grinding, the mill uses compressed air which enters the mill through a number of nozzles. The feed particles enter the mill through a separate inlet, which is an injector mounted on the top plate.

7.1.3 Approach

In Chapter 6 the equation 6.1 was used to predict the median size of the mill product for different combinations of feedrate and nozzle pressure. This empirical equation was based on pilot plant experiments and can be considered a black box model.

In this chapter a more physically based model will be described that relates the PSD of the end product to process inputs, conditions in the mill and material properties. The latter were determined by the off-line breakage tests described in Chapter 4.

A simple linear grinding model can be represented by mass flows, and particle size vectors and a mill matrix as was first done by BROADBENT. The grinding model can then be written down schematically as

$$
\begin{bmatrix} q_{P,1} \\ \vdots \\ q_{P,i} \\ \vdots \\ q_{P,n} \end{bmatrix} = \begin{bmatrix} B_{11} & 0 & \cdots & \cdots & 0 \\ \vdots & \ddots & \ddots & & \vdots \\ B_{j1} & & B_{ji} & \ddots & \vdots \\ \vdots & & & \ddots & 0 \\ B_{n1} & \cdots & B_{ni} & \cdots & B_{nn} \end{bmatrix} \begin{bmatrix} q_{F,1} \\ \vdots \\ q_{F,i} \\ \vdots \\ q_{F,n} \end{bmatrix}
$$

Physically this means that in such a process the feed particles are loaded once and discharged directly. The elements of the lower triangularity of the transfer matrix B represent the breakage functions of the feed q_F. The length of this vector equals the number of size classes ranging from q_{F1}, q_{F2}, ...to q_{Fn}.

In grinding practice the 1st size class traditionally contains the largest particles, while the nth class contains the finest particles. A higher number of classes, n, will give more accurate simulation results, but also requires more computational time. In the following paragraphs a shorter matrix notation will be used

$$q_P = B \cdot q_F \qquad (7.1)$$

Jetmilling is a autogenous grinding process, which means that the material hold-up in the mill serves as the grinding medium. The particles that are continuously fed to the

mill have a finite residence time during which they are loaded repetitively by mutual collisions. This makes the description of the jet milling process far more complex. The changes in the particle population cannot be computed using the simple transfer matrix of equation 7.1. Mathematical equations for particle breakage and transfer in the model are functions of the hold-up itself. This gives the model a non-linear character.

The model derived in this chapter is a phenomenological Population Balance Model that contains expressions for size reduction and particle transfer based on the well-known comminution laws and force equilibria of particles in a flow field. These expressions are a function of the conditions in the mill, and are therefore time-dependent. The additional process knowledge to develop this model was collected by two kinds of experiment:

1. Pilot plant experiments carried out with the 10-inch spiral jet mill in open circuit and in combination with the free vortex classifier (see Chapter 6).

2. Off-line breakage tests: Impact of particles on a fixed target and compression tests. The results are presented in Chapter 4.

7.2 Population balance model

7.2.1 Description of a continuous grinding process

In a population balance model (PBM) the product flows are expressed as PSD-density vectors. The continuity equation is to be solved for each size class.

$$\frac{\partial}{\partial t}(Conservation) = In - Out + Generation \qquad (7.2)$$

In the literature many publications can be found dealing with population balances applied for the mathematical description of crystallisation, granulation and precipitation processes. Grinding processes were also extensively described by mathematical models. Examples are the work by GRIESHAMER BROUSSAUD, GOLDMAN and DOROKHOV.

The PBMs with relevance to grinding are mostly volume based as the total mass of product remains constant during the process implying that disappearance of mass in certain size classes will result in the appearance of mass in other size classes. The conservation equation of the ith size class for a continuous grinding process can be written as

$$\frac{\partial \, m_{m,i}(t)}{\partial t}$$

$$= \Phi_F(t) q_{F,i}(t) - \Phi_P q_{P,i}(t) - M(t) \left[S_i(t) q_{m,i}(t) + \sum_{j=1}^{i} B_{ij}(t) S_j(t) q_{m,i}(t) \right] \qquad (7.3)$$

In the population balance model the mass balance is solved for each defined size class ($m_{m,i}$). The total mass of material present in the mill chamber $M(t)$ and the particle size density are calculated and normalised after each time step by

$$M(t) = \sum_{i=1}^{n} m_{m,i} \text{ and } q_{m,i} = \frac{m_{m,i}}{M(t)}$$

Particles can leave or enter a certain size class i either as a result of breakage or by transport in and out the mill. Articles about solution methods of PBMs were written by HOUNSLOW, MELOY and RAMKRISHNA. The integration scheme and size grid have to be chosen carefully. In this Chapter the selection was made by trial and error and the use of 64 size classes was found sufficient. This was twice as many as the number of size classes provided by the laser diffraction instruments used.

Terms for mass transfer: The mass transfer over the mill is described by the flowrates and particle size densities of the feed Φ_F and discharge Φ_p. The particle size density of the discharge flow is determined by the internal transfer of particles in the rotating flow field of the spiral jet mill.

Terms for particle breakage: EPSTEIN was the first person split the process of breakage into two steps, namely the probability of selection and the distribution of broken particles over other smaller size classes.

The *selection for breakage function, S,* can be seen as a death term. It is the rate at which particles leave a certain size class due to breakage. Not every particle in the mill will break upon colliding with another particle or with the wall. The applied forces onto the particles have a distribution as has also the particle strength. A certain percentage will survive when submitted to weak forces. Therefore the probability for a particle to break during an event of loading will be smaller than unity. After loading the broken, unbroken and new particles will usually be mixed before the next event of loading. Before a particle is discharged from the mill it is also loaded several times.

If the change of particle fraction $q_{m,1}$ due to breakage is denoted by $dq_{m,1}$, then the following equation is valid:

$$\frac{dq_{m,1}(t)}{dt} = -S_1 q_{m,1}(t) \qquad\qquad (7.4)$$

The number of particles in size class $q_{m,1}$ which is selected for breakage during a time step, dt, will leave size class $q_{m,1}$.

The *breakage function, B,* is an equivalent of a birth term. For a certain fraction q_i the disappearance is related to a parameter S_i, but there are also particles appearing from the coarser fractions. The parameter b_{ij} expresses how broken particles leaving coarser size classes ($j<i$) will appear in size class i.

$$\frac{dq_{m,i}(t)}{dt} = -S_i q_{m,i}(t) + \sum b_{ij} S_j q_{m,j}(t) \qquad\qquad (7.5)$$

Here b_{ij} denotes the breakage function. The summation form can be presented in matrix form where the breakage matrix B_{ij} is a diagonal matrix. I is the unity matrix. $q_i(t)$ is the PSD given as a vector.

$$dq_i(t) = -\left[I - B_{ij} \right] \cdot S_i \cdot q_i(t) \cdot dt \qquad\qquad (7.6)$$

Closed circuit grinding: The model for a continuous mill can be extended for closed circuit grinding by adding terms that describe the performance of an external classifier. Figure 7-2 shows the configurations of the grinding plant with the symbols for the various flows.
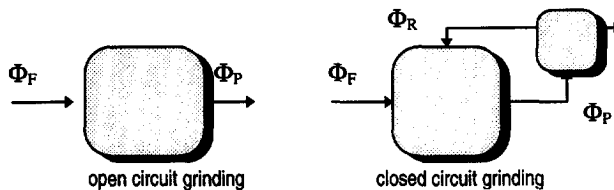
Figure 7-2 Basic configurations of the modelled grinding plants.

The term $Y_i(t)$ is the separation efficiency of the external classifier that expresses which fraction of the powder flow leaving the mill is recirculated to the mill for regrinding. The dead time before the product is returned to the mill is represented by τ.

$$\Phi_R(t) \cdot q_R(t) = Y(t) \cdot \Phi_P(t-\tau) \cdot q_P(t-\tau) \qquad\qquad (7.7)$$

The population balance of the closed circuit grinding plant becomes:

$$\frac{\partial\, m_m(t)}{\partial\, t}$$

$$= \Phi_F(t)q_F(t) - \Phi_P q_P(t) - M(t)[I - B_{ij}]S(t)q_m(t) + \Phi_R q_R(t)$$

(7.8)

7.3 Extension to a multiple zone model

7.3.1 Model assumptions

Phenomena like grinding and particle transfer are very dependent on local flow patterns and solid concentrations. To obtain a more physically based model the mill has been divided into zones where particles are submitted to size reduction due to collisions and particle transfer based on forces in the flow field. A variety of effects have to be included for in the grinding model depending on the material to be ground and the type of mill. It must be realised that the following assumptions were made to reduce the PBM equations:

1. The zones in the mill were well-mixed.

2. No agglomeration or growth occurred.

3. Empirical expressions for particle breakage and transfer are simple functions of operating conditions and particle properties.

4. There is no effect of shape on the physical processes. The particles are modelled as spheres.

7.3.2 Division into zones

An early multiple zone model was already described by HENDRY in 1966. Concentric zones were defined in the mill as shown in Figure 7-3. In the following paragraph this concept will be used to model the spiral jet mill.

Figure 7-3 The zones model of the spiral jet mill connected the external classifier.
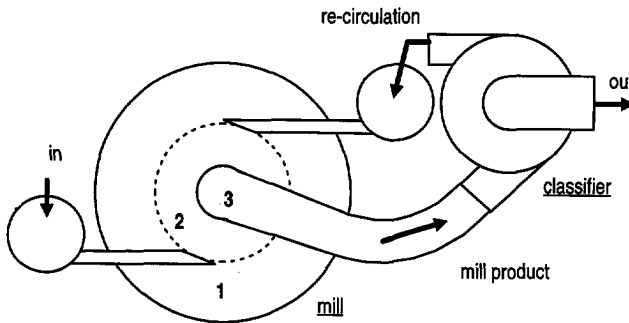
The jet mill chamber is divided into three subsystems called the *grinding zone (1)*, *transfer zone (2) and discharge zone (3)*. The number of zones is limited in order to save computational time. Between these zones mass exchanges occur, which connect the separate subsystems. The external classifier is in fact the fourth subsystem of the closed circuit grinding system. In Figure 7-1 the four subsystems of the closed circuit grinding system are shown schematically. The hold-ups PSD of the product in the zones are calculated by population balances. The population balance for zone 2 can be written as

$$\frac{\partial q_{m2}(t)}{\partial t} = -\left[I - B_{ij}\right]M_{m2}S \cdot q_{m2}(t) + P_{12}q_{m1}(t) - P_{21}(t)q_{m2}(t) \qquad (7.9)$$

The term M_{m2} represents the total mass of particles present in zone 2. The function P_{12} expresses the transfer of particles from zone 1 to zone 2.

In the jet mill system particles are classified as a result of different trajectories in the flow fields. Similar to classifier theory, S-shaped functions are used to describe the particle transport. Several researcher have stated that the PSD of the end product is strongly related to the flow pattern at the outlet of the jet mill [SCHÄFER, SCHÄDEL, MÜLLER].

The term P_{12} is a statistical function that expresses the amount of particles transferring from zone 1 to 2. P_{21} represents the transport function in the reverse direction. The stochastic approach makes it possible to describe the separation results inclusive of the efficiency of separation. A cumulative log-normal distribution is used for the classification behaviour.

$$P_{12}(x) = 1 - \frac{1}{2}\left[1 + erf\left(\frac{ln(x) - ln(x_{50,12})}{\sqrt{2}ln(\sigma_{12})}\right)\right] \qquad (7.10)$$

The function $P_{12}(x)$ represents the probability of a particle with a certain size x to transfer from zone 1 to zone 2.

The pilot plant experiments indicated that the hold-up has a strong influence on the mill performance. Therefore empirical relations were used and the cut size and the imperfection of the S-shaped transfer functions were made time dependent. The star * indicates the nominal value, in a situation without disturbance of the hold-up. Thus a higher hold-up leads to a larger x_{50} and a wider spread of the particle size.

$$x_{50,12}(t) = x^*_{50,12}\left(1 + K_{x12}M_m^2(t)\right) \quad and \quad \sigma_{12}(t) = \sigma^*_{12}\left(1 + K_{s12}M_m^2(t)\right) \qquad (7.11)$$

7.3.3 Process variables

Combination of population balances, comminution and classification behaviour will provide a complete model of the pilot plant. Figure 7-4 illustrates the interactions between the processes in the closed circuit jet mill plant.
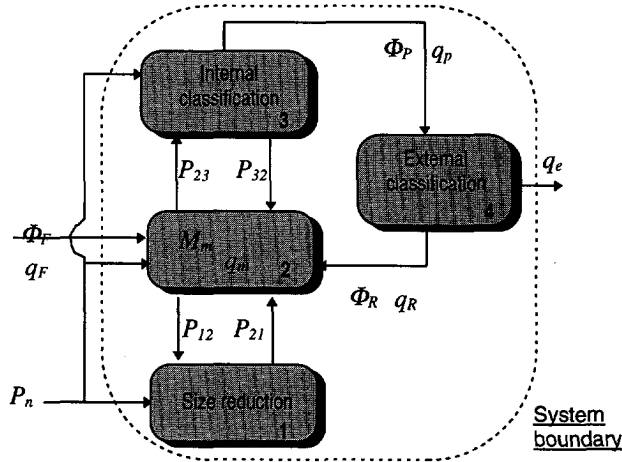
Figure 7-4 Interactions between processes described by mill model.

The input variables of the jet mill are:

1. Solid feed rate Φ_F

2. Particle size distribution of the feed q_F

3. Pressure on the nozzles P_n

4. Control air to the external classifier $\Phi_{air,C}$

The output of the system is given by :

1. Particle size distribution of the product q_P

2. Mass flow of the product Φ_P

7.4 Functional forms of breakage functions

7.4.1 Selection for breakage

AUSTIN [1971] gave an overview of the mathematical description of breakage processes. A classical equation for the selection function is

$$S = \alpha \left(\frac{x}{x_{max}} \right)^{\lambda} \qquad (7.12)$$

It will be clear that the parameters α en λ are strongly dependent on operating conditions and material properties. The following sections discuss some extensions made to the original selection function. In the dynamic model the selection function contained terms that took into account the influence of the hold-up, K_H, the energy input, K_E, and the particle properties K_P.

$$S(t) = K_H \cdot K_E \cdot K_P \qquad (7.13)$$

These terms are expressed as:

$$K_H = \left(\frac{C_H^{\beta}(t)}{C_H^{\beta}(t) + K_2} \right); \; K_E = \left(P_n(t) \cdot d_n^2 \right); K_P = \alpha \cdot \left(\frac{x}{x_{max}} \right)^{\lambda}$$

<u>Effect of particle size (K_P)</u>: The selection function decreases monotonously as a function of the particle size. At constant pressure level and hold-up the selection function can be represented by the original exponential curve. The power λ indicates how rapidly the breakage rate decrease with size, as is shown in Figure 7-5. This breakage behaviour, which is a material property, was investigated by single particle impact tests and compression tests described in Chapter 4. The following parameters based on impact tests were used in the model: Material CW $\lambda=0.7$; Material PW $\lambda=1.7$.
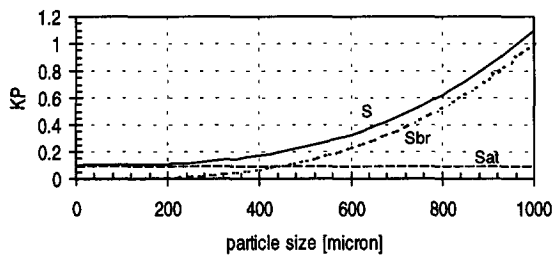
Figure 7-5 Terms for breakage $K_{P,B}$ and attrition $K_{P,A}$.

In a jet mill two breakage modes occur, and therefore the selection function was split. The normal breakage is expressed by $K_{P,B}$. A second selectivity function, $K_{P,A}$, was introduced to separately describe attrition. As a first approach the attrition was assumed to be a constant over the size range as is shown Figure 7-5. These selection terms are multiplied by the breakage functions as described in paragraph 7.4.2 and represent two different comminution modes.

Effect of hold-up (K_H): The concentration of particles in the grinding zone, C_H, has a distinct influence on the grinding rate as the selection for breakage is related to the number of collisions and the particle loading during a collision. In the selection function an empirical term is used to take into account the mill-hold-up.
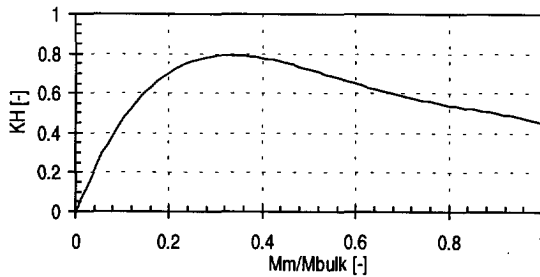
Figure 7-6 Hold-up term KH in selection function versus C_H=Mm/Mbulk.

The concentration-term plotted in Figure 7-6 displays an optimum for the grinding rate. If too few particles are present in the turbulent flow field of the grinding zone the probability of collision will be low and the grinding rate drops.

A high particle concentration $C_H(t)$ reduces the volume of the turbulent jets. Furthermore the maximum velocity that the particles can reach goes down as the free path before collision is shorter. These effects have a negative influence on the number of effective collisions and the selection for breakage rate drops.

Effect of energy input: The pneumatic energy supplied to the mill is proportional with the nozzle pressure, the number of nozzles and the square of the nozzle diameter. The theory of nozzle flows is dealt with in Appendix A. The grinding rate at a constant particle concentration, is assumed to be proportional to the energy input, as is shown in Figure 7-7.
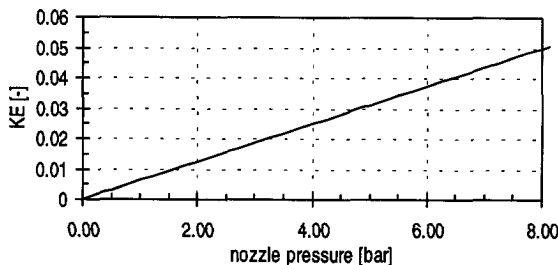
Figure 7-7 Energy term KE in S-function.

The total selection for breakage is the product of the three terms discussed above. It will be a combined effect of material properties, amount of material in the mill and the energy input.

7.4.2 Breakage distribution function

The cumulative breakage function B_{ij} ($i{\geq}j$) predicts how broken particles of a certain size class, j, appear in smaller size classes, i. The breakage function is divided into two components, one to express normal breakage and the other for attrition.

$$B_{ij,B} = \frac{K_{P,B}}{2K_P}\left[1 + erf\left(\frac{ln(\,rf_B x_i\,/\,x_j\,)}{\sqrt{2}\,ln\sigma_B}\right)\right] \qquad\qquad (7.14)$$

and

$$B_{ij,A} = \frac{K_{P,A}}{2K_P}\left[1 + erf\left(\frac{ln(\,rf_A x_i\,/\,x_j\,)}{\sqrt{2}\,ln\sigma_{At}}\right)\right] \qquad\qquad (7.15)$$

In which $K_P = K_{PB} + K_{PA}$ and $B_{ij} = B_{ij,B} + B_{ij,A}$

The B_{ij} is not normalised, but the simulation program takes this into account.

A typical breakage function is shown in Figure 7-8 and illustrates how fragments of a larger particle are distributed over the smaller size classes.
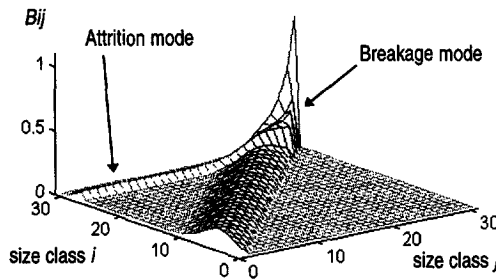
Figure 7-8 Breakage function B_{ij}.

Comment: In this model it is presumed that the breakage function is only related to material properties rather than the process conditions. The impact experiments showed a reduction factor of 2.5 for our test material at an impact velocity of 200 meters per second. The breakage function, is assumed to be only size dependent. For the attrition a reduction factor of 7.0 was taken, based on the discussion in Chapter 4.

7.5 Functional form of external classification

In the closed circuit plant the coarse fraction in the mill product was recirculated to the jet mill for regrinding by an external classifier. The separation in a vortex flow of that classifier is disadvantageously influenced by stochastic disturbances that are primarily due to the turbulence of the air stream, the particle wall interactions and the particle-particle interactions.

These disturbances cause an inefficiency in the classification process as particles may be displaced into another particle stream than was to be expected on the basis of the equilibrium between the centrifugal and the drag forces. The classification function of the external classifier was expressed by the statistical PLITT equation.

$$Y_{class} = R_d + (1 - R_d)\left(1 - e^{-0.963\left(\frac{x}{x_{50}}\right)^m}\right) \qquad (7.16)$$

The cut-size depended on the operating conditions of the LCC20 classifier which could be tuned by the fan at the outlet. The dead flux, R_d, was also determined by experiments and varied from 25 to 55 percent.

7.6 Simulation experiments

7.6.1 Default model parameters

The PBM described in the previous paragraphs was implemented in a computer model. Table 7-1 contains the default values of the parameters used for the simulations.

Table 7-1 Default parameters of jet mill model

Process	Description	Parameter	Value	Equation
Breakage	Power [-]	λ	1.7	7.14
	Constant [-]	K_1	1.0	7.14
	Reduction factors [-]	Rf_1; Rf_2	2.5; 7.0	7.15; 7.16
Transfer	Cut size [μ]; spread zone 12 [-]	$X_{50,12}$; $\sigma_{50,12}$	14.0; 1.5	7.11
	Cut size [μ]; spread zone 23 [-]	$X_{50,23}$; $\sigma_{50,23}$	6.0; 1.5	7.12
Classifier	Cut size [μ]	X_{50c}	10.0	7.17
	Dead flux [%]	R_d	35	7.17
	Residence time [s]	τ	30	7.7

In the following section the influences of the model parameters and the changes of process inputs are investigated.

7.6.2 Effect of the breakage parameters

Importance of attrition term: Figure 7-9 compares the simulation results obtained from a model that only contained a term for normal breakage and a model that contained an extra term for attrition.
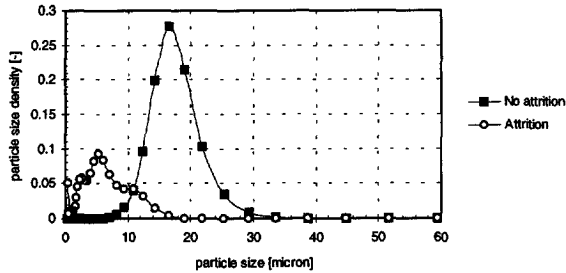
Figure 7-9 Predicted PSD of jet mill product for model based on pure breakage and model extended with attrition term.

The first model did not produce enough fines at all. With the same internal classification function the simulated hold-up of the spiral jet mill increased dramatically up and beyond realistic values. After extension of the model with equations for attrition the simulation results agreed better with the experimental data.

7.6.3 Dynamic responses of the product flow

Response of mass flows: In the open circuit configuration of the plant the external classifier was switched off, thus no particles were recirculated to the mill chamber. Figure 7-10 shows the evolution of the production rate with time using the default parameter values. The experimental data was obtained with the in-line cell.
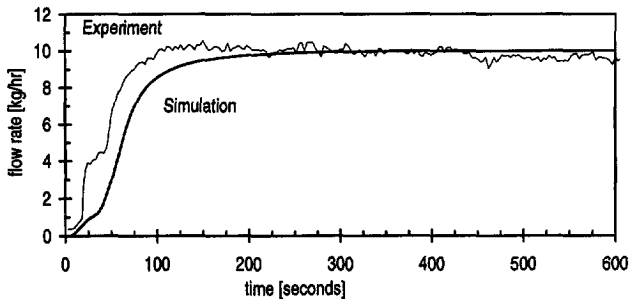
Figure 7-10 Evolution of production rate with time. Open circuit jet mill.

From these simulations it turned out that the process got into a steady state condition after about 150 seconds. This time scale was consistent with some experimental

results due to FRICKE who showed that a stationary condition was established after 180 to 250 minutes in on a spiral jet mill with approximately the same dimensions.

Differences between the measured and simulated curves could be explained by uncertainties during start-up. Nevertheless the experiments and the simulations showed good resemblance. The time delay before the material left the mill indicated that there had to be some kind of mass built up inside the mill chamber.

Remark: The differences between the literature values and the experiments and simulations in this project can also be explained by differences in grindability of the test materials. Simulations confirmed that with higher selectivity for breakage shorter times to steady state were obtained.

Response of particle size distribution: Figure 7-11 shows the evolution of the cumulative undersizes x_{10}, x_{50} and x_{90} in time during a test run. The smooth lines are the simulation results.
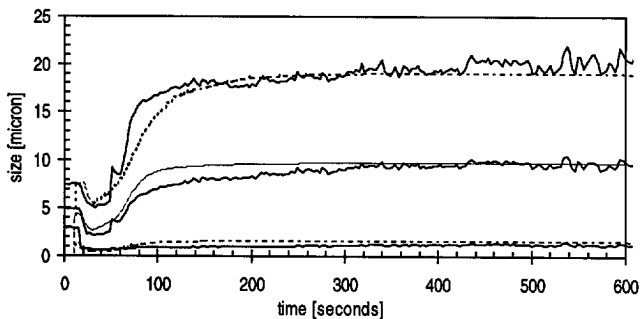
Figure 7-11 PSD of the product in the steady state conditions. Open circuit jet mill.

From the computer simulations we learned that around a critical feedrate the hold-up in the mill reached the value of the bulk density. This was in fact a physical restriction to the hold-up which explained the unstable mill performance. Beyond that range the calculated hold-up by the model are unrealistic. It is proposed to extend the model with stochastic equations to take into account the frequency and extent of the mill loading.

7.6.4 Residence time distributions

The mill simulation program has the possibility to simulate an injected pulse of material with a given size and to trace its fragments in the output. This allowed the determination of the residence time distribution of this material.

Figure 7-12 shows how the particles were moving through the mill after an injection of 10 grams of 10 and 100 micron tracer particles in the central zone (2). During the first few seconds the amount of tracer in zone 2 decreased as the particles were transferred to zone 1 where they were ground. Gradually the tracer fragments started to reappear in zone 2 before they left the mill.
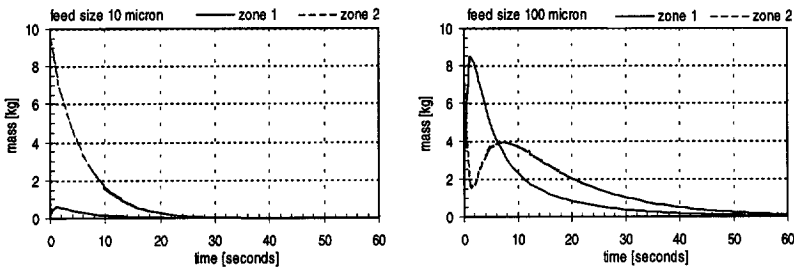
Figure 7-12 Evolution of mass in zones 1 and 2 after a pulse injection.

Figure 7-13 shows the residence time distribution for feed particles with different sizes.
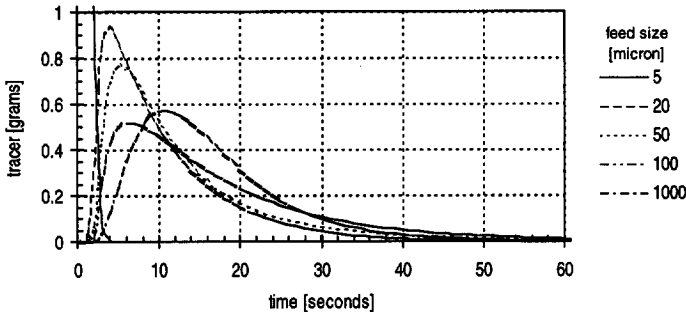
Figure 7-13 Residence time distributions of particles with different sizes.

The recirculating flow from the external classifier usually contains a large amount of fines due to the dead flux. In this section it is investigated what the influence is of those particles on the mill. Four different size classes 5, 10, 20 and 50 micron were injected in the mill. The mean residence time for the indicated sizes varied from 1 seconds for the smallest to 15 seconds for the largest particles. The residence time distribution of the fresh feed material was represented by the 1000 micron curve.

The simulation results corresponded with hold-up experiments. They indicated that the tracer mass of fine particles in the solid feed, such as with recirculation, leave the

mill almost instantly (by-passed), while coarser particles remain a longer time inside the mill.

7.6.5 Comparison between open circuit and closed circuit grinding

In this section the open circuit and closed circuit simulations will be compared. The mill was operated at a pressure of 6.0 bar. The feedrate was adjusted such that the x_{50} was maintained at a constant value of 8.9 micron.

Figure 7-14 shows how the mass flows and the built-up of material evolving over the course of a simulation run. The time needed to reach 95 percent of the nominal rate was 90 seconds in the case of open circuit grinding. This simulation result agreed with times found in the pilot plant experiments. The hold-up stabilised within the same time span at a level of 180 grams.

Figure 7-14 Mass flow leaving the mill versus for open circuit grinding (left). Built-up of hold-up versus time (right). $x_{10}=1.2$; $x_{50}=8.0$; $x_{90}=15.5$ micron.

For the closed circuit grinding tests the product specification was maintained the same. The cut-size of the classifier was 9.5 micron, the dead flux was 30 percent and the sharpness was 1.8. Model results are presented in Figure 7-15. Under these conditions a recirculating load of 29.5 grams per second was obtained at a feed rate of 16.2 grams per second. The indicates an increase of the throughput of the grinding plant by 35 percent at the same energy input.

In the closed circuit configuration it took a longer time to reach the steady, as was also found in practice. The time needed to reach 95% of the nominal rate increased to 158 seconds in closed circuit. Figure 7-15 shows that the total hold up in the jet mill chamber was almost doubled when the external classifier was activated.
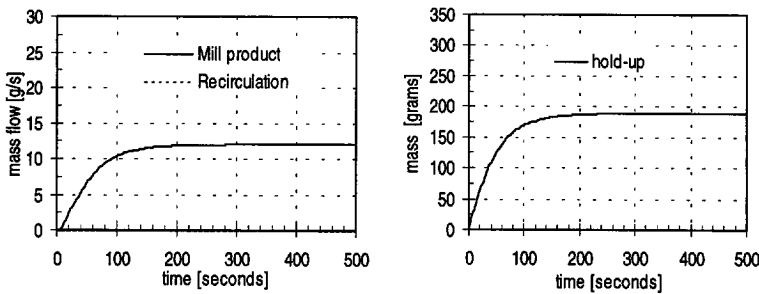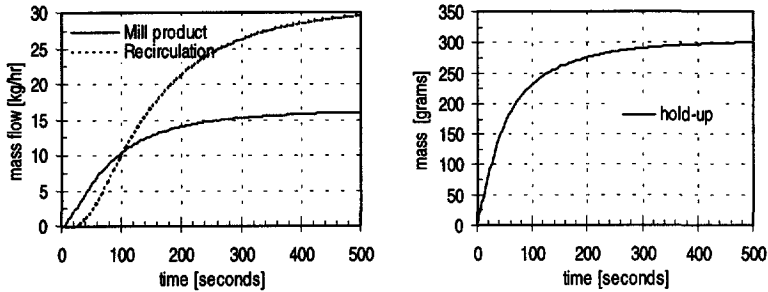
Figure 7-15 Mass flow leaving the mill versus for closed circuit grinding (left). Built-up of hold-up versus time (right). x10=1.2; x50=8.0; x90=15.5 micron.

7.7 Conclusions

A dynamic model was developed to describe the performance of the open and closed circuit jet mill plant. In order to obtain a more realistic description of the local processes inside the mill a multi zone model was constructed. The mill chamber was divided in a number of functional compartments, that is the grinding zone, the vortex zone and the outlet zone.

The breakage parameters obtained from the single particle impact tests gave a good description of the breakage in the large particle size range. Use of the breakage function in the simulation program indicated that the fracture mechanism alone was not sufficient for the creation of fine particles. Therefore an attrition term was added in order to be able to produce realistic results.

The PBM model was able to simulate the dynamic behaviour of the mill based on the interaction between the grinding rate and the discharge rate which are both strongly related to the mill hold-up. The accumulation of material occurred and could lead to unstable mill performance as the volume of the material in the mill reached the physical limit. Instabilities could be predicted but not simulated.

The external classifier was modelled by the empirical Plitt function. Simulations indicate that for a reduction of the deadflux of 30% the throughput can be increased with approximately 10%.

The results of the simulations have been compared on the basis of the distribution of particles and particle sizes in the milling chamber. Small particles were instantaneously by-passed to the mill outlet while the average residence time of the coarse particles corresponded with the measured one based on the hold-up and feedrate.

The stochastic nature of the particle collisions and the variation in particle size, shape and strength require a statistical description of the jet mill process. The current jet mill model contains many empirical parameters. Also the number of zones should be extended. It is proposed to implement similar equations for the mechanisms in computational fluid dynamics model. The turbulence intensities and particle concentration should be related to the breakage kinetics.

List of symbols

B_{ij}	breakage distribution function	[-]
d_n	nozzle diameter	[mm]
C	concentration	[m^3/ m^3]
K	constant	[-]
M_H	mass of hold-up	[grams]
P	pressure	[bar]
q_i	size class i in mill chamber	[-]
$q_{F,i}$	size class i of fresh feed	[-]
r_f	reduction factor of breakage mode	[-]
R_d	deadflux	[-]
S	selection for breakage	[kg/s]
x	particle size	[micron]

Greek

λ	power in selection function	[-]
Φ_p	Product flow	[kg/hr]
σ	variance	[-]
τ	delay time	[s]

Literature

Austin, L. G.; Barahona, C. A.; Weymont, N. P.; Suryanarayanan, K., An improved simulation model for semi- autogenous grinding, *Powder Technology,* 47(3), 265-83, 1986

Austin, L. G.; Trimarchi, T.; Weymont, N. P., An analysis of some cases of non-first-order breakage rates, *Powder Technology,* 17(1), 109-13, 1977

Austin, L.G., A review: Introduction to the Mathematical Description of grinding as a rate process, *Powder Technology,* 5, 1-17, 1971 - 72

Austin, L.G., Bhatia, V.K., Note on Conversion of Discrete Size Interval Values of Breakage Parameters S and B to Point values and Vice Versa, *Powder Technology,* 7, 107-110, 1973

Austin, L.G., Luckie, P.T., Note on influence of Interval Size on the first-order hypothesis of grinding, *Powder Technology,* 4, 109-110, 1970

Austin, L.G., Luckie, P.T., The estimation of non-normalised breakage parameters from batch grinding tests, *Powder Technology,* 5, 267-271, 1971 - 72

Austin, L.G., Perez, J.W., A Note on Limiting Size Distributions from Closed Circuit Mills, *Powder Technology,* 291-293, 1977

Austin, L.G., Shoji, K., Bell, D., Rate equations for non-linear breakage in mills due to material effects, *Powder Technology,* 31, 127-133, 1982

Austin, L.G., Shoji, K., Bhatia, V.K., Jindal, V., Savage, K., Klimpel, R.R, Some results on the description of size reduction as a rate process in various mills, *Ind. eng. chem.,* 1976

Bascur, O. A.; Freeh, E. J.; Herbst, J. A., Dynamic simulation for estimation of industrial grinding circuit control characteristics, *ISA Trans.,* 25(2), 77-83, 1986

Blickle, T.; Menyhart, Mrs. J.; Virag, T., Analysis of grinding kinetics and the change of particle size distribution and numericality in a jet mill, *Hung. J. Ind. Chem.,* 4(1-2, Suppl.), 109-116, 1976

Broadbent, S.R. Gallcott, T.G., A matrix analysis of processes involving particle assemblies, 99-121, 1956

Broussaud, A., Fourniget, G., Guillaneau, J.C., Conil, P., Guyot, O., Conception et gestion assistees par ordinateur des circuits de broyage, *Journees d'etudes sur les nouvelles techniques de broyage et l'economie d'energie,* 1989

Broussaud, A.; Conil, P.; Vedrine, H.; Matos, C. F.; Ferrao, C. N., Modeling of an autogenous grinding and flotation process. Application to the industrial processing of the Moinho complex sulfide ore, *Comm. Eur. Communities, [Rep.] EUR,* 3, 931-60, 1992

Chand, P., Sarda, S.P., An analytical approach to fluid energy mills, *Bulk Solids Handling,* 6 (1), 151-156, 1986

Cross, M., Method for extracting product size distributions from empirical comminution models, *Powder Technology,* 1982

Dorokhov, I.N., Arutyunov, S.Y. and Eskin, D.I., Mathematical Description of the Processes of Jet Grinding, , 27/5, 514-517, 1993

Dorokhov, I.N., Eskin, D.I., Phuc, T.H., Mathematical modeling and design of the fine grinding mills, *8th European Symposium on Comminution, Stockholm,* 1994

Fan, L.S., Srivastava, R.C., A stochastic model for particle disintegration-I. Grinding mechanism, *Chem.Eng.Sci.,* 36 (1981), 1091-1096, 1980

Fricke, H.M., Polke, R., Schadel, G., Wellmann, J., Verweilzeitmessungen in der Spiralstrahlmuhle, *Dusseldorf 1988, Techn.Entwicklung Verfahrenstechnik,* 1988

Frühwein, P., Mathematical simulation as a tool for optimizing comminution processes with respect to particle size distribution of product, *Ger.Chem.Eng.,* 2 (1979), 305-311, 1979

Furuya M., Nakajima Y., Tanaka T.,, Theoretical analysis of closed-circuit grinding system based on comminution kinetics, *Int.Eng.Chem. Proc.Des.Dev.,* V.10, 449,

Gardner, R. P.; Rogers, R. S.; Verghese, K., Short-lived radioactive tracer methods for the dynamic analysis and control of continuous comminution processes by the mechanistic approach, *Int. J. Appl. Radiat. Isot.,* 28(10-11), 861-871, 1977

Gardner, R.P., Austin, L.G., Prediction of size-weight distributions from selection and breakage data, *Symposium Zerkleinern Fragmentation size reduction, Frankfurt,* 2, 232-248, 1962

Gardner, R.P., Sukanjnajtee, K., A combined tracer and back calculation method for determining particle breakage functions in ball milling., *Powder Technology,* 7(1973), 169-179, 1973

Gardner, R.P., Verghese, K., A model with closed form analytic solution for steady state closed circuit comminution processes, *Powder Technology,* 11, 87-88, 1975

Goldman, M., Barbery, G., Flament, F., Modeling load and product distribution in autogenous and semi-autogenous mills: pilot plant tests, *CIM Bull.,* 84(946), 80-6, 1991

Goldman, M.; Barbery, G., Wear and chipping of coarse particles in autogenous grinding: experimental investigation and modeling, *Miner. Eng.,* 1(1), 67-76, 1988

Gommeren, H. J. C., Heitzmann, D. A., Kramer, H. J. M., Heiskanen, K., Scarlett, B., Dynamic modeling of a closed circuit jet mill, *Int. J. Miner. Process.,* 44-45, 497-506, 1996

Gommeren, H.J.C., Heitzmann, K., Scarlett, B., Modelling and control of jet mill plant, *Control of particulate processes, Engineering foundation, Kananaskis, Canada,* 1995

Gommeren, H.J.C., Heitzmann, D.A., Kramer, H.J.M., Heiskanen, K., Scarlett, B., Dynamic modeling of a closed loop jet mill, *8th European Symposium on Comminution, Stockholm,* II, 574-585, 1993

Gommeren, H.J.C., Heitzmann, D.A., Kramer, H.J.M., Heiskanen, K., Scarlett, B., Dynamic modeling of a closed circuit jet mill, *1st international particle technology forum, august 17-19, 1994, Denver,* part II, 197-201, 1994

Gommeren, H.J.C., Heitzmann, D.A., Scarlett, B., Estimation of operating ranges of jet mills using dynamic modelling, *Procedes de Broyage, Toulouse 96,* 10, 43-50, 1996

Grady, D.E., Particle size statistics in dynamic fragmentation, *Journal Appl.Phys.,* 68 no. 12, 6099-6105, 1990

Griesshammer,G., Weigelt, V., Digitale simulation eines Muehlen- Sichter- Kreislaufes. Zerkleinern; 35 Vortraege., *Symposion in Cannes,* 69 Nr 1292 - 1326 teil 1, 1971

Hartley, D.G., Hayward, P.C., Sterns, U.J. and Weller, K.R., The Use of Mathematical Models of Grinding and Classification to Optimize Grinding Circuits at the Mt. Lyell Copper Concentrator, Tasmania, *Min Eng,* , 48-55, 1983

Heiskanen, K., On the estimation of system parameters in mathematical simulation of batch grinding, *Dissertation,* 1978

Heiskanen, K., The modelling of autogenous grinding, *Automation in mining, mineral and metal processing, IFAC,* 1989

Hendry, R., A mathematical model for fluid energy mills, *proc. 2nd European symp on size reduction, a'dam Dechema Monogr.,* 57, 695-727, 1966

Hogg R., Agglomeration models for process design and control, *Powder Technology,* 69, 69-76, 1992

Hounslow, M.J., A discretized Population Balance for Continuous Systems at Steady State, *AIChE Journal,* vol.36, no 1, 106-116, 1990

Hounslow, M.J., Ryall, R.L., Marshall, V.R.,, A Discretized Population Balance for Nucleation, Growth and Aggregation, *AIChE Journal,* vol 34, no 11, 1821-1831, 1988

Kelly, E.G., Spottiswood, D.J., The breakage function, what is it really?, *Minerals engineering,* 3-5, 405-414, 1990

Koka, V.R., Trass, O., Estimation of breakage parameters in grinding operations using a direct search method, *Int. J. Miner. Process.,* 23, 137-150, 1988

Leite, M.r.m., A non linear kinetic model for full autogenous grinding simulation, *Preprints xvii int.mineral procesing congress, Dresden, september 1991,* vol. 1, 357-370, 1991

Lippek, E.; Dombrowe, H., Simulation of a grinding circuit which includes high-pressure grinding rolls, *ZKG Int.,* 49(3), 124-32, 1996

Loveday, B.K., An analysis of comminution kinetics in terms of size distribution parameters, *Journal of the South African Institute of Mining and Metallurgy,* 113-130, 1967

Lynch, A.J. and Morrell, S., The Understanding of Comminution and Classification and Its Practical Application in Plant Design and Operation, *Comminution-Theory & Pract SME Symp,* Ch.30, 405-426, 1992

Meloy, T.P., Ferrara, G., Bevilacqua, P. and Williams, M.C., Size distribution of comminuted porous materials: the oops region, *Powder Technology,* 83, Issue 1,, 43-48, 1995

Mular, A. L.; Ye, G. Y.; Chen, Z. M.; Lovering, J. R., Simulation of a semi- autogenous grinding circuit, *Miner. Process. Extr. Metall. Rev.,* 2(3), 157-202, 1987

Nakajima, Y.; F., M.; Tanaka, T., Theoretical analysis of a closed - circuit grinding system based on comminution kinetics, *Ind. Eng. Chem., Process Des. Develop.,* 10(4), 449-56, 1971

Narasimhan, K.S., sastri, S.R.S, How to estimate size distribution of crushed products, *solids handling mag.,* june, 202-210, 1975

Paramanthan, B.K. and J. Bridgwater, Material behaviour and kinetics of attrition, *Chem. Eng. Sc.,* 38 (2), 207-224, 1983

Peterson, T.W., Similarity Solutions for the Population Balance Equation Describing Particle Fragmentation, *Aerosol Sci. Technol.,* 5, 93-101, 1986

Peterson, T.W., Scotto, M.V., Sarofim, A.F., Comparison of comminution Data with analytical solutions of the fragmentation equation, *Powder Technology,* 45, 87-93, 1985

Pitchumani, B., venkateswarlu, D., Matrix representation of batch and continuous size reduction processes, *Fine particles processing,* vol.1, 148-163, 1980

Plitt, L.R., A mathematical model of the hydrocyclone classifier, *CIM Bulletin,* vol.69, No.776, P.114-123, 1976

Popplewell, L.M., O.H. Campanella, Peleg, M., Simulation of bimodal size distributions in aggregation and disintegration processes, *Chem.Eng.Progress,* 85(8), 56-62, 1989

Ramkrishna, D., The status of population balances, *Reviews in Chemical engineering,* 1985

Reddy, I. G., Kinetic study of simulated closed - circuit grinding, *Chem. Age India,* 19(2), 101-5, 1968

Schönert, K., Mathematische Simulation von Zerkleinerungsprozessen, *Chem.Ing.Techn.,* vol.43, 316-367, 1971

Stanley, G.G., Milling and Classification, *SAIMM, Johannesburg,* 1/3, 121-217, 1987

Stanley, G.G., Mechanims in the autogenous mill and their mathematical representation, *j.of.the south african institue of mining and metallurgy,* nov 74, 77-80, 1974

Tanaka, T.; Nakajima, Y.; Furuya, M., Closed circuit grinding theory based on the comminution kinetics and its application to jet milling mechanism, *DECHEMA (Deut. Ges. Chem. Apparatew.) Monogr.,* 69(1), 515-526, 1972

Valenzuela, J.; del Villar, R.; Bourassa, M.; Arnaud, S. St., Development of an empirical dynamic simulator for the analysis of control strategies in an autogenous grinding circuit, *CIM Bull.,* 88(995), 60-8, 1995

Valery, W.; Morrell, S., The development of a dynamic model for autogenous and semi-autogenous grinding, *Miner. Eng.,* 8(11), 1285-97, 1995

Viswanathan, K., Theoretical expression for the distribution function of comminution kinetics, *Ind.Eng. Chem.Fundam.,* 24, 339-343, 1985

Viswanathan, K. and B.P. Mani, Optimum method of calculation of product distribution from a distributed fracture model, *Int. J. Miner. Process.,* 11, 155-162, 1983

Viswanathan, K., Mani, B.P., Distribution function of comminution kinetics- modelling and experimental study, *Int. J. Miner. Process.,* 9, 385-392, 1982

Watson, D., Cropton, R.W.G. and Brookes, G.F., Modelling Methods for a Grinding/Classification Circuit and the Problem of Plant Control, , manuscript, C112-117, 1970

Weichert, R., Fracture Physics in Comminution, *7th European Symposium on Comminution, Ljubljana,* 3-20, 1990

Williams, M.C., Meloy, T.P., Tarshan, M., Solution approaches to the dynamic population balance modeling of a closed grinding network, *8th European Symposium on Comminution, Stockholm,* 249-255, 1994

Chapter 8

Fluid dynamics of jet mills

This chapter contains a study into the flow patterns of jet mills using computational fluid dynamics and flow measurements, described in respectively paragraph 8.2 and 8.3. Some design features of a jet mill are discussed in paragraph 8.4. This chapter ends with conclusions and discussions.

8.1 Introduction

The flow patterns in the jet mill chamber are important with respect to the size reduction as well as to the classification of particles. The study of flow patterns was performed to acquire physical insight in how these internal processes relate to the performance of a jet mill.

In jet mills the size reduction of particles is primarily the result of mutual collisions. When sufficient impact energy is available for the built-up of the required stress field a particle will break. The efficiency of grinding depends on the rate of particle entrainment and the final velocity the particles can achieve.

The quality of the product of the jet mill, defined as a desired PSD, depends largely on the internal classification in the vortex around the central outlet.

The fluid dynamics appeared to have a strong influence on the comminution as well as the classification processes in the mill. Three steps were taken for the investigating of the flow patterns in the jet mill:

1. *Literature review.* Important work was done by RUMPF, MUSCHELKNAUTZ AND KÜRTEN. Pressure gradients over the mill chamber were related to velocity profiles inside the mill. Furthermore visualisation experiments were carried out with light-emitting material to determine the grinding zones inside spiral jet mills.

2. *Flow simulations.* The experiments mentioned above are time consuming and have many practical limitations. In this project the package Fluent was used as a tool to carry out flow simulations that helped to understand the fundamentals of the flow inside the mill. In this sense they had the same purpose as the real jet mill experiments.

3. *Flow observations and measurements.* The 10-inch jet mill was equipped with a transparent base plate to observe the flow patterns inside the mill chamber. CCD-recordings revealed the flow behaviour under different operating conditions. The entrainment and acceleration of the particles by an expanding jet was investigated with phase Doppler measurements.

8.2 Computational fluid dynamics

8.2.1 Hardware and software

Computational Fluid Dynamics (CFD) software describes the fluid flow and heat transfer by solving the conservation equations for mass, momentum and energy. These partial differential equations are to be solved for machine geometries which are divided into a large number of small grid elements. The numerical solution progresses in time and space and finally should converge to a numerical description of the complete flow field in the machine or reactor that is modelled. The flow simulations described in this thesis were carried out with Fluent Version 4.43.

8.2.2 Building a computational grid

The first step in the flow simulation was the definition of the geometry of the simulated parts of the jet mill. As an example, the set-up of a grid for the mill chamber will be described here. In the cylindrical wall eight nozzles were placed at equal distances. Under the assumption that the flow pattern is axi-symmetric only a wedge shaped segment of the mill chamber was modelled. This approach strongly reduced the calculation time.

Figure 8-1 shows how the segment of the mill chamber was divided into small computational cells. Five different types of cells were used. The air entered the chamber through the inlet cells with a given velocity and direction. Live cells are the

actual computational cells in which the flow pattern develops itself. The mill contents leaves the chamber through the outlet cell. The rotating flow leaving the segment on one side enters a similar neighbouring segment by definition of the cyclic cells.

Grid (49 X 49 X 19)

Outlet cells

Wall cells

Cyclic cells

Inlet cells
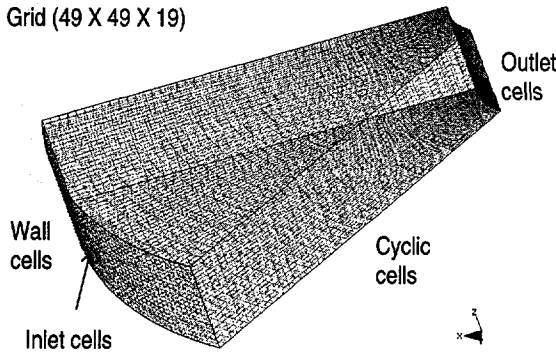
Figure 8-1 Composite grid of a segment of the spiral jet mill with different cells.

8.2.3 Definition of physical models

The flow in a jet mill contains two interacting phases. This section deals with the properties of the media and models used for the simulation.

Material properties: For the expanding air the standard viscosity was used, while the local density was calculated by the ideal gas law. The temperature of the air at the nozzle inlet was 20 degrees Celsius. The density of the solid material was 1010 kilograms per cubic meter.

Table 8-1 Physical constants used for CFD simulation.

$T_l = 293$	Ambient temperature	[K]
$k = 1.4$	Ratio of specific heats for air (Cp/Cv = 1.005/0.718)	[-]
$M_{air} = 28.969$	Molecular mass	[g/mol]
$R_{GAS} = 287$	Gas constant	[J/kg.K]

Navier-Stokes: The three-dimensional state of stress of a fluid element, schematically shown in Figure 8-2, can be written in Cartesian tensor notation.

Figure 8-2 Three-dimensional state of stress of element and coordinate system.

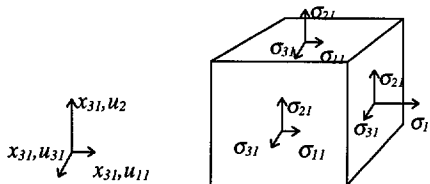Variable u denotes a mean velocity and u' is used for fluctuations around the mean value. The principle of momentum conservation applied to the fluid element for the x_i-component is

$$\frac{\partial u_i}{\partial t} + u_l \frac{\partial u_i}{\partial x_l} = \frac{1}{\rho} \frac{\partial}{\partial x_l} \left(-p\delta_{il} + \sigma_{il} \right) + f_i \equiv -\frac{1}{\rho} \frac{\partial p}{\partial x_i} + \frac{1}{\rho} \frac{\partial \sigma_{il}}{\partial x_l} + f_i \qquad (8.1)$$

Where f_i is the x_i-component of the body force, such as gravity or Coriolis, per unit mass and ρ is the instantaneous density. The viscous stress is proportional to the rate of strain. These N.S.-equations are used by the CFD package [FLUENT].

Turbulence: In order to study the statistics of turbulence information is required at two locations in the flow, plotted as point P and P* in Figure 8-3. Usually a correlation between velocities fluctuations u' at these points is used [KAY, NIEUWSTADT].
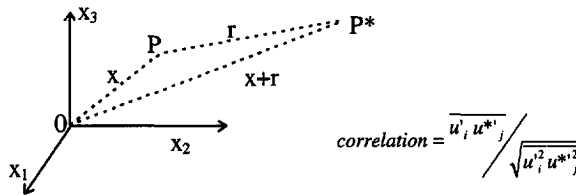
Figure 8-3 Notation for spatial covariances of two points in the flow.

Therefore the N.S.-equations is multiplied by u'_j, plus u_i times the x_j-component equations for point P*. The ensemble is averaged and the equation is re-arranged into the turbulent energy equation

$$\frac{\partial}{\partial t} (\tfrac{1}{2}\overline{u'^2_i}) + u_i \frac{\partial}{\partial x_l} (\tfrac{1}{2}\overline{u'^2_i}) =$$
$$-\overline{u'_i u'_l} \frac{\partial u_i}{\partial x_l} - \frac{\partial}{\partial x_l} (\overline{p * u'_l}/\rho + \tfrac{1}{2}\overline{u'^2_i u'_l}) - \varepsilon - \Phi_{visc} + \overline{f *_i u'_i} \qquad (8.2)$$

The dissipation-term can be interpreted as the mean rate at which the turbulence does work against viscous stresses. The mean-flow generation term can be expressed as

$$-\overline{u'_i u'_j}(1/2)(\partial u_i / \partial x_l + \partial u_l / \partial x_i) \qquad (8.3)$$

which is the product of each Reynolds-stress with the corresponding mean rate of strain and is therefore the rate at which the mean flow does work on the turbulence. The turbulent diffusion terms are just a special case of the corresponding terms in the $\overline{u'_i u'_j}$ -equation.

CFD software packages normally contain turbulence models which are approximations of the real physics. The required model parameters used in the empirical statistical expressions are derived from experimental flow data.

For the simulations of in this project the Re-Normalised Group (RNG) model was used to describe turbulence. This approach involves the progressive scaling of the shortest wavelength whose effect on the larger wavelengths can be retained in an average form as a contribution to a transport coefficient. The velocity field is represented by a discrete set of components $u(k,t)$ on the interval $0<k<k_o$. Here k_o denotes the largest wave number that is present. The flow field can be defined through the dissipation rate

$$\varepsilon = \int_0^{k_o} 2vk^2 E(k)dk \qquad\qquad (8.4)$$

In which $E(k)$ is the energy spectrum. A wavenumber cut-off is to be chosen. Then the NAVIER-STOKES equation is solved in two stages:

1. Solve the N.S.-equation on the interval $k_1 \leq k \leq k_0$. Substitute that solution for the mean effect of high k-modes into the N.S.-equation on $0 \leq k \leq k_1$. This results in an increment to the viscosity: $v_0 \rightarrow v_1 = v_0 + \delta v_0$

2. Re-scale the basic variables so that the N.S.-equation on $0 \leq k \leq k_1$ looks like the original N.S.-equation on $0 \leq k \leq k_0$

This procedure is repeated for a wave number cut-off $k_2 \leq k_1 \leq k_0$. The underlying physics of the RNG method can be summarised as follows. In the viscous range of wave numbers, it is reasonable to suppose that the turbulence is critically damped [YAKHOT].

The use of the RNG model for the jet mill simulations required values for the turbulence intensity and the characteristic length to set-up the set of conservation equations. For the simulations a turbulence intensity of 10% was used, while the characteristic length was put equal to the diameter of the nozzles.

Particle tracking: When a particle, or a cloud of particles of low concentration, is introduced into an air stream the response of the particles depends on the relative velocity of the particle and the fluid. This relative velocity determines the drag force which causes the motion of the particle. It was assumed that there is no particle interaction and further that the presence of the particles does not change the basic flow pattern.

The dispersed phase is solved by tracking a large number of particles through the calculated flow field. The dispersed phase can exchange momentum, mass and energy with the fluid phase. A fundamental assumption made in this model is that the dispersed second phase occupied a low volume fraction, less than 10 volume percent. This assumption implies that the motions of particles is controlled by local dynamic forces.

Comment: Hold-up measurements of the jet mill chamber indicated that the actual concentration of solids varied from 10 to 45 volume percent. Under these dense particle flow conditions the flow pattern motion is also controlled by particle-particle collision and particle fluid interactions [SOO]. The high concentration of particles inside the mill makes the CFD problem much more complex. For example, the motion of the particles present in the mill chamber also influences the turbulence of the fluid stream, and vice versa. These particles are accelerating, decelerating and spinning while they move in the local pressure gradients. In the simulations presented in the following sections these effects were ignored.

8.2.4 Entrainment and acceleration of particles by gas jets

Some opposed jet mills, such as the Pulva FP or the Alpine AFG-R contain Laval nozzles that generate supersonic velocities. MUSCHELKNAUTZ stated that for straight nozzles the jet expansion after the nozzle is very strong, resulting in a considerable acceleration of the fluid. The fluid velocity with pressure ratios as used in jet mills reaches therefore 90 to 94 percent of the velocity attained by Laval nozzles. The fact that Laval nozzles have to be operated at the pressure for which they are designed makes them less flexible. This explains, combined with the high manufacturing cost, why most commercial jet mills are equipped with straight nozzles.

An air jet in a fluidised bed generates several areas in its surrounding that have specific properties depending upon nozzle diameter and the distances between the nozzles. For a given gas velocity the jet penetration increases with increasing nozzles diameter and therefore with increasing mass flow. Forms to correlate jet penetration in fluidised beds are described by YATES. In a turbulent free jet of circular cross-section the average velocity v in the middle of the jet after a distance ten times the nozzle diameter downstream drops and can be estimated by

$$\frac{v}{v_0} = 6.5 \cdot \frac{d}{l_{max}} \tag{8.5}$$

The average initial air velocity at the exit of the nozzle is denoted by v_o. The active path for particle acceleration is defined as $l_{max} = C \cdot d$. Beyond this distance from the

nozzle outlet the velocity drops to one-third of the velocity at the nozzle outlet. Here the jet velocity is too low to entrain sufficient numbers of particles and too weak to generate effective particle collisions that result in breakage.

Figure 8-4 shows the calculated particle trajectories in the simulated flow field of a free air jet. The particles, ranging in size from one to 100 microns were injected near the nozzle outlet.
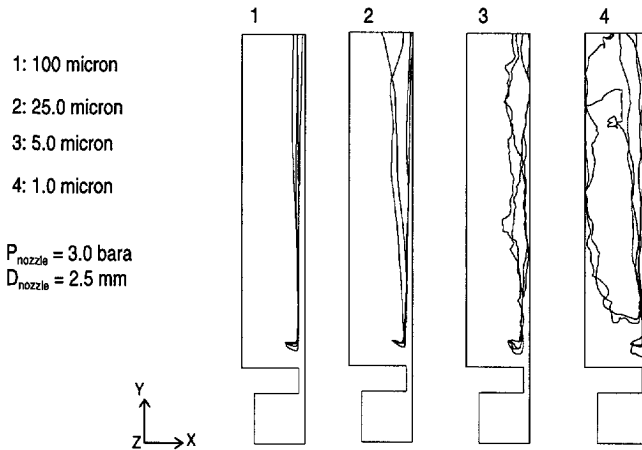
1: 100 micron

2: 25.0 micron

3: 5.0 micron

4: 1.0 micron

P_{nozzle} = 3.0 bara
D_{nozzle} = 2.5 mm

Figure 8-4 Trajectories of particles with different sizes in an expanding air jet.

The simulation results indicate that the particles were dragged towards the jets and taken up by the jet. The acceleration time and distance depended on the drag forces experienced and the inertia of the particles. The final velocities that the particles could reach in the jet depended on their size. For an equal tracking time the trajectories of the fine particles were much longer. The flow simulations confirmed literature that most entrainment of particle occurred in the vicinity of the nozzle outlet [MILOJEVIC].

The particle trajectories showed that the kernel of the jet remained dilute. This was explained by the large velocity and pressure gradients that prevented the particles from entering the core where the velocities and the turbulence intensities were highest. Thus only a fraction of the pneumatic energy input by the jets wa used for particle acceleration. GREGOR expressed the efficiency of particle acceleration by a nozzle as the ratio of the kinetic energy supplied to the particles and the total pneumatic energy of the jet.

Around the jet a shear layer was found where the particle concentration was elevated due to the vacuum created by the turbulent gas flow around the jet perimeter. These stream lines entrained the particles in the direct vicinity of the jet where they could be

accelerated to high velocities. The larger particles in that layer followed straighter trajectories than fines that were more vulnerable to the forces in the turbulent eddies and convection streamlines.

A number of flow simulations were carried out in order to study the opposed jet configuration. Figure 8-5 shows the velocity vectors of two jets that are expanding towards each other. The flow was assumed to be symmetrical in the horizontal plane.
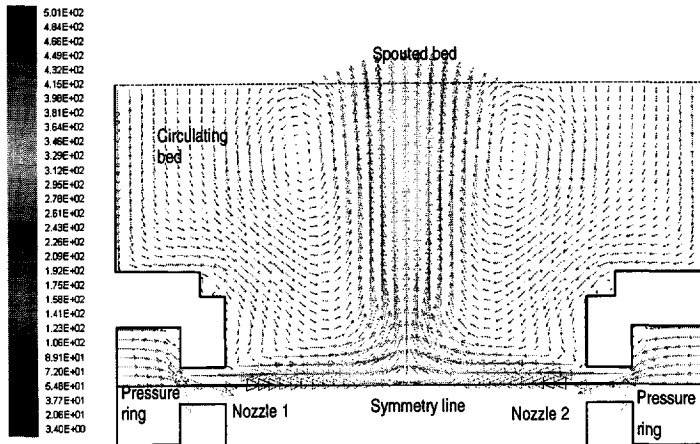
Figure 8-5 Velocity vectors of two opposed jets.

At the focal point of the two jets the average velocity in the axial direction was zero. Here the air flow was diverted and a kind of spouted bed was formed which dragged away the particles from the grinding zone. The simulation shows how a portion of the bed was recirculated and entrained again by the jets.

Figure 8-6 show a contour plot of the turbulence intensity created by the two opposed jets.

Figure 8-6 Particle trajectories in opposed jets. 100 micron (left), 5 micron (right).
Contour plots of turbulence intensity in W/m^2. $d_n = 3.0$ mm, $P_n = 3.0$ bar.

The right hand plot shows how the highest intensities were found at the cross section. The trajectories indicated that particles larger than 40 microns were able to pass the highly turbulent zone and enter the opposed jet. T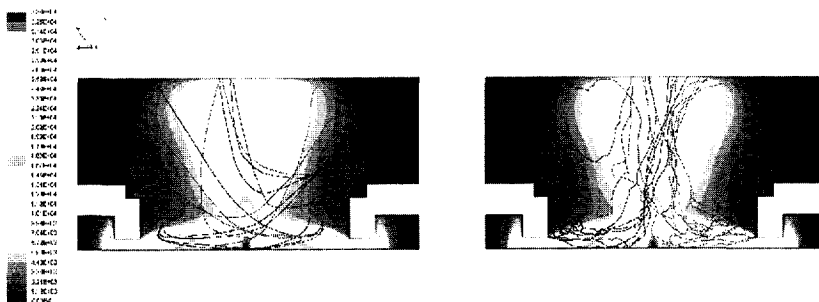hose particle were able to collide with particles present in the opposed jet. Fines however, were dragged away from the focus point of the jets as is shown in Figure 8-6. Mutual collisions between those particles only occurs in the turbulent flows of the individual jets.

8.2.5 The circulating flow in the jet mill chamber

The particle size classified in the vortex can be determined from the balance between the drag force and the centrifugal force acting on that particle. For this calculation the velocity profiles in the mill are required. ZHAO reported about tracer experiments on a 12-inch jet mill with nozzles angled at 75 degrees to the tangent. The radial velocity near the wall was in the order of five times lower than the average radial velocity. A back-flow towards the outer wall occurred in the central region between the axial walls. The large differences in radial velocities along the axis of the mill caused a poor classification of the jet mill.

In this project CFD simulations were carried out to get a three dimensional picture of the flow patterns inside the mill chamber. Figure 8-7 shows the results for the 10-inch spiral jet mill equipped with 8 nozzles of 2.0mm in diameter. The nozzle angle was 71 degrees from the tangent.
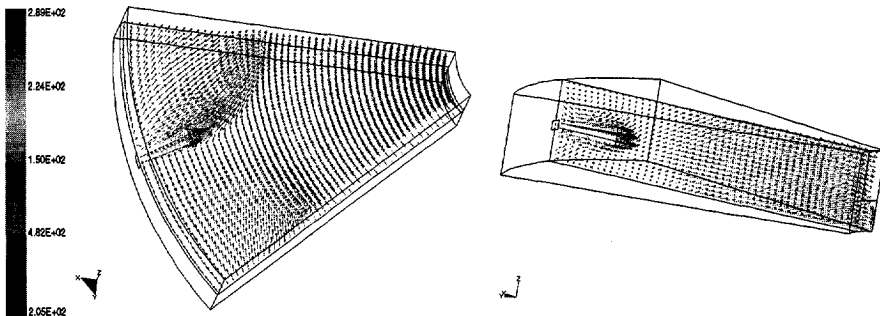
Figure 8-7 Top view of mill segment (left). Velocity vectors in horizontal plane of jet mill chamber. Side view (right).

The flow simulations showed a strong dependency of the value and direction of the velocity components on the position in the mill chamber. Slowly circulating flows created by negative pressure gradients at the vicinity of the expanding jets dragged particles from the bulk to the jet surface. The average radial velocity was in the

direction of the central outlet, though short cut flows existed along the upper and lower walls of the mill chamber.

Figure 8-8 shows a contour plot of the velocities in the axial and radial planes of a spiral jet mill. As a numerical tracer experiment a number of 7-micron particles were injected in the calculated flow field at a radial distance of 10 centimetre from the outlet of the mill. The calculated trajectories indicate that the particles stabilised in an orbit in the mill chamber. These particle were neither hit by the jets, nor dragged to the central outlet, which caused an accumulation that ultimately led to unstable mill performance when the local density of the circulating bed reached the bulk density. Then the vortex collapsed. This phenomenon occurred during pilot plant experiments with an overloaded jet mill.
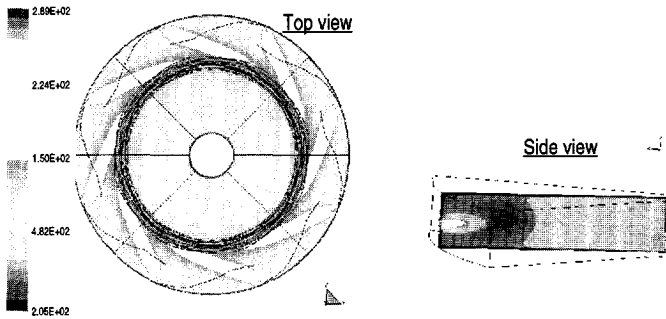
Figure 8-8 Contour plot of velocity levels and trajectories of 5 micron particles in spiral jet mill.

Figure 8-9 shows how 20 micron particles, injected at the same point, were transferred to the outer zone by the centrifugal forces, where they were continuously entrained and accelerated by the jets.
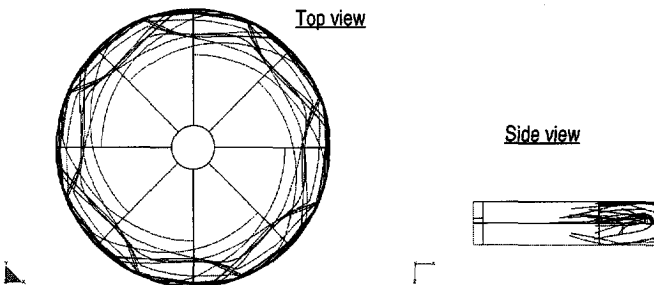
Figure 8-9 Trajectories of 20 micron particles.

Figure 8-10 shows the trajectories of particles with a diameter of 2 micron. These small particles were more rapidly dragged towards the central outlet and added to the

product flow leaving the jet mill. A portion of these fines was conveyed back to the grinding zone along the mill walls, as can be seen in the right hand plot.
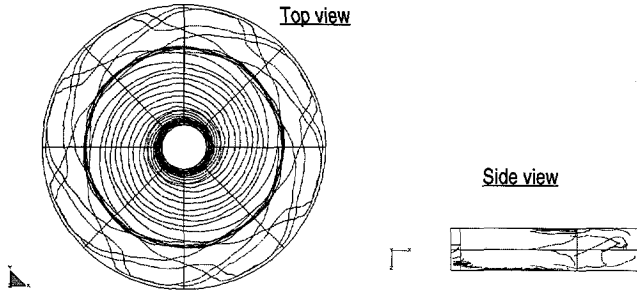
Figure 8-10 Trajectories of 2 micron particles.

Comment: Similar to the turbulent flow conditions in air classifiers the particle motion in jet mills is not only influenced by settling caused by a centrifugal force field, but also by turbulent transport phenomena like eddy diffusion [SCHUBERT].

8.3 Observation and measurement of flow patterns

8.3.1 Visualisation of flow in mill chamber

A transparent base plate, as shown on Photo 8-1, was mounted on the spiral jet mill in order to study the flow patterns with a CCD camera.
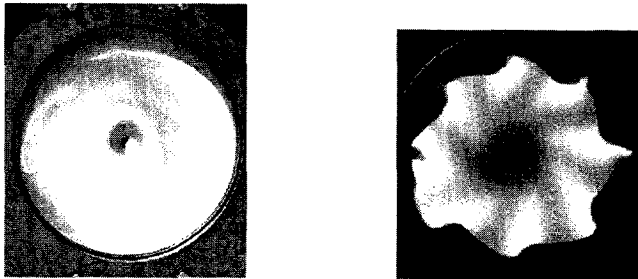
Photos 8-1 Collapsing vortices in overloaded jet mill (left) and light emitting material in the grinding zones (right).

The vortex flow was recorded for combinations of solid feedrates and nozzle pressures. At higher loading of the mill the vortices started to collapse resulting in an instantaneous discharge of the mill contents. This phenomenon was also observed as peaks in the product flow by the in-line measurements on the mill outlet using the LD-instrument.

KÜRTEN reported that most of the size reduction occurred inside the highly turbulent jets. Grinding experiments were carried out with tribo-luminescent materials that visualised the zones where particle collisions were most frequent and intense. Communication appeared to took place at the front and the back of the jet, as well as in a closed circular layer around the centre of the expanding jet.

Photos 8-1 (right) shows an example of a light pattern obtained when sugar was ground on the 10-inch spiral jet mill.

The location of the grinding zone was related to the angle and the diameter of the nozzles, the operating pressure and the solids concentration inside the chamber. The dark curved patterns were due to the blockage of emitted light by slowly circulating mass. Around the central outlet vortex flow no grinding occurred since the local velocities were too low.

Test runs carried out with 4 nozzles showed light emission on spots where the jets hit the mill wall, indicating that a significant amount of breakage occurred as a result of wall collisions. Furthermore the vortex was less symmetrical and coarse particles bounced against the wall and escaped through the mill outlet. Similar effects were reported by RUMPF, who suggested that for small scale jet mills with a diameter of approximately 15 centimetre, the minimum amount of nozzles is 6 to 8. Larger spiral jet mills, varying from 70 up to 200 centimetres, should be equipped 12 up to 20 nozzles.

8.3.2 Phase Doppler measurements on single jet

Experimental set-up: Figure 8-11 depicts the schematic arrangement of the TSI phase Doppler instrument used for the measurements of the expanding jet. The beam splitter created two separate beams out of the incident laser light, while the lens focused the laser beams at the sampling point where an interference pattern was formed. The angle of intersection, 2γ, is related to the beam separation and the focal length of the lens.
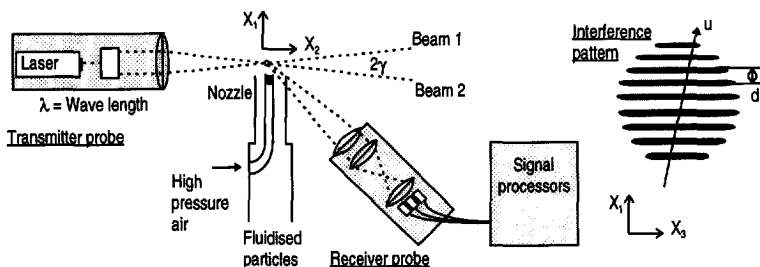

Figure 8-11 Set-up of Phase Doppler instrument for measurement on a single jet.

The velocity measurements were carried out with a 2mm straight nozzle mounted in a fluidised particle bed.

Figure 8-11 shows the set-up for the measurement of the axial component u_1 in the free jet from the nozzle. The incident beams lie in the x_1x_2-plane. On the right side a schematic cross section through the fringe patterns in the x_1x_3-plane is shown caused by the interference of the laser beams. Two sets of laser beams with different colours (blue and green) were used to measure in two planes. A review about phase Doppler was published by LAUTERBORN and VOGEL.

Signal processing: The scattered light by a particle moving through this interference pattern is focused onto a set of photo multipliers located in the receiver probe which record an output current proportional to the light intensity.

The phase angle between these so-called Doppler bursts is proportional to the detector spacing and the fringe spacing, d. As the particle crosses through the fringes only the u_1 component contributes to the recorded signal. The component perpendicular to the x_2-axis do not cross fringes.

The frequency spectrum f_D output is obtained by Fourier transformation of the Doppler burst caused by a passing particle. The following properties of the scattering particle can be obtained from the signals [HIRLEMANN]:

1. The axial component of the particle velocity, u_1, is linearly related to the temporal frequency, f_D, of the scattered fringe pattern.

$$u_1 = (\frac{\lambda}{2 \sin \gamma / 2} - \gamma) \times f_D \qquad (8.6)$$

2. The diameter of a spherical particle, x_p, is linearly related to the spatial frequency of the scattered fringe pattern.

$$\Delta = \frac{\pi x_p}{\lambda} \left[(\sin \tau_1 - \sin \tau_2) - pm (\sin \tau_1^{'} - \sin \tau_2^{'}) \right] \qquad (8.7)$$

Measurement: The expanding jet surrounded by the dispersed particle bed generated several areas in its vicinity. Figure 8-12 shows the sampling points of the phase Doppler-measurements. The points A are on the jet centre line, while the points B are located in the shear layer or outside the jet.
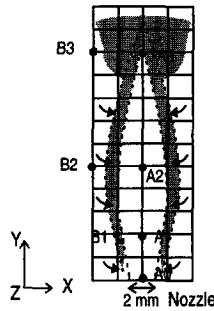
Figure 8-12 Sample points of phase Doppler velocity measurements. Points A1 to A3 are on the centre line, points B outside the jet.

As an example the results of a 2.0 mm straight nozzle with an operating pressure of approximately 3.0 bar are presented. In the kernel of the jet no particles were detected with the laser Doppler instrument, thus no velocities could be measured. The measurements were continued at point B_1.

Figure 8-13 shows the particle velocities in the radial and axial direction of the jet. The velocities distribution ranged from -6 and +6 meters per second, both in the x- and y-directions. The RMS-value of the velocities was 3.5 meters per second.
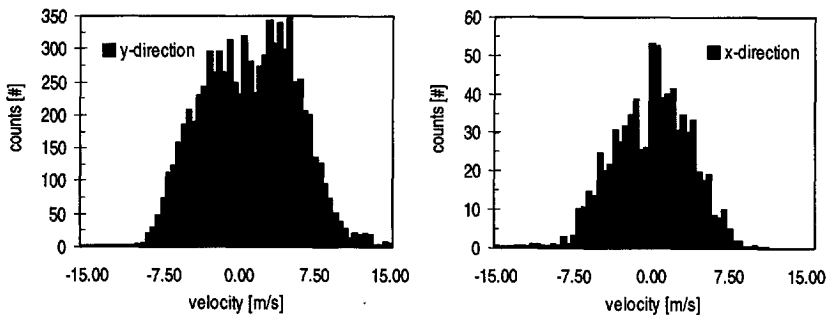
Figure 8-13 Velocity distribution for the axial (y) and radial (x) directions. Sampling location B1.

Figure 8-14 show the peak that was found at a velocity of approximately 70 meters per second, which was assumed to be caused by particles in the shear layer of the jet. This velocity was in the order of 10 times higher than the velocities in the circulating bed near the jet. The RMS-value was a factor of 5.5 higher.

Figure 8-14 Velocity distribution for the axial direction of the jet. Sampling point B1.

Comment: The free shear layers are important because of the rapid rate at which they entrain air and particles from the surrounding bed. JOHNSTON stated that the growth rate of a turbulent jet was of the order $\partial\delta/\partial x \approx 0.1$, which is much higher than the rate at which fluid could be captured by a laminar diffusion process.
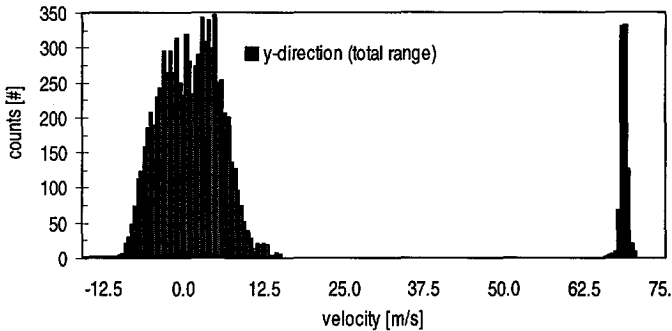
8.4 Some design features of jet mills

In this section some approaches will be discussed that can be used to improve the performance of jet mills. Crucial for the efficiency of size reduction in jet mills are

1. The level of particle entrainment into the high velocity jet.

2. The collisions of particles with other particles or a target.

Pulsating jets: The machine builder BLF Poitemill used the concept of pulsating jets hitting the particle bed to enhance the solid loading. A standard opposed jet mill was equipped with two rows of opposed jets placed above each other in the mill body that were alternately switched. BLF claimed that the grinding efficiency improved compared to the standard opposed jet mills. A danger of these pressure pulses might be their negative effect on the classification.

Multiple jets: The AFG can be equipped with Mega nozzles. The idea behind the multiple jets is the increase the effective area for entrainment by dividing one nozzle into a number of smaller nozzles with an equal total cross section. As the multiple jets expand they form one single jets at a certain distance from the outlets. This type of nozzle is expected to enhance the loading of the jets.

Ejector nozzle: Pre-loading of the jet before expansion gives a higher grinding efficiency. The dense and high turbulent flow inside the nozzle already makes particles collide against other particles and the ejector wall. The Pulva FP mill

[KARVINEN] generates a air-particle suspension which is accelerated in two opposed Laval nozzles.

Target impact: In case of tougher materials like PE a pre-grinder can reduce the feed particles to a critical size below which grinding in a free jet becomes possible. Figure 8-15 shows the incorporation of a target in an ejector unit.
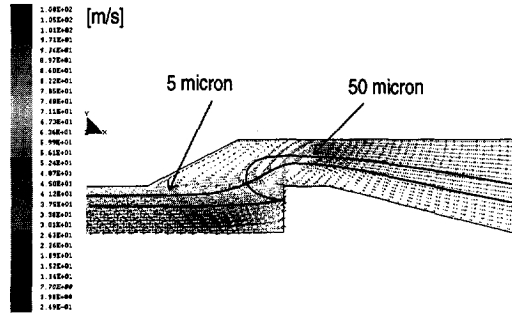
Figure 8-15 Velocity vectors in a solid feed injector with an incorporated target

The small feed particles follow air stream without hitting the target, whilst the coarse particles impact upon the target and their fragments dragged with the air flow. The ejector nozzle and the impact pre-grinder are suitable for processing non-abrasive materials.

8.5 Conclusions and discussions

A free jet expanding in a fluidised particle bed entrains particle mainly at the vicinity of the nozzle outlet. Here a relatively slowly rotating flow exists transferring particles from the bulk to the jet shear layer. The Phase Doppler measurements confirmed the CFD simulations that only a thin shear layer of the jet actually contains particles. The concentration of particles in kernel of jets was very low, which indicated that the pneumatic energy of the jet was not effectively used for particle acceleration.

The experiments with light emitting material confirmed literature that size reduction mainly takes places around the jets. The locations corresponded with parts of the flow field in the CFD simulations where high turbulence intensities were highest and where sufficient particles were available.

The CFD simulations showed that larger particles require a longer distance to be accelerates to maximum velocity and follow straighter trajectories than the fines. Compared to opposed jet mills, spiral jet mills of the same capacity usually contain a

larger number of nozzles, but with smaller diameters. Therefore the jets are shorter and not capable to accelerate the coarser particles to the critical impact velocity.

The CFD simulations showed that in opposed jets only relatively coarse particles, larger than 40 microns, are able to cross the focal point and enter the other opposed jets. Small particles follow streamlines and are dragged away from the focal points of the jets. These particles are primarily broken by collisions in the turbulences of the single jet.

Extension of the CFD code with statistical equations that relate breakage kinetics to flow conditions, similar to the equations discussed in Chapter 6, can be useful for the simulation of jet mills and attrition phenomena in fluidised beds.

So far the CFD simulations performed in this project provided insight in the nature of the jetmilling process. The numerical results agreed reasonably well with the Phase Doppler.

The real processes occurring in jet mills are very complicated. In fact, for each particle the equations of motion and the geometry of the collision (angle, partner, velocity) have to be solved [TALMAN]. Furthermore the current CFD-software is not able to cope with two-way interaction between the solids and the air flow. Though statistical techniques like Monte-Carlo help to reduce the computational time, a complete simulation of the particle-fluid flow in a jet mill is extremely time consuming.

List of symbols

f	frequency	$[s^{-1}]$
P_n	nozzle pressure	[bar]
d_n	nozzle diameter	[mm]
η	viscosity	
σ	stress	$[N/m^2]$
δ	jet diameter	[mm]
Δ	spatial frequency	$[s^{-1}]$
Φ	flow rate	[kg/hr]
ρ	density	$kg/m^3]$
λ	wave length	$[10^{-9} m]$
u,v	velocity	[m/s]

References

Ayazi Shamlou, P., Liu, Z., Yates, J.G., Hydro-dynamic influences on particle breakage in fluidized beds, *Chem.Eng.Sci.*, 45,4, 809-817, 1990

Butler, P.B., Schmitt, R.G., Influence of particle melding on a shocked particle laden gas, *Powder Technology,* vol.70, 163-173, 1992

Byron Bird, R., Stewart W.E., Lightfoot E.N., *Transport Phenomena,* 1960

Cleaver, J.A.S., Ghadiri, M., Tuponogov, V.G., Yates, J.G. and Cheesman, D.J., Measurement of jet angles in fluidized beds, *Powder Technology,* 85, iss 3, 221-226, 1995

Devulapalli, B. and Rajamani, R.K., A Comprehensive CFD Model for Particle Size Classification in Industrial Hydrocyclones, *Hydrocyclones,* 1996

Dodge, F.T., Green, S.T., Johnson, J.E., Characterization of injection nozzles for gas solid flow applications, *J.of Fluid Engin.,* 113, 469-475, 1991

Doss, E.D., Srinivasan, M.G., Modeling of wall friction for multi-species solid-gas flows, *transactions of the asme,* 108, 486-490, 1986

Drain, L.E., The laser doppler technique, *book,* 1986

Ebert, F., Interaction between the motion of particles and their turbulent carrier fluid flow, *part.part.syst.charact.,* 9, 116-124, 1974

Grace, J.R., Contacting modes and behaviour classification of gas-solid and other two-phase suspensions, *Canadian J. Chem. Engin.,* 64, 353-363, 1986

Gregor, W, Schönert, K., The Efficiency of the Particle Acceleration in a Jet Pipe, *Powder Technology,* 34, 81-86, 1983

Gregor, W.; Schönert, K., Efficiency of particle acceleration in a jet mill, *Chem.-Ing.-Tech.,* 54(8), 764-5, 1982

Gumula, S.,Pytko, P., Transport and separation of dust particles in vortex type flow, *Proceeding Partec,* 10, 1995

Jing, Y., Jianyan, Ch., Qihong, W., Study of velocity field in jet mill, *Journal of chemical industry and engineering (China),* 4, 444-450, 1990

Kay, J.M., Nedderman, R.M., Fluid mechanics and transfer processes, Cambridge, *Univ.Pr.,* 1985

Kirch, F., Löffler, F., 2-component laser-doppler measurements of velocities in a gas cyclone, for the determination of turbulent data, *Partec 86,* 1986

Kürten, H., Zerkleinerungsuntersuchungen an tribolumineszierenden Stoffen, *Chem.Ing.Tech.*, 38, 331-342, 1966

Kürten, H.; Rumpf, H., Flow direction and comminution conditions in a spiral jet mill, *Chem.-Ing.-Tech.,* 38(11), 1187-92, 1966

Lede, J., Barillon, B., Villermaux, J. and Marcant, S., Modelisation des trajectoires de particules projetees par un jet gazeux sur une surface plane. Comparaison avec l'experience, *Powder Technology,* 83, Issue 2, 173-186, 1995

Leschonski, K., Two phase flow techniques as applied in characterization, *Proceedings of the 25th anniversary conference Particle size analysis, 17-19 Sept. 1991, LOUGHBOROUGH,* 409-425, 1991

Littman, H., Morgan, M.H. III, Jovanovic, S.Dj., Paccione, J.D., Grbavcic, Z.B. and Vukovic, D.V., Effect of particle diameter, particle density and loading ratio on the effective drag coefficient in steady turbulent gas-solids transport, *PT,* 84, Issue 1, July 1995, 49-56, 1995

Löffler, F., Muhr, W., Die abscheidung van feststofteilchen und tropfen an kreiszylindern infolge van tragheitskraften, *Chem.Ing.Techn.,* 44, 510-515, 1972

Maly, K, Untersuchung der partikel-stromung wechselwirkung in windsichtem, *Particle Technology, A'dam,* 1980

Milojevic, D., Borner, T., Durst F., Prediction of Turbulent Gas-Particle flows measured in a plain confined Jet, *Partec 86,,* 485, 1986

Morris, G.J., Jurewicz, Palmer, G.M., Gas-solid flow in a fluidically oscillating jet, *transactions of the asme,* 114, 362-370, 1992

Nieuwstadt, F.T.M., Turbulentie, Epsilon, Uitgaven, Utrecht, 1992.

Muschelknautz, E., Giersiepen, G., Rink, N., Strömungsvorgänge bei der Zerkleinerung in Strahlmühlen, *Chem.Ing.Techn.,* 42, 6-15, 1970

Muschelknautz, E.; Giersiepen, G.; Rink, N., Flow processes on grinding in jet mills, *Chem.-Ing.-Tech.,* 42(1), 6-15, 1970

Neesse, Th., Espig, D., Particle transfer from a turbulent gas stream to a sediment layer at the wall, - a microprocess of cyclone separation, *Partec 86,* 1986

Neilson, J.H., Gilchrist, A., An analytical and experimental investigation of the velocities of particles entrained by gas flow in nozzles, *J.Fluid Mech.,* 33, part 1, 131-149, 1968

Okuda S., Choi W.S., Gas mixture flow in various types of convergent-divergent nozzles, *J.Chem.Eng. of Japan,* 11, 432-438, 1978

Perry (editor), J.H., Gas-solids systems, *Chemical Engineer's Handbook (Perry),* section 20, 1-96, 1963

Rama Ratnam, S.R., Viswanathan, K., Mani, B.P., Studies on attrition in fluidized beds, *J.Pow.Bulk.Sol.Tech.*, 8-4, 1-9, 1984

Rudoff, R.C., Sankar, S.V., Bachalo, W.D., Using the phase doppler particle analyzer for in-situ sizing of fine spherical particles, *Proceedings of the 25th anniversary conference Particle size analysis, 17-19 Sept. 1991, LOUGHBOROUGH*, 206-214, 1991

Schetz, J.A., Injection and mixing in turbulent flow, *Progress in astronautics and aeronautics series*, vol. 68, 1980

Schönert, K., Gregor, V., The efficiency of particle acceleration in a jet pipe, *Powder Technology*, vol.34, 81-86, 1983

Schubert, H., Bohme, St., Classificaton in Turbulent 2-phase flows, *Partec 86*, , 419-425, 1986

Schurr, G.A., Zhao, Q.Q., Fluid mechanic considerations for fine grinding in a fluid energy mill, *8th European Symposium on Comminution, Stockholm*, vol., 536-547, 1994

Shuvalov, S. I., Motion of particles of a grindable material in the chamber of a jet mill, *Izv. Vyssh. Uchebn. Zaved., Khim. Khim. Tekhnol.*, 38(6), 87-91, 1995

Smith, R.A., Klinzing, G.E., Investigation of particle velocities in a gas-solid system, *AIChE Journal*, 32, no.2, 313-315, 1986

Talman, J.A., Computer simulations of a jet mill, *quarterly report for the japanese-german center berlin*, 1994

Tanaka, T., Yonemura, S., Discrete Particle Simulation of Dispersed Particulate Flows, 373, 1993

Tsuji, Y., Kawaguchi, T., Tanaka T., Discrete particle simulation of two-dimensional fluidized bed, *Powder Technology*, 77, 79-87, 1993

W.D. McComb, The Physics of Fluid Turbulence, *Oxford Engineering Science Series*, 25, 1996

Wendt, J.F., Computational Fluid Dynamics, An introduction, *A Von Karman Institute Book*, 1995

Yakhot, V., Orszag, S.A., Renormalisation Group Analysis of Turbulence, *Journal of Computing*, Vol.1, no.1, 1986

Yates, J.G., Cobbinah, S.S., Cheesman, D.J., Jordan, S.P., Particle attrition in fluidized beds containing opposing jets, *AIChE symposium series, advances in fluidized systems*, 87-281, 13-19, 1991

Yuu, S., Umekage, T., Direct simulation for dilute gas particle turbulent jet, *FED, ASME 1991, gas-solids fows*, vol. 121, 3-9, 1991

Chapter 9

Conclusions and perspectives

Jet milling is a grinding technique that is suitable for the production of fine powders down to a particle size of several microns. The principle of autogenous grinding make it suitable for heat sensitive and abrasive materials that cannot be ground on mechanical mills.

Product quality is the factor which determines whether a specific grinding technique is appropriate. The product of a jet mill is a fine powder with a well-defined and narrow particle size distribution. The particles are loaded during mutual collisions after acceleration in the mill chamber by expanding air jets. However, the energy efficiency of jet mills is extremely low and it is estimated that less than one percent of the energy supplied is actually used for particle breakage. Most of the energy is dissipated in the turbulent flow.

As a result of the autogenous grinding principle, the performance of a jet mill is very sensitive to changes in the hold-up of the mill chamber. Experiments confirmed that an optimal mass and composition of the material present in the grinding chamber exists. However this poses a dilemma as the optimal hold-up for grinding did not coincide with the required hold-up for internal classification.

The decoupling of the grinding and classification processes by the use of an external classifier provided the extra degrees of freedom required for the optimisation of the overall process. One of the major results of this project was that the pilot plant experiments showed that this closed circuit jet mill plant allowed an energy reduction up to 50 percent compared with the traditional open circuit configuration.

The forward light scattering method of particle size measurement was found to be most suitable for realtime measurements in the dispersed product flow of the jet mill. The signal acquisition time was 4 milliseconds and was fast enough to measure in the

fast moving product flow. For this purpose a custom made sampling cell that could be mounted on the mill outlet was designed and built.

The numerical processing on a PC of the raw light signals by deconvolution into a PSD required approximately one second. The obscuration signal caused by the passing product flow was used to determine the mass flow rate leaving the mill. Performance tests showed that the measured PSD depended on the type of instrument, the numerical processing of the signals and the sampling method. Below 2 percent by volume the measurement of coarse particles was poor. A method was investigated based on the correlation of fluctuations on the detector rings in order to enhance the accuracy in the extremes of the particle size distribution.

The light scattering instruments that are commercially available are usually based on laser diffraction and intended for laboratory use. In the past 20 years both the hardware and software of these instruments has been improved which has resulted in sophisticated devices. However, installation on an industrial plant requires a sensor with a simplified interface that provides a single control signal based on the aspect of the PSD that needs to be monitored or controlled. The sensor must be built into a robust probe and contains components that can resist heat and vibrations.

As an alternative to laser diffraction an instrument based on the scattering of incoherent halogen light was tested. This instrument contained a relatively simple LCD mask instead of a multi-channel light sensitive diode. This mask can be customised to fit the size ranges to be measured on a mill. This incoherent technique is less sensitive to contamination of the sampler windows as a result of the absence of speckles.

The mill product ground on the automated jet mill plant that was equipped with real-time PSD measurements was of a constant quality. The high reproducibility was possible as the influences of individual operators during manual start-up and shut-down of the gjet mill plant were excluded, as was the influence of overfeeding. Finally the real-time PSD measurements in the grinding plant were used in a feed back control loop that enabled closer operation to the specification limit which directly reduced the degree of overgrinding of the product.

Off-line quality analysis of grinding product is laborious, vulnerable to segregation errors during sampling and the measurement frequency is low. All this makes the results statistically poor. The continuous measurements allow an on-line tuning of the mill plant to disturbances such sudden changes in the grinding properties of the solid feed or pressure drops in the air supply system. This reduced the amount of batches

that need to be reprocessed. From an industrial point of view the remote monitoring and operation offers advantages for an operator who does not need to work in the dusty and noisy environment of the jet mill plant. Furthermore one person could supervise several jet mill plants. Finally the on-line measurement was used in a feedback control loop that was able to maintain the product quality with an accuracy of one micron at the desired level.

The real-time PSD measurements were also a useful tool for the analysis of the grinding system. A specially designed in-line cell allowed the investigation of the dynamic behaviour of the spiral jet mill under different combinations of set points. During the pilot plant experiments the product quality and the process conditions such as solid feedrate, pressure on the nozzles and pressure level in the mill chamber were logged and stored in a data base. If problems with the product quality were later detected, the origin of the disturbance can be traced.

It appeared that the jet mill was very sensitive to overloading since an increase of the solid feed with 10 percent could cause a transition to complete unstable mill performance. Under these conditions the grinding rate was insufficient compared to the discharge rate and the hold-up increased dramatically. Ultimately the vortex in the mill, which is responsible for the internal classification, collapsed, resulting in an instant discharge. In overloaded operating conditions the PSD and the mass flow of the product fluctuated with a frequency of 15 to 20 times per minute. These unstable flow patterns in the chamber were also observed through a transparent base plate that was mounted on the spiral jet mill. These instabilities could also be predicted by the PBM model.

New applications of powders demand a stricter control of the PSD, especially in the fine particle range below 10 microns. This makes the role of classifiers more important. A free vortex type of classifier was used in closed circuit with the spiral jet mill as it effectively used the air flow of the mill. Due to the absence of moving parts the product was treated more gently than in mechanical classifiers which reduced contamination and deposition of melted material on the machine parts. Powders with a median size down to 5 micron were produced. However, in the fine range the dead flux of this classifier increased up to 50 percent, causing unnecessary loading of the mill. For cut-size below 5 microns the free vortex classifier is not suitable, especially as the scale and throughput of the unit grows.

A classifier that can be more easily scaled up and has a low cut-size is the Coanda classifier. This type of classifier normally requires a lot of processing air, in

combination with a jet mill it can more effectively utilise the grinding air. Extra air can be added to adjust the classification performance.

A number of tests were performed with an opposed jet mill. This mill in principle is able to grind the same material to the same specification as on a spiral jet mill. Furthermore it appeared to be more suitable for granules which are tougher, such as PW, since the opposed jets cause more direct particle collisions. The mechanical energy input from the rotor resulted in extra heat development which sometimes caused the deposition of melted polymers in the mill outlet. The median size of the mill product could be controlled by varying the rotor speed and the product quality could be well predicted by the calculations. This mill was also controlled with a real-time particle sizing system. An optimum operating point was found where the product was finest and the throughput largest.

In fact inside an opposed jet mill with an integrated rotor an internal recirculation of material also takes place, which has an analogy with the closed circuit spiral jet mill plant. These overall grinding systems are self-stabilising as an equilibrium between the grinding rate and discharge rate is established.

In this project a mechanistic model was developed that described the dynamic behaviour of the open and closed circuit jet mill plant. Predominant phenomena occurring in local zones of the grinding plant were modelled by statistical functions that described particle breakage and particle transfer. These functions contained parameters that could be characterised as machine, material and operating variable. The material parameters were determined by single particle impact tests. These tests were compared with the results of compression tests. The test material CW and PW showed good results during the impact tests and the grindability corresponded with the findings in the jet mill plant experiments. The other material such as NL, PC, PE showed hardly any reduction during the off-line impact tests and also could not be ground in jet mills.

Simulations with the PBM based on pure breakage gave no realistic results due to the fact that the production of fines was insufficient. This made the hold-up increase to extreme levels and no steady state could be reached. This behaviour of the model supported the idea that attrition is a predominant comminution mode in a jet mill. The population balance model of the jet mill was extended with terms that took the attrition into account.

The adapted population balance model was capable of predicting the dynamic behaviour of the open and closed circuit jet mill plant. The increase in throughput by the use of an improved classifier were predicted.

However, the population balance model contained a number of obscure uncertain parameters with an uncertain physical basis. Research at the machine and particle level should provide more insight in the underlying physics. CFD simulations and LDV measurements in the mill chamber provided further insight of the two phase flow, that can be useful for improvements of the mill design.

216

Appendix A: Air flow through a nozzle

The air supplied to a jet mill serves as the energy carrier for grinding as well as the transport medium for the product.

Airflow: The fluid flow through a nozzle will increase with higher nozzle pressure until the linear velocity in the nozzle throat reaches the local velocity of sound (a_1), in other words Mach number (M_1) is one.
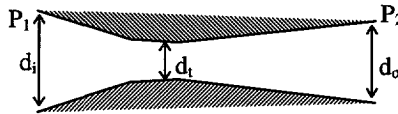

Figure: Nozzle

The value of P_1/P_2 for which this just occurs is the critical pressure ratio (R_c). The actual pressure in the nozzle will not fall below P_1R_c, even if a much lower pressure exists downstream. The critical pressure ratio is obtained from the following theoretical equation, under the assumption that the fluid behaves as a perfect gas and flow without friction through the nozzle

$$R_c^{(1-k)/k} + \left(\frac{k-1}{2}\right)\beta^4 R_c^{2/k} = \frac{k+1}{2} \qquad (A.1)$$

In which β is the ratio of the expansion. In case of jet mills β is considered very small. In this case R_c can be calculated by

$$R_c = \left(\frac{2}{k+1}\right)^{k/(k-1)} \qquad (A.2)$$

For the calculation of the flow rate through the nozzle only the conditions (T_1, P_1, $\rho1$) on the high pressure side need to be known. The mass flow in kilograms per second is determined with

$$\Phi_M = A_2 P_1 \sqrt{k\left(\frac{M_{MOL}}{R_{GAS}T_1}\right)\left(\frac{2}{k+1}\right)^{(k+1)/(k-1)}} \qquad (A.3)$$

The air supplied to the jet mill was 20 degrees Celsius (293 K). For a mill containing n nozzles with a diameter d_n the air flow rate is estimated by

$$\Phi_M = Const \cdot d_n \cdot n_n \cdot P_1 \qquad (A.4)$$

Substitution of the following parameters for air

$T_1 = 293$	*Ambient temperature*	*[K]*
$k = 1.4$	*Ratio of specific heats for air (Cp/Cv = 1.005/0.718)*	*[-]*
$M_{MOLL} = 28.969$	*Molecular mass*	*[g/mol]*
$R_{GAS} = 287$	*Gas constant*	*[J/kg.K]*

A similar equation was derived by Dr.-ing H. RUMPF [1966] for an air flow with temperature 288 K. The air consumption in normal cubic meters per second of a spiral jet mill can be estimated by

$$\Phi_{air} = 143 \cdot d_n \cdot n_n \cdot P_1 \tag{A.5}$$

In which: d_n = nozzle diameter in meters; n_n = number of nozzles; P_1 = nozzle pressure in bar.

VISWANATHAN [1987] used the following equation

$$\Phi_{VOL} = \sqrt{7} N \frac{\pi}{4} d^2 P_1^{2/7} \left(1 - P_1^{-2/7}\right) \tag{A.6}$$

Energy input: The energy is supplied to the jet mill as gas kinetic energy and therefore this should be the measure for energy input [SCHURR]. The kinetic energy at the throat is given by

$$E_{KIN} = \frac{1}{2} \Phi_{air} v_t \tag{A.7}$$

with $v_t = \sqrt{\dfrac{kRT}{M}}$

VISWANATHAN used an alternative method. He calculated the energy supplied to the mill from the work done by the adiabatic expansion (W) of the fluid flow (Φ_v).

$$E_{exp} = W \cdot \Phi_v \tag{A.8}$$

References

Hanisch, H., Schubert, H., Clemens, P., Energy considerations in particle bed comminution, *proc. partec 86*, 223, 1986

Patuscha, L., Mielczarek, E., Otinowski, H., Energy consumption during pneumatic jet milling, *Archives of mining science*, 33 (1), 127-136, 1988

Viswanathan, Jet mill design: a complete method, *Bulk solids handling*, vol.7, no.4, 1987

Schurr, G.A., Zhao, Q.Q., Fluid mechanic consideration for fine grinding in a fluid energy mill, *8th Eur. Symp. on Comminution*, vol.II, 562-573, 1994

Samenvatting

Bestudering van een closed circuit jet mill installatie

gebruikmakend van on-line deeltjesgroottemetingen

Jetmilling is een techniek die bijzonder geschikt is voor de produktie van fijne poeders met een smalle deeltjesgrootteverdeling (DGV) uit bros voedingsmateriaal. De DGV bepaald voor een belangrijk deel het uiteindelijk gedrag van het materiaal in de opvolgende processtappen zoals chemische reacties, verbranding, drukwerk en coating.

Voordelen van jetmilling zijn, behalve de nauwkeurig gedefinieerde DGV, de vermijding van excessieve warmteontwikkeling en contaminatie tijdens het vermalen. Dit maakt jetmilling erg aantrekkelijk voor de verwerking van plastics, farmaceutische produkten en voedingsmiddelen. Een belangrijk nadeel is het hoge energieverbruik.

In een jet mill, oftewel luchtstraalmolen, worden de deeltjes opgenomen en versneld door sterk expanderende luchtstralen die de maalkamer binnenkomen door een aantal inspuitstukken. Turbulentie is het voornaamste mechanisme voor intense onderlinge botsingen tussen deeltjes waardoor deze mechanisch belast worden en breken.

In dit project zijn twee typen jet mills onderzocht, namelijk de spiral jet mill en de opposed jet mill. In een spiral jet mill zijn zowel de verkleining alsook de afscheiding van deeltjes afhankelijk van de roterende stroming in de kamer. De optimale molenbelading voor elk van deze processen conflicteerd en maakt een gelijktijdige optimalisatie onmogelijk. Daarom werd de spiral jet mill aan een externe classificator gekoppeld. Met deze configuratie, een zogenaamde closed circuit maalinstallatie, kon een aanzienlijke energiebesparing worden bereikt.

Ter vergelijking is ook een opposed jet mill getest. In deze molen staan de luchtstralen op elkaar gericht en vindt de afscheiding van fijne deeltjes plaats door een geïntegreerde classificatorrotor. Instellingen van het persluchtniveau, de voeding en de rotorsnelheid zijn systematisch onderzocht.

Verstoringen op de perslucht en schommelingen in de voedingssamenstelling kunnen ertoe leiden dat de DGV van het molenprodukt varieert. Daarom worden jet mills in de industriële praktijk vaak beneden hun maximale capaciteit gehouden om de produktie van afgekeurd (te grof) materiaal te voorkomen. Verder moet de maalinstallatie voor het opstarten en stilzetten nauwkeurig worden afgeregeld, hetgeen erg omslachtig is en veel expertise vereist.

Dit onderstreept het belang van een geautomatiseerde maalinstallatie die is uitgerust met een continu DGV-meetinstrument. Een speciaal ontwikkelde meetcel werd op de molenuitlaat geplaatst voor gebruik met een laserdiffractie (LD) apparaat. Als een robuuster en goedkoper alternatief is er ook een meetmethode gebaseerd op de verstrooiing van halogeenlicht onderzocht.

De real-time DGV metingen aan de jet mill installatie werden samen met andere procesvariabelen continu opgeslagen in de procescomputer. De verzamelde kennis werd voor de validatie en de optimalisatie van een voorspellend populatiebalansmodel gebruikt. Aparte botsings- en compressieproeven zijn uitgevoerd met het testmateriaal om het breekgedrag te karakteriseren.

Voor regeling van het maalproces is een absolute nauwkeurigheid van de DGV nie vereist. Met principle components analysis (PCA) is de LD data bestudeerd. Het bleek da met PCA de meetdata sneller en eenvoudiger konden worden verwerkt in een stuursignaa dan met de gebruikelijke deconvolutiemethoden.

De reproduceerbaarheid van de produktkwaliteit van de geautomatiseerde opstelling wer verhoogd door uitsluiting van bedieningsfouten. Door de continue monitoring van d produktkwaliteit kon tevens de hoeveelheid afgekeurd materiaal verminderd worden. Ee regelkring gebaseerd op de on-line DGV metingen maakte het mogelijk om de mole dichter tegen de specificatiegrenzen te laten werken. Hierdoor werd de hoeveelheid te fij vermalen materiaal sterk gereduceerd.

Het laatste gedeelte van dit projekt richtte zich op de bestudering van d stromingspatronen. Numerieke simulaties zijn uitgevoerd van de vortex in d molenkamer en met Phase Doppler apparatuur is de opname en versnelling van deeltjes i de expanderende luchtstralen gemeten.

Acknowledgement

Erik Gommeren is geboren op 19 april 1966 te Bergen op Zoom.

1976 - 1980	Mavo Heilige Geest, Bergen op Zoom.
1980 - 1985	Atheneum B, Moller Lyceum, Bergen op Zoom.
1985 - 1990	Studie Werktuigbouwkunde aan de Technische Universiteit Delft.
1990 - 1991	Onderzoeker op het Instituto des Pesquisas Technologicas, São Paulo, Brazilië.
1991 - 1992	Militaire dienst: Trompettist in de muziekkapel Johan Willem Friso.
1993 - 1997	Werkzaam als Assistent in Opleiding aan het Laboratorium Apparatenbouw voor de Procesindustrie van de Technische Universiteit Delft.
1998	Werkzaam bij DuPont de Nemours, Experimental Station, Wilmington, Delaware, Verenigde Staten.